AN EXPERIMENTAL AND THEORETICAL INVESTIGATION INTO THE ACOUSTIC SPECTRA OF SOLIDS HAVING CYLINDRICAL SYMMETRY

A thesis submitted to the Faculty of Engineering of the University of Aston in Birmingham for the degree of,

Doctor of Philosophy

by

GAYATHRI AMBATI

PREFACE

This thesis describes research carried out at the Electrical Engineering Department of the University of Aston in Birmingham from 1973 to 1975. No part of this thesis has been submitted for a qualification at another university, but the contents of Chapter 3 are to appear in the following publication:

Ambati, G., Bell, J.F.W., Sharp, J.C.K. : 'In plane vibrations of annular rings',(accepted for publication), Journal of Sound and Vibration, 1976.

I wish to express my thanks to Dr. J.F.W. Bell, Reader, for the guidance and discussions during the course of this research. I also wish to express my thanks to the University of Aston in Birmingham for providing a research grant and to Prof. J.E. Flood, Head of the Department of the Electrical Engineering, for providing necessary facilities throughout the research period.

Gambati

December 1975

SUMMARY

A highly sensitive acoustic line pulse-echo system was developed to measure and classify the spectra of a range of isotropic solids having cylindrical geometry. In a number of cases, these have been compared with exact theoretical solutions and in others they have been used to test the extent to which approximate solutions are valid.

A theory for contour vibrations in thick disks was developed and numerical solutions obtained for a wide range of disk thickness-to-diameter ratios. These numerical eigenvalues and the resonant spectra of the specimen, which is in the form of a disk resonator (with no restriction on its thickness), have been used to determine the elastic constants of the specimen material.

The in plane vibrations of annular rings, which is the general case of the disk at one extreme and the narrow ring at the other, have been analysed. Six series of resonances were identified, in which every disk mode progresses to a particular ring mode as the hole diameter is increased.

The thick disk theory has been extended to the thick annular disk and numerical eigenvalues evaluated for a full range of hole sizes, Poisson's ratio and disk thicknesses upto one radius. The correspondence of the resonances in thick disks to those in cylindrical shells was examined. The six series of resonances observed in annular rings were present and in addition, there is one series each of pure radial (compressional), finite frequency and asymptotic (compressional) modes.

Several limiting cases obtained by simplifying the thick annular disk frequency equation, using various approximations,

were investigated. Of these, the most important one is the frequency equation which yields the cut-off frequencies (plane strain) of an infinite hollow cylinder. These features agree exactly with those of other researchers. It is shown that a material modulus transformation yields the plane stress (annular ring) results from the plane strain results.

The interaction of a thin layer of gas on a vibrating body was investigated by constructing a series of tuning forks with various narrow gaps between the tines. An electronic system was constructed for this investigation which enabled the fork to be driven into resonance and the subsequent decrement received from the fork was analysed to give the decrement parameters. A reactive component changing the frequency and a lossy component changing the logarithmic decrement were found by changing the gas pressure.

Finally, the solution of non-axisymmetric vibrations in a disk-shaft combination has been considered. Resonant spectra were obtained for disk-shafts of various disk and shaft dimensions and the way in which their various modes of vibration were coupled together, was examined.

LIST OF PRINCIPAL SYMBOLS

a	=	Disk radius
b	=	Hole/Shaft radius
h	=	Thickness of the disk
l	=	Length of the shaft/rod
X_{ij}, Y_{ij}, a_{ij}, b_{ij}	=	Elements of the determinants
A_i, B_i, C_i	=	Amplitude coefficients
p, q, r	=	Integers
E	=	Young's modulus
σ	=	Poisson's ratio
ρ	=	Density
Θ^2	=	$2/(1-\sigma)$
c	=	$\frac{(1-\sigma)^2}{(1-2\sigma)}$
C	=	Velocity of sound
C_0	=	$\sqrt{E/\rho}$, Rod velocity
C_p	=	$C_0/\sqrt{(1-\sigma^2)}$, Plate velocity
C_s	=	C_p/Θ , Shear velocity
C_c	=	$\sqrt{c}\, C_p$, Compressional (bulk) velocity
r, θ, z	=	Cylindrical coordinates
J_n, Y_n, I_n, K_n	=	Bessel functions of first and second kind
k, h, α, β, ν	=	Wavenumbers
ζ	=	$p\pi/l$, Longitudinal wavenumber
u_r , u_θ , u_z	=	Displacement functions
ξ_r , ξ_θ , ξ_z	=	Radial, tangential and axial components of displacement
$W_n(x)$	=	$x \frac{Z_{n-1}(x)}{Z_n(x)}$, where W = M,L,N,P for Z = J,Y,I,K, respectively
Δ , $\tilde{\omega}$	=	Dilatational and rotational strains
γ	=	b/a , Inner to outer diameter ratio

η = $2a/h$, Diameter-to-thickness ratio

ε_r , ε_θ , ε_z = Strain components

σ_r , σ_θ , σ_z = Stress components

Bulk modulus = $\rho C_c^2 = \dfrac{E(1-\sigma)}{(1+\sigma)(1-2\sigma)}$

Plate modulus = $\rho C_p^2 = \dfrac{E}{(1-\sigma^2)}$

Shear modulus = $\rho C_s^2 = \dfrac{E}{2(1+\sigma)}$

T_{rr}, $T_{r\theta}$, T_{rz} = Stress resultants

K = $\omega a/C$ = Dimensionless eigenvalue

δ, $\lambda\delta$, $K\Theta$ = αa, βa, νa, respectively

K_p = $K = \omega a/C_p$

K_s = $K\Theta = \omega a/C_s$

K_0 = $K/\sqrt{(1-\sigma^2)} = \omega a/C_0$

K_c = $K/\sqrt{c} = \omega a/C_c$

(m,n) = Integers defining number of nodal circles and nodal diameters associated with modes

f, λ = Frequency and wavelength

ω = Angular frequency

m, S = Mass and stiffness

Q = A factor to estimate the energy lost per cycle

Z_m , Z_s = Impedance of mass and spring

CONTENTS

CHAPTER 1

GENERAL INTRODUCTION

The acoustic spectra of solid bodies has been the subject of investigation for many years. Exact solutions of simple geometries are readily available and their resonant spectra give an insight into the behaviour of various phenomena, when they are used as sensors. Although, the application of thin disk numerical values for the determination of material constants, using a pulse-echo technique originally developed by Bell[1], has been successful, problems were encountered due to finite thickness of the disk[2]. These problems have now been overcome by the theory developed for contour vibrations of thick disks(Chapter 2 of this thesis). The numerical solutions of this theory and the resonant spectra of the disk can be used to determine the elastic constants of the disk material with high accuracy. The fabrication problems encountered, when disk shaped resonators are used as sensors, can also be avoided with the use of this analysis.

The acoustic spectra of solids can be obtained by the pulse-echo technique using an acoustic resonance detector. The investigations were limited to solid resonators having cylindrical geometry. The technique, basically consists of the specimen (resonator) coupled to one end of a magnetostrictive line (transducer). The other end of the line is connected to the coil which is fed by burst of oscillations from the transmitter, to excite resonances in the specimen. Thus, the electrical part of the system is remote from the specimen under investigation, which gives a practical importance to the system. The echos received from the resonator are then analysed to yield the resonant spectra of the specimen. Some of the properties of the specimen such as elastic constants and internal friction can also be deduced from the echo signal.

Further, with this method, it was possible to excite higher resonant modes using various drive techniques described in Appendix A.2.2. A determination of these higher modes affords the oppourtunity of studying, in detail, several interesting phenomena. Firstly, from the frequencies of higher modes, one can determine phase velocity dispersion over a wide frequency range. Secondly, to the extent that one can develop confidence in the theoretical solutions for the phase velocity, one can use the measured frequencies to give an indication of any possible frequency dependence of the elastic constants[3]. Finally, the measurement of frequencies of higher modes helps in classifying various resonances as the resonator progresses from one form to another.

The various applications of this pulse-echo method have resulted in:

(1) Measurement of elastic constants of thin disk materials[2] and thick disk materials (chapter 2 of this thesis),

(2) Measurement of internal friction in solids[4],

(3) Measurement of high temperature[5] and fluid properties such as density, viscosity and pressure[6] (also, chapter 6 of this thesis).

(4) Investigation of vibration spectra in various solids having cylindrical geometry[7](chapters 3,4,5 and 7 of this thesis).

The electronic system used to measure the acoustic spectra of solids is described in Appendix A.2.2.

CHAPTER 2

ELASTIC CONSTANT MEASUREMENT FROM THE SPECTRA OF THICK DISK RESONATORS

2.1 Introduction

The contour extensional vibrations of thin disks, which involve no transverse displacement, were solved by Love[8]. Due to the complexity of the resulting equations and the lack of a ready method for exciting these modes, they seemed to him "not to be of sufficient physical importance". However, with the advent of high speed digital computers and the development of the piezoelectric vibrators, these equations have become important and have been solved by Onoe[9] and Holland[10].

In practice, all disks have a finite thickness-to-diameter ratio. Resonant-frequency equations for vibrations in thick disks that are available in the literature[11,12,13] are valid only for radial modes. Further, they are in the form of correction factors, which are limited to a fairly small thickness-to-diameter ratios. Mosley has obtained a thickness correction to the radial mode frequencies of an isotropic disk by a method similar to the Pochhammer-Chree approximate frequency equation for the longitudinal resonances of the rod. But, this correction factor is valid only for disks with thickness-to-diameter ratios less than 0.125. Lucey, however, defined a boundary between a thick disk and a thick rod and derived equations for the resonant frequency in terms of the planar and axial frequency constants, but, these equations are valid only for the fundamental mode of radial vibration. Rasband[14] has recently given a solution for non-axisymmetric vibrations of a free cylinder or a disk, by satisfying, partially, the boundary conditions on the cylindrical and flat surfaces, but the resulting frequency equations are so complex that their numerical solution becomes very expensive. Moreover, the solution is not unique and requires different frequency equations to be used for different modes of vibration. Furthermore, the theoretical results were not verified experimentally.

In this chapter, the frequency equations for axisymmetric and non-axisymmetric vibrations of a disk, with any thickness-to-diameter ratio, are derived by reducing the three dimensional equations of motion to the equivalent two dimensional equations. The distribution of the displacement along the thickness direction is taken as sinusoidal, without any loss of generality, to reduce the complexity of the problem and to enable the numerical solution of the frequency equations, to be obtained at a reasonable cost in computer time. The frequency equations will also predict the effect of thickness on the resonant frequencies of fundamental as well as higher modes of vibration. The theoretical frequency values are compared with the experimental spectrum, which is measured by means of a Pulse echo technique. A marked agreement is observed between the two results over a wide range of disk thickness-to-diameter ratios. These results are also compared with those of Moseley and Lucey. A method is also proposed, by which, the elastic constants of thick disk material can be determined precisely, using the experimental resonant spectrum and the numerical eigen values.

2.2 Contour Vibrations in Thick Disks

The contour vibrations in thick disks consist of two families of modes of circumferential order zero; one is the radial modes characterised by the absence of rotation and the other is the tangential modes characterised by the absence of dilatation; but, for each circumferential order greater than zero, there is only one family of compound modes, the vibrations being compounded of both dilatational and rotational strains.

The derivation of the dilatation, rotation and their associated displacement functions in thick disks, whose radius is 'a' and thickness h, is given in Appendix A.2.1. In this section, the frequency equation for the compound modes of vibration is derived and then the radial mode frequency equation is obtained as a special case of the compound mode frequency equation.

2.2.1 Compound Modes

For compound modes of vibration, $n > 0$ and the radial, tangential and axial components of displacement, given by eqns.(A.2.13),(A.2.15), are

$$\xi_r = \{A_1 \frac{dJ_n(\alpha r)}{dr} + B_1 \frac{dI_n(\beta r)}{dr} + \frac{nC_1}{r} J_n(\nu r)\} \cos n\theta$$

$$\xi_\theta = -\{\frac{nA_1}{r} J_n(\alpha r) + \frac{nB_1}{r} I_n(\beta r) + C_1 \frac{dJ_n(\nu r)}{dr}\} \sin n\theta \qquad (2.2.1)$$

$$\xi_z = \{A_1 \phi_1 J_n(\alpha r) - B_1 \phi_2 I_n(\beta r)\} \cos n\theta$$

The boundary conditions, for free motion at $r = a$, are

$$T_{rr} = 0 \quad \text{at } r = a$$
$$T_{r\theta} = 0 \quad \text{at } r = a \qquad (2.2.2)$$
$$\text{and} \quad T_{rz} = 0 \quad \text{at } r = a$$

where the stress resultants T_{rr}, $T_{r\theta}$ and T_{rz}, given by eqns.(A.2.3), can be rewritten as

$$T_{rr} = \frac{hE}{(1+\sigma)(1-2\sigma)} \{(1-\sigma) \frac{\partial \xi_r}{\partial r} + \frac{\sigma}{r} (\xi_r + \frac{\partial \xi_\theta}{\partial r}) + \frac{2\sigma}{h} \xi_z\}$$

$$T_{r\theta} = \frac{hE}{2(1+\sigma)} \{\frac{\partial \xi_\theta}{\partial r} - \frac{\xi_\theta}{r} + \frac{1}{r} \frac{\partial \xi_r}{\partial \theta}\} \qquad (2.2.3)$$

$$T_{rz} = \frac{h^2 E}{\pi^2 (1+\sigma)} \frac{\partial \xi_z}{\partial r}$$

Substitution of eqns.(2.2.1) and (2.2.3) into eqn.(2.2.2) yields the frequency equation, formed by the determinant of the coefficients A_1, B_1 and C_1, as given below:

$$F(K) = \left| X_{ij} \right| = 0 \quad , \qquad i,j = 1 \text{ to } 3 \qquad (2.2.4)$$

where i and j identify the row and the column of the 3×3 determinant, respectively, and the elements of the determinant are given by

$$X_{11} = J_n(\delta)\{M_n(\delta) - n(n+1) + \frac{K^2 \Theta^2}{2}\}$$

$$X_{12} = \frac{I_n(\lambda\delta)}{\lambda\delta} \{N_n(\lambda\delta) - n(n+1) + \frac{K^2 \Theta^2}{2}\}$$

$$X_{13} = n J_n(K\Theta)\{M_n(K\Theta) - (n+1)\}$$

$$X_{21} = nJ_n(\delta)\{M_n(\delta) - (n+1)\}$$

$$X_{22} = \frac{nI_n(\lambda\delta)}{\lambda\delta}\{N_n(\lambda\delta) - (n+1)\}$$

$$X_{23} = J_n(K\Theta)\{M_n(K\Theta) - n(n+1) + \frac{K^2\Theta^2}{2}\} \qquad (2.2.5)$$

$$X_{31} = J_n(\delta)\{M_n(\delta) - n\}(\delta^2 - K^2/c)$$

$$X_{32} = -\frac{I_n(\lambda\delta)}{\lambda\delta}\{N_n(\lambda\delta) - n\}(\lambda^2\delta^2 + K^2/c)$$

$$X_{33} = 0$$

where K is a dimensionless eigen value defined as

$$K = \omega a\sqrt{\frac{\rho(1-\sigma^2)}{E}} \qquad (2.2.6)$$

$$\Theta^2 = \frac{2}{1-\sigma}\ , \quad c = \frac{(1-\sigma)^2}{(1-2\sigma)}\ ,$$

$M_n(x)$ and $N_n(x)$ are defined as, $M_n(x) = x\frac{J_{n-1}(x)}{J_n(x)}$, $N_n(x) = x\frac{I_{n-1}(x)}{I_n(x)}$,

respectively, and δ and $\lambda\delta$ are the wavenumbers given by

$$\delta = \alpha a = \frac{\pi\eta}{2}\sqrt{\frac{G(\psi+1)}{(1-\sigma)}}$$

$$\text{and} \quad \lambda\delta = \beta a = \frac{\pi\eta}{2}\sqrt{\frac{G(\psi-1)}{(1-\sigma)}} \qquad (2.2.7)$$

where G and ψ are given by

$$G = \{\frac{2K^2(3-4\sigma)}{\pi^2\eta^2(1-\sigma)} - 1\} \qquad (2.2.8)$$

$$\psi = \left[1 + \frac{4(G+1)(1-\sigma)^2}{G^2(3-4\sigma)}\{1 - \frac{2(G+1)(1-\sigma)}{c(3-4\sigma)}\}\right]^{\frac{1}{2}}$$

and $\eta = \frac{2a}{h}$, is the diameter-to-thickness ratio of the disk.

For a given n, the m^{th} solution of eqn.(2.2.4) is designated by K_{mn}, where n is the number of nodal diameters and (m-1) is the number of nodal circles. Thus, K_{mn} refers to all of the antisymmetric extensional modes of vibration. The resonant frequency of the mode associated with the eigenvalue K_{mn} is similarly designated by f_{mn}. Thus, the first solution of the first antisymmetric compound mode is designated by K_{11} and so on.

The Case when $\lambda\delta$ is Imaginary

It may be noted, from eqns.(2.2.7), that the wavenumber δ is always real whereas $\lambda\delta$ is real if $\psi>1$ and is imaginary if $\psi<1$. This corresponds to the condition that $\lambda\delta$ is real if $K/\sqrt{c}<\pi\eta/2$ and is imaginary if $K/\sqrt{c}>\pi\eta/2$. Hence, for $\lambda\delta$ imaginary, the elements of the determinant become

$$X_{12} = \frac{J_n(\bar{\lambda}\delta)}{\bar{\lambda}\delta}\{M_n(\bar{\lambda}\delta) - n(n+1) + \frac{K_{mn}^2\Theta^2}{2}\}$$

$$X_{22} = \frac{nJ_n(\bar{\lambda}\delta)}{\bar{\lambda}\delta}\{M_n(\bar{\lambda}\delta) - (n+1)\} \qquad (2.2.9)$$

$$X_{32} = \frac{J_n(\bar{\lambda}\delta)}{\bar{\lambda}\delta}\{\bar{\lambda}^2\delta^2 - \frac{K_{mn}^2}{c}\}\{M_n(\bar{\lambda}\delta) - n\}$$

where $\bar{\lambda}^2\delta^2 = -\lambda^2\delta^2$ and the remaining elements of the determinant are given by eqn.(2.2.5). The frequency equation(2.2.4), then, gives the relation between the dimensionless eigenvalue K_{mn} and the dimensionless parameters σ, the Poisson's ratio and η, the diameter-to-thickness ratio. Since, the solutions to eqn.(2.2.4) exists for all integer values of $n\geq 1$ and since there is an infinite number of solutions for each value of n, namely, m = 1,2,3,..∞,etc., the symbol K_{mn} represent infinite number of modes of propagation, which are solutions of eqn.(2.2.4).

The thin disk frequency equation for the compound modes may be obtained, from eqn.(2.2.4), as a limiting case. For instance, when $1/\eta\to 0$, $\delta\to K_{mn}^T$, $\lambda\delta\to\infty$, $N_n(\lambda\delta)\to\infty$ and $\lambda^2\delta^2 >> K_{mn}^2/c$. Thus, eqns.(2.2.5) reduce to

$$X_{11} = \{M_n(K_{mn}^T) - n(n+1) + \frac{(K_{mn}^T)^2\Theta^2}{2}\},$$

$$X_{12} = 1, \quad X_{13} = n\{M_n(K_{mn}^T\Theta) - (n+1)\}$$

$$X_{21} = n\{M_n(K_{mn}^T) - (n+1)\}, \quad X_{22} = n, \qquad (2.2.10)$$

$$X_{23} = \{M_n(K_{mn}^T\Theta) - n(n+1) + \frac{(K_{mn}^T)^2\Theta^2}{2}\},$$

$$X_{31} = 0, \quad X_{32} = 1, \text{ and } X_{33} = 0.$$

The thin disk frequency equation, then, becomes

$$F(K_{mn}^T) = (X_{13}\, X_{21} - X_{11}\, X_{23}) = 0 \qquad (2.2.11)$$

where

$$F(K_{mn}^T) = \{M_n(K_{mn}^T) - n(n+1) + \frac{(K_{mn}^T)^2\Theta^2}{2}\}\{M_n(K_{mn}^T\Theta) - n(n+1) + \frac{(K_{mn}^T)^2\Theta^2}{2}\}$$
$$- n^2\{M_n(K_{mn}^T) - (n+1)\}\{M_n(K_{mn}^T\Theta) - (n+1)\}\ , \qquad (2.2.12)$$

which is same as the compound mode frequency equation in the theory of generalised plane stress[10], and K_{mn}^T denotes compound modes of thin disk. The numerical solution of the frequency equations (2.2.4) and (2.2.11) is given in section 2.3.

2.2.2 Radial Modes

The radial modes of vibration, with circumferential order n equal to zero, are characterised by the absence of rotation. Consequently, $\tilde{\omega} = 0$, $\xi_\theta = 0$ and ξ_r and ξ_z are independent of θ. Hence, the radial mode frequency equation can be obtained, as a special case, by setting $n = 0$ in eqn.(2.2.4). Then, eqn.(2.2.4) reduces to

$$\begin{vmatrix} Y_{11} & Y_{12} \\ Y_{31} & Y_{32} \end{vmatrix} \times |Y_{23}| = 0 \qquad (2.2.13)$$

where the elements of the above determinants can be obtained by setting $n = 0$ in eqn.(2.2.5). Then, the radial mode frequency equation is given by

$$F(K_{mR}) = \begin{vmatrix} Y_{11} & Y_{12} \\ Y_{31} & Y_{32} \end{vmatrix} = 0 \qquad (2.2.14)$$

where

$$F(K_{mR}) = \delta^2(\delta^2 - \frac{K_{mR}^2}{c})\{\frac{K_{mR}^2\Theta^2}{2} N_1(\lambda\delta) + \lambda^2\delta^2\}$$
$$-\lambda^2\delta^2(\lambda^2\delta^2 + \frac{K_{mR}^2}{c})\{\frac{K_{mR}^2\Theta^2}{2} M_1(\delta) - \delta^2\} \qquad (2.2.15)$$

and K_{mR} is the designated radial mode, which is given by the m^{th} solution

of eqn.(2.2.14), where (m-1) represents the number of nodal circles. Thus, the first (or lowest) branch of the symmetric radial mode is designated by K_{1R} and so on. For $\lambda\delta$ imaginary, the corresponding frequency equation is given by

$$\delta^2\left(\delta^2 - \frac{K_{mR}^2}{c}\right)\left\{\frac{K_{mR}^2\Theta^2}{2} M_1(\bar{\lambda}\delta) - \bar{\lambda}^2\delta^2\right\} - \bar{\lambda}^2\delta^2\left(\bar{\lambda}^2\delta^2 - \frac{K_{mR}^2}{c}\right)\left\{\frac{K_{mR}^2\Theta^2}{2} M_1(\delta) - \delta^2\right\} = 0 \qquad (2.2.16)$$

where $\bar{\lambda}^2\delta^2 = -\lambda^2\delta^2$ so that $\bar{\lambda}\delta$ is real. The numerical solution of the frequency equation is described in section 2.3.

The thin disk frequency equation for radial modes may be obtained as a special case of eqn.(2.2.14). For example, when $1/\eta \to 0$, $N_1(\lambda\delta) \to \lambda\delta$ and $\lambda^2\delta^2 >> K_{mR}^2/c$. Thus, eqn.(2.2.15) can be rewritten in the form, as

$$\left\{\frac{K_{mR}^2\Theta^2}{2\delta^2} M_1(\delta) - 1\right\} = \frac{(\delta^2 - K_{mR}^2/c)}{\lambda^2\delta^2}\left\{\frac{K_{mR}^2\Theta^2}{2\lambda\delta} + 1\right\} \qquad (2.2.17)$$

Further, as $1/\eta \to 0$, $\delta \to K_{mR}^T$ and $\lambda\delta \to \infty$; substituting these in the above equation, yields

$$M_1(K_{mR}^T) = \frac{2}{\Theta^2} = (1 - \sigma) \quad , \qquad (2.2.18)$$

which is a well known radial mode frequency equation in the theory of generalised plane stress[2,8] and K_{mR}^T is the eigenvalue for the radial modes of vibration in thin disk.

2.3 Numerical Solution Of The Frequency Equation:

Each of the frequency equations(2.2.4), (2.2.11) and (2.2.14) relates the eigenvalue K with η and σ . For a given n, η and σ , the frequency eqn. reduces to a transcedental equation in K only. Two methods based on iterative procedures are described to compute the roots K_m, m =1,2,3,...,etc., of the frequency equation, and their merits and demerits, with respect to the computer time, are discussed.

For a desired value of n, η and σ, the value of F(K) is computed for an assumed value of K using an 'Interval-division iteration technique', and the result is designated by 'Error'. Thereafter, the computation is

carried out at a specified value of ΔK till the error becomes less than a specified value of 'Error 1'. During the computation, if the magnitude of the error becomes less than one-tenth of error 1, then the interval ΔK is set to one-tenth of its previous value and the computation is carried out using this interval. This process is repeated until a change of sign of the error occurs in any interval, which gives an indication of a root in that interval. If a change of sign occurs, then the interval of ΔK is set to one-tenth of its previous value and the direction of scanning is reversed. This process is repeated until a root with the error less than an allowable 'Relative error'(i.e., the error divided by the root) of, say, 1 in 10^5, is obtained.

In the second method, for a chosen value of n, η and σ, the error is computed for an assumed value of K. If the magnitude of this error is not less than a specified value, then the value of K for the successive iteration is determined, using Newton-Raphson method, as

$$K_{i+1} = \{ K_i - \frac{F(K_i)}{F'(K_i)} \} \qquad (2.3.1)$$

where $F'(K)$ is the derivative of $F(K)$ with respect to K and K_{i+1} and K_i are the values of K at $(i+1)^{th}$ and i^{th} iterations, respectively. The value of the error is computed again for this value of K and so on, until the K value, for which the magnitude of the error is less than an allowable 'Relative error', is obtained.

The major demerits of the first method are: (a) the number of iterations required for yielding a root with an acceptable accuracy are, indeed, very large. (b) Secondly, the possible chances of the computation sticking between two successive iterations without yielding the required result, are high. (c) Finally, this method requires a prior knowledge of the approximate value of the root, otherwise it may require about one hundred iterations to take the value of the root from an assumed value to an approximate value, which is rather expensive. The merits of Newton-Raphson method, on the otherhand, are: (a) It does not require prior knowledge of

the approximate value of the root. (b) It convergs very rapidly to the exact value of the root with in, say, two or three iterations.

The only difficulty in Newton-Raphson method is in obtaining the derivative of the complicated frequency equation. But, this difficulty can be overcome by determining the value of F(K) on either side of the root and then evaluating the derivative by the formula, provided that dK is small, given below:

$$\frac{dF(K_i)}{dK} = \frac{F(K_i) - F(K_{i-1})}{K_i - K_{i-1}} \qquad (2.3.2)$$

and hence eqn.(2.3.1) now becomes,

$$K_{i+1} = K_i - \frac{(K_i - K_{i-1})\, F(K_i)}{\{F(K_i) - F(K_{i-1})\}} \qquad (2.3.3)$$

where K_i is the eigenvalue at the i^{th} iteration.

The Newton-Raphson method was found to be 20 to 25 times faster than the interval-division method and hence results in an enormous saving of computer time. The use of eqn.(2.3.3) in place of eqn.(2.3.1) results in further reduction of computer time. The ICL 1905E computer has been used for all the computations of eigen values.

The computations were carried out for 12 modes for Poisson's ratio σ from 0.0 to 0.5 in the interval of 0.01 and the tables of K values, for thickness-to-diameter ratios from 0.0 to 0.5, are available from the author. However, the variation of K values of all the modes with the Poisson's ratio is shown in Figs.2.1 to 2.6, for various η's. The computations were restricted to a few specific modes only, because these are the only modes basically required for the measurement of elastic constant of the disk material, by a method proposed here. Further, these are, mainly, the modes of resonances which can be excited experimentally by pulse-echo technique[1].

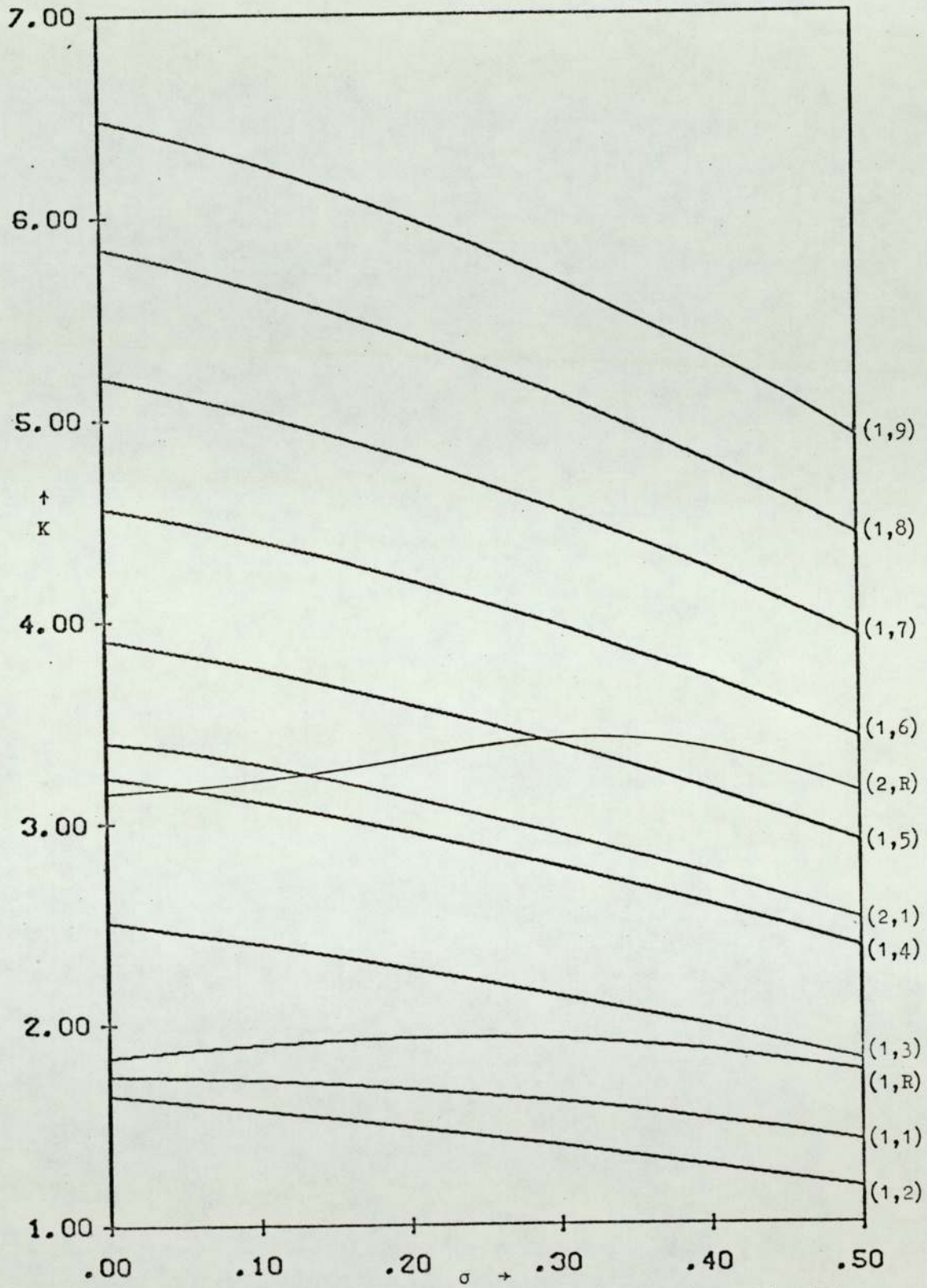

Fig.2.1 Graph of K versus σ for thickness-to-diameter ratio =0.5. The differing trends of the K values for radial and compound modes are the basis for the measurement of Poisson's ratio.

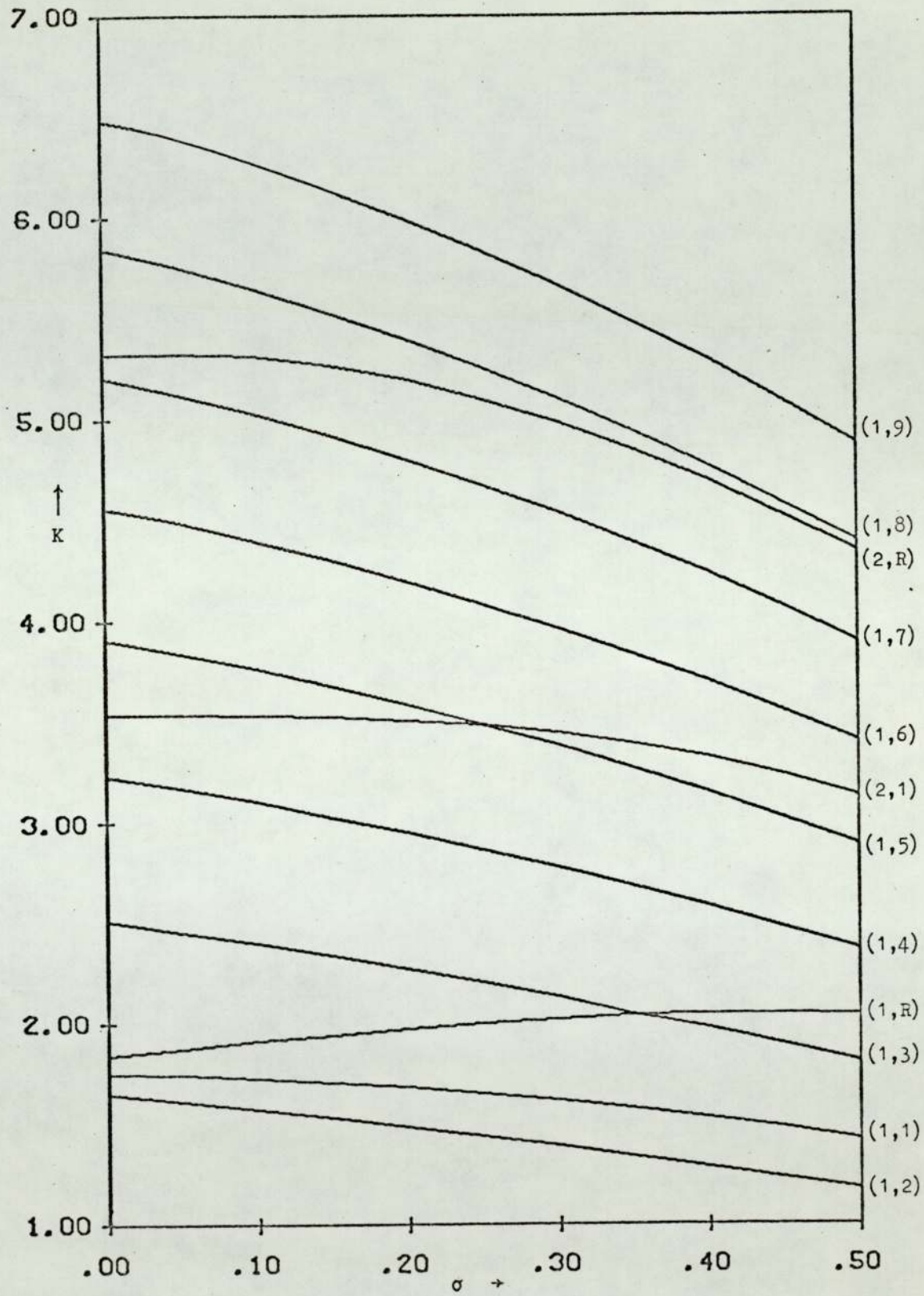

Fig.2.2 Graph of K versus σ for thickness-to-diameter ratio =0.25.

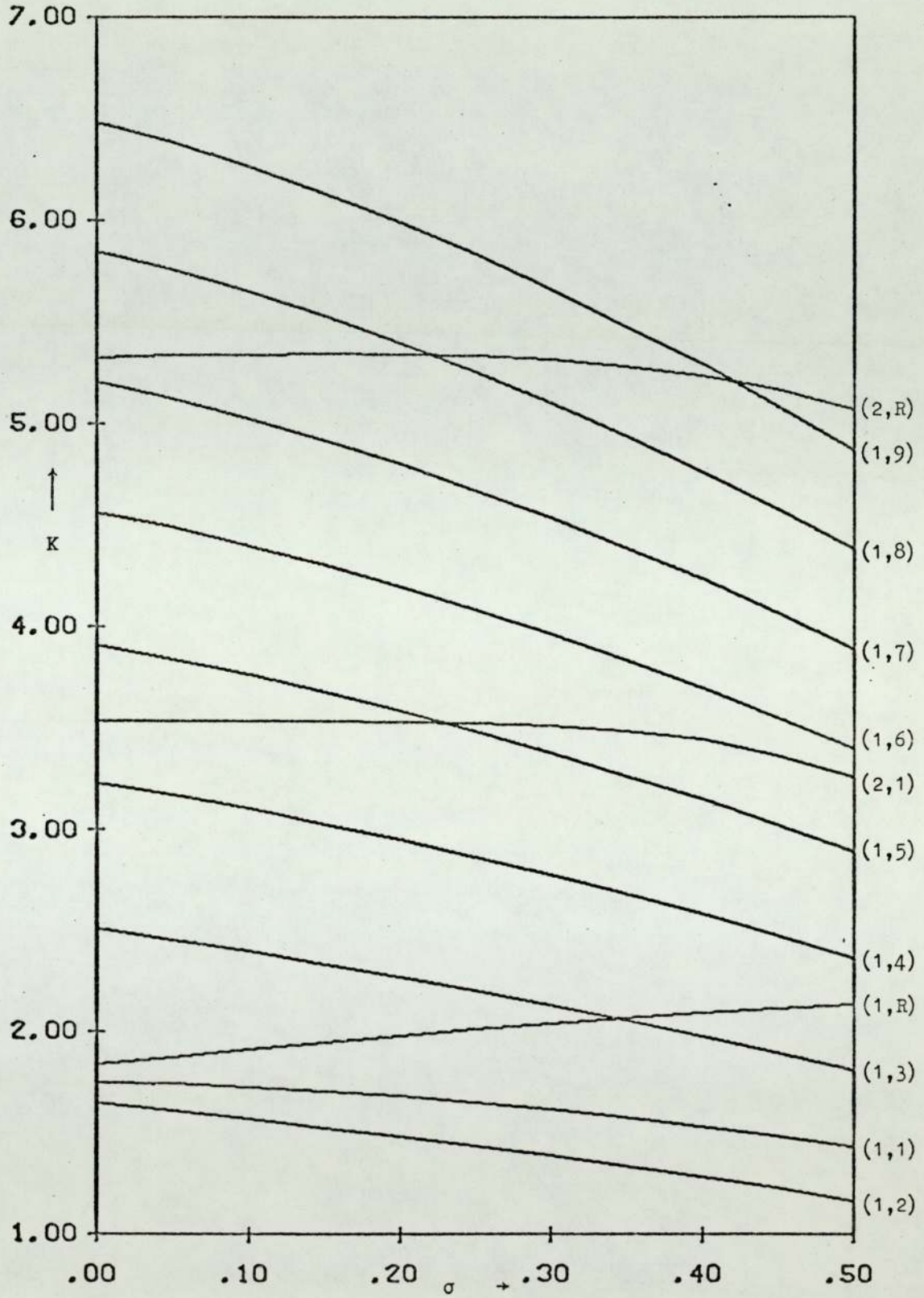

Fig.2.3 K versus σ for thickness-to-diameter ratio =0.125.

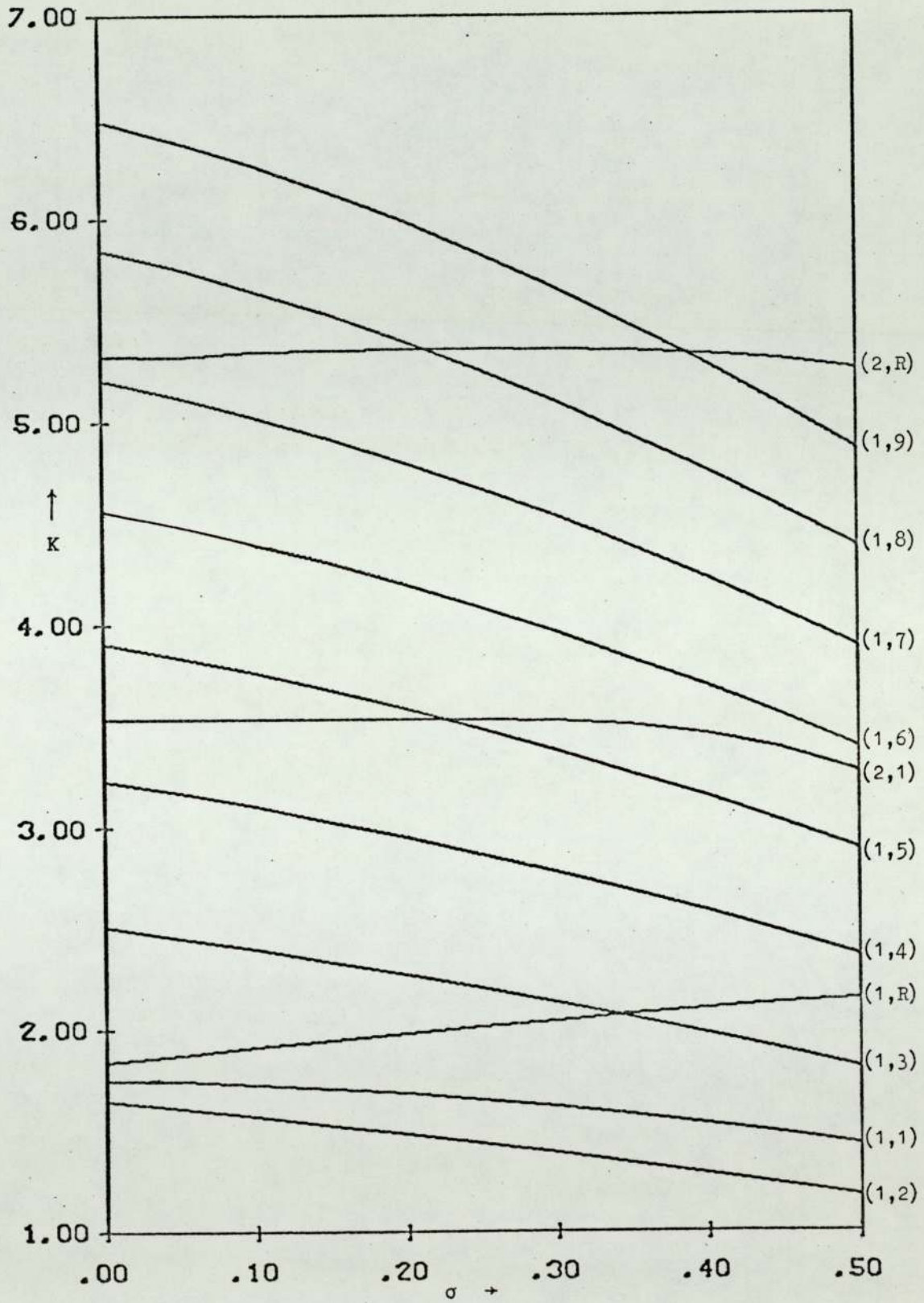

Fig.2.4 Graph of K versus σ for thickness-to-diameter ratio =0.08.

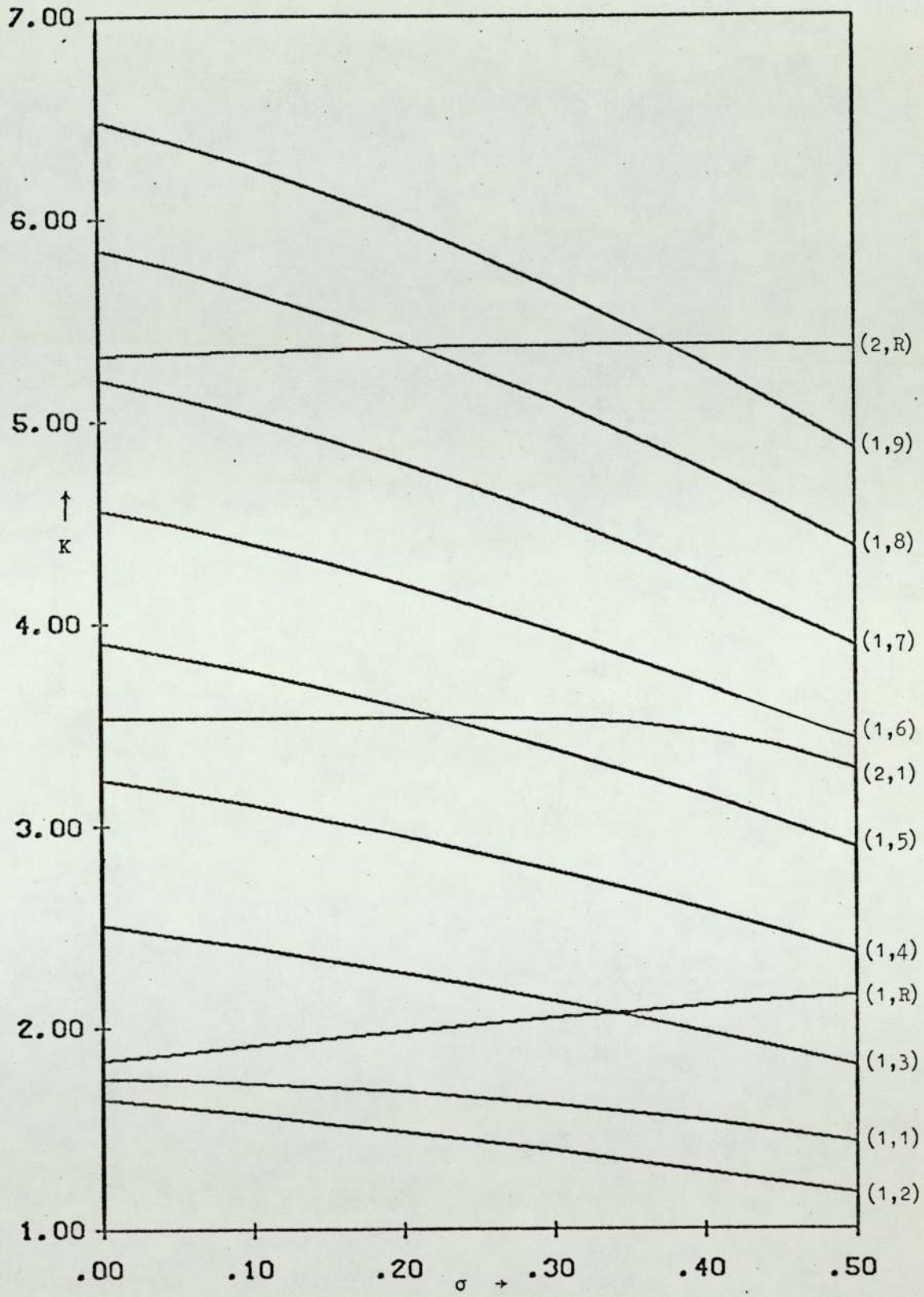

Fig.2.5 Plot of K versus σ for thickness-to-diameter ratio =0.05.

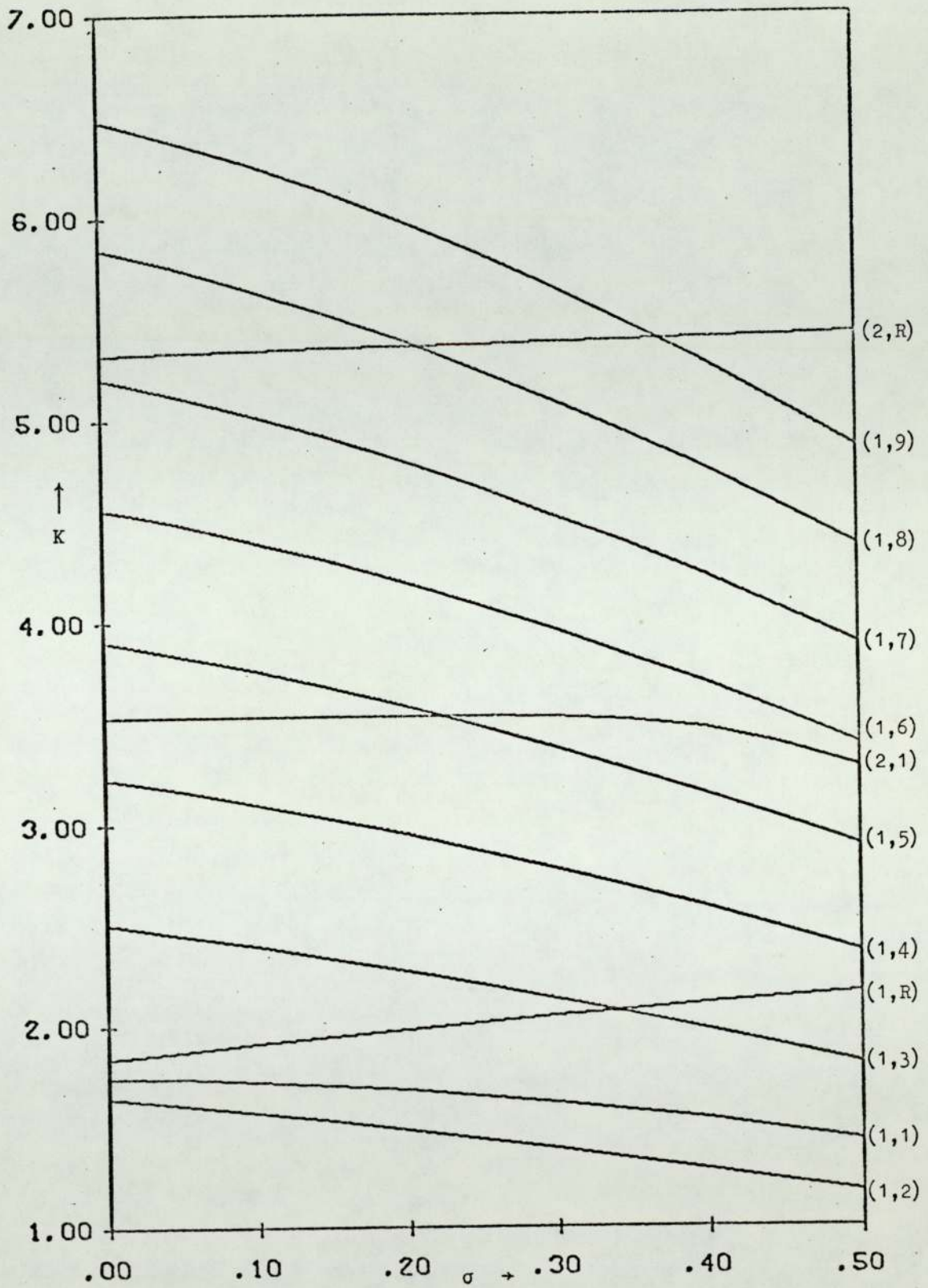

Fig.2.6 K values versus σ for thin disks.

2.4 Comparison of Experimental and Theoretical Results

The experimental apparatus used to measure the spectra of thick disk resonators is described in Appendix A.2.2. The method of measuring the resonant frequency of a mode is also described in Appendix A.2.2. Measurements were carried out on steel and aluminium disks of various thickness-to-diameter ratios and the results are given in Tables 2.1 and 2.2, respectively, together with the theoretical values of frequency which have been calculated, from the corresponding K values, using eqn.(2.2.6). The theoretical and experimental results agree within the limit of experimental accuracy. The physical properties of the disks are as given below:

	Steel Disk	Aluminium Disk
Diameter(2a)	5 cms.	5 cms.
Thickness(h)	2.5 cms.	2.5 cms.
Density(ρ)	7.8×10^3 kg/m^3	2.7×10^3 kg/m^3
Young's Modulus(E)	2.12×10^{11} N/m^2	0.71×10^{11} N/m^2
Poisson's Ratio(σ)	0.28	0.33

The disks of various thickness-to-diameter ratios were obtained by first choosing a disk with a thickness of 2.5 cms. and then gradually grinding the thickness away until only a thin disk remained.

2.5 Elastic Constant Measurement

A method is proposed here by which the Poisson's ratio σ and the Young's modulus E of the material of thick disks can be determined with good sensitivity by measuring the natural frequencies of extensional vibration. Other methods for the determination of σ are available in the literature, but they either use the ratio of a pair of flexural resonances[15] or are applicable to piezoelectric materials[16,17] only.

The method proposed here, however, uses the type of excitation described in Appendix A.2.2, which is equally applicable to all materials and also to disks of all thickness-to-diameter ratios. In section 2.2, the theory of radial and compound modes of vibration of thick disk has

Mode \ 1/η	Frequencies in KHZ											
	0.50		0.25		0.167		0.125		0.10		0.00	
	Calculated	Measured	Calculated	Measured	Calculated	Measured	Calculated	Measured	Calculated	Measured	Calculated	Measured
1,R	66.623	66.065	69.635	69.333	70.042	69.715	70.173	69.890	70.232	70.070	70.302	70.524
2,R	117.380	116.801	174.051	173.396	181.994	182.004	183.959	184.479	184.756	184.839	185.925	185.466
2,1	102.826	98.995	119.476	118.111	121.044	120.148	121.502	120.863	121.698	121.220	121.966	121.417
1,1	56.091	55.245	56.306	55.684	56.329	55.557	56.352	55.625	56.358	55.547	56.340	56.166
1,2	48.607	48.227	48.602	48.175	48.601	48.099	48.600	48.181	48.601	48.274	48.575	48.370
1,3	74.622	73.828	74.591	73.890	74.586	73.874	74.580	73.986	74.579	74.117	74.542	74.425
1,4	97.190	96.317	97.107	96.455	97.091	96.366	97.076	96.305	97.071	96.508	97.017	96.944
1,5	118.267	117.012	118.232	116.839	118.198	116.886	118.168	117.156	118.160	117.273	118.082	117.594
1,6	138.934	138.157	138.688	137.685	138.636	137.630	138.581	137.409	138.564	137.568	138.460	138.066
1,7	159.124	158.241	158.779	157.286	158.700	157.869	158.616	157.671	158.594	157.548	158.451	157.619
1,8	179.098	180.268	178.851	178.164	178.553	178.405	178.474	178.649	178.315	178.735	178.205	177.641
1,9	198.929	197.124	198.381	197.620	198.217	198.507	198.018	197.769	197.947	196.483	197.766	196.902

Table 2.1 The table shows the agreement between theoretical and experimental frequencies for a steel disk of various thicknesses. Diameter = 5.0 cms., the value of Poisson's Ratio used in the calculations is 0.28, which is a recognised value for steel[65].

Mode \ 1/η	Frequencies in KHZ													
	0.500		0.334		0.250		0.200		0.125		0.080		0.000	
	Calculated	Measured	Calculated	Measured	Calculated	Measured	Calculated	Measured	Calculated	Measured	Calculated	Measured	Calculated	Measured
1,R	65.768	64.895	69.154	69.190	70.128	70.158	70.551	70.573	70.984	71.179	71.139	71.346	71.245	71.405
2,R	118.421	118.493	152.119	150.261	169.248	169.000	176.303	175.237	182.622	181.217	184.523	185.183	185.921	186.227
2,1	99.239	100.856	113.599	112.220	117.621	117.102	118.746	118.129	120.539	119.948	120.987	121.180	121.309	121.739
1,1	54.589	53.656	54.801	54.360	54.867	54.237	54.897	54.389	54.928	54.220	54.940	54.842	54.947	54.670
1,2	46.458	46.268	46.800	46.567	46.799	46.688	46.798	46.123	46.797	46.249	46.796	46.828	46.794	46.930
1,3	71.951	71.125	71.925	71.510	71.914	71.734	71.907	71.005	71.901	71.813	71.897	71.935	71.894	71.995
1,4	93.825	93.158	93.759	92.924	93.728	93.183	93.700	92.832	93.692	92.860	93.683	92.801	93.674	94.040
1,5	114.309	113.895	114.272	112.760	114.212	113.315	114.173	113.045	114.137	113.126	114.117	113.840	114.100	113.592
1,6	134.346	134.104	134.151	133.640	134.054	133.510	133.988	133.441	133.926	132.968	133.890	133.620	133.860	134.640
1,7	153.954	152.992	153.685	153.852	153.543	152.642	153.498	152.520	153.349	152.123	153.294	152.544	153.241	152.052
1,8	173.372	172.682	173.010	170.523	172.822	172.540	172.690	171.559	172.549	171.667	172.310	171.740	172.385	172.001
1,9	192.623	192.475	192.293	190.100	191.964	191.415	191.887	190.321	191.601	190.200	191.472	190.600	191.383	191.293

Table 2.2 This table confirms the close agreement between the calculated and the experimentally measured frequencies of an aluminium disk for various thicknesses. Diameter = 5.0 cms., The value of Poisson's Ratio used for calculations is 0.33 for aluminium[65].

been given and the combination of the families of these resonances enable the elastic constants to be determined with a greater accuracy. The compound modes having nodal diameters, all decrease with Poisson's ratio whereas the pure radial modes K_{1R} and K_{2R} and the compound mode K_{21}, which has a nodal circle and a nodal diameter, have a completely different dependence on σ, for each η, and hence, the comparison of these modes with the adjacent compound modes yields Poisson's ratio with good sensitivity.

The theoretical K values (or frequency values) corresponding to the η of the disk under investigation, are compared with the measured spectrum of resonances(Table 2.1 for steel and 2.2 for aluminium) and the lowest resonance is at once identified to be f_{12}. Since the value of K_{14} is approximately twice the value of K_{12}, f_{14} mode can also be easily identified. From the K values, shown in Figs.2.1 to 2.6, corresponding to the η of the disk, an approximate value of σ, for which the f/K ratios of these two modes are equal, is determined. With the help of the other K values corresponding to this η and σ, the mode numbers of the rest of the resonances can be identified.

The relation between K and f is given by the equation $K = cf$, where $c = (2\pi a/C_p)$ is a constant for a given disk, C_p being the plate velocity. The K_{1R} mode is compared with K_{13}, K_{21} with K_{15} and K_{2R} with K_{18} and K_{19}. Thus, the ratios $(\frac{f_{1R} - f_{13}}{f_{13}}) \times 100$, $(\frac{f_{21} - f_{15}}{f_{15}}) \times 100$, $(\frac{f_{2R} - f_{18}}{f_{2R}}) \times 100$ and $(\frac{f_{2R} - f_{19}}{f_{2R}}) \times 100$ can be calculated from measured resonant frequency. The sensitivity is defined as $\frac{1}{R}\frac{dR}{d\sigma}$, where R is the frequency ratio mentioned above. The value of Poisson's ratio σ for each ratio and for the η concerned can then be determined from the Figs.2.7 to 2.12, corresponding to the η of the disk under investigation. Although, the σ values obtained independently from the four ratios may result in an ambiguity, there are certain advantages in doing so. For certain materials, for example, in thin aluminium disk, the resonances f_{1R} and f_{13} are so close to each other

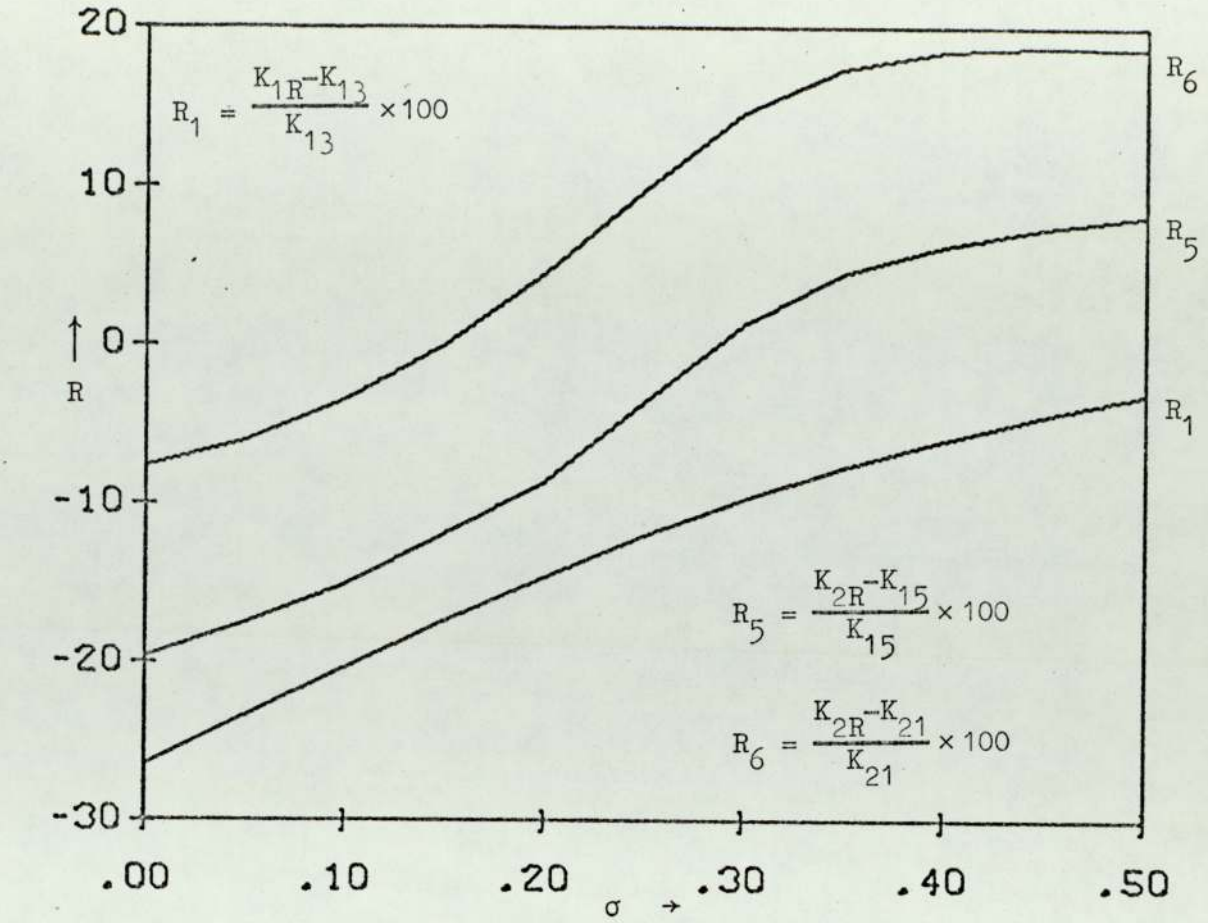

(a)

Thickness-to-diameter ratio = 0.50.

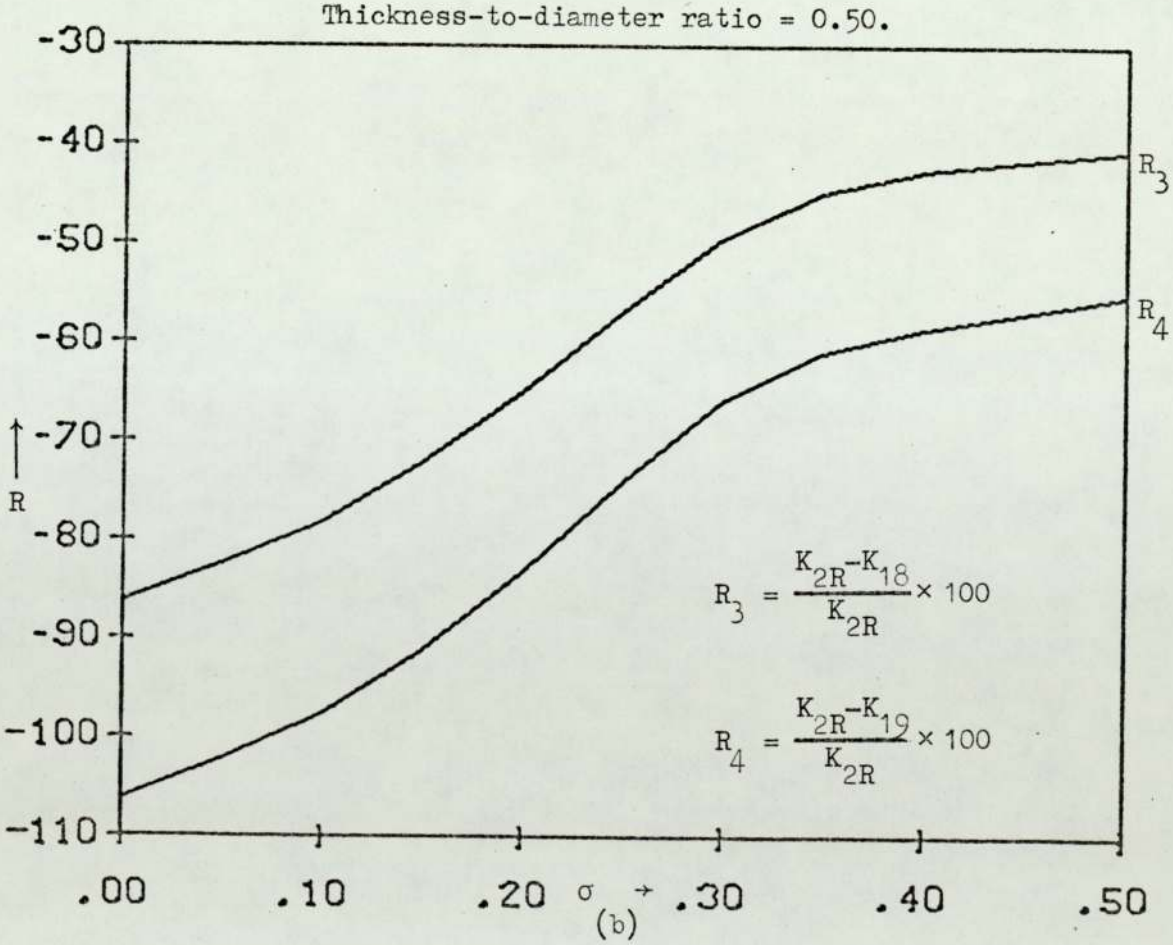

(b)

Fig.2.7 Graph of R versus σ, where R is the percentage ratio of two frequencies. The graphs indicate the sensitivity of different methods. The measure of the sensitivity is $\frac{1}{R}\frac{dR}{d\sigma}$.

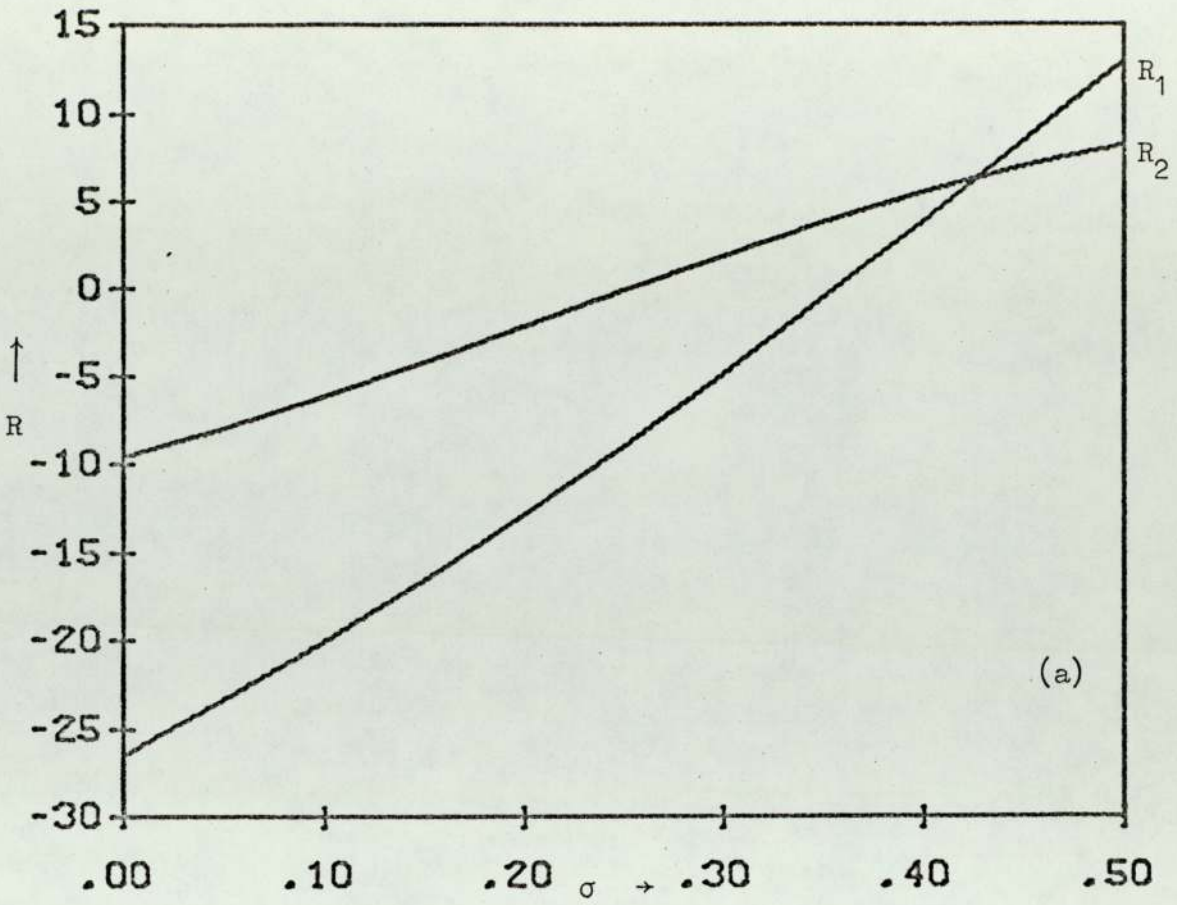

$$R_1 = \frac{K_{1R} - K_{13}}{K_{13}} \times 100,\ R_2 = \frac{K_{21} - K_{15}}{K_{15}} \times 100,\ R_3 = \frac{K_{2R} - K_{18}}{K_{2R}} \times 100,\ R_4 = \frac{K_{2R} - K_{19}}{K_{2R}} \times 100$$

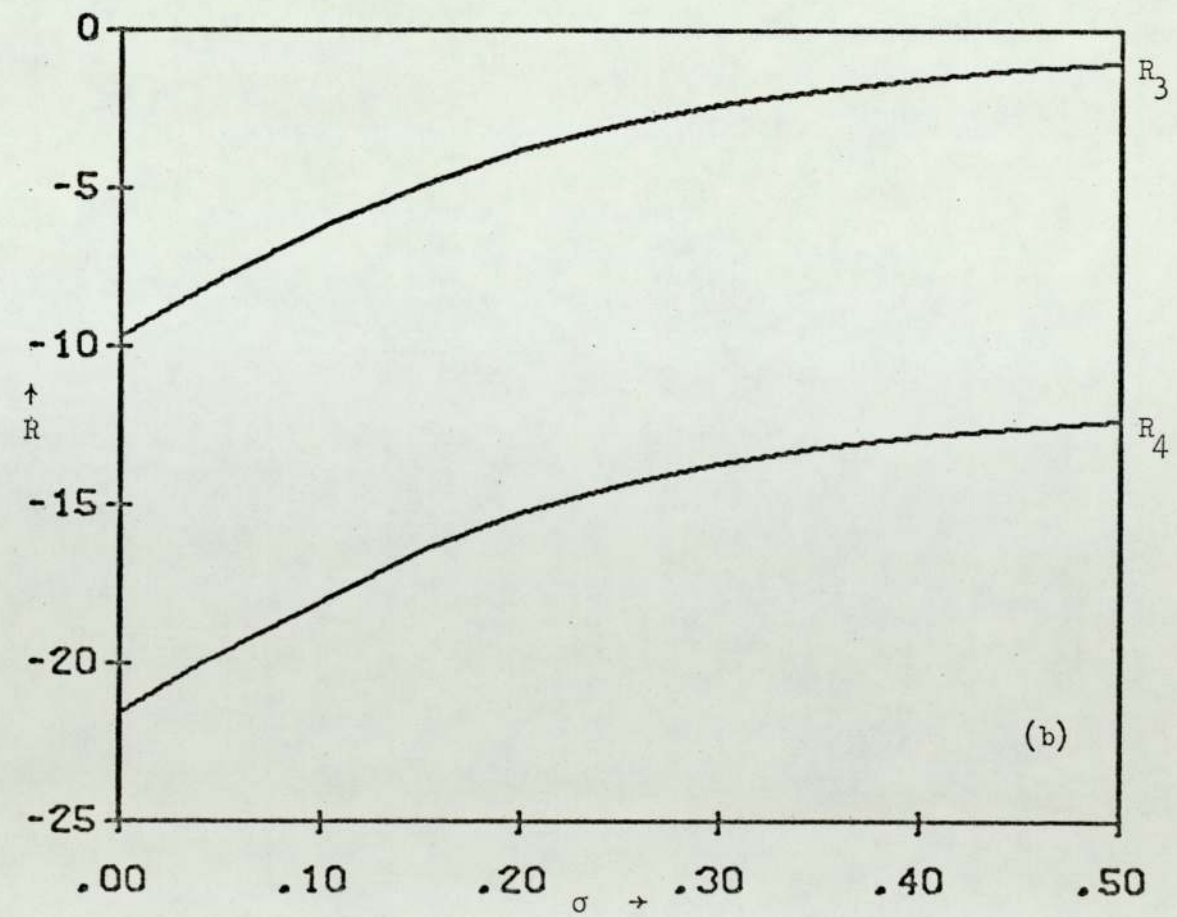

Fig.2.8 Graph of R versus σ for thickness-to-diameter ratio =0.25.

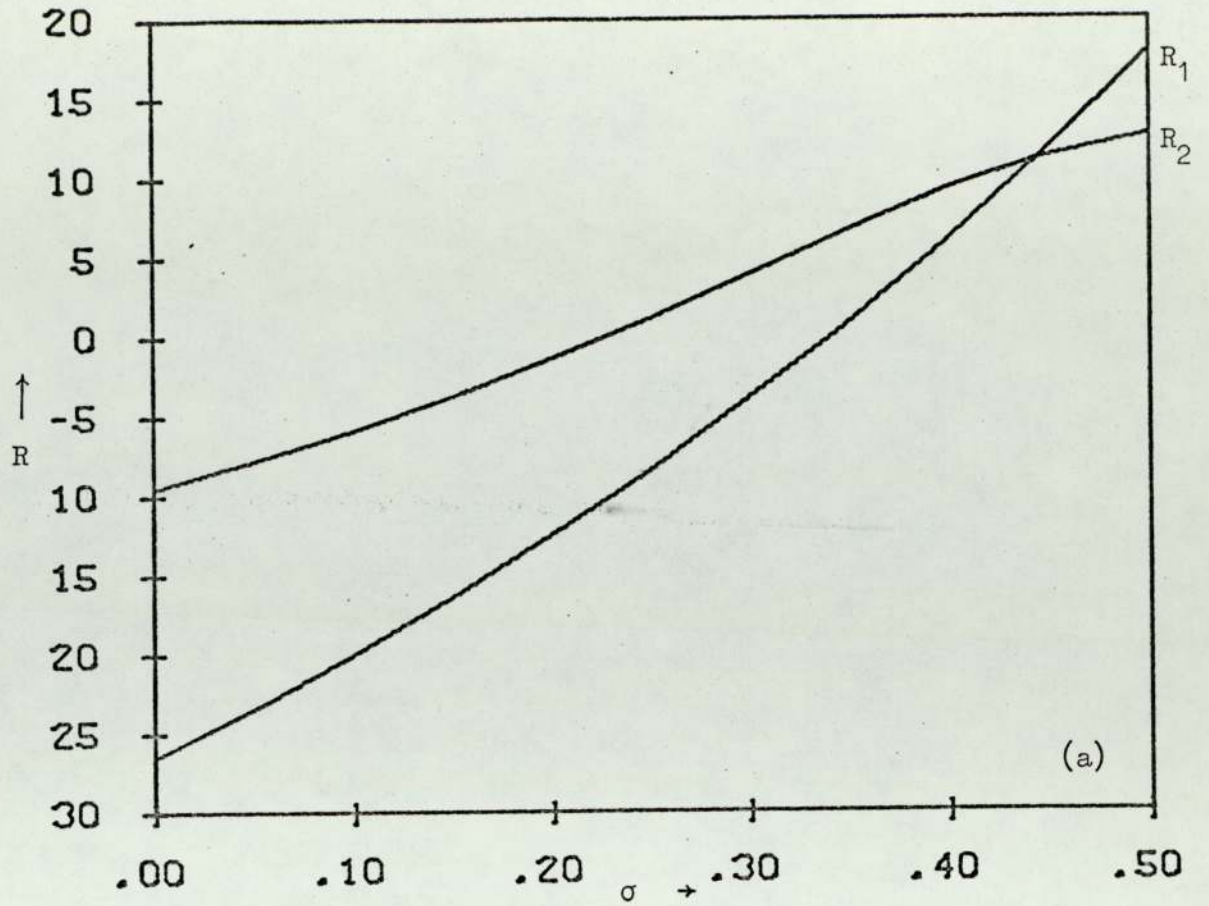

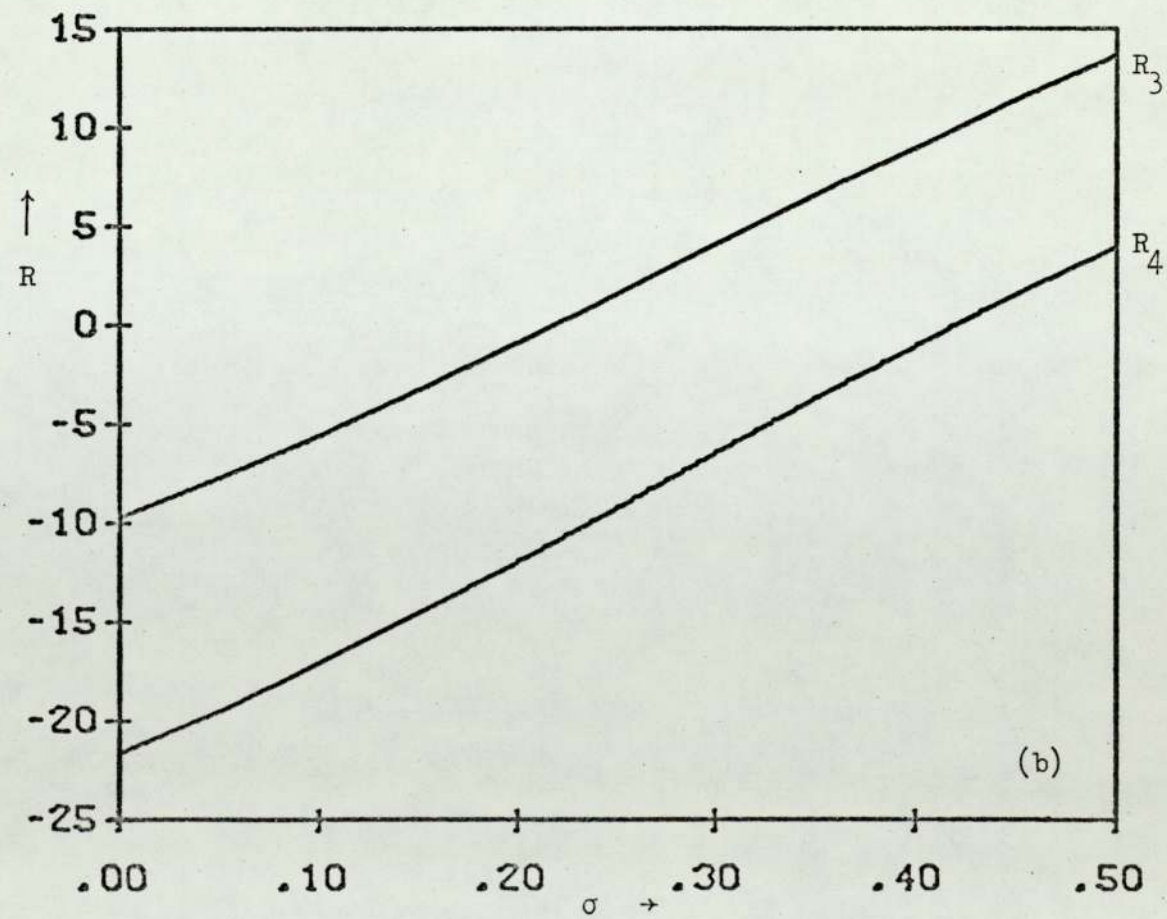

Fig.2.9 Plot of R versus σ for thickness-to-diameter ratio =0.125.

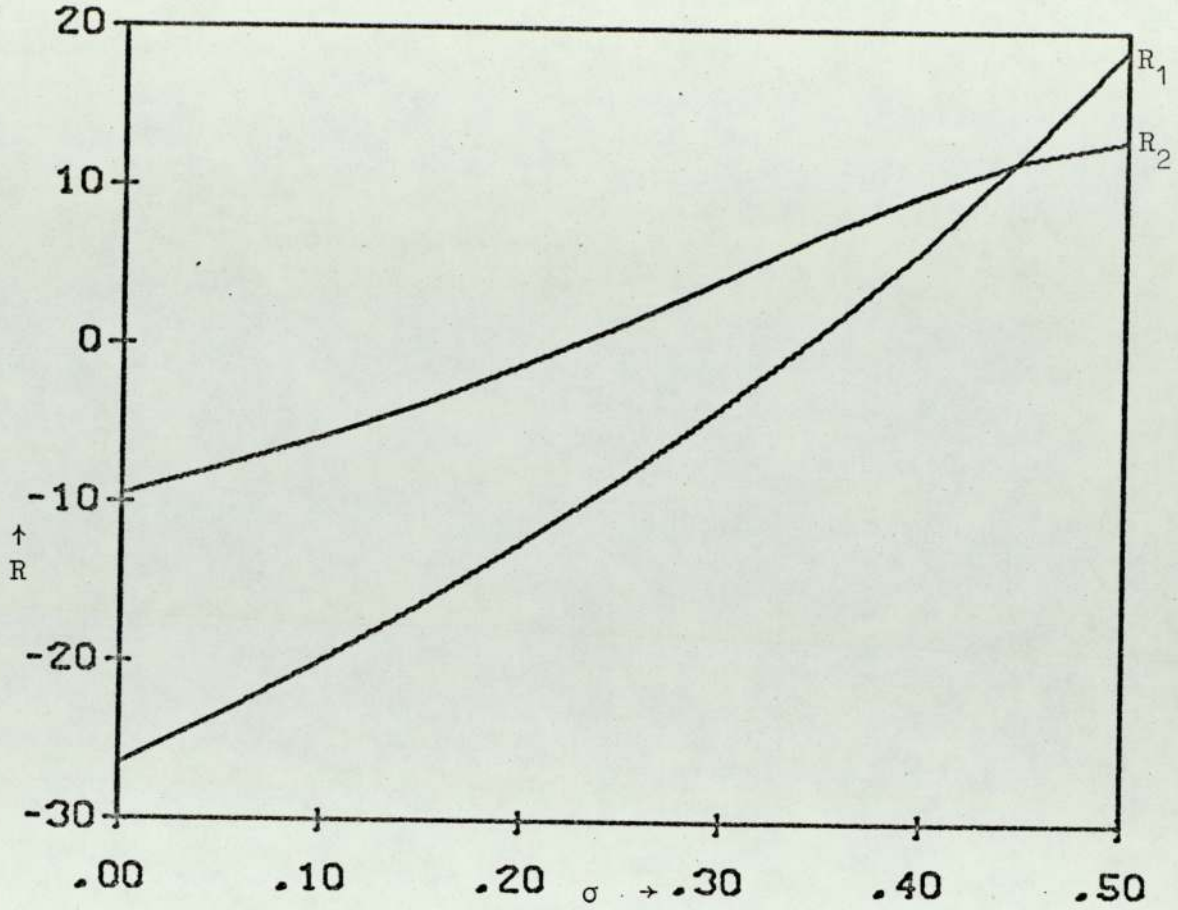

(a)

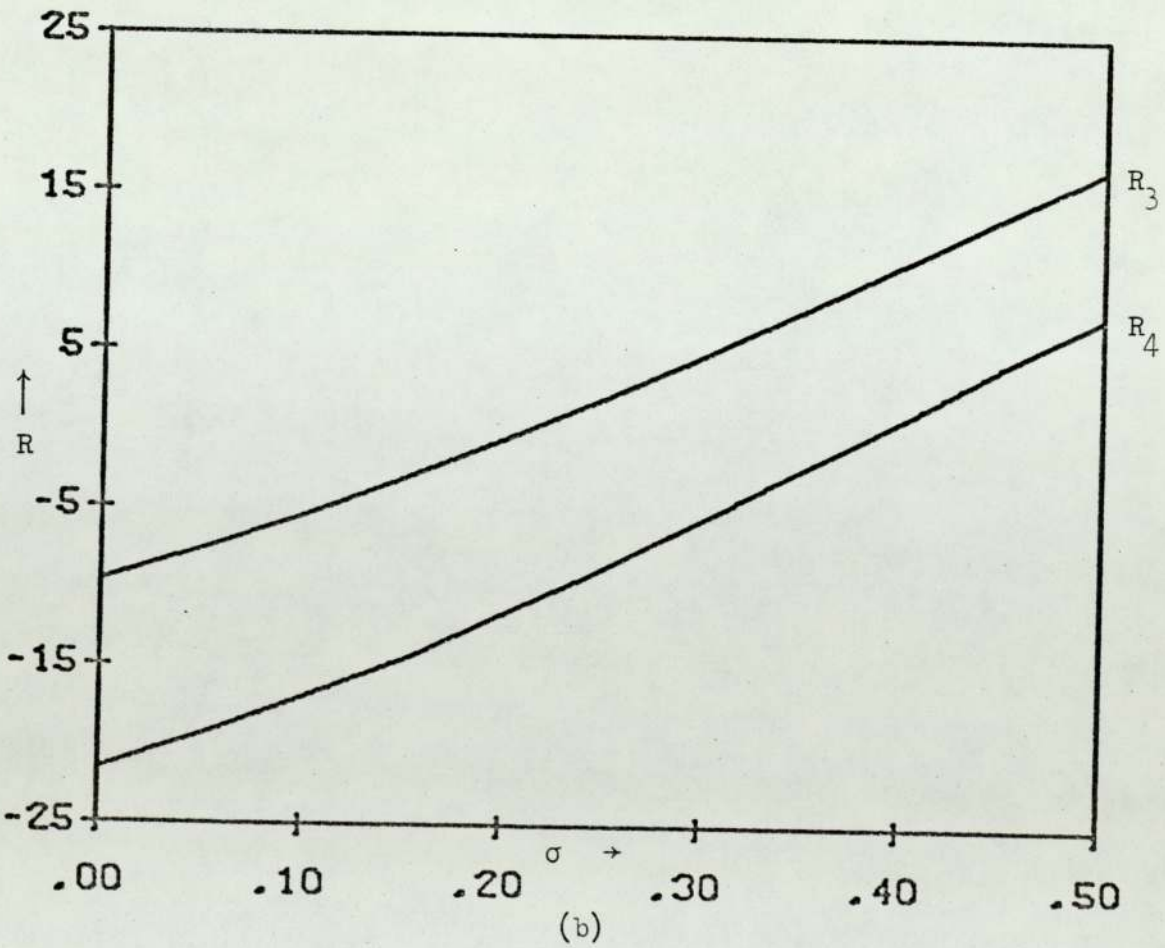

(b)

Fig.2.10 Graph of R versus σ , for thickness-to-diameter ratio = 0.0834.

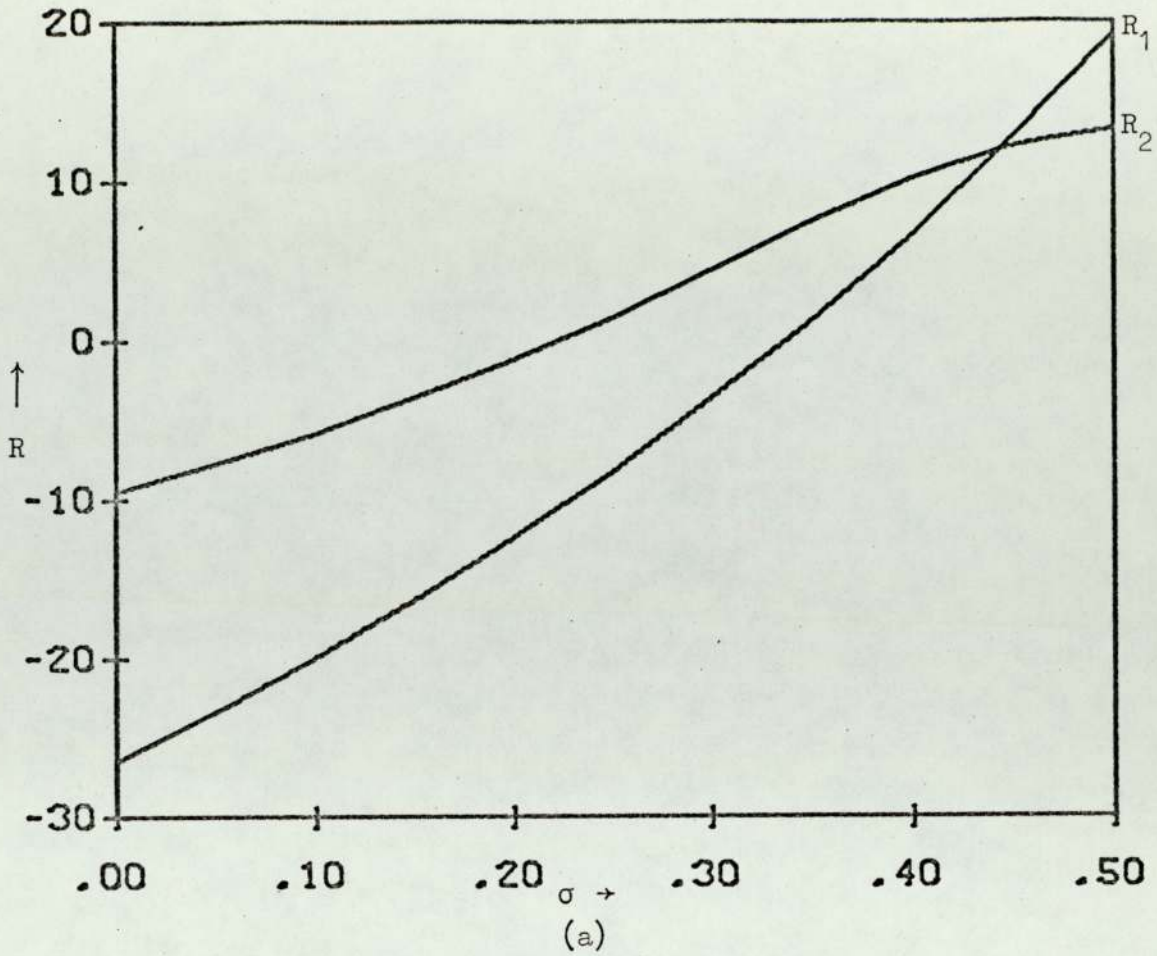

(a)

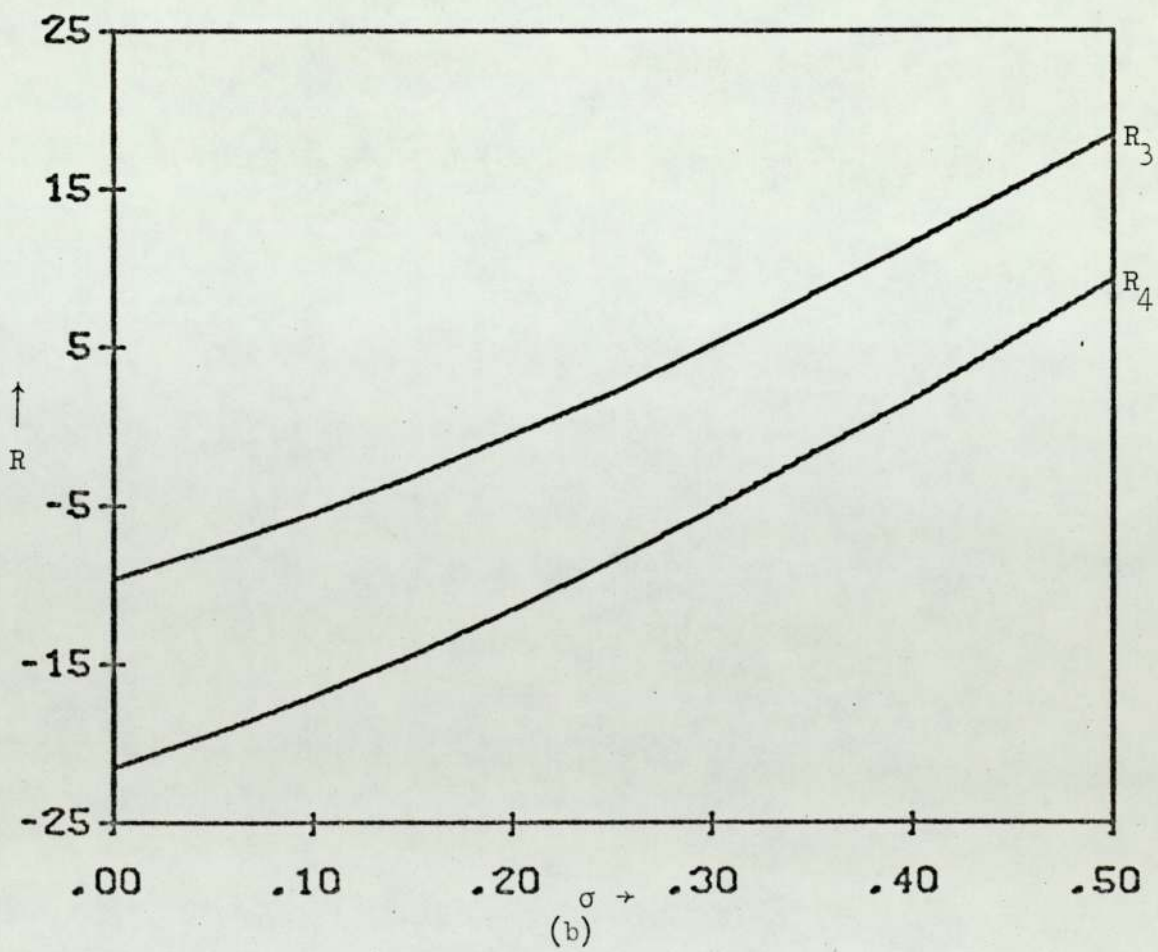

(b)

Fig.2.11 Plot of R versus σ, for thickness-to-diameter ratio = 0.05.

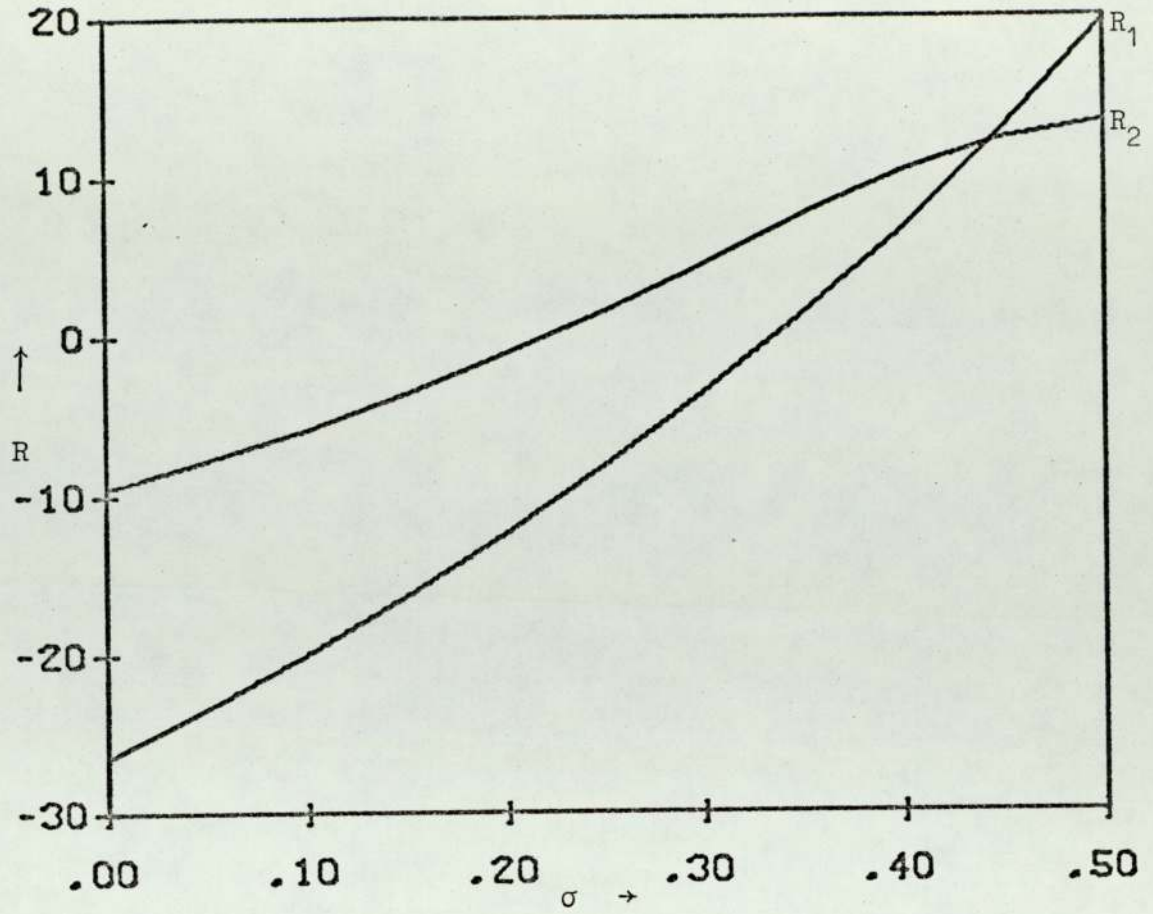

(a)

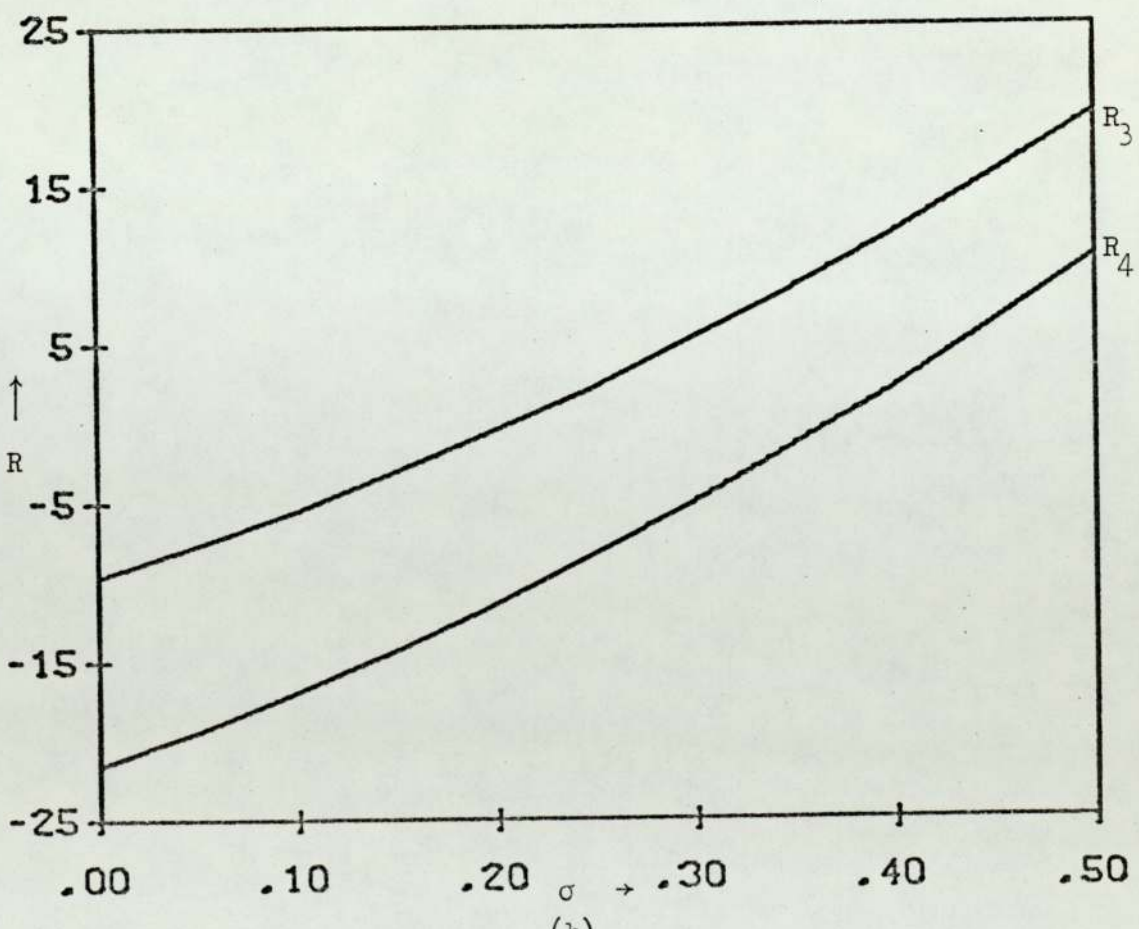

(b)

Fig.2.12 Graph of R versus σ , for thin disks.

that they may not be easily detected and hence the sensitivity of the ratio $(f_{1R} - f_{13})/f_{13}$ is very poor that it may not yield the correct value of σ. One has to, then, go in for other ratios for determining the σ of the disk. Further, the value of σ obtained from one ratio can be checked with the value obtained from other ratio, which indicates the correct value of σ.

The value of the Young's modulus E of the material under test can be computed from the formula

$$E = 4\pi^2 a^2 \rho(1-\sigma^2)(f/K)^2 \qquad (2.5.1)$$

where f and K refer to any particular mode and ρ is the mass density per unit volume.

The experiments were conducted on disks of various materials and thicknesses. The agreement between theory and experiment is excellent, as can be seen from Tables 2.1 and 2.2. Tables 2.3 and 2.4 show the values of σ, obtained independently from each ratio, for steel and aluminium, respectively over a wide range of thickness-to-diameter ratios.

This method of determining σ was first developed by the author for the measurement of variation of σ with the magnetic field[2] and was later used to measure the variation of σ, of thin disk material, with the temperature[18].

2.6 Discussion

The results of the present thick disk theory are now compared with those of the existing theories and the experiment, in order to show the validity and the applicability of the present theory to disks of larger thickness-to-diameter ratios. Moseley's thickness correction[11] to the natural frequencies of the disk radial modes is given by

$$K^M_{mR} = K^T_{mR}\left[1 - \frac{1}{6}\left\{\frac{K^T_{mR}\sigma}{\eta(1-\sigma)}\right\}^2\right] \qquad (2.6.1)$$

Lucey's thickness correction[12] to the fundamental radial mode of vibration in a thick disk is given by

1/η	f_{1R}	f_{13}	$\left(\frac{f_{1R}-f_{13}}{f_{13}}\right)\times 100$	σ	f_{21}	f_{15}	$\left(\frac{f_{21}-f_{15}}{f_{15}}\right)\times 100$	σ
0.500	66.065	73. 828	-10.515	0.2844	98.995	117.012	-15.400	-
0.250	69.333	73.890	- 6.168	0.2858	118.111	116.839	1.103	0.2887
0.167	69.715	73.874	- 5.630	0.2850	120.148	116.886	2.791	0.2875
0.125	69.890	73.986	- 5.536	0.2840	120.863	117.156	3.164	0.2857
0.100	70.070	74.111	- 5.453	0.2842	121.220	117.273	3.366	0.2866
0.000	70.524	74.425	- 5.242	0.2848	121.417	117.594	3.251	0.2791

1/η	f_{2R}	f_{18}	$\left(\frac{f_{2R}-f_{18}}{f_{2R}}\right)\times 100$	σ	f_{2R}	f_{19}	$\left(\frac{f_{2R}-f_{19}}{f_{2R}}\right)\times 100$	σ
0.500	116.80	180.27	-54.340	0.2735	116.80	197.12	-68.770	0.2850
0.250	173.40	178.16	- 2.750	0.2750	173.40	197.62	-13.950	0.2834
0.167	182.00	178.41	1.980	0.2820	182.00	198.51	- 9.070	0.2761
0.125	184.48	178.65	3.160	0.2830	184.48	197.77	- 7.210	0.2874
0.100	184.84	178.74	3.310	0.2780	184.84	196.48	- 6.299	0.2794
0.000	185.47	177.64	4.219	0.2811	185.47	196.90	- 6.166	0.2830

Table 2.3 The table gives the values of σ derived, independently, from four frequency ratios, for steel disk, over a wide range of thickness-to-diameter ratios.

1/η	f_{1R}	f_{13}	$\left(\frac{f_{1R}-f_{13}}{f_{13}}\right)_{\times 100}$	σ	f_{21}	f_{15}	$\left(\frac{f_{21}-f_{15}}{f_{15}}\right)_{\times 100}$	σ
0.500	64.895	71.125	-8.750	0.3265	100.856	113.895	-11.450	-
0.334	69.190	71.500	-3.231	0.3360	112.220	112.760	- 0.481	0.3351
0.250	70.158	71.734	-2.197	0.3334	117.102	113.315	3.342	0.3397
0.200	70.573	71.005	-0.608	0.3330	118.129	113.045	4.248	0.3366
0.125	71.179	71.813	-0.883	0.3340	119.948	113.126	6.030	0.3374
0.080	71.346	71.935	-0.819	0.3325	121.180	113.840	6.450	0.3375
0.000	71.405	71.995	-0.820	0.3319	121.739	113.592	7.172	0.3441

1/η	f_{2R}	f_{18}	$\left(\frac{f_{2R}-f_{18}}{f_{2R}}\right)_{\times 100}$	σ	f_{2R}	f_{19}	$\left(\frac{f_{2R}-f_{19}}{f_{2R}}\right)_{\times 100}$	σ
0.500	118.493	172.682	-45.730	0.3380	118.493	192.475	-62.440	0.3370
0.334	150.261	170.523	-13.500	0.3380	150.261	190.100	-26.170	0.3350
0.250	169.000	172.540	- 2.100	0.3310	169.000	191.415	-13.310	0.3390
0.200	175.231	171.559	2.100	0.3325	175.237	190.321	- 8.600	0.3377
0.125	181.217	171.667	5.270	0.3250	181.217	190.200	- 4.960	0.3310
0.080	185.183	171.740	7.220	0.3370	185.183	190.600	- 2.925	0.3425
0.000	186.227	172.001	7.639	0.3356	186.227	191.293	- 2.720	0.3331

Table 2.4 This table shows the values of σ derived from four ratios, independently, over a wide range of thickness-to-diameter ratios of aluminium disk.

$$K^{L}_{mR} = K^{T}_{mR}\left[1 - \frac{1}{3(1-\sigma^2)}\left(\frac{2K^{T}_{mR}}{\pi\eta}\right)^2\right]^{\frac{1}{2}} \qquad (2.6.2)$$

where the superscripts M, L and T refer to Moseley, Lucey and the thin disk (generalised plane stress) theories, respectively.

The frequency values of the fundamental radial resonance for aluminium disk, as predicted by eqns.(2.6.1), (2.6.2) and eqn.(2.2.14), are shown in Fig.2.13(a), together with the experimental results. The second radial mode frequencies for aluminium are shown in Fig.2.13(b). The corresponding results for steel are shown in Fig.2.14(a) and (b), respectively. It may be noted from the figures that the results of the present theory closely agree with the experimental results over a wide range of thickness-to-diameter ratios.

Fig.2.15 shows the variation of theoretical frequencies of the first two compound modes, for n=1, with thickness-to-diameter ratio and these results closely agree with the experimental values, as may be seen from Table 2.2. The figure also shows that the variation for the second mode is larger than that for the first mode. This remarkable feature is held by the higher modes, for all n and is dealt with in greater detail in Chapters 4 and 5.

The graphs of normalised K values of first and second radial modes are shown in Fig.2.16(a) and (b), respectively, as a function of σ and $1/\eta$. They predict the departure from the respective thin disk radial mode frequencies, as a function of thickness-to-diameter ratio and can be readily used to obtain the necessary frequency correction for a disk with a given thickness-to-diameter ratio. Alternatively, the exact K values for the radial modes may be computed from the frequency equation(2.2.14), for the desired σ and η .

It may be noted, from Figs.2.1 to 2.6, that the modes K_{2R} and K_{21} have an entirely different dependence on σ, for different η's. For example, K_{2R} decreases with σ for $2 < \eta < 8$, but almost remains constant,

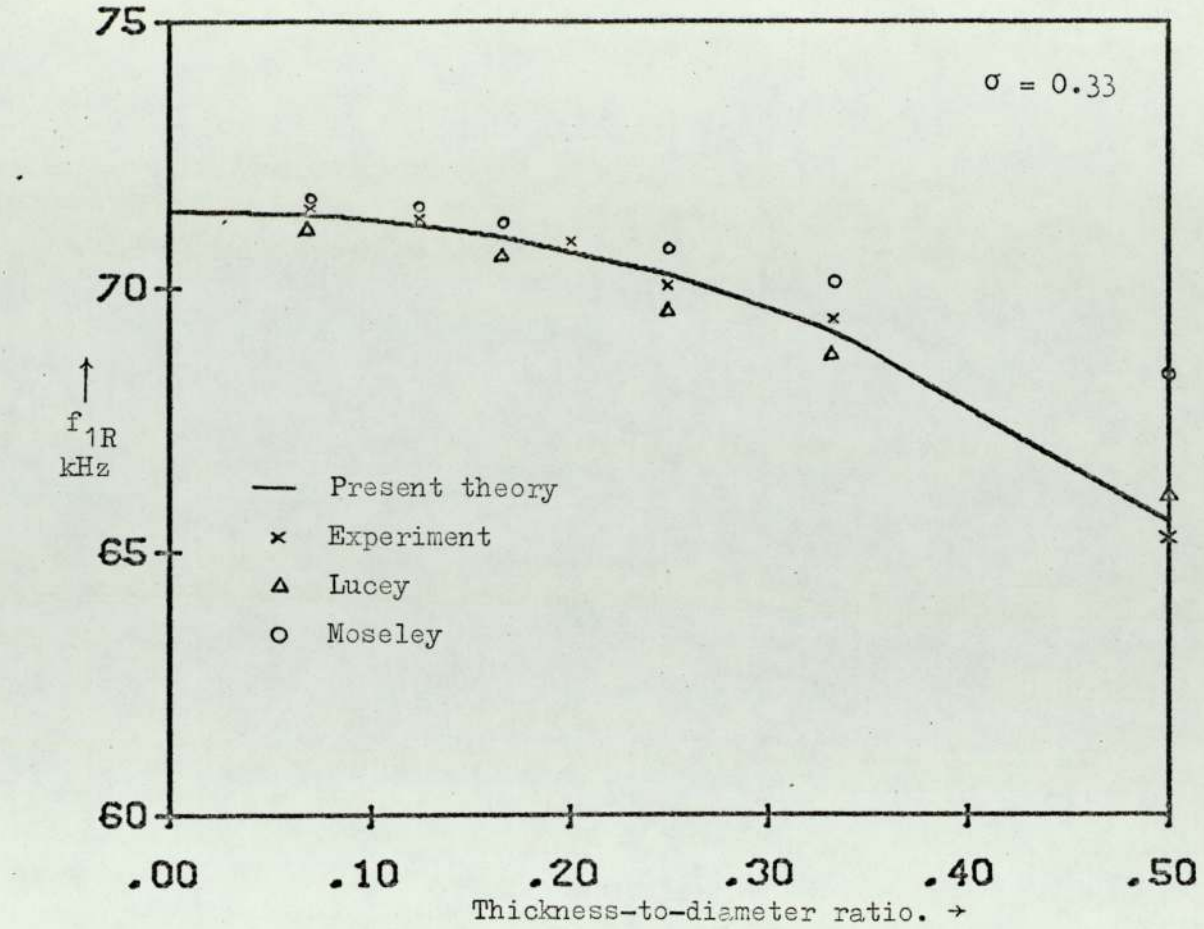

(a)

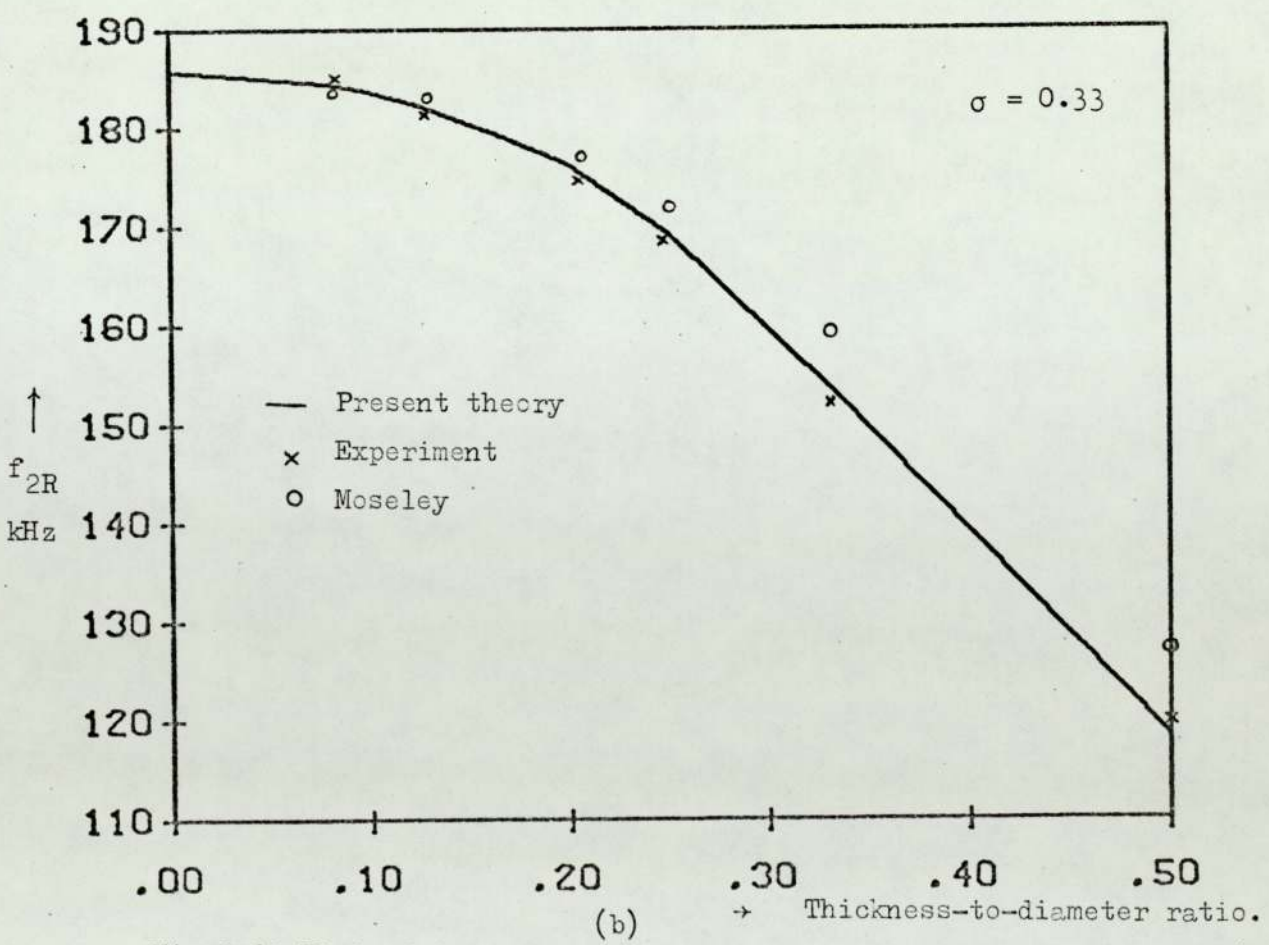

(b)

Fig.2.13 Plot of frequency versus thickness-to-diameter ratio for (1,R) and (2,R) modes in aluminium disk. Comparison of various results.

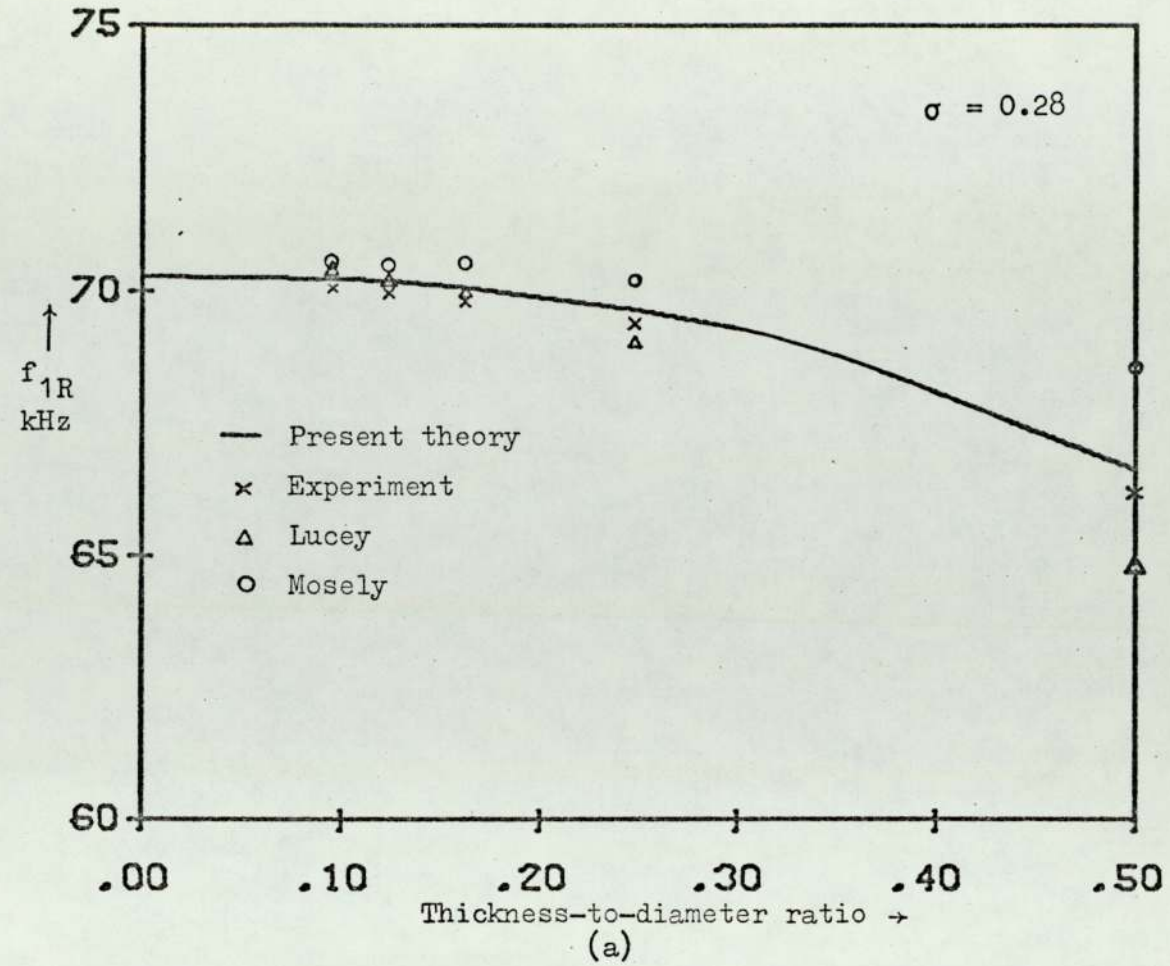

(a)

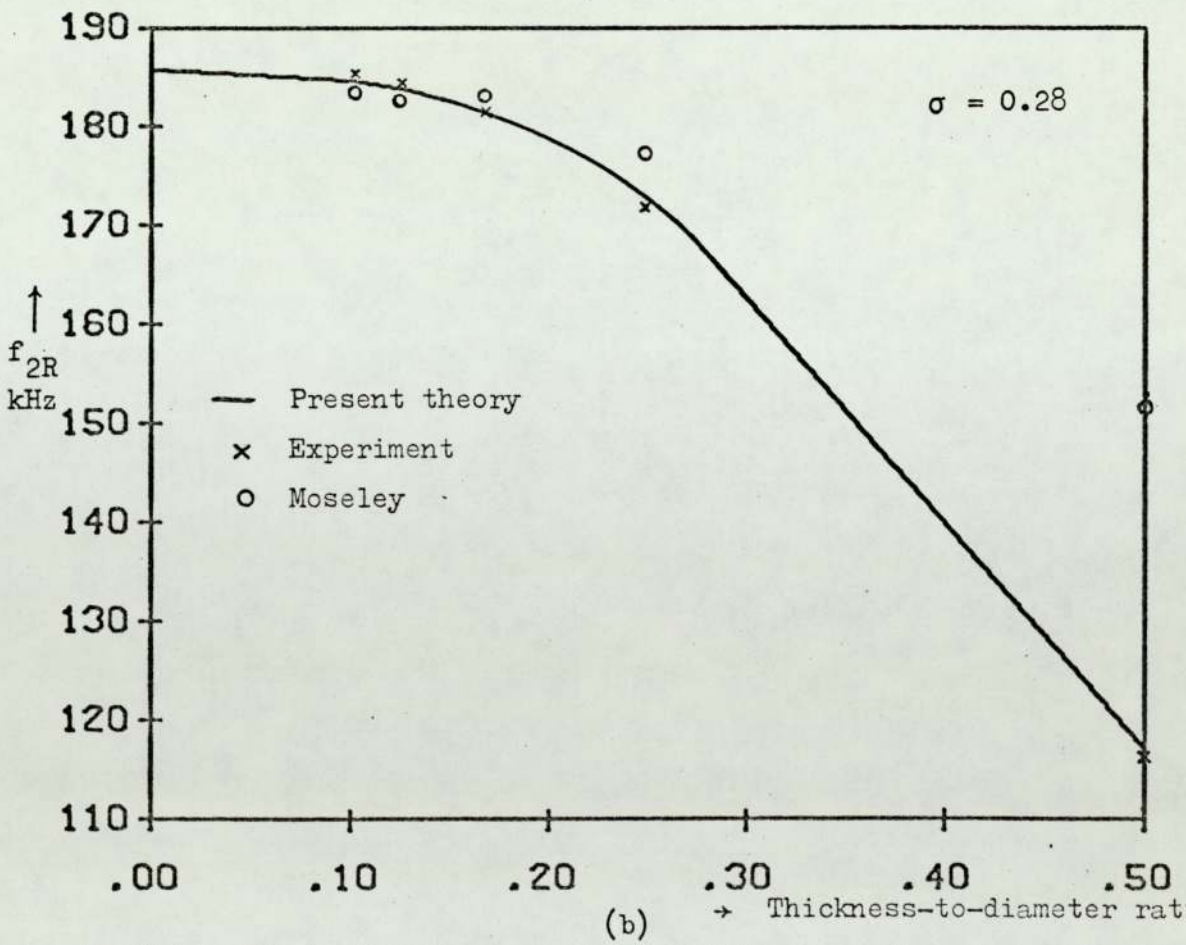

(b)

Fig.2.14 Graph of frequency versus thickness-to-diameter ratio for (1,R) and (2,R) modes in steel disk. Comparison of various results.

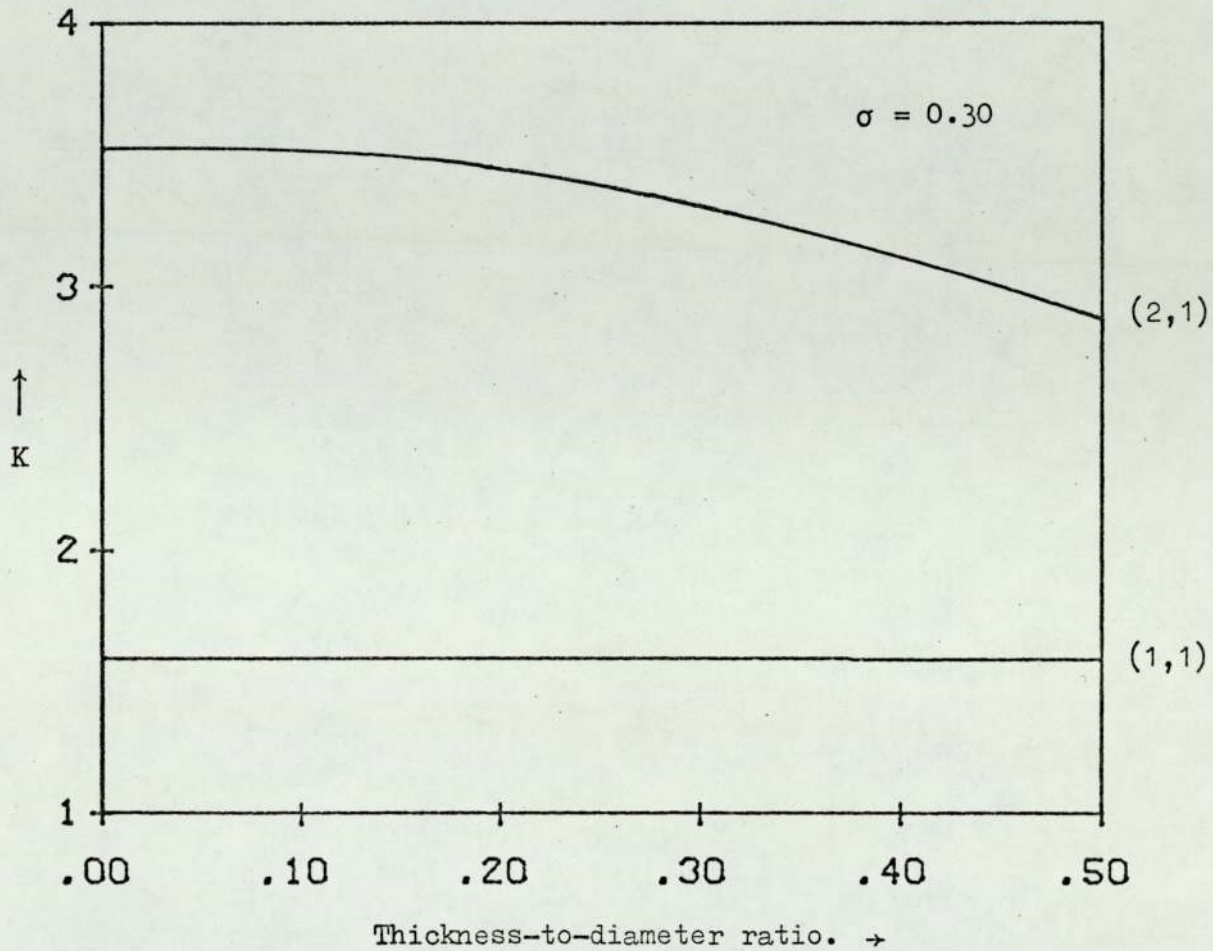

Fig.2.15 plot of theoretical frequencies versus thickness-to-diameter ratio, for the first two compound modes for n = 1. Note that mode (2,1) varies with thickness-to-diameter ratio whereas (1,1) does not.

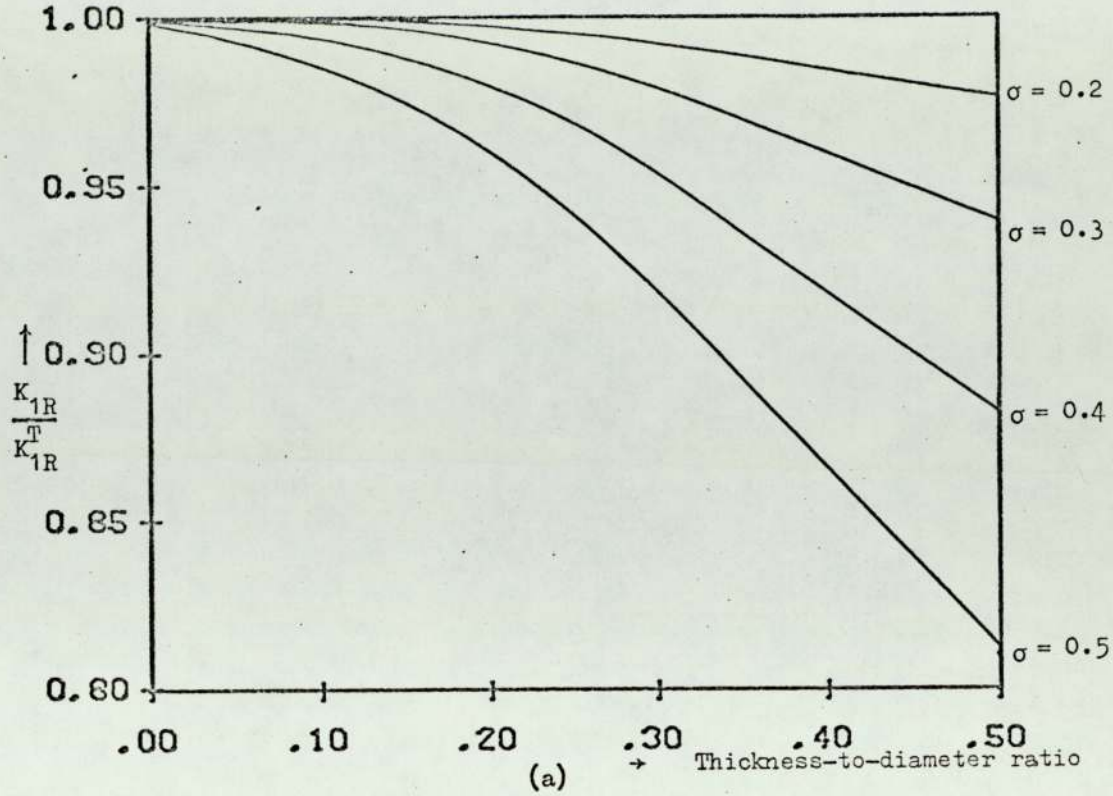

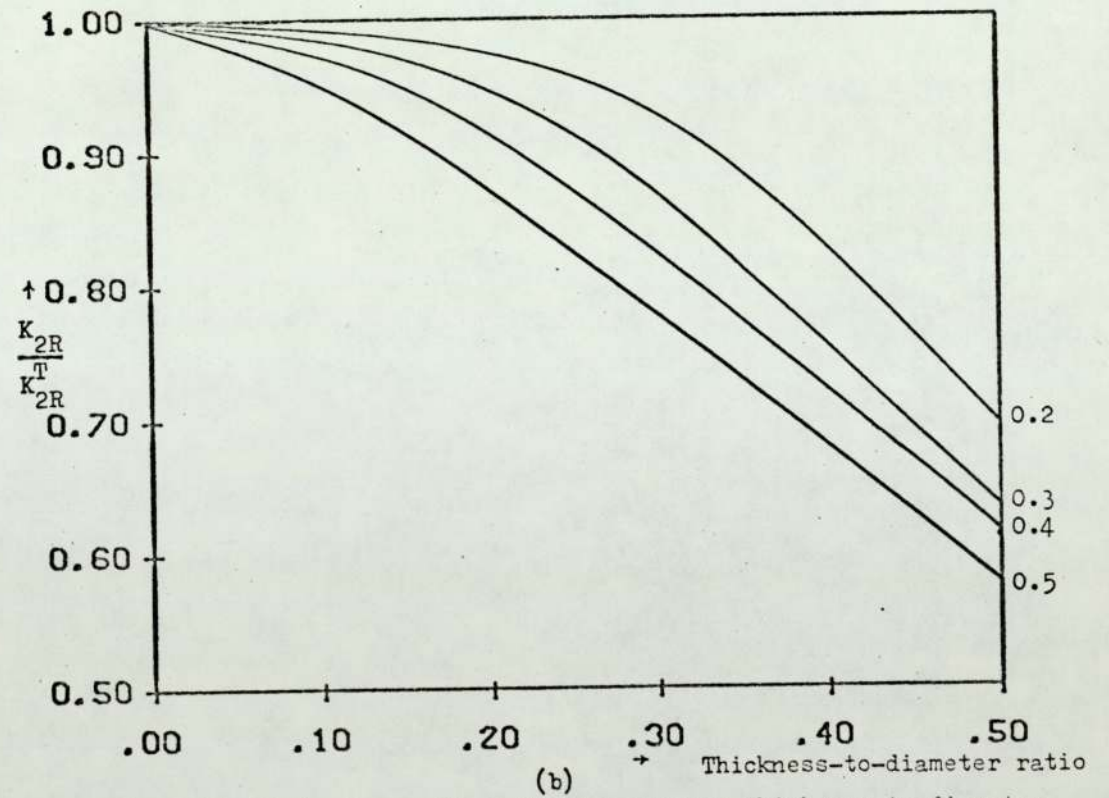

Fig.2.16 Plot of normalised K values versus thickness-to-diameter ratio, as a function of σ, for the first two radial modes.

They predict the departure from the thin disk frequencies and can be readily used for any frequency correction.

for $\eta>8$. However, for $\eta=2$, it has a completely different dependence on σ, as can be seen from Fig.2.1. The mode K_{21}, on the other hand, decreases with σ for $\eta<4$, but has a different dependence on σ for $\eta\geq 4$. Thus, for $\eta=2$, the use of the ratio $(K_{21}-K_{15})/K_{15}$ may not yield the correct value of σ, for the material under consideration (see Tables 2.3 and 2.4), because the variation of K_{15} with σ is same as that of K_{21}, as shown in Fig.2.1. Since K_{2R} has a different dependence on σ, for $\eta=2$, it is appropriate to compare K_{2R} with K_{15} or K_{21}. For this reason, the graphs of the percentage ratios $(K_{2R}- K_{15})/K_{15}$ and $(K_{2R}- K_{21})/K_{21}$ versus σ have been shown in Fig.2.7(a), which may be used in place of the percentage ratio $(K_{21}- K_{15})/K_{15}$ for $\eta=2.0$.

Tables 2.3 and 2.4 show the Poisson's ratio of steel and aluminium, respectively, derived from the measurement of pairs of neighbouring resonances, over a wide range of thickness-to-diameter ratios. There is an excellant agreement between the values of the Poisson's ratio obtained independently from the four ratios. The method described in this chapter, for the measurement of elastic constants, is preferable and advantageous over the method proposed by Martincek[15], which uses a pair of flexural resonances, because the latter method requires different arrangements to excite two neighbouring flexural resonances, whereas in the method proposed here, all the resonances could be excited by means of a single arrangement described in Appendix A.2.2.

CHAPTER 3

CONTOUR VIBRATIONS OF ANNULAR RINGS

3.1 Introduction

The vibrations of solid bodies have been solved for only a few simple geometries and modes. Exact solutions of the wave equations of thin narrow rings vibrating in flexure or extension[8,19,20] and of thin disks[8,9] vibrating only radially or only tangentially are readily obtained. The theory due to Buckens[21] for rings, although takes into account the shear stresses, is not valid when the thickness of the ring is large. The numerical solution of compound modes of disks required the use of digital computers. A study of this work[2] indicated that the vibration problem of an annular ring, introducing a second boundary, would be soluble at a reasonable computational cost. The frequency equations thus obtained are valid for the whole range of ring thicknesses. The results obtained from the solution of these frequency equations would then identify the disk counterparts of the ring modes and vice versa.

The disk resonances consist of two series of pure radial and pure tangential modes, in the absence of nodal diameters and a series of compound modes which have both radial and tangential components of displacement. There are six series of narrow ring counterparts of these disk resonances, each disk mode moving to a particular ring mode as the diameter of the central hole is increased. Flexural modes approach zero frequency, the extensional series have finite frequencies and there is one series each of compound shear and compound plate modes, both of which approach infinite frequency as do the two pure torsional and radial modes.

Typically, the finite frequency extensional ring mode series must go to a disk series of which the pure radial mode is the first, but the counterparts of the higher modes are not self evident. Practically, useful data on the effect of a small hole in a disk or on a finite width ring, has hitherto been only available as approximations. The eigenvalues, in the form of a dimensionless frequency constant, have been

evaluated for steps of hole size from the disk case to that of an indefinitely narrow ring and for a wide range of values of Poisson's ratio. The theoretical results are compared with the measurements of the spectra of a range of annulae and by exploring the pattern of vibrations with a probe pick-up.

Table 3.1 shows a classification of disk modes defined by (m,n) where m is the number of nodal circles- a centre nodal point being included - and n, the number of nodal diameters. There are two series with no nodal diameters, the tangential modes where the first (1,T) has one nodal circle and the movement is purely rotational and the radial modes where the first (1,R) has a node at the centre and the movement is purely radial. Thus (1,T) and (2,R) are equivalents, there being no tangential equivalent to (1,R).

In thin rings and disks it can be assumed that no stresses are acting along the thickness direction. The frequency is thus independent of thickness and consequently the radius is normally taken as the dimension. In the case of annular rings, by taking the width as the dimension, the modes which move to infinite narrow ring frequency, approach a constant K value. Similarly, for the modes which move to zero frequency the simplest presentation of results is obtained by taking (mean radius)^2/width. The theoretical results usually appear in terms of plate or shear velocities. By choosing an appropriate velocity, the K value can be made independent of Poisson's ratio for a particular series of modes as the thin ring condition is approached. Rod, plate and shear velocities are appropriate for extensional, radial and tangential modes, respectively.

Tables 3.2 and 3.3 summarise the main features of disk and narrow ring modes and include the corresponding frequency equations. Where the motion is predominantly radial, a radial drive is used and tangential vibrations require an angled or a tangential drive. The drive point normally becomes an antinode for the drive direction. Nodal lines refer

Table 3.1

Classification of disk modes

n \ m	1	2	3	4
	Circular nodes			
0	1,T	2,T	3,T	4,T
	Pure torsion			
0	1,R	2,R	3,R	4,R
	Finite	Pure radial		
1	1,1	2,1	3,1	4,1
	Flexural	Finite	Shear wave	Plate wave
2	1,2	2,2	3,2	4,2
3	1,3	2,3	3,3	4,3

Nodal diameters

Shear wave

Table 3.2 Characteristics of disk resonances

Mode Series	Typical nodal patterns	Remarks	Source of frequency term
Pure torsional disk	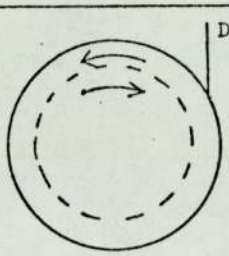 Mode (1,T)	The dynamic balance condition requires at least one nodal circle. The centre is always an antinode. This series consists of (1,T); (2,T); (3,T)...	Solution of equation $K_s J_o(K_s)/J_1(K_s) = 2$ where $K_s = \omega a/C_s$ Formal solution by Love.
Pure radial disk	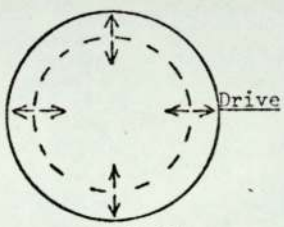 Mode (2,R)	The dynamic balance condition does not require a nodal circle. The centre is always a node. This series consists of (1,R); (2,R); (3,R) ...	Solution of equation $K_p J_o(K_p)/J_1(K_p) = 1-\sigma$ where $K_p = \omega a/C_p$ Normally attributed to S E Poisson. Formal solution by Love.
Compound disk	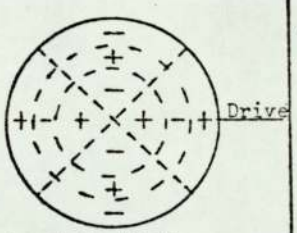 Mode (3,2)	This series consists of (1,1) and higher order modes.	Solution of equation (3.4.1), where $K_s = \omega a/C_s$ $K_p = \omega a/C_p$ $K_o = \omega a/C_o$ M.Onoe and R.Holland

Table 3.3

Characterisitics of Ring Resonances

Mode Series	Typical nodal pattern	Remarks	Source of frequency term
Extensional	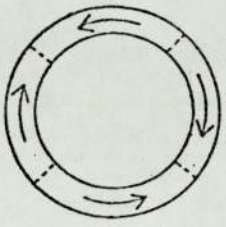 Mode n=2	This is the finite frequency series. The energy is mainly in hoop strain.	$K_o = (n^2 + 1)^{\frac{1}{2}}$ $K_o = \omega a/C_o$ $n = 0,1,2 \ldots$ Lord Rayleigh
Flexural	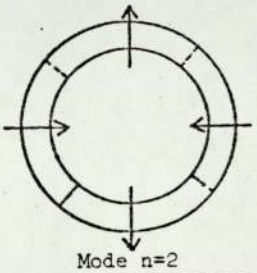 Mode n=2	The frequencies approach zero. The energy is flexural and the ring length is unchanged.	$K_o = \frac{2}{\sqrt{3}} \frac{1-\gamma}{(1+\gamma)^2} \frac{n(n^2-1)}{(n^2+1)^{\frac{1}{2}}}$ $K_o = \omega a/C_o$ $n = 2,3 \ldots$ R Hoppe
Compound	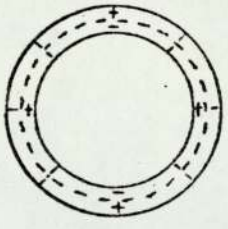 Mode p=1	The frequencies approach infinity as plate or shear waves. The disk counterparts are S(3,2) P(4,2).	$K(1-\gamma) \rightarrow p\pi$ $K = \omega a/C_s$ or $K = \omega a/C_p$ $p = 1,2,3 \ldots$

to radial or tangential movements. In general, a node for one component of motion is an antinode for its orthogonal counterpart. The phase of the various regions is indicated by arrows or polarity signs.

This chapter is a continuation of the work of Sharp[18], who obtained theoretical and experimental results for the flexural series of resonances in an annular ring. The lower order radial[22] and torsional[23] modes were already well known. The author's contribution was to develop the experimental techniques by using tangential and angular drives and also a double wire drive. The former enabled the finite frequency series of resonances to be identified and the latter was particularly useful in exciting the weak higher order modes. The theoretical results for the finite frequency and higher order modes were also obtained.

It is shown in chapter 4 that the frequency equation (3.2.1) used by the author, for obtaining the numerical eigenvalues, can be derived as a limiting case, from the thick annular disk frequency equation(4.2.3), by equating the thickness-to-diameter ratio to zero. Several limiting cases obtained, by simplifying the frequency determinant (3.2.1) using various approximations, were also investigated. This resulted in the elucidation of the finite frequency mode series and the higher order shear and plate mode series and the resolution of the inner boundary node paradox. The completed work has been published jointly[7].

3.2 Spectra of In plane Vibrations

A general solution to the wave equations of motion may be obtained by first establishing the differential equations for various wave motions in the appropriate coordinates, cylindrical in this case. The boundary conditions for the system, in this case that the radial and tangential stresses must vanish at the inner and outer perimeters, are then used to obtain the frequency equation for compound modes of vibration. The frequency equations for radial and tangential modes of vibration are then obtained by setting n=0, in the compound mode frequency equation. These

will consist of simultaneous algebraic equations containing amplitude constants and the eigenvalue (K) giving the frequency in terms of the dimensions of the resonator and a wave velocity. There will be an infinite number of numerical solutions, each corresponding to a mode of vibration. If required, the amplitude constants can also be evaluated to obtain the eigen function of the mode expressing the components of stress or strain throughout the resonator.

3.2.1 Frequency Equation for Compound Modes

In Appendix A.3.1, the procedure for obtaining the frequency equation is outlined for compound modes. The frequency equation is then obtained as:

$$F(K^T) = \begin{vmatrix} a_{11} & a_{12} & a_{13} & a_{14} \\ a_{21} & a_{22} & a_{23} & a_{24} \\ a_{31} & a_{32} & a_{33} & a_{34} \\ a_{41} & a_{42} & a_{43} & a_{44} \end{vmatrix} = 0 \qquad (3.2.1)$$

where

$$a_{11} = - J_n(K^T)\{M_n(K^T) - n(n+1) + (K^T\Theta)^2/2\} ,$$

$$a_{12} = - Y_n(K^T)\{L_n(K^T) - n(n+1) + (K^T\Theta)^2/2\} ,$$

$$a_{13} = n J_n(K^T\Theta)\{M_n(K^T\Theta) - (n+1)\} ,$$

$$a_{14} = n Y_n(K^T\Theta)\{L_n(K^T\Theta) - (n+1)\} ,$$

$$a_{21} = - n J_n(K^T)\{M_n(K^T) - (n+1)\} ,$$

$$a_{22} = - n Y_n(K^T)\{L_n(K^T) - (n+1)\} ,$$

$$a_{23} = J_n(K^T\Theta)\{M_n(K^T\Theta) - n(n+1) + (K^T\Theta)^2/2\} ,$$

$$a_{24} = Y_n(K^T\Theta)\{L_n(K^T\Theta) - n(n+1) + (K^T\Theta)^2/2\} ,$$

$$a_{31} = - J_n(K^T\gamma)\{M_n(K^T\gamma) - n(n+1) + (K^T\gamma\Theta)^2/2\} ,$$

$$a_{32} = - Y_n(K^T\gamma)\{L_n(K^T\gamma) - n(n+1) + (K^T\gamma\Theta)^2/2\} ,$$

$$a_{33} = n J_n(K^T\gamma\Theta)\{M_n(K^T\gamma\Theta) - (n+1)\} ,$$

$$a_{34} = n Y_n(K^T\gamma\Theta)\{L_n(K^T\gamma\Theta) - (n+1)\}$$

$$
\begin{aligned}
a_{41} &= -\, n\, J_n(K^T\gamma)\{M_n(K^T\gamma) - (n+1)\} \quad , \\
a_{42} &= -\, n\, Y_n(K^T\gamma)\{L_n(K^T\gamma) - (n+1)\} \quad , \\
a_{43} &= J_n(K^T\gamma\theta)\{M_n(K^T\gamma\theta) - n(n+1) + (K^T\gamma\theta)^2/2\} \quad , \\
a_{44} &= Y_n(K^T\gamma\theta)\{L_n(K^T\gamma\theta) - n(n+1) + (K^T\gamma\theta)^2/2\}
\end{aligned}
\tag{3.2.2}
$$

It may be recognised that eqn.(3.2.1) is the frequency equation for the compound modes of vibration in a thin disk with a central hole[7,18]. This equation has an infinite number of numerical solutions for each n, designated by K^T_{mn}, each representing a mode of vibration.

3.2.2 Frequency Equations for Radial and Tangential Modes

The frequency equations for pure radial and pure torsional modes, for which the displacements are independent of θ and n=0, can be derived, as a limiting case, from eqn.(3.2.1). Putting n=0 in eqn.(3.2.1), the frequency equation degenerates into

$$D_1 \cdot D_2 = 0 \tag{3.2.3}$$

where

$$D_1 = \begin{vmatrix} b_{11} & b_{12} \\ b_{31} & b_{32} \end{vmatrix} \quad \text{and} \quad D_2 = \begin{vmatrix} b_{23} & b_{24} \\ b_{43} & b_{44} \end{vmatrix} \tag{3.2.4}$$

where

$$
\begin{aligned}
b_{11} &= J_1(K^T)\{M_1(K^T) - (1-\sigma)\} \quad , \\
b_{12} &= Y_1(K^T)\{L_1(K^T) - (1-\sigma)\} \quad , \\
b_{31} &= J_1(K^T\gamma)\{M_1(K^T\gamma) - (1-\sigma)\} \quad , \\
b_{32} &= Y_1(K^T\gamma)\{L_1(K^T\gamma) - (1-\sigma)\} \quad , \\
b_{23} &= J_1(K^T\theta)\{M_1(K^T\theta) - 2\} \\
b_{24} &= Y_1(K^T\theta)\{L_1(K^T\theta) - 2\} \\
b_{43} &= J_1(K^T\gamma\theta)\{M_1(K^T\gamma\theta) - 2\} \\
b_{44} &= Y_1(K^T\gamma\theta)\{L_1(K^T\gamma\theta) - 2\}
\end{aligned}
\tag{3.2.5}
$$

Then, the frequency equations for the radial and tangential modes will be

$$D_1 = 0 \tag{3.2.6}$$

and $D_2 = 0$, (3.2.7)

respectively. Thus, eqn.(3.2.3) indicates that the extensional and shear modes of vibration can exist uncoupled in the case of axially symmetric motion.

The numerical solutions are obtained by evaluating frequency eqns. (3.2.1), (3.2.6) and (3.2.7) for fixed values of n, γ and σ with successive steps of K^T. This method was used to identify and follow the frequency variation of various modes as γ and σ values are changed. Fig.3.1 illustrates the frequency variation of compound modes, for n = 1, $\gamma = 0.9$ and $\sigma = 0.3$. Solutions are obtained for values of σ from 0.0 to 0.5 in steps of 0.05 and for γ values from 0.0 to 0.9 in steps of 0.2 and are given in Appendix A.3.2. The precise values shown in the various tables in Appendix A.3.2 were obtained by interpolating between positive and negative values about the zero value of F(K) by the Newton-Raphson method, described in Chapter 2. If required, the amplitude constants can also be evaluated to obtain the eigen function of the mode expressing the components of stress or strain throughout the resonator.

3.3 Comparison with Experimental Results

Six resonators progressing in form from a disk to a narrow ring were cut from steel and aluminium rods of diameter 7.6 cms. and 5.0 cms., respectively. By driving them at an angle and radially, as described in Appendix A.2.2, all the lower order resonances and few higher order resonances can be measured. The degree of coupling to a particular resonance depends on the direction of vibration at the point of drive. A radial drive gives good coupling, if the radial component of the particular mode is large, while an angular drive enables the excitation of torsional modes, for which the shear component is large. When two frequencies are close together, a double drive at different points can, by phasing, suppresses one mode in favour of the other. Employing a probe of fine wire as a receiver, the various resonances could be easily

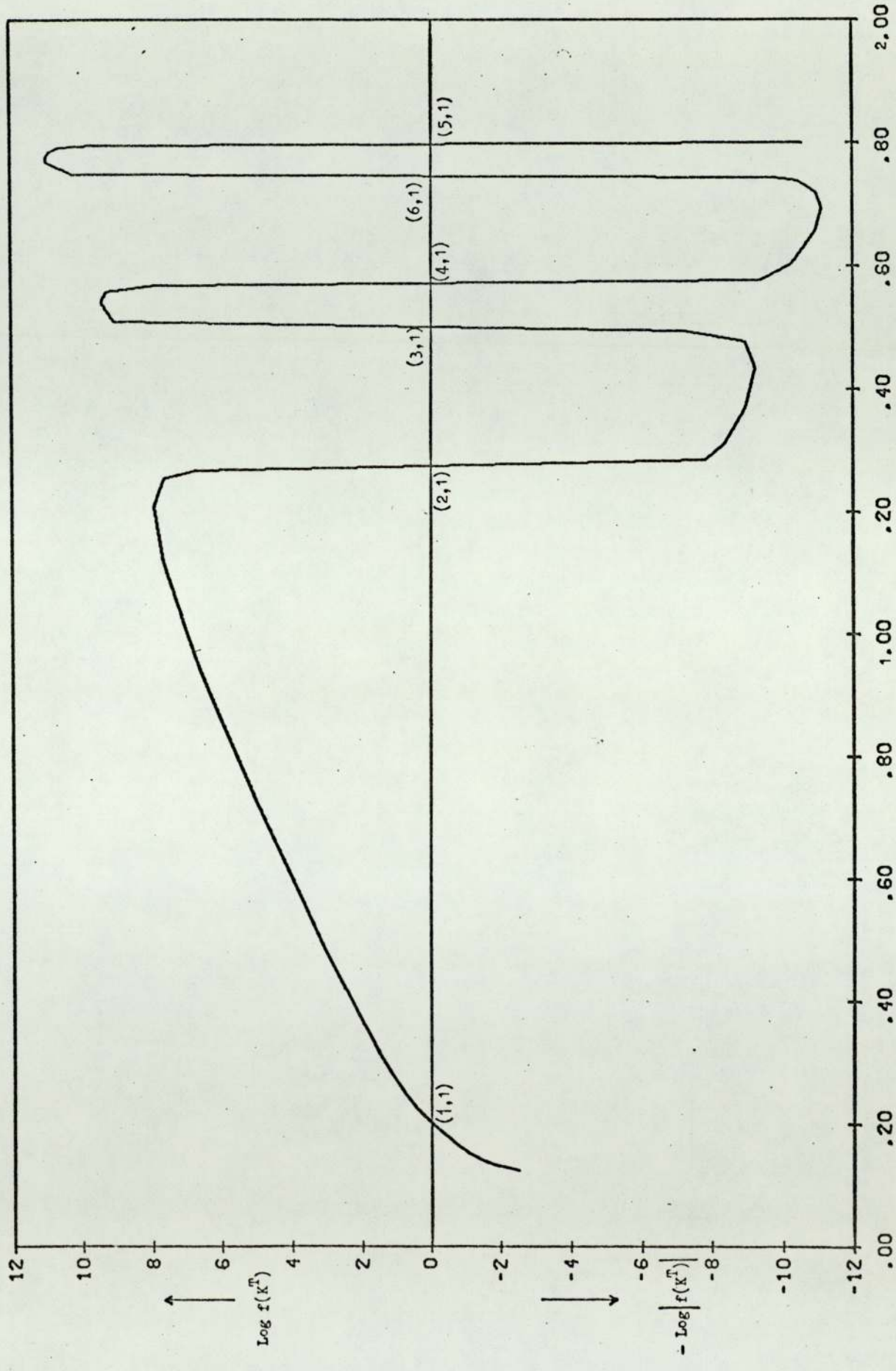

Fig.3.1 The solutions of the annular ring compound mode frequency equation for n=1, γ=0.9 and σ =0.3.

identified. The detailed vibration pattern across the face of a resonator can also be explored with this probe. As a node is traversed, the amplitude falls to zero and then rises with reverse phase.

The data obtained from the experiments on steel and aluminium disks, are tabulated in Tables 3.4 and 3.5, respectively, together with the theoretical K^T values taken from the tables given in Appendix A.3.2. The frequencies shown in the tables are as observed in spectral order. Poisson's ratio and the plate velocity were calculated from the (1,3) and (1,R) disk modes, using the results given in Reference 2 and the method described in Chapter 2. This enabled the K^T values to be obtained from the tables. Then, the constancy of the value of C_p calculated for every mode shows the agreement between theory and experiment. The theory is for an indefinitely thin specimen whereas the diameter-to-thickness ratio of the disks used was about 12. Certain modes such as the (1,R), (2,R) and all lower and higher order compound modes are sensitive to thickness while the flexural series of modes (1,2),(1,3) etc., are not (see Chapters 2 and 4). It may also be seen that these tables completely confirm the close agreement between the theoretical and experimental results for the flexural and finite frequency extensional modes, over the whole range of hole size, but the higher order resonances follow the theoretical values only over a sufficient range of hole size. In effect, the result is a validation of the method of measuring frequency and lends confidence to calculated K^T values beyond the range of direct observation.

3.4 Limiting Cases

The two limiting cases of the annular ring are a thin disk and a thin ring. The frequency equations for these cases can be derived from eqn.(3.2.1), by making suitable approximations. This is helpful in classifying the various disk and ring resonances.

Table 3.4 The theoretical and experimental results for steel annular ring. Radius = 3.809 cms., σ = 0.280 , C_p = 5426 m/sec.

These values are derived from disk modes (1,3) and (1,R) modes, using the method described in Reference 2.

Y	Mode	1,2	1,1	1,R	1,3	2,2	1,4	1,T	1,5	2,3	2,1	1,6	3,1	2,4	3,2	1,7	2,T
0.00	f kHz	31.741	36.864	46.288	48.848	57.659	63.628	69.564	77.182	79.092	80.198	90.618	92.560	100.996	102.884	103.452	114.049
	K^T	1.4070	1.6319	2.0363	2.1592	2.5299	2.8101	3.0813	3.4203	3.4789	3.5330	4.0106	4.0957	4.4387	4.5513	4.5896	5.0593
	C_p m/s	5399	5406	5440	5414	5455	5419	5403	5401	5441	5433	5408	5409	5446	5410	5395	5395
0.1646	f kHz	28.989	37.381	42.071	47.961	55.403	63.340	70.862	77.081	78.419	85.561	90.201	94.405	100.703	91.405	103.568	119.124
	K^T	1.3215	1.6410	1.8582	2.1546	2.4443	2.8094	3.1484	3.4195	3.4773	3.7711	4.0097	4.2174	4.4322	4.0610	4 5886	5.2951
	C_p m/s	5250	5452	5419	5327	5425	5396	5387	5395	5397	5430	5384	5357	5438	5387	5402	5416
0.3324	f kHz	19.032	38.152	35.156	41.007	55.332	60.438	76.855	76.276	75.831	90.886	90.417	109.844	97.116	104.338	103.729	137.310
	K^T	0.8524	1.6890	1.5634	1.8219	2.4462	2.6606	3.4122	3.3638	3.3690	3.9977	3.9909	4.8685	4.3211	4.6122	4.5827	6.0492
	C_p m/s	5344	5406	5382	5387	5414	5437	5391	5427	5387	5441	5422	5400	5379	5414	5417	5432
0.50	f kHz	12.712	37.901	30.133	30.452	57.051	48.784	93.378	67.090	78.350	100.505	84.550	143.220	99.029	129.981	101.067	-
	K^T	0.5648	1.5722	1.3285	1.3400	2.4992	2.1612	4.0877	2.9688	3.4333	4.4339	3.7318	6.3373	4.3429	5.7489	4.4356	-
	C_p m/s	5386	5424	5429	5438	5463	5402	5467	5408	5462	5425	5422	5409	5457	5411	5453	-
0.66	f kHz	7.794	35.739	26.446	19.593	55.860	33.790	134.365	49.388	77.699	134.739	65.399	-	100.092	144.805	81.459	-
	K^T	0.3440	1.5904	1.1752	0.8807	2.4588	1.5150	5.9448	2.1987	3.4356	5.9614	2.9057	-	4.4233	6.4303	3.6198	-
	C_p m/s	5276	5378	5386	5324	5437	5338	5409	5376	5413	5409	5387	-	5416	5389	5386	-
0.8341	f kHz	-	33.123	23.574	8.778	52.799	16.307	-	25.453	74.003	-	35.864	-	96.751	-	47.465	-
	K^T	-	1.4727	1.0505	0.3951	3.2689	0.7276	-	1.1420	3.2689	-	1.5940	-	4.2599	-	2.1081	-
	C_p m/s	-	5383	5371	5317	5417	5364	-	5334	5418	-	5385	-	5436	-	5389	-

Table 3.4 (Contd.) Steel annular ring

γ	Mode	1,8	4,2	2,R	2,5	3,3	1,9	4,1	3,4	1,10	2,6	4,3	5,2	3,5
0.00 (Disk)	f kHz	116.593	118.283	121.729	122.387	122.516	129.235	134.447	139.813	141.816	142.216	144.531	154.806	158.260
	K^T	5.1618	5.2375	5.3854	5.3863	5.3977	5.7284	5.9664	6.1995	6.2585	6.3060	6.4000	6.2049	7.0011
	C_p m/s	5406	5405	5410	5438	5432	5399	5393	5397	5423	5397	5405	5415	5410
0.1646	f kHz	116.590	118.038	108.357	121.202	112.321	129.313	141.844	137.500	141.844	141.341	143.446	-	-
	K^T	5.1607	5.2137	4.7753	5.3443	4.9865	5.7234	6.2370	6.0355	6.2543	6.2605	6.3886	-	-
	C_p m/s	5407	5418	5431	5428	5391	5407	5443	5452	5428	5403	5374	-	-
0.3324	f kHz	116.525	121.454	116.216	119.256	108.887	129.208	150.374	122.999	142.078	141.073	144.719	-	-
	K^T	5.1588	5.3594	5.1559	5.3047	4.8413	5.7280	6.6626	5.4471	6.2508	6.2197	6.3782	-	-
	C_p m/s	5406	5424	5394	5380	5383	5399	5402	5404	5440	5428	5410	-	-
0.5	f kHz	115.287	138.244	-	117.086	136.017	129.021	-	139.310	141.528	133.897	140.396	-	-
	K^T	5.0835	6.1275	-	5.1697	6.0276	5.6910	-	6.1421	6.2702	5.9062	6.2049	-	-
	C_p m/s	5428	5400	-	5420	5401	5426	-	5428	5399	5426	5415	-	-
0.66	f kHz	97.763	-	-	121.839	161.574	114.018	-	-	129.499	142.990	-	-	129.479
	K^T	4.3308	-	-	5.3620	7.1475	5.0314	-	-	5.7317	6.2766	-	-	5.7363
	C_p m/s	5403	-	-	5438	5410	5423	-	-	5407	5452	-	-	5402
0.8341	f kHz	59.700	-	-	119.291	-	72.702	-	-	86.055	142.219	-	-	-
	K^T	2.6434	-	-	5.2765	-	3.2001	-	-	3.8147	6.2648	-	-	-
	C_p m/s	5405	-	-	5411	-	5437	-	-	5399	5433	-	-	-

Table 3.5 This table shows the agreement between the theory and experiment for an aluminium annular ring. Radius = 2.5 cms. σ = 0.33, C_p = 5423 m/sec., These values are derived from (1,R) and (1,3) disk modes[2].

Y	Mode	1,2	1,1	1,R	1,3	2,2	1,4	1,T	1,5	2,3	2,1	1,6	3,1
0.00 (Disk)	f kHz	46.730	54.670	71.405	71.995	85.013	94.040	102.790	113.592	116.310	121.739	134.640	137.123
	K^T	1.3579	1.5945	2.0674	2.0862	2.4766	2.7183	2.9723	3.3110	3.4019	3.5202	3.8844	3.9791
	C_p m/s	5406	5386	5425	5421	5392	5434	5432	5389	5370	5432	5445	5399
0.30	f kHz	30.570	56.340	55.730	63.550	81.130	91.270	109.120	113.120	112.144	185.101	133.710	156.493
	K^T	0.8903	1.6477	1.6067	1.8549	2.3736	2.6460	3.1656	3.2933	3.2746	5.3904	3.8799	4.5647
	C_p m/s	5394	5371	5448	5382	5369	5418	5415	5396	5379	5394	5413	5385
0.50	f kHz	18.934	56.689	45.427	45.117	84.280	72.452	135.823	99.377	114.870	147.025	124.370	-
	K^T	0.5537	1.6447	1.3121	1.3098	2.4468	2.1057	3.9430	2.8868	3.3489	4.2697	3.6237	-
	C_p m/s	5371	5414	5438	5414	5410	5404	5411	5407	5388	5409	5391	-
0.70	f kHz	9.754	53.498	38.486	25.408	82.314	45.236	-	66.201	115.026	-	88.645	-
	K^T	0.2874	1 5399	1.1235	0.7522	2.3951	1.3184	-	1.9425	3.3528	-	2.5989	-
	C_p m/s	5331	5457	5381	5306	5399	5390	-	5353	5389	-	5358	-
0.90	f kHz	2.632	48.481	34.331	7.711	76.009	14.993	-	24.001	107.359	-	35.219	-
	K^T	0.0799	1.4025	0.9944	0.2292	2.2146	0.4394	-	0.7106	3.1301	-	1.0424	-
	C_p m/s	5171	5430	5423	5286	5391	5360	-	5305	5387	-	5307	-

Table 3.5 (Contd.)

Y	Mode	2,4	1,7	3,2	2,T	1,8	4,2	2,5	3,3	2,R	1,9	4,1	3,4	4,3
0.00 (Disk)	f kHz	148.480	152.052	153.680	167.180	172.001	177.670	179.780	180.380	186.227	191.293	197.770	207.650	217.890
	K^T	4.3327	4.4468	4.4611	4.8718	5.0023	5.1608	5.2435	5.2647	5.3951	5.5536	5.7600	6.0389	6.3286
	C_p m/s	5383	5371	5411	5390	5401	5408	5386	5382	5422	5411	5393	5401	5413
0.30	f kHz	144.743	152.179	149.490	191.706	171.351	175.917	178.140	159.355	169.927	190.848	213.793	182.730	216.572
	K^T	4.2266	4.4450	4.3594	5.5555	5.0010	5.1172	5.1841	4.6314	4.9393	5.5521	6.2252	5.3225	6.3182
	C_p m/s	5379	5378	5387	5420	5382	5400	5398	5405	5404	5400	5395	5393	5384
0.50	f kHz	144.513	147.902	175.851	-	169.027	-	172.029	-	-	189.513	-	-	-
	K^T	4.2202	4.3037	5.1237	-	4.9305	-	5.0094	-	-	5.5193	-	-	-
	C_p m/s	5379	5398	5391	-	5385	-	5394	-	-	5393	-	-	-
0.70	f kHz	148.902	112.118	-	-	135.560	-	181.798	-	-	159.131	-	-	-
	K^T	4.3320	3.2723	-	-	3.9529	-	5.2871	-	-	4.6345	-	-	-
	C_p m/s	5399	5382	-	-	5387	-	5401	-	-	5393	-	-	-
0.90	f kHz	139.974	49.518	-	-	64.917	-	172.991	-	-	82.561	-	-	-
	K^T	4.0791	1.4347	-	-	1.8875	-	5.0367	-	-	2.4008	-	-	-
	C_p m/s	5390	5421	-	-	5402	-	5395	-	-	5402	-	-	-

3.4.1 Thin Disk Frequency Equations

The limiting case obtained when γ is equated to zero, corresponds to a thin disk. For this case, as $\gamma \to 0$, $Y_n(K^T\gamma) \to \infty$ and $Y_n(K^T\gamma\theta) \to \infty$. Thus, by dividing the elements a_{i2} , i= 1 to 4, by $Y_n(K^T\gamma)$ and the elements a_{4j}, j= 1 to 4, by $Y_n(K^T\gamma\theta)$, the frequency equation (3.2.1) simplifies to

$$\begin{vmatrix} a_{11} & a_{13} \\ a_{21} & a_{23} \end{vmatrix} = 0 \qquad (3.4.1)$$

where the elements of the determinant are given in eqn.(3.2.1), and $n \geq 1$. The above equation represents the frequency equation of compound modes of vibration in thin disks, as given by Love[8], Onoe[9], Holland[10] and Ambati[2].

The frequency equations for the axisymmetric vibrations(i.e., pure radial and pure torsional), whose displacements are independent of θ, can be obtained by equating n, in eqn.(3.4.1), to zero. Then, eqn.(3.4.1), reduces to

$$b_{11} \cdot b_{23} = 0 \qquad (3.4.2)$$

where the elements b_{11} and b_{23} are given in eqn.(3.2.5).

The frequency equations for the pure radial and torsional modes are, therefore, given by

$$M_1(K^T) = (1 - \sigma) \qquad (3.4.3)$$

and $$M_1(K^T\theta) = 2$$

respectively, where the wave velocities associated with these modes are the plate and the shear velocities, respectively. Equations (3.4.1) and (3.4.3) can be identified to be same as those derived from the theory of generalised plane stress[8,9,10].

3.4.2 Vibrations of a Thin Circular Ring

The frequency equations for the vibrations of a thin ring, which can approach zero, finite or infinite frequency, can be derived, as a special case when $\gamma \to 1$, from eqn.(3.2.1). For a thin ring, γ can be

written as

$$\gamma = (1 - d\gamma) \tag{3.4.4}$$

where $d\gamma$ is small such that $d\gamma \to 0$, as $\gamma \to 1$. Then, using the Taylor series expansion for the Bessel functions, we obtain

$$\begin{aligned} Z_{n-1}(\gamma x) &= \{1 - (n-1)\, d\gamma\}\, Z_{n-1}(x) + x\, d\gamma\, Z_n(x) \\ Z_n(\gamma x) &= (1 + n\, d\gamma)\, Z_n(x) - x\, d\gamma\, Z_{n-1}(x) \end{aligned} \tag{3.4.5}$$

where $Z = J, Y$ and $x = K^T$, $K^T\theta$ and it should be noted that the second-order terms in $d\gamma$ are neglected, since $d\gamma << 1$. Thus, those of the elements of the determinant in eqn.(3.2.1), which involve γ, become

$$\begin{aligned} a_{3i} &= Z_n(K^T)\Big[(1+ n\, d\gamma)\{n(n+1) - \frac{(K^T\theta)^2}{2}\} + d\gamma(1+\sigma)\frac{(K^T\theta)^2}{2} \\ &\qquad - (1+ d\gamma_1)\, W_n(K^T)\Big] \\ a_{3j} &= Z_n(K^T\theta)\Big[n(1+ d\gamma)\, W_n(K^T\theta) - \{n(n+1) + d\gamma_3\}\Big] \\ a_{4i} &= Z_n(K^T)\Big[\{n(n+1) + d\gamma_2\} - n(1+ d\gamma)\, W_n(K^T)\Big] \\ a_{4j} &= Z_n(K^T\theta)\Big[(1+ d\gamma_1)\, W_n(K^T\theta) - (1+ n\, d\gamma)\{n(n+1) - \frac{(K^T\theta)^2}{2}\}\Big] \end{aligned} \tag{3.4.6}$$

where $Z = J$ for $i = 1$, $j = 3$

$= Y$ for $i = 2$, $j = 4$

and

$$W_n(x) = x\,\frac{Z_{n-1}(x)}{Z_n(x)}\ , \quad d\gamma_1 = d\gamma\{n^2 - \frac{(K^T\theta)^2}{2}\}\ , \tag{3.4.7}$$

$$d\gamma_2 = n\, d\gamma\{n(n+1) - (K^T)^2\}, \quad d\gamma_3 = n\, d\gamma\{n(n+1) - (K^T\theta)^2\}$$

Substituting eqns.(3.4.6) and (3.4.7) into eqn.(3.2.1) and simplifying, yields the frequency equation, for $d\gamma \simeq 0$ (i.e., $\gamma \simeq 1$), as

$$\begin{aligned} &\left[(K^T)^2 - \frac{4(1-\gamma)^2\, n^2(n^2-1)^2(1-\sigma^2)}{3(1+\gamma)^4\,(n^2+1)}\right]\left[(K^T)^2 - \frac{4(n^2+1)(1-\sigma^2)}{(1+\gamma)^2}\right] \\ &\{J_n(K^T)Y_{n-1}(K^T) - J_{n-1}(K^T)Y_n(K^T)\} \\ &\{J_n(K^T\theta)Y_{n-1}(K^T\theta) - J_{n-1}(K^T\theta)Y_n(K^T\theta)\} = 0 \end{aligned} \tag{3.4.8}$$

Using the following Gray and Mathews theorem for Bessel functions[24]

$$\{J_n(x)Y_{n-1}(x) - J_{n-1}(x)Y_n(x)\} = \frac{1}{x}$$

eqn.(3.4.8) becomes

$$\left[(K^T)^2 - \frac{4(1-\gamma)^2 n^2 (n^2-1)^2 (1-\sigma^2)}{3(1+\gamma)^4 (n^2+1)}\right] = 0 \ ,$$

i.e.,
$$K^T = \frac{2(1-\gamma)\ n(n^2-1)}{(1+\gamma)^2}\sqrt{\frac{(1-\sigma^2)}{3(n^2+1)}} \qquad (3.4.9)$$

or
$$\left[(K^T)^2 - \frac{4(n^2+1)(1-\sigma^2)}{(1+\gamma)^2}\right] = 0 \ , \text{ i.e., } K^T = \frac{2}{(1+\gamma)}\sqrt{(n^2+1)(1-\sigma^2)} \qquad (3.4.10)$$

It may be ascertained that equations (3.4.9) and (3.4.10) are the frequency equations of the low frequency in plane flexural and the finite frequency extensional vibrations, respectively, of the thin ring[8]. But, eqns.(3.4.9) and (3.4.10) do not predict the high frequency extensional vibrations of the ring which tend to infinity, as $\gamma \to 1$. However, the frequency equation for high frequency vibrations can be obtained by assuming that $K^T \to \infty$, as $\gamma \to 1$. Then, using this condition in eqn.(3.2.1), yields the product of two 2 x 2 determinants, as

$$\begin{vmatrix} Y_{11} & Y_{12} \\ Y_{41} & Y_{42} \end{vmatrix} \times \begin{vmatrix} Y_{25} & Y_{26} \\ Y_{55} & Y_{56} \end{vmatrix} = 0 \qquad (3.4.11)$$

where $Y_{11} = J_n(K^T)$, $Y_{12} = Y_n(K^T)$, $Y_{41} = J_n(K^T\gamma)$, $Y_{42} = Y_n(K^T\gamma)$

$$Y_{25} = J_n(K^T\theta),\ Y_{26} = Y_n(K^T\theta),\ Y_{55} = J_n(K^T\gamma\theta),\ Y_{56} = Y_n(K^T\gamma\theta). \qquad (3.4.12)$$

Substituting eqns.(3.4.12) and the following asymptotic expansions, valid for high argument values of Bessel functions,

$$J_n(x) = \frac{1}{\sqrt{\pi x}}\left[\cos(x - \frac{n\pi}{2}) + \sin(x - \frac{n\pi}{2})\right] ,$$
$$Y_n(x) = \frac{1}{\sqrt{\pi x}}\left[\sin(x - \frac{n\pi}{2}) - \cos(x - \frac{n\pi}{2})\right], \qquad (3.4.13)$$

in eqn.(3.4.11) and simplifying, yields the frequency equation for the high frequency modes of the ring, as

$$\sin K^T(1-\gamma).\ \sin K^T\theta(1-\gamma) = 0 \ , \qquad (3.4.14)$$

which leads to,

$$\sin K^T(1-\gamma) = 0 \text{ , i.e.,; } K^T(1-\gamma) = p\pi \text{ , } p = 1,2,3,... \qquad (3.4.15a)$$

$$\text{or } \sin K^T\Theta(1-\gamma) = 0 \text{ , i.e.; } K^T\Theta(1-\gamma) = q\pi \text{ , } q = 1,2,3,... \qquad (3.4.15b)$$

Eqns.(3.4.15a) and (3.4.15b) show that the high frequency compound vibrations are effectively of pure plate or pure shear waves, respectively. This can be appreciated as for large K^T values, the nodal circles are indefinitely closer together than the nodal radii.

Similarly, it can be shown that the first radial mode of the annular ring, predicted by eqn.(3.2.6), tends, as $\gamma \to 1$, to the ring frequency given by

$$K^T = \frac{2}{(1+\gamma)} \sqrt{1-\sigma^2} \text{ ,} \qquad (3.4.16)$$

which is same as eqn.(3.4.10), when n=0. The second and higher radial modes in the disk progress to high frequency ring modes, given by eqn. (3.4.15a) and all the disk torsional modes tend to the ring high frequencies given by the eqn.(3.4.15b).

3.5 Discussion of Results

A complete picture, summarised in Table 3.6 is now available of the ways in which disk and ring resonances constitute the limiting cases of annular ring resonances. The pure radial and pure torsional modes are solutions of eqns.(3.2.6) and (3.2.7), respectively, where the associated velocities are those of plate and shear waves. The frequency increases rapidly with hole size, the nodal circles are crowded together, and the energy arising from the curvature becomes less and less. As a result, the edges of the ring become antinodes and the width of the ring, $a(1-\gamma)$, becomes an integral number of half wavelengths, the integer being the number of nodal circles. Putting $a(1-\gamma) = p\lambda/2$, gives the ratio of phase velocity C_{phase}, to plate velocity C_p, for radial modes, as

$$\frac{C_{phase}}{C_p} = \frac{K^T(1-\gamma)}{p\pi} \qquad (3.5.1)$$

Table 3.6 Correspondence of disk and ring modes

	Torsion (Shear)	Radial (Plate)
Disk	1,T 2,T 3,T ...	2,R 3,R 4,R ...
Ring	p= 1 2 3	p= 1 2 3
	Flexural	Finite Frequency
Disk	1,2 1,3 1,4 ...	1,R 1,1 2,2 2,3 ...
Ring	n= 2 3 4	n = 0 1 2 3
	Compound Shear	
Disk	2,1 3,2 3,3 ...	4,1 5,2 5,3 ...
Ring	q = 1	q = 2
	Compound Plate	
Disk	3,1 4,2 4,3 ...	5,1 6,2 6,3
Ring	p = 1	p = 2

and the ratio of C_{phase} to the shear velocity C_s , for the torsional modes, as

$$\frac{C_{phase}}{C_{shear}} = \frac{K^T\Theta(1-\gamma)}{q\,\pi} \qquad (3.5.2)$$

The modes (1,T) and (2,R) each having one nodal circle are the lowest modes of their series. Figs.3.2 and 3.3, which gives C_{phase}/C , where C is either C_s or C_p , show the ways in which the shear and plate velocities are approached as γ increases.

It may be seen that in both cases, C_{phase}/C goes to unity for all modes, establishing that the waves travel with the velocities appropriate to the wave equations and are not dispersive. The curves are not of a particularly regular form and the plateau which occurs in Fig 3.2 is a feature of a similar perturbations in other modes. In the case of the velocity ratios, for torsional modes, there is no dependence on σ , but this is not true for radial modes, as can be noted from Tables 3.7 and A.3.2.

The compound modes of disks which have nodal diameters but no nodal circles, (1,n) are the direct counterparts of the flexural modes of rings, being the solutions of eqn.(3.4.9). Fig.3.4 shows the progression, for steel, from the finite frequency disk resonances to zero frequency resonances of the thin ring. Table A.3.3 gives the K_0^T values, where $K_0^T = \omega a/C_0$, C_0 being the longitudinal velocity, for the full range of σ and γ. As the narrow ring region is approached, the frequency becomes less dependent on Poisson's ratio and the slope finally follows the Hoppe equation[25] of Table 3.3.

The finite frequency ring modes and their disk counterparts are of particular interest. It is reasonably evident that the 1,R disk mode becomes the n=0 ring-extensional mode, but, the disk counterparts of the higher n value ring modes are not self evident. In early experiments using radial drive, the transformations from n=0 to (1,R) and n=1 to (1,1)

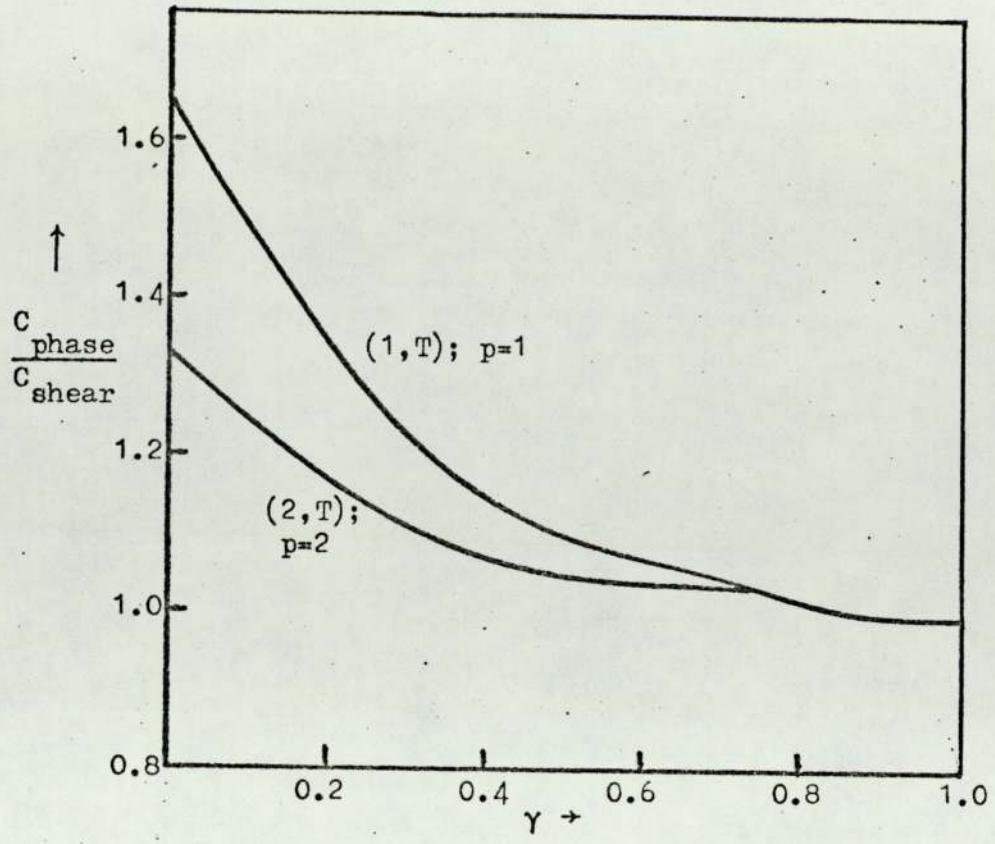

Fig.3.2 In pure torsional modes, the wave velocity approaches that of shear waves for the narrow ring. This velocity has no dependance on σ other than as a shear velocity.

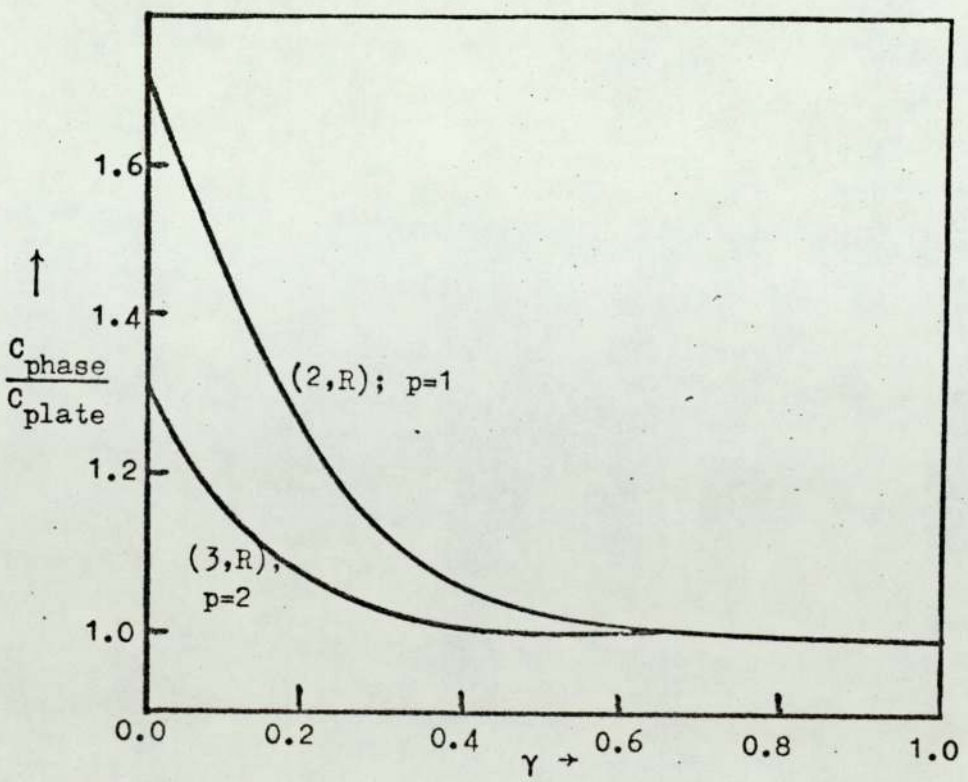

Fig.3.3 The first two pure radial modes for steel (σ = 0.3), p=1 and 2, respectively. The velocity has a small dependence on σ outside the plate velocity term.

modes were readily followed. Higher modes required drives with a tangential component. This extensional character of the strain results in large hoop stresses whereas in the distortion modes the stress is mainly flexural. The eigen functions of the ring (Rayleigh[19]) show n to be the ratio of tangential to radial displacement and in disks a similar feature appears. The experiments established that the n = 2,3,...,n, ring modes, as given by eqn.(3.4.10), have the disk counterparts of (2,2), (2,3),..., (2,n) modes. For disks, there is one nodal circle but, as the hole size increases it remains in the same position. Consequently, as the inner boundary pierces the node, the vibrational amplitude goes to zero, reverses in phase and the inner and outer boundary amplitudes finally becomes equal as the extensional ring condition is reached. The results for steel are shown in Fig 3.5 and the complete data is given in Table A.3.4. With the exception of (1,R), the curves have similar undulations which are thought to arise from the nodal circle effect described above. The (1,R) disk frequency is greater than that of the (1,1) mode and the curves cross at a low γ value as the frequencies move to the $K_0^T = 1$ and $K_0^T = \sqrt{2}$ ring values, respectively. The crossover occurs for all values of σ, the position being $\gamma = 0.372$ and 0.143 for $\sigma = 0.5$ and 0.0, respectively. The final rise in frequency as the narrow ring condition is reached becomes more prominent at higher modes.

There remains those compound modes which, like pure torsional and plate modes, approach infinite frequency as $\gamma \to 1$, the asymptotic values being the solutions of equation (3.4.15a) for plate waves and equation (3.4.15b) for shear waves, where p and q are the number of nodal circles. The way in which the limit is approached is shown for two plate modes - (3,1) and (4,2) - and for two shear modes (2,1) and (3,2) - in Fig.3.6. Values of K_p^T were obtained by solving eqn.(3.2.1) for $\sigma = 0.25$ for all four modes and $K_p^T(1-\gamma)$ is plotted against γ, where $K_p^T = K^T$. For the two plate modes, the asymptotic value of K^T is π and for the shear modes, it

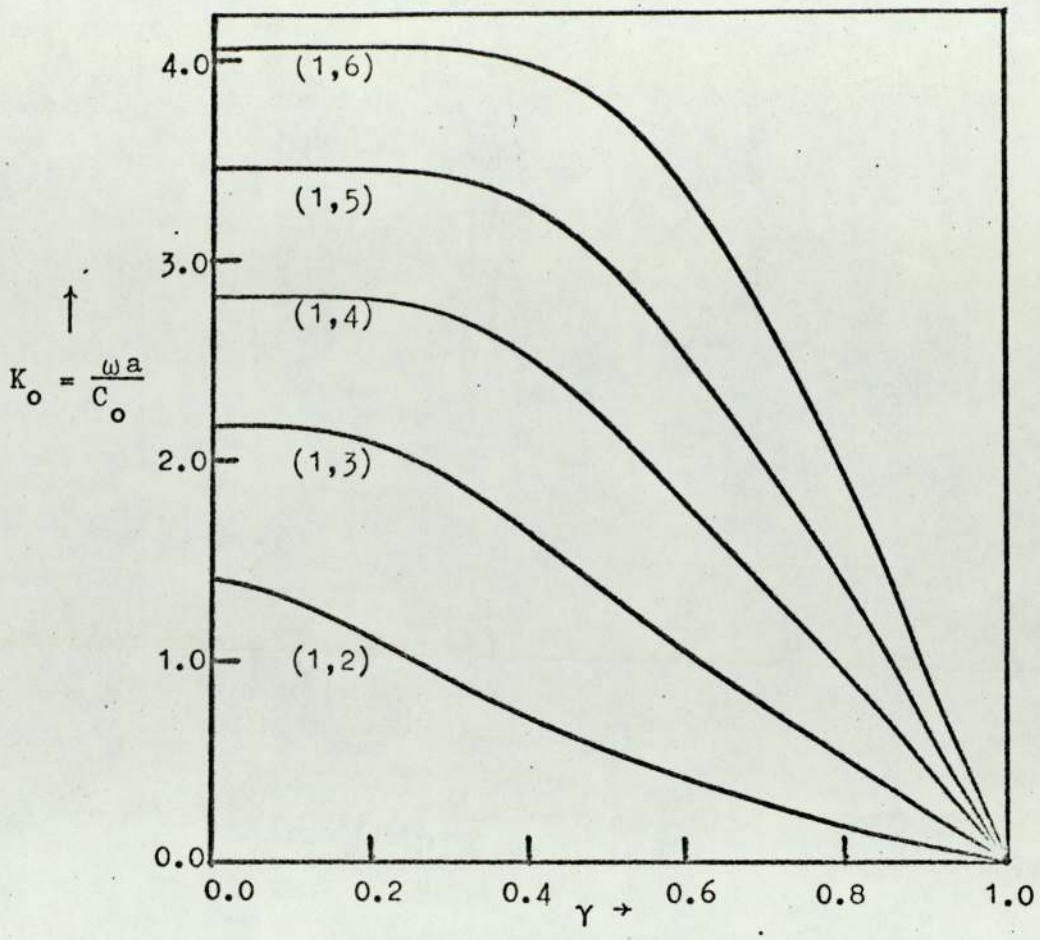

Fig.3.4 The flexural modes for steel ($\sigma = 0.3$), showing that they approach to zero frequency for narrow rings. These modes have no nodal circles.

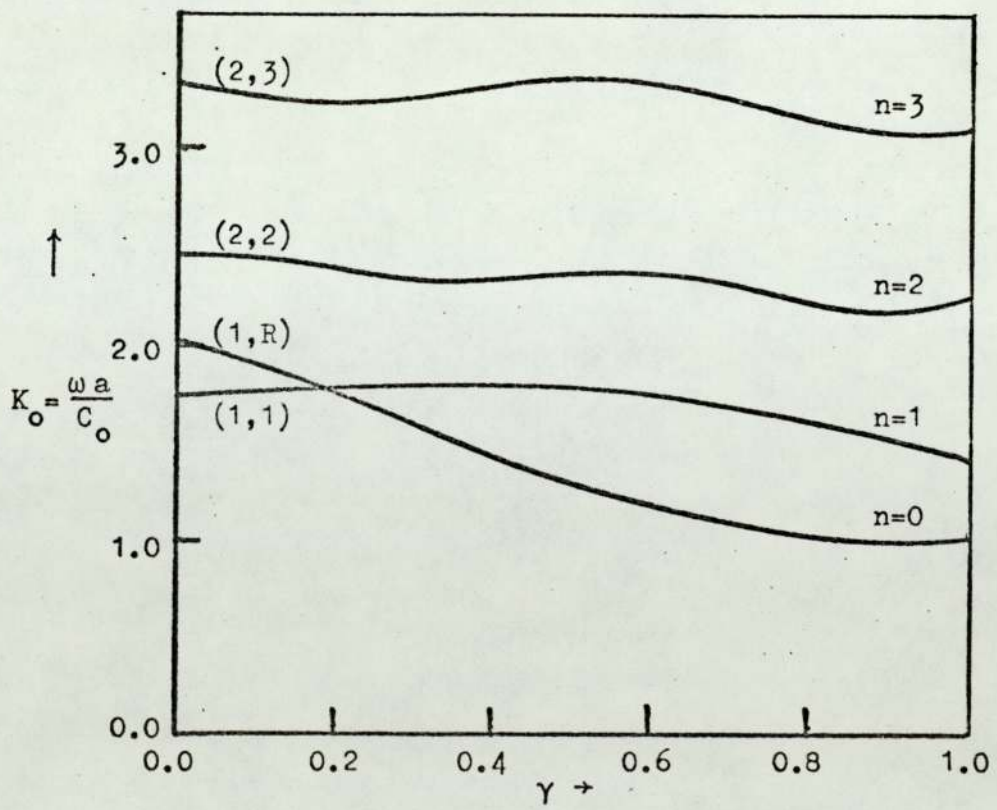

Fig.3.5 In the finite frequency modes, the dependence of frequency on Poisson's ratio falls to zero in the narrow ring condition, the values being in the ratio's $1:\sqrt{2}:\sqrt{5}:\sqrt{10}$. The movement is purely radial for the first mode and becomes increasingly tangential for higher modes.

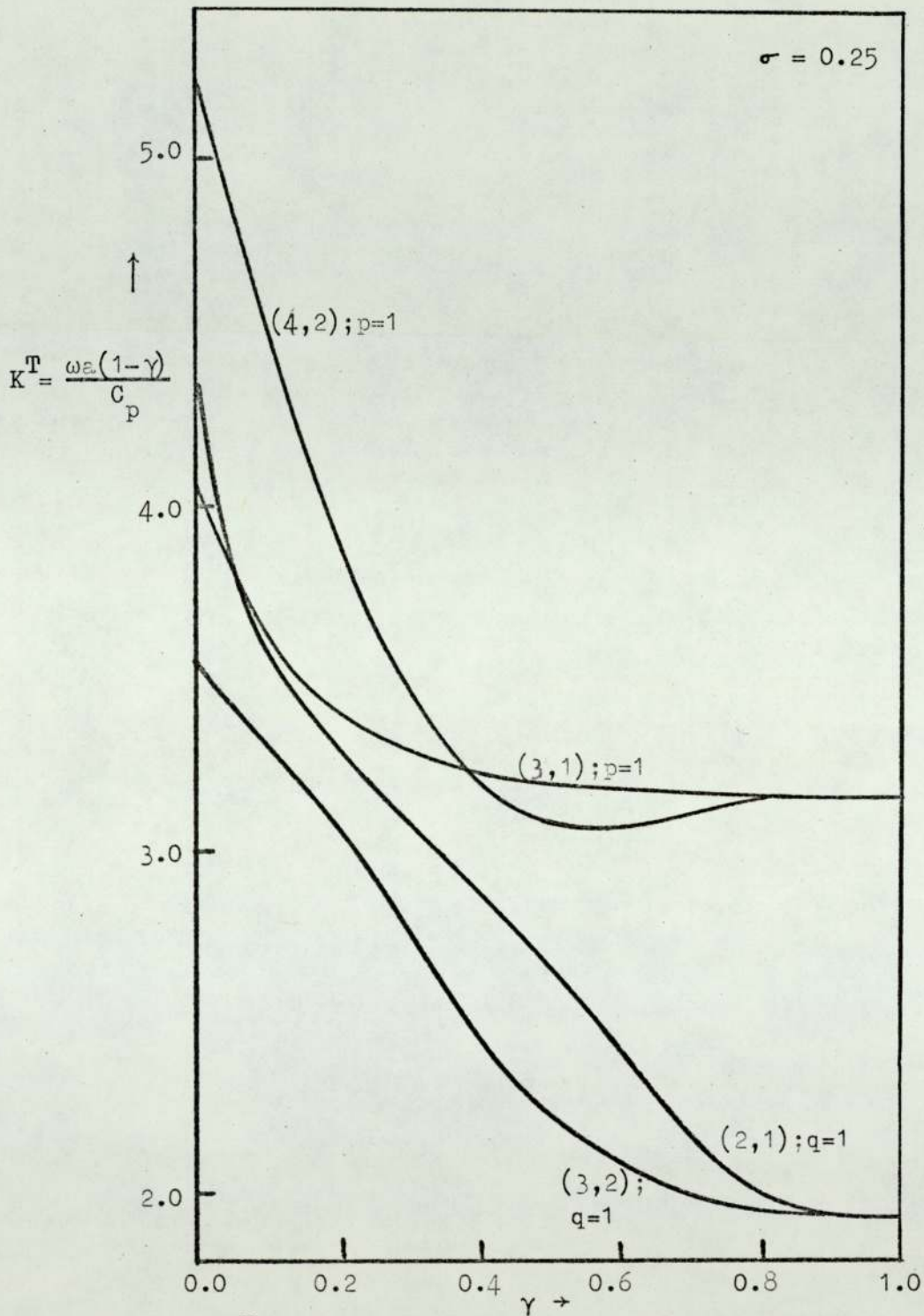

Fig.3.6 The $K_p^T(1-\gamma)$ values for the (3,1) and (4,2) plate modes and the (2,1) and (3,2) shear modes plotted as a function of γ. The asymptotic values reached are π and $\pi C_s/C_p$, establishing the compound plate and shear mode series, respectively.

is equal to $\pi/1.633$. The ratio of C_p/C_s is 1.633 for $\sigma = 0.25$ giving a $K_s^T(1-\gamma)$ value of π, where $K_s^T = K^T\theta$ and p, the number of nodal circles, is therefore unity for all four modes. The eigen values for these four modes are given in Table 3.8, for $\gamma = 0.9$.

Other modes were investigated for $\gamma = 0.99$, $\sigma = 0.25$ and the results are summarised in Table 3.9 which gives the C_{phase}/C values of eqn.(3.4.15). The original disk modes are identified by the (m,n) values. The lowest mode is the (2,1) which heads the series (2,1),(3,2),(3,3),... and higher series are (3,1),(4,2),(4,3),... and so on. The prefix letter gives the wave type and the suffix number the p value. Thus, the (5,1) disk mode with four nodal circles becomes the p = 2 narrow ring mode, two circles having been lost. The departure of the wave velocity ratio from unity is very small. It changes slightly with the number of nodal diameters and was found to have a similar small dependence on Poisson's ratio. Table 3.10 shows the actual progression of $K_p^T(1-\gamma)$ solutions of eqn.(3.2.1). The disk solutions are in the sequence (2,1),(3,1),(4,1), ..., but, because of the difference between shear and plate wave velocities, the sequence is different for narrow rings. For example, the (5,1), a plate mode has a higher frequency than the (6,1), a shear mode.

The disappearance of nodal circles as the hole is developed in the disk occurs in the cases of the (2,1) and higher finite frequency modes and the higher compound modes. The phenomenon was observed in detail for the (2,1) mode by using rings of increasing hole size and investigating the phase and amplitude at the ring boundaries with a pick-up probe. The nodal circle did not change position significantly with hole size and disappeared as already described earlier in this section. This is an apparent paradox, as for a particular hole size, the inner boundary can be a node, meaning in this case that there is no radial movement ($\xi_r = 0$). In terms of the boundary condition T_{rr} given by eqn.(A.3.6), the radial stress associated with the $(\partial \xi_r/\partial r)$ term is

Mode \ γ	For all σ's						
	0.00	0.10	0.30	0.50	0.70	0.90	1.0
K_{1T}	5.1356	5.1424	5.4703	4.8138	10.720	31.482	Infinity
K_{2T}	8.4173	8.4574	9,6003	12.856	21.070	62.865	infinity

Table 3.7 The (1,T) and (2,T) pure torsional modes, $K_s = \omega a/C_s$. Note that they are independent of σ .

Mode \ σ	$K^T\Theta(1-\gamma)$		$K^T(1-\gamma)$	
	K^T_{21}	K^T_{32}	K^T_{31}	K^T_{42}
0.0	3.1531	3.1678	3.1440	3.1421
0.1	3.1534	3.1690	3.1435	3.1409
0.2	3.1537	3.1701	3.1428	3.1393
0.3	3.1540	3.1712	3.1419	3.1367
0.4	3.1543	3.1723	3.1398	3.1301
0.5	3.1545	3.1828	3.1103	3.0790

Table 3.8 The limiting values approached, for (2,1),(3,2) shear modes and (3,1),(4,2) plate modes, for $\gamma = 0.90$.

m / n	2	3	4	5	6
1	S1.000003(1)	P0.999998(1)	S1.00000007(2)	P1.000004(2)	S
2	Finite	S1.000051(1)	P0.999984(1)	S (2)	P
3	frequency	S1.000159(1)	P0.999970(1)	S (2)	P
4	modes	S1.000275(1)	P0.999939(1)	S (2)	P

Table 3.9 Wave velocity ratios for a narrow ring, ($\gamma = 0.99$).

Nodal circles (p)	1	2	3	4
Plate	3.14(3,1)	6.28(5,1)	9.42(7,1)	12.57(9,1)
Shear	1.92(2,1)	3.85(4,1)	5.77(6,1)	7.70(8,1)

Table 3.10 Narrow ring $K_p^T(1-\gamma)$ values, $\gamma = 0.99$.

cancelled out by the $\left(\frac{\sigma}{r} \frac{\partial \xi_\theta}{\partial \theta} \right)$ term which produces the hoop stress. There is thus no net radial force and therefore no radial movement.

To summarise, every disk mode has been followed to its narrow ring counterpart which can approach zero, finite or infinite frequency. The general solution of the annulus given in equation (3.2.1) contains the Rayleigh[19] and Hoppe[25] ring resonances and the Poisson[20], Love and Holland disk resonances. Five figure Tables of frequency eigen values for a full range of annulus geometry and Poisson's ratio are available with the author.

A feature of the change from disk to thin ring is the disappearance of one or more nodal circles in certain cases. Typically, all modes with one nodal circle and two or more nodal diameters loose the nodal circle to become the finite frequency extensional ring series. The $m = 2,4,\ldots,$ compound mode series of disks will move to shear ring modes having $q = 1, 2,\ldots,$ circles and the $m = 3,5,\ldots$ series become $p = 1,2,\ldots,$ plate ring modes. This creates the apparent paradox that the inner free boundary of an annulus can be a node. In fact, the force at the edge arising from a radial strain is balanced by the hoop stress arising from a tangential strain.

CHAPTER 4

SPECTRA OF THICK ANNULAR DISKS

4.1 Introduction

In the previous chapter, the analysis of contour vibrations in a thin disk with a central hole was considered. In this chapter, the theory developed in chapter 2 is extended to deal with the in plane vibrations of a thick annular disk and the numerical results compared with the experimental frequency measurements carried out on disks of various thicknesses and hole sizes.

The exact and approximate solutions of the wave equations of thin cylindrical shells[23,26,27,28,29,30] vibrating in flexure or extension and of solid cylinders[14,31,32,33] vibrating only longitudinally or only tangentially, can be readily obtained. Rasband[14] has recently given a solution for axisymmetric and nonaxisymmetric vibrations of a free cylinder or a disk, but the resulting frequency equations are very complicated and neither the numerical nor the experimental results were given. Shaw[34] had provided experimental data(resonance frequencies) for radial and edge modes of vibration in barium titanate disks, for thickness-to-diameter ratios in the range 0.15 to 0.80, but these results are not valid for materials other than barium titanate or for disks with thickness-to-diameter ratios less than 0.15. These results are also not of much use for other modes of vibration such as compound or torsional vibrations. Further, in these papers, the case of nonaxisymmetric vibrations of a thick disk with a central hole, was not considered.

The solutions for nonaxisymmetric vibration of thick disks is given in chapter 2, which takes into account the coupling between contour and thickness modes of vibration. A study of this work indicated that the general case of a thick disk with a central hole, introducing a second boundary while increasing the number of elements in the frequency determinant from nine to thirty six, can be solved at a reasonable cost in computer time. These results would then identify the thick disk

counterparts of the shell modes and vice versa.

The resonances in a thick disk consist of one series each of radial, tangential and compound modes. The radial modes have radial and axial components of displacement, the tangential modes have the tangential component and the compound modes have all three components of displacement. There are nine series of shell counterparts of these thick disk resonances, each thick disk mode moving to a particular shell mode as the hole diameter is increased. There are two series of pure radial modes (radial plate or shear and radial compressional), one series of pure torsional modes, as in the case of a ring, both approaching infinite frequency, one series of flexural modes which approach zero frequency, two series of extensional modes which have finite frequencies and one series each of compound plate, compound shear and compound compressional modes,all approaching infinite frequency as do the pure radial and torsional modes, for $\gamma \to 1$. This classification of thick disk/shell modes is shown in Table 4.1, in which the modes are defined by (m,n), where (m-1) is the number of nodal circles and n, the number of nodal diameters. The two series with no nodal diameters are the tangential modes where the first mode (1,T), with purely rotational movement, has one nodal circle and the radial modes where the first mode (1,R), with radial and axial movement, has a node at the centre.

Various limiting cases that can be obtained from the frequency equations of thick annular disk are shown in Fig.4.1, together with the corresponding velocities and wave-numbers.

4.2 Compound Modes

The three dimensional equations of motion and the choice of the components of displacement are given in Appendix A.2.1. A general solution to these wave equations of motion may be obtained by reducing them to an equivalent two dimensional equations of motion, also described in Appendix A.2.1. The boundary conditions on the cylindrical surface

n \ m	1	2	3	4	5	6
	Nodal circles					
0	1,T	2,T	3,T	4,T	5,T	6,T
	Pure torsional modes					
0	1,R	2,R	3,R	4,R	5,R	6,R
	Pure radial modes					
1	1,1	2,1	3,1	4,1	5,1	6,1
2	1,2	2,2	3,2	4,2	5,2	6,2
3	1,3	2,3	3,3	4,3	5,3	6,3
4	1,4	2,4	3,4	4,4	5,4	6,4

Nodal diameters

Finite Flexural

Finite frequency Shear

Plate or axial shear

Compressional Shear

Table 4.1 Classification of thick annular disk modes.

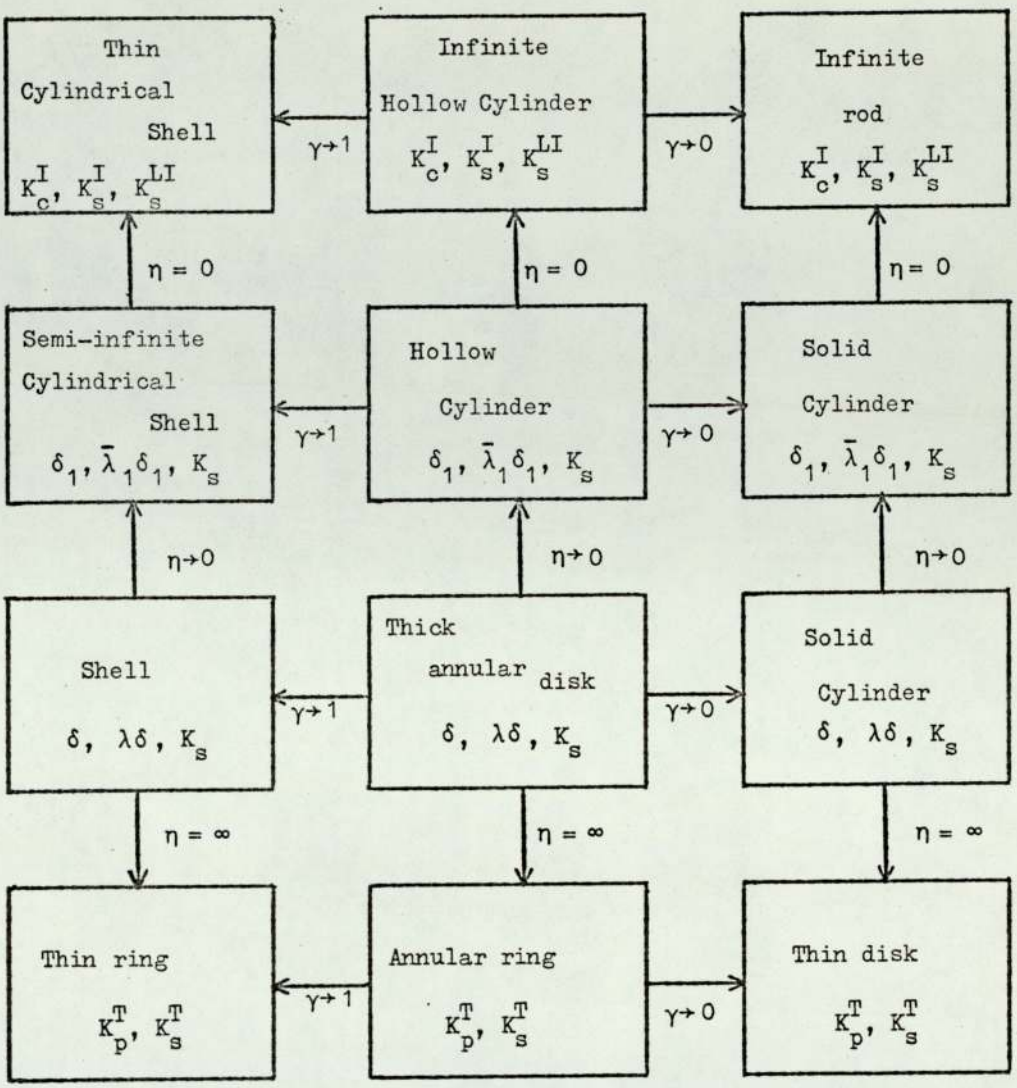

(a) Various limiting cases

Velocity	C_c	C_p	C_s
Infinite rod	K_c^I	K_s^{LI}	K_s^I
Thick disk	$\lambda\delta$	δ	K_s
Disk	-	K_p^T	K_s^T

$K_p = K$, $K_s = K\Theta$, $K_c = K/\sqrt{c}$,

$\delta_1 = \sqrt{K_s^2 + \frac{\pi^2 \eta^2}{\Theta^2}}$, and

$\bar{\lambda}_1\delta_1 = \sqrt{K_c^2 - \frac{\pi^2 \eta^2}{\Theta^2}}$,

η = Diameter-to-thickness ratio.

(b) Wavenumbers and the velocities associated with them.

Fig.4.1 Cylindrically symmetrical resonators showing the various limiting forms.

of the system, in this case that the radial, axial and tangential stresses must vanish at the inner and outer surfaces, are then used to obtain the frequency equation for compound modes of vibration. This will consist of simultaneous algebraic equations containing amplitude constants and the eigen value(K) giving the frequency in terms of the dimensions of the resonator and a wave velocity. There will be an infinite number of numerical solutions, each corresponding to a mode of vibration. If required the amplitude constants can also be evaluated to obtain the eigen function of the mode expressing the components of stress or strain throughout the resonator.

The derivation of the wave equations of motion in terms of the dilatation Δ and the rotation $\tilde{\omega}$ is given in Appendix A.2.1. The solutions of these equations are given by eqns.(A.2.10). Then, following the same procedure as given in Appendix A.2.1, the radial, tangential and axial components of the displacement can be derived, respectively,as

$$\xi_r = \left[A_1 \frac{dJ_n(\alpha r)}{dr} + A_2 \frac{dY_n(\alpha r)}{dr} + B_1 \frac{dI_n(\beta r)}{dr} + B_2 \frac{dK_n(\beta r)}{dr} + \frac{nC_1}{r} J_n(\nu r) + \frac{nC_2}{r} Y_n(\nu r) \right] \cos n\theta$$

$$\xi_\theta = -\left[\frac{nA_1}{r} J_n(\alpha r) + \frac{nA_2}{r} Y_n(\alpha r) + \frac{nB_1}{r} I_n(\beta r) + \frac{nB_2}{r} K_n(\beta r) + C_1 \frac{dJ_n(\nu r)}{dr} + C_2 \frac{dY_n(\nu r)}{dr} \right] \sin n\theta \qquad (4.2.1)$$

$$\xi_z = \{A_1 \phi_1 J_n(\alpha r) + A_2 \phi_1 Y_n(\alpha r) - B_1 \phi_2 I_n(\beta r) - B_2 \phi_2 K_n(\beta r)\} \cos n\theta$$

where ϕ_1 and ϕ_2 are given by eqns.(A.2.16), α, β, ν are given by eqns.(A.2.9), n is the circumferential order, J and Y are the Bessel functions, I and K are the modified Bessel functions, of first and second kind, respectively, and A_1, A_2, B_1, B_2, C_1, and C_2 are the amplitude constants. In the above equations, the time factor $\exp(j\omega t)$ has

been omitted for convenience.

The boundary conditions for a disk with radius 'a', thickness 'h' and a concentric hole of radius 'b', are

$$\begin{aligned} T_{rr} &= 0 \quad \text{at } r = a, & T_{rr} &= 0 \quad \text{at } r = b \\ T_{r\theta} &= 0 \quad \text{at } r = a, & T_{r\theta} &= 0 \quad \text{at } r = b \\ T_{rz} &= 0 \quad \text{at } r = a, & T_{rz} &= 0 \quad \text{at } r = b \end{aligned} \tag{4.2.2}$$

where the stress resultants T_{rr}, $T_{r\theta}$ and T_{rz} given by eqns.(A.2.3), have been expressed in terms of the displacements. The frequency equation for compound modes of vibration can then be obtained by satisfying the boundary conditions given in eqns.(4.2.2). Thus, substitution of eqns. (4.2.1) and (A.2.3) into eqns.(4.2.2) yields the compound mode frequency equation, formed by the determinant of the coefficients of the amplitude constants A_1, B_1, C_1, A_2, B_2 and C_2, as follows:

$$F(K) = |X_{ij}| = 0 \quad ; \quad i,j = 1 \text{ to } 6 \tag{4.2.3}$$

where, $X_{11} = - J_n(\delta)\{M_n(\delta) - n(n+1) + K^2\theta^2/2\}$,

$X_{12} = - Y_n(\delta)\{L_n(\delta) - n(n+1) + K^2\theta^2/2\}$,

$X_{13} = - I_n(\lambda\delta)\{N_n(\lambda\delta) - n(n+1) + K^2\theta^2/2\}$,

$X_{14} = K_n(\lambda\delta)\{P_n(\lambda\delta) + n(n+1) - K^2\theta^2/2\}$,

$X_{15} = n\, J_n(K\theta)\{M_n(K\theta) - (n+1)\}$,

$X_{16} = n\, Y_n(K\theta)\{L_n(K\theta) - (n+1)\}$,

$X_{21} = - n\, J_n(\delta)\{M_n(\delta) - (n+1)\}$,

$X_{22} = - n\, Y_n(\delta)\{L_n(\delta) - (n+1)\}$,

$X_{23} = - n\, I_n(\lambda\delta)\{N_n(\lambda\delta) - (n+1)\}$,

$X_{24} = n\, K_n(\lambda\delta)\{P_n(\lambda\delta) + (n+1)\}$,

$X_{25} = J_n(K\theta)\{M_n(K\theta) - n(n+1) + K^2\theta^2/2\}$,

$X_{26} = Y_n(K\theta)\{L_n(K\theta) - n(n+1) + K^2\theta^2/2\}$,

$$
\begin{aligned}
X_{31} &= J_n(\delta)\{M_n(\delta) - n\}(\delta^2 - K^2/c) , \\
X_{32} &= Y_n(\delta)\{L_n(\delta) - n\}(\delta^2 - K^2/c) , \\
X_{33} &= - I_n(\lambda\delta)\{N_n(\lambda\delta) - n\}(\lambda^2\delta^2 + K^2/c) , \\
X_{34} &= K_n(\lambda\delta)\{P_n(\lambda\delta) + n\}(\lambda^2\delta^2 + K^2/c) , \\
X_{35} &= X_{36} = 0 ,
\end{aligned}
\tag{4.2.4}
$$

and the remaining eighteen elements can be obtained from the corresponding elements given above by replacing δ, $\lambda\delta$ and K by $\gamma\delta$, $\gamma\lambda\delta$ and γK, respectively, where K is the required eigenvalue, which can be obtained from the solution of the frequency equation, δ and $\lambda\delta$ are the wave-numbers given by eqns.(2.2.7), $\eta = 2a/h$, is the diameter-to-thickness ratio, $\gamma = b/a$, is the ratio of the inner radius to the outer radius of the disk, $K\Theta = \nu a$ and

$$
\begin{aligned}
M_n(x) &= x\, J_{n-1}(x)/J_n(x) , \\
L_n(x) &= x\, Y_{n-1}(x)/Y_n(x) , \\
N_n(x) &= x\, I_{n-1}(x)/I_n(x) , \\
P_n(x) &= x\, K_{n-1}(x)/K_n(x) .
\end{aligned}
\tag{4.2.5}
$$

The case when $\lambda\delta$ is imaginary:

When $\lambda^2\delta^2 < 0$, the elements of the determinant which involve $\lambda\delta$, become

$$
\begin{aligned}
X_{13} &= - J_n(\bar{\lambda}\delta)\{M_n(\bar{\lambda}\delta) - n(n+1) + K^2\Theta^2/2\} , \\
X_{14} &= - Y_n(\bar{\lambda}\delta)\{L_n(\bar{\lambda}\delta) - n(n+1) + K^2\Theta^2/2\} , \\
X_{23} &= - n\, J_n(\bar{\lambda}\delta)\{M_n(\bar{\lambda}\delta) - (n+1)\} , \\
X_{24} &= - n\, Y_n(\bar{\lambda}\delta)\{L_n(\bar{\lambda}\delta) - (n+1)\} , \\
X_{33} &= J_n(\bar{\lambda}\delta)\{M_n(\bar{\lambda}\delta) - n\}(\bar{\lambda}^2\delta^2 - K^2/c) , \\
X_{34} &= Y_n(\bar{\lambda}\delta)\{L_n(\bar{\lambda}\delta) - n\}(\bar{\lambda}^2\delta^2 - K^2/c) , \\
X_{43} &= -J_n(\gamma\bar{\lambda}\delta)\{M_n(\gamma\bar{\lambda}\delta) - n(n+1) + \gamma^2K^2\Theta^2/2\} ,
\end{aligned}
$$

$$
\begin{aligned}
X_{44} &= -\, Y_n(\gamma\bar{\lambda}\delta)\{L_n(\gamma\bar{\lambda}\delta) - n(n+1) + \gamma^2K^2\theta^2/2\} \quad , \\
X_{53} &= -\, n\, J_n(\gamma\bar{\lambda}\delta)\{M_n(\gamma\bar{\lambda}\delta) - (n+1)\} \quad , \\
X_{54} &= -\, n\, Y_n(\gamma\bar{\lambda}\delta)\{L_n(\gamma\bar{\lambda}\delta) - (n+1)\} \quad , \\
X_{63} &= J_n(\gamma\bar{\lambda}\delta)\{M_n(\gamma\bar{\lambda}\delta) - n\}(\bar{\lambda}^2\delta^2 - K^2/c) \quad , \\
X_{64} &= Y_n(\gamma\bar{\lambda}\delta)\{L_n(\gamma\bar{\lambda}\delta) - n\}(\bar{\lambda}^2\delta^2 - K^2/c) \quad ,
\end{aligned}
\tag{4.2.6}
$$

where $\bar{\lambda}^2\delta^2 = -\lambda^2\delta^2$ and the remaining elements of the frequency equation are given by eqns.(4.2.4). Then, equation (4.2.3) gives natural frequencies of vibration in terms of the dimensions (thickness and diameter) of the disk resonator and the wave velocity. The numerical solutions of the frequency equation, for desired values of n, η, γ and σ, can be obtained on similar lines as described in section 2.3. There will be an infinite number of numerical solutions, each corresponding to a mode of vibration.

Comprehensive tables of K values for γ from 0.0 to 1.0, Poisson's ratio from 0.0 to 0.5 and for disk thickness-to-diameter ratios from 0.0 to 0.5, are given in Appendix A.4. However, the extensive tables of K values are available from the author. For thickness-to-diameter ratios greater than 0.5, the thick annular disk transforms to a hollow cylinder[12] and a change in the vibration spectra is expected. Thus, the numerical results obtained from this theory for thickness-to-diameter ratios greater than 0.5 may not accurately represent the true results. However, the theoretical results for the vibration spectra of hollow cylinders can be found in the literature[26,27]. The validity of the present theory for infinite hollow cylinders is shown in chapter 5 and its applicability to semi-infinite hollow cylinders is suggested, in chapter 8, for further work.

4.3 Axisymmetric Vibrations

Axisymmetric vibrations may consist of purely radial or purely torsional vibrations in which cases the motions are independent of the angular coordinate θ and n=0. Thus, setting n=0, the frequency equation (4.2.3) degenerates into the product of two sub-determinants, as

$$D_3 \, D_4 = 0 \tag{4.3.1}$$

where

$$D_3 = \begin{vmatrix} Y_{11} & Y_{12} & Y_{13} & Y_{14} \\ Y_{31} & Y_{32} & Y_{33} & Y_{34} \\ Y_{41} & Y_{42} & Y_{43} & Y_{44} \\ Y_{61} & Y_{62} & Y_{63} & Y_{64} \end{vmatrix} \tag{4.3.2}$$

$$D_4 = \begin{vmatrix} Y_{25} & Y_{26} \\ Y_{55} & Y_{56} \end{vmatrix} \tag{4.3.3}$$

and

$$\begin{aligned}
&Y_{11} = J_1(\delta)\{\tfrac{K^2\theta^2}{2} M_1(\delta) - \delta^2\}, \quad Y_{12} = Y_1(\delta)\{\tfrac{K^2\theta^2}{2} L_1(\delta) - \delta^2\} \\
&Y_{13} = I_1(\lambda\delta)\{\tfrac{K^2\theta^2}{2} N_1(\lambda\delta) + \lambda^2\delta^2\}, \quad Y_{14} = K_1(\lambda\delta)\{\tfrac{K^2\theta^2}{2} P_1(\lambda\delta) - \lambda^2\delta^2\} \\
&Y_{31} = \delta^2 J_1(\delta)(\delta^2 - \tfrac{K^2}{c}), \quad Y_{33} = \lambda^2\delta^2 I_1(\lambda\delta)(\lambda^2\delta^2 + \tfrac{K^2}{c}) \\
&Y_{32} = \delta^2 Y_1(\delta)(\delta^2 - \tfrac{K^2}{c}), \quad Y_{34} = -\lambda^2\delta^2 K_1(\lambda\delta)(\lambda^2\delta^2 + \tfrac{K^2}{c}) \\
&Y_{41} = J_1(\gamma\delta)\{\tfrac{K^2\theta^2}{2} M_1(\gamma\delta) - \delta^2\}, \quad Y_{43} = I_1(\gamma\lambda\delta)\{\tfrac{K^2\theta^2}{2} N_1(\gamma\lambda\delta) + \lambda^2\delta^2\} \\
&Y_{42} = Y_1(\gamma\delta)\{\tfrac{K^2\theta^2}{2} L_1(\gamma\delta) - \delta^2\}, \quad Y_{44} = K_1(\gamma\lambda\delta)\{\tfrac{K^2\theta^2}{2} P_1(\gamma\lambda\delta) - \lambda^2\delta^2\} \\
&Y_{61} = \delta^2 J_1(\gamma\delta)(\delta^2 - \tfrac{K^2}{c}), \quad Y_{63} = \lambda^2\delta^2 I_1(\gamma\lambda\delta)(\lambda^2\delta^2 + \tfrac{K^2}{c}) \\
&Y_{62} = \delta^2 Y_1(\gamma\delta)(\delta^2 - \tfrac{K^2}{c}), \quad Y_{64} = -\lambda^2\delta^2 K_1(\gamma\lambda\delta)(\lambda^2\delta^2 + \tfrac{K^2}{c})
\end{aligned} \tag{4.3.4}$$

and

$$\begin{aligned}
&Y_{25} = K\theta\, J_1(K\theta)\{M_1(K\theta) - 2\}, \quad Y_{26} = K\theta\, Y_1(K\theta)\{L_1(K\theta) - 2\} \\
&Y_{55} = K\gamma\theta\, J_1(K\gamma\theta)\{M_1(K\gamma\theta) - 2\}, \quad Y_{56} = K\gamma\theta\, Y_1(K\gamma\theta)\{L_1(K\gamma\theta) - 2\}
\end{aligned} \tag{4.3.5}$$

Then, the frequency equations

$$D_3 = 0 \qquad (4.3.6)$$

and $$D_4 = 0 \qquad (4.3.7)$$

correspond to the radial and tangential modes of vibration, respectively. It may be noted that these two types of vibration are uncoupled when the motion is independent of the angular coordinate θ, whereas they are coupled for a nonzero n, when the motion is axially asymmetric. For a given value of η, γ and σ, there are infinite number of values of K satisfying the frequency equation. Numerical solutions obtained by evaluating eqns.(4.3.6) and (4.3.7), for a desired value of η, γ and σ, are designated by K_{mR} and K_{mT}, which refer to the radial and tangential modes, respectively. Tables of K values for the first few radial modes are given in Appendix A.4.

It may be noted that the tangential mode frequency equation (4.3.7) in thick annular disks is same as the corresponding annular ring equation (3.2.7) derived in chapter 3, the rotational velocity being the same as in the theory of generalised plane stress[16].

4.4 Comparison with Experiment

The resonators used, for the measurement of the spectra, were aluminium disks with diameter of 5 cms. and thickness-to-diameter ratios of 0.5, 0.25 and 0.125, respectively. For each disk, a concentric hole of diameter 1.5 cms. corresponding to $\gamma = 0.3$, was machined and the resonant spectrum was measured using the method described in Appendix A.2.2. Then, the hole diameter of each disk was increased in steps of 1 cm. and at each step the family of resonances were measured. This procedure was repeated until each disk approximated to a shell.

The radial, angular and double drive techniques were employed to measure the resonant spectrum of the specimens. The radial drive excites lower order resonances including the second finite frequency modes and a few of higher order resonances (asymptotic modes) which tend for $\gamma \to 1$, to

plate or axial shear modes as $\eta \to \infty$ or 0, respectively. The modes excited by the angular and tangential drives include torsional and first finite frequency modes and a few of high frequency asymptotic modes which approach shear frequencies as $\gamma \to 1.0$. The double drive at different points was useful, in particular, when two frequencies are close together, as it can, by phasing, suppress one mode in favour of the other. The coupling in radial drive was strong to those modes which have large radial component, while the angular drive gave a good coupling to those modes having large tangential component.

The theoretical frequency values of the modes were calculated from the corresponding K values, using eqn.(2.2.6). The calculated and the measured results are given in Tables 4.2 to 4.4. The frequencies are given in spectral order of thick disks. The Poisson's ratio of the specimen material was calculated from the (1,R) and (1,3) thick disk modes, using the method described in Chapter 2. This enabled the K values for the theoretical results, to be obtained from the tables given in Appendix A.4. Then, tables 4.2 to 4.4 confirm the close agreement between the theoretical and experimental frequency values, for in plane flexural and two finite frequency series of resonances, over the whole range of hole sizes and disk thicknesses. But, the higher order resonances follow the theoretical results over a sufficient range of hole sizes for a wide range of disk thickness-to-diameter ratios, thus establishing the validity of the present theory beyond the range of direct measurement.

4.5 Limiting Cases

The validity of the present theory for in plane vibrations of thick annular disks, can be further demonstrated by studying a number of limiting cases.

Table 4.2 The theoretical and experimental resonant spectra of aluminium thick annular disk. Diameter = 5.0 cms., Thickness-to-diameter ratio = 0.50, Poisson's ratio = 0.33, as calculated from (1,R) and (1,3) thick disk modes.

Mode \ γ	Frequencies in kHz									
	0.00		0.30		0.50		0.70		0.90	
	Calculated	Measured	Calculated	Measured	Calculated	Measured	Calculated	Measured	Calculated	Measured
1,2	46.458	46.268	31.302	30.230	19.660	19.328	10.340	9.770	2.960	2.708
1,1	54.589	53.656	56.294	55.478	55.794	55.553	52.310	51.792	47.775	46.516
1,R	65.768	64.895	53.989	52.901	44.665	44.632	38.378	38.136	34.027	34.101
1,3	71.951	71.125	64.589	64.720	46.211	45.472	26.958	25.906	8.071	7.976
2,2	83.794	83.012	81.019	80.874	82.370	82.017	79.844	78.614	74.111	74.082
1,4	93.825	93.158	91.575	92.320	73.965	72.599	47.065	45.349	15.843	15.032
2,1	99.239	100.856	103.780	103.334	109.210	108.606	111.348	110.915	110.735	110.251
1,T	102.430	102.767	109.090	108.972	135.880	135.130	213.790	-	-	-
3,2	103.782	103.039	112.722	111.513	117.512	116.431	118.127	117.538	118.706	117.477
2,3	112.349	111.485	110.615	109.920	110.825	111.694	107.264	107.031	100.454	99.913
3,1	113.274	112.587	136.490	137.040	148.490	147.730	218.550	-	-	-
1,5	114.309	113.895	113.814	112.510	100.951	101.048	69.117	67.815	24.940	23.862
2,R	118.421	118.493	108.718	107.810	107.930	107.026	108.540	108.250	108.957	109.124
4,1	132.675	131.724	149.906	149.234	169.201	168.766	236.265	-	-	-

Table 4.2 (Contd.) Aluminium thick annular disk., Thickness-to-diameter ratio = 0.50.

Mode \ γ	Frequencies in kHz									
	0.00		0.30		0.50		0.70		0.90	
	Calculated	Measured	Calculated	Measured	Calculated	Measured	Calculated	Measured	Calculated	Measured
1,6	134.346	134.104	134.215	133.940	126.304	125.032	92.215	91.114	35.920	34.499
2,4	137.092	137.352	136.907	137.140	134.991	134.741	129.995	129.198	122.093	122.797
3,3	138.024	138 194	129.746	128.315	131.642	131.146	136.810	135.497	133.020	132.709
4,2	139.223	139.241	158.910	157.635	170.267	169.935	232.268	-	-	-
3,R	143.160	143.934	143.529	143.020	166.670	165.873	235.600	-	-	-
3,4	149.560	150.334	154.697	154.972	151.975	151.092	161.278	160.650	156.454	156.068
1,7	153.954	152.992	153.284	152.671	149.616	148.531	115.964	115.461	49.450	50.410
5,2	160.950	160.825	160.622	160.136	184.650	183.623	243.372	-	-	-
4,3	162.449	163.260	170.583	171.230	185.739	185.017	244.368	-	-	-
2,T	167.880	167.452	191.450	190.941	256.370	-	-	-	-	-
1,8	173.372	172.682	173.306	172.932	171.195	172.584	139.763	139.486	65.050	64.732
4,4	181.266	180.175	194.391	195.422	203.109	-	253.150	-	-	-
1,9	192.623	192.475	192.569	191.212	191.559	190.341	163.295	164.219	82.733	82.825

Table 4.3 The spectra of thick annular aluminium disk. Diameter = 5.0 cms., Thickness-to-diameter ratio = 0.25, σ = 0.33, as calculated from (1,R) and (1,3) thick disk modes.

Mode \ γ	Frequencies in kHz									
	0.00		0.30		0.50		0.70		0.90	
	Calculated	Measured	Calculated	Measured	Calculated	Measured	Calculated	Measured	Calculated	Measured
1,2	46.799	46.688	30.990	30.419	19.358	18.833	10.181	9.891	2.732	-
1,1	54.867	54.237	56.821	56.548	56.464	56.310	52.902	52.718	47.871	46.266
1,R	70.128	70.158	55.079	54.534	45.118	44.852	38.658	38.575	34.220	34.165
1,3	71.914	71.734	64.300	63.235	45.682	44.689	26.568	26.006	7.629	7.429
2,2	85.040	84.706	81.677	81.134	83.969	83.106	82.027	81.041	75.882	74.928
1,4	93.728	93.183	90.699	89.886	73.334	72.587	46.520	45.584	15.026	14.719
1,T	102.430	101.601	109.090	108.371	135.880	134.347	-	-	-	-
1,5	114.212	113.315	113.611	112.490	100.360	99.962	68.415	68.060	24.112	23.586
2,3	116.460	116.039	112.670	113.520	114.810	114.625	114.350	113.945	106.630	105.982
2,1	117.621	117.102	130.650	130.796	147.003	146.374	207.215	206.126	214.004	-
1,6	134.054	133.510	133.958	133.819	125.867	126.387	91.377	90.603	35.085	34.757

Table 4.3 (Contd.) Thickness-to-diameter ratio = 0.25. Thick aluminium annular disk.

Mode \ γ	Frequencies in kHz									
	0.00		0.30		0.50		0.70		0.90	
	Calculated	Measured	Calculated	Measured	Calculated	Measured	Calculated	Measured	Calculated	Measured
3,1	136.010	135.487	151.913	150.752	186.690	186.248	235.650	-	-	-
2,4	147.750	146.549	145.050	145.450	144.740	144.639	146.600	146.023	137.650	137.040
3,2	149.010	148.231	143.820	142.838	170.426	170.012	209.590	-	217.450	-
1,7	153.543	152.642	153.423	153.670	149.050	148.622	114.870	113.945	49.361	48.993
4,2	163.001	162.019	170.270	169.004	187.980	187.187	233.520	-	-	-
2,R	169.248	169.001	158.928	158.138	185.445	185.072	207.970	207.638	216.097	215.409
1,8	172.822	172.540	172.703	172.900	170.610	169.450	138.558	137.995	64.468	63.818
3,3	174.788	173.952	154.737	154.012	182.973	183.447	216.071	-	223.650	-
1,9	191.964	191.415	191.835	191.808	190.910	189.523	160.934	159.129	82.811	82.529
4,1	196.530	195.151	207.456	206.348	236.748	-	-	-	-	-
3,4	197.920	197.697	178.400	177.940	190.330	189.725	224.340	-	-	-

Table 4.4 The theoretical and experimental resonant spectra of aluminium thick annular disk. Diameter = 5.0 cms., Thickness-to-diameter ratio = 0.125, σ = 0.33, as calculated from (1,R) and (1,3) thick disk modes.

Mode \ γ	Frequencies in kHz									
	0.00		0.30		0.50		0.70		0.90	
	Calculated	Measured	Calculated	Measured	Calculated	Measured	Calculated	Measured	Calculated	Measured
1,2	46.797	46.249	30.790	30.734	19.180	18.993	10.019	9.912	2.745	-
1,1	54.928	54.220	56.955	57.074	56.631	56.528	53.027	53.178	48.018	47.341
1,R	70.984	71.179	55.309	55.791	45.197	45.231	38.707	38.429	34.256	34.235
1,3	71.901	71.813	64.083	64.135	45.326	45.106	26.207	26.013	7.756	7.364
2,2	85.273	85.127	81.774	81.304	84.241	84.013	82.418	82.107	76.216	75.871
1,4	93.692	92.860	91.291	90.744	72.872	72.038	45 902	45.578	15.105	14.653
1,T	102.430	102.780	109.090	109.668	135.880	135.853	-	-	-	-
1,5	114.137	113.126	113.556	113.912	99.841	99.671	67.592	66.927	24.346	23.478
2,3	117.061	116.983	112.839	112.345	115.285	114.978	115.361	115.196	107.590	107.011
2,1	120.539	119.948	133.222	133.142	147.800	147.381	218.488	-	-	-
1,6	133.926	132.968	133.799	134.539	125.326	124.904	90.386	90.031	35.561	35.021

Table 4.4 (Contd.) Spectra of thick aluminium annular disk. Thickness-to-diameter ratio = 0.125, σ = 0.33.

Mode \ γ	Frequencies in kHz									
	0.00		0.30		0.50		0.70		0.90	
	Calculated	Measured	Calculated	Measured	Calculated	Measured	Calculated	Measured	Calculated	Measured
3,1	136.838	136.382	156.240	156.581	212.060	-	-	-	-	-
2,4	148.994	148.346	145.611	144.259	145.313	144.869	148.755	148.289	139.961	139.372
3,2	152.735	151.372	149.066	148.566	175.922	175.631	231.609	-	-	-
1,7	153.349	152.123	153.288	152.464	148.632	148.053	113.746	113.286	49.398	49.461
4,2	166.447	165.903	174.868	174.204	205.048	-	-	-	-	-
1,8	172.549	171.667	172.499	171.748	170.203	169.837	137.336	136.857	64.834	64.125
3,3	180.502	179.313	158.739	158.778	201.966	201.138	-	-	-	-
2,R	182.622	181.217	168.271	168.365	216.875	-	-	-	-	-
1,9	191.601	190.200	191.551	191.050	190.492	189.983	160.934	160.175	82.795	82.485
4,3	194.705	194.031	211.008	210.921	-	-	-	-	-	-
4,1	205.088	204.651	213.635	214.441	265.342	-	-	-	-	-
3,4	206.840	206.067	182.790	182.461	205.971	-	-	-	-	-

4.5.1 Thick Disk Resonators

For thick disks, the inner radius $b \to 0$ and hence $\gamma \to 0$. Thus, equating γ to zero, the frequency equation (4.2.3) simplifies to

$$\begin{vmatrix} X_{11} & X_{13} & X_{15} \\ X_{21} & X_{23} & X_{25} \\ X_{31} & X_{33} & X_{35} \end{vmatrix} = 0 \quad , \tag{4.5.1}$$

which is the frequency equation (2.2.4) derived in chapter 2 for the compound modes of vibration in thick isotropic disks; where the elements of the determinant are given in eqn.(4.2.4).

The frequency equations for the axisymmetric vibrations (i.e., pure radial and pure torsional modes) can be derived, as special cases, by equating n to zero, in equation (4.5.1). Equation (4.5.1), then, simplifies to

$$\begin{vmatrix} X_{11} & X_{13} \\ X_{31} & X_{33} \end{vmatrix} |X_{25}| = 0 \tag{4.5.2}$$

where the elements of the above equation are given in eqns.(4.3.4) and (4.3.5). Thus, the frequency equation

$$\begin{vmatrix} X_{11} & X_{13} \\ X_{31} & X_{33} \end{vmatrix} = 0 \tag{4.5.3}$$

corresponds to the radial modes of vibration[35], and the frequency equation

$$|X_{25}| = 0 \tag{4.5.4}$$

corresponds to the tangential modes of vibration in thick disks, which may be identified to be same as the frequency equation of torsional vibrations in thin disks[8]. The frequencies of the tangential modes[16] are the same for a thick disk as for a thin disk, which has been experimentally verified(see Tables 4.2 to 4.4).

4.5.2 Vibrations of a Shell

For this case, η is finite and the hole size is large such that $\gamma \to 1$. For higher compound modes, such as (3,n), (4,n),(5,n),...,etc., it is observed that the values of K and Kγ become large and tend to infinity as the value of γ approaches unity. The Bessel functions can, therefore, be approximated by the first term of their asymptotic expansions, as

$$\begin{aligned} J_n(x) &= \frac{1}{\sqrt{\pi x}} \{ \cos(x - \tfrac{n\pi}{2}) + \sin(x - \tfrac{n\pi}{2}) \} , \\ Y_n(x) &= \frac{1}{\sqrt{\pi x}} \{ \sin(x - \tfrac{n\pi}{2}) - \cos(x - \tfrac{n\pi}{2}) \} , \\ I_{n-1}(x) &= I_n(x) = \frac{e^x}{\sqrt{2\pi x}} , \\ K_{n-1}(x) &= K_n(x) = \sqrt{\frac{\pi}{2x}}\, e^{-x} . \end{aligned} \tag{4.5.5}$$

Further, since $K \to \infty$, as $\gamma \to 1$, the wavenumbers δ and $\lambda\delta$ given in eqns. (2.2.7), reduce to

$$\delta = \sqrt{K^2\Theta^2 + \frac{\pi^2\eta^2}{\Theta^2}} \quad \text{and} \quad \lambda\delta = \sqrt{\frac{\pi^2\eta^2}{\Theta^2} - \frac{K^2}{c}} \tag{4.5.6}$$

Then, by using the approximation that the terms in K^2 are large compared to other terms in eqn.(4.2.3), the frequency equation reduces to the product of three 2 × 2 determinants, as

$$\begin{vmatrix} J_{n-1}(\delta) & Y_{n-1}(\delta) \\ J_{n-1}(\gamma\delta) & Y_{n-1}(\gamma\delta) \end{vmatrix} \times \begin{vmatrix} J_n(K\Theta) & Y_n(K\Theta) \\ J_n(K\gamma\Theta) & Y_n(K\gamma\Theta) \end{vmatrix} \times \begin{vmatrix} I_n(\lambda\delta) & K_n(\lambda\delta) \\ I_n(\gamma\lambda\delta) & K_n(\gamma\lambda\delta) \end{vmatrix} = 0 \tag{4.5.7}$$

Substituting the asymptotic approximations of eqns.(4.5.5), valid for high argument values of Bessel functions, in eqn.(4.5.7) and simplifying yields the following equation

$$\sin \delta(1 - \gamma) \cdot \sin K\Theta(1 - \gamma) \cdot \sin \lambda\delta(1 - \gamma) = 0 \tag{4.5.8}$$

This leads to

$$\sin \delta(1-\gamma) = 0 \ , \ \text{i.e.,} \ \delta(1-\gamma) = p\pi \ , \quad p = 1,2,3,\ldots, \tag{4.5.9a}$$

$$\text{or} \quad \sin K\Theta(1-\gamma) = 0, \ \text{i.e.,} \ K\Theta(1-\gamma) = q\pi \ , \quad q = 1,2,3,\ldots, \tag{4.5.9b}$$

$$\text{or} \quad \sin \bar{\lambda}\delta\,(1-\gamma) = 0, \ \text{i.e.,} \ \bar{\lambda}\delta\,(1-\gamma) = r\pi \ , \quad r = 1,2,3,\ldots, \tag{4.5.9c}$$

where p, q, r are integers, $\lambda\delta = j\bar{\lambda}\delta$ and $\bar{\lambda}\delta = \sqrt{\frac{K^2}{c} - \frac{\pi^2\eta^2}{\Theta^2}}$, is real.

Among axisymmetric vibrations, all pure (except 1,R and 2,R) radial modes such as K_{3R} , K_{4R} etc., and all torsional modes of vibration such as K_{1T} , K_{2T} etc., tend to infinite frequency values for $\gamma \to 1$. Using this assumption, the radial mode frequency equation (4.3.6) reduces to

$$\begin{vmatrix} J_1(\delta) & Y_1(\delta) \\ J_1(\gamma\delta) & Y_1(\gamma\delta) \end{vmatrix} \times \begin{vmatrix} I_0(\lambda\delta) & K_0(\lambda\delta) \\ I_0(\gamma\lambda\delta) & K_0(\gamma\lambda\delta) \end{vmatrix} = 0 \tag{4.5.10}$$

Using the asymptotic approximations, from eqns.(4.5.5), for n=0, the frequency equation (4.5.10) reduces to

$$\sin \delta\,(1-\gamma) \ \sin \bar{\lambda}\delta(1-\gamma) = 0 \tag{4.5.11}$$

which, then, gives

$$\sin \delta(1-\gamma) = 0 \ , \ \text{i.e.,} \ \delta\,(1-\gamma) = p\pi \ , \quad p = 1,2,3,\ldots \tag{4.5.12a}$$

$$\text{or} \quad \sin \bar{\lambda}\delta\,(1-\gamma) = 0 \ , \ \text{i.e.,} \ \bar{\lambda}\delta(1-\gamma) = r\pi \ , \quad r = 1,2,3,\ldots \tag{4.5.12b}$$

Similarly, using the assumption that $K \to \infty$ as $\gamma \to 1$ and the asymptotic approximations for Bessel functions, in the tangential mode frequency equation (4.3.7), leads to

$$\sin K\Theta(1-\gamma) = 0 \ , \ \text{i.e.,} \ K\Theta(1-\gamma) = q\pi \ , \quad q = 1,2,3,\ldots \tag{4.5.13}$$

It is clear that eqn.(4.5.13) corresponds to shear modes. It may be noted from Table 4.1 that $\delta \to K^T$ for $\eta \to \infty$ and tends to K_s^{LI} for $\eta \to 0$ and hence eqns.(4.5.12a) and (4.5.12b) represent, depending on η, plate or axial shear and compressional modes, respectively. The velocities corresponding to the wavenumbers $K\Theta$, δ and $\bar{\lambda}\delta$ will be shear, plate (or axial shear) and compressional, respectively, where the compressional velocity C_c is given by

$$C_c = \frac{C_p(1-\sigma)}{\sqrt{(1-2\sigma)}} \qquad (4.5.14)$$

Table 4.5(a) shows how the high frequency axisymmetric and nonaxisymmetric modes in thick disks progress to corresponding shear, plate and compressional modes in cylindrical shells. However, eqns.(4.5.12a) and (4.5.12b) do not describe the lowest two finite frequency modes of the shell (i.e., 1,R and 2,R disk radial modes), for which the assumption that $K \to \infty$ as $\gamma \to 1$ is not valid.

As $\gamma \to 1$, these two modes approach finite frequency values. For a shell, γ can be written as $\gamma = (1 - d\gamma)$, where $d\gamma \to 0$ as $\gamma \to 1$. Thus, using the Taylor series expansion for the Bessel functions, and neglecting the second and higher-order terms in $d\gamma$, we obtain

$$\begin{aligned}
Z_0(\gamma x) &= Z_0(x) + x\, d\gamma\, Z_1(x) \;, \quad Z_1(\gamma x) = (1+d\gamma) Z_1(x) - x\, d\gamma\, Z_0(x), \\
I_0(\gamma x) &= I_0(x) - x\, d\gamma\, I_1(x) \;, \quad I_1(\gamma x) = (1+d\gamma) I_1(x) - x\, d\gamma\, I_0(x), \\
K_0(\gamma x) &= K_0(x) + x\, d\gamma\, K_1(x) \;, \quad K_1(\gamma x) = (1+d\gamma) K_1(x) + x\, d\gamma\, K_0(x),
\end{aligned} \qquad (4.5.15)$$

where $Z = J, Y$ and $x = \delta, \lambda\delta$. Then, the elements of the determinant in eqn.(4.3.2), which involve γ, become

$$\begin{aligned}
X_{4i} &= Z_1(\delta) \left[\left(\frac{K^2\Theta^2}{2} - d\gamma_1\right) W_1(\delta) + \delta^2 (d\gamma_2 - 1) \right] \;, \\
X_{4j} &= Z_1(\lambda\delta) \left[\left(\frac{K^2\Theta^2}{2} - d\gamma_3\right) W_1(\lambda\delta) - d_1 \lambda^2\delta^2 (d\gamma_2 - 1) \right] \;, \\
X_{6i} &= \delta^2 \left(\delta^2 - \frac{K^2}{C}\right) Z_1(\delta) \left[(1 + d\gamma) - d\gamma\, W_1(\delta) \right] \;, \\
\text{and } X_{6j} &= \lambda^2\delta^2 \left(\lambda^2\delta^2 + \frac{K^2}{C}\right) Z_1(\lambda\delta) \left[d_1(1 + d\gamma) - d\gamma\, W_1(\lambda\delta) \right] \;,
\end{aligned} \qquad (4.5.16)$$

where $i = 1,2$; $j = 3,4$;

$Z = J$, $W = M$, for $i = 1$,
$= Y$, $= L$, for $i = 2$,
$= I$, $= N$, for $j = 3$,
$= K$, $= P$, for $j = 4$,

$d_1 = 1$, for $Z = I$,
$= -1$, for $Z = K$,

and $$d\gamma_1 = d\gamma\left(\frac{K^2\theta^2}{2} - \delta^2\right), \quad d\gamma_2 = d\gamma\left(\frac{K^2\theta^2}{2} - 1\right)$$

$$d\gamma_3 = d\gamma\left(\frac{K^2\theta^2}{2} + \lambda^2\delta^2\right) \qquad (4.5.17)$$

Substituting eqns.(4.5.16) and (4.5.17) into eqn.(4.3.2) and simplifying, yields the frequency equation for $\gamma \to 1$, as

$$\left[K^4 - K^2\left\{\frac{4}{(1+\gamma)^2} + \frac{\pi^2\eta^2}{4}\right\} + \frac{\pi^2\eta^2(1-\sigma^2)}{(1+\gamma)^2}\right]\{J_1(\delta)\,Y_0(\delta) - J_0(\delta)\,Y_1(\delta)\}\{I_1(\lambda\delta)K_0(\lambda\delta) + I_0(\lambda\delta)K_1(\lambda\delta)\} = 0 \qquad (4.5.18)$$

Using the following identities[36,37],

$$J_1(x)Y_0(x) - J_0(x)Y_1(x) = 1/x \quad , \quad \text{and}$$
$$I_1(x)K_0(x) + I_0(x)K_1(x) = 1/x \quad , \qquad (4.5.19)$$

eqn.(4.5.18) reduces to

$$\left[K^4 - K^2\left\{\frac{4}{(1+\gamma)^2} + \frac{\pi^2\eta^2}{4}\right\} + \frac{\pi^2\eta^2(1-\sigma^2)}{(1+\gamma)^2}\right] = 0 \quad , \qquad (4.5.20)$$

which is the frequency equation for the lowest two vibrations of cylindrical [8,38] shells. The two positive real roots of eqn.(4.5.20) for annular disks (i.e., $\eta \geq 2$), can be obtained, using the binomial expansion, as

$$K^s_{1R} = \frac{2}{(1+\gamma)}\left[1 + \frac{\pi^2\eta^2\sigma^2\,(1+\gamma)^2}{\{16 - \pi^2\eta^2\,(1+\gamma)^2\}}\right]^{\frac{1}{2}} \qquad (4.5.21a)$$

and $$K^s_{2R} = \frac{\pi\eta}{2}\left[1 - \frac{16\,\sigma^2}{\{16 - \pi^2\eta^2\,(1+\gamma)^2\}}\right]^{\frac{1}{2}} \qquad (4.5.21b)$$

where the superscript s refers to the shell. These two equations represent the shell counterparts of the first two radial vibrations of thick disk, respectively. Table 4.5(b) shows the experimental frequencies of first two radial modes of an aluminium shell with $\gamma = 0.9$ and diameter 5 cms., and the theoretical frequencies calculated from eqns.(4.5.21), for $\eta = 2, 4$ and 8. There is a good agreement between the theory and the experiment.

1/η / Mode	0.50			0.25			0.125		
	$K\Theta(1-\gamma)$	$\delta(1-\gamma)$	$\overline{\lambda}\delta(1-\gamma)$	$K\Theta(1-\gamma)$	$\delta(1-\gamma)$	$\overline{\lambda}\delta(1-\gamma)$	$K\Theta(1-\gamma)$	$\delta(1-\gamma)$	$\overline{\lambda}\delta(1-\gamma)$
3,R		3.1471			3.1457			3.1440	
4,R			3.1421			3.1410			3.1435
3,1	3.1539			3.1540			3.1540		
4,1		3.1463			3.1446			3.1429	
5,1			3.1374			3.1366			3.1498
4,2	3.1963			3.1711			3.1712		
5,2		3.1485			3.1452			3.1403	
6,2			3.1248			3.1246			3.1384
4,3	3.2139			3.1988			3.1995		
5,3		3.1498			3.1425			3.1357	
6,3			3.1071			3.1076			3.1222
4,4	3.2084			3.2356			3.2382		
5,4		3.1511			3.1396			3.1238	
6,4			3.0867			3.0880			3.1034

Table 4.5(a) This table shows the progression of high frequency thick disk modes to shear, plate(or axial shear) and compressional modes of the shell. $\gamma = 0.90$, $\sigma = 0.30$.

Mode / 1/η	K_{1R}		K_{2R}	
	Calculated	Measured	Calculated	Measured
0.50	33.977	34.101	109.006	109.124
0.25	34.182	34.165	216.185	215.409
0.125	34.228	34.235	432.885	-

Table 4.5(b) The theoretical and experimental frequencies of the first two radial modes of an aluminium shell. $\sigma = 0.33$, $\gamma = 0.9$, $2a = 5$ cms.

4.5.3 Vibrations of an Annular Ring

The frequency equation for the compound modes of vibration of annular rings can be obtained, as a limiting case, from the corresponding frequency equation (4.2.3), by equating the thickness-to-diameter ratio to zero. Therefore, for a thin disk, as $\eta \to \infty$, $\delta \to K^T$, $\lambda\delta \to \infty$ and hence $M_n(\delta) \to M_n(K^T)$, $L_n(\delta) \to L_n(K^T)$, $N_n(\lambda\delta) \to \lambda\delta$ and $K_n(\lambda\delta) \to 0$. Substituting these in eqn.(4.2.3), dividing the elements X_{3j}, X_{6j}; j=1 to 6, by $\lambda\delta$, and elements X_{i3}, X_{i4}; i=1 to 6 by $\lambda^2\delta^2$ and simplifying yields

$$F(K^T) = \begin{vmatrix} X_{11} & X_{12} & X_{15} & X_{16} \\ X_{21} & X_{22} & X_{25} & X_{26} \\ X_{41} & X_{42} & X_{45} & X_{46} \\ X_{51} & X_{52} & X_{55} & X_{56} \end{vmatrix} = 0 \quad , \qquad (4.5.22)$$

which is the frequency equation (3.2.1) derived, independently, in chapter 3 for compound modes of an annular ring, where the elements of the above determinant are given by eqns.(4.2.4), by replacing δ by K^T.

4.6 Discussion

Table 4.6 summarises the thick disk and shell resonances, which constitute the limiting cases of the corresponding resonances of the thick annular disk. In contrast to only one series of finite frequency modes in the case of a thin ring, there are two series of finite frequency modes in a cylindrical shell. There are two series of asymptotic modes for radial resonances of a shell whereas there is only one for pure radial modes of a ring. For compound modes of vibration, there are three series of asymptotic modes in a cylindrical shell as opposed to only two series in a thin ring, as shown in Tables 4.6 and 3.6, respectively. However, the pure torsional modes remain the same in both cases.

The pure radial modes are solutions of eqn.(4.3.6). The frequency increases rapidly with hole size, for all modes except the two lowest

	Torsion	Radial
Thick Disk	(1,T),(2,T),(3,T),...	(3,R),(5,R),... (4,R),(6,R),...
Shell	p= 1 2 3 ...	p= 1 2 ... q= 1 2 ...
	Flexural	**Finite Frequency**
Thick Disk	(1,2),(1,3),(1,4),...	(1,R) (1,1) (2,2) (2,3) (2,4) ... (2,R) (2,1) (3,2) (3,3) (3,4) ...
Shell	n= 2 3 4 ...	n= 0 1 2 3 4 ...
	Compound Shear	
Thick Disk	(3,1),(4,2),(4,3),...	(6,1),(7,2),(7,3),...
Shell	q= 1	q= 2
	Compound Plate (or axial shear)	
Thick Disk	(4,1),(5,2),(5,3),...	(7,1),(8,2),(8,3),....
Shell	p= 1	p= 2
	Compound Compressional	
Thick Disk	(5,1),(6,2),(6,3),...	(8,1),(9,2),(9,3),...
Shell	r= 1	r= 2

Table 4.6 Correspondence of thick disk and cylindrical shell resonances.

modes given by eqn.(4.5.20), making the width of the shell, $a(1-\gamma)$, to be an integral number of half wavelengths, the integer being the number of nodal circles. The ratio of the phase velocity C_{phase} to the plate velocity C_p or compressional velocity C_c can be obtained, for radial modes, from eqns.(4.5.12a & b), as

$$\frac{C_{phase}}{C_{plate}} = \frac{K(1-\gamma)}{p\pi} = \frac{K}{\delta} \qquad (4.6.1)$$

$$\frac{C_{phase}}{C_c} = \frac{K_c(1-\gamma)}{r\pi} = \frac{K_c}{\lambda\delta} \qquad (4.6.2)$$

where $K_c = K/\sqrt{c}$, $a(1-\gamma) = p\lambda/2$ in eqn.(4.6.1) and $a(1-\gamma) = r\lambda/2$ in eqn. (4.6.2). The modes (3,R) and (4,R) are the lowest modes of these series, respectively. Figs.4.2 show the variation of C_{phase}/C_{plate}, with γ, for modes (3,R) and (5,R), for thickness-to-diameter ratios 0.5, 0.25 and 0.125, respectively. The figures show that as γ approaches unity, the ratio C_{phase}/C_{plate} approaches the value K/δ. The figures also show that, for $\gamma \simeq 1$, as the thickness-to-diameter ratio approaches zero, the velocity ratio approaches unity, indicating that, ultimately, this mode propagates with plate velocity as in the thin ring. Figs.4.3 show the ways in which the ratio C_{phase}/C_c, where C_c is the compressional velocity, approaches unity as $\gamma \to 1$.

The compound modes of thick disks which have nodal diameters but no nodal circles, (1,n) are the direct counterparts of the flexural modes of shells. Fig.4.4 shows the progression from finite frequency disk resonances to zero frequency resonances of the thin shell, for the first four flexural modes, for $\eta = 2$, $\sigma = 0.3$. Table A.4.1 gives K values for these modes, for a full range of σ, γ and η. As γ approaches the shell region, the frequency (i.e., $K_o = \omega a/C_o$, value) becomes independent of σ, as in the case of a thin ring.

It is of particular interest to study the finite frequency modes of the cylindrical shell and their thick disk counterparts. There are

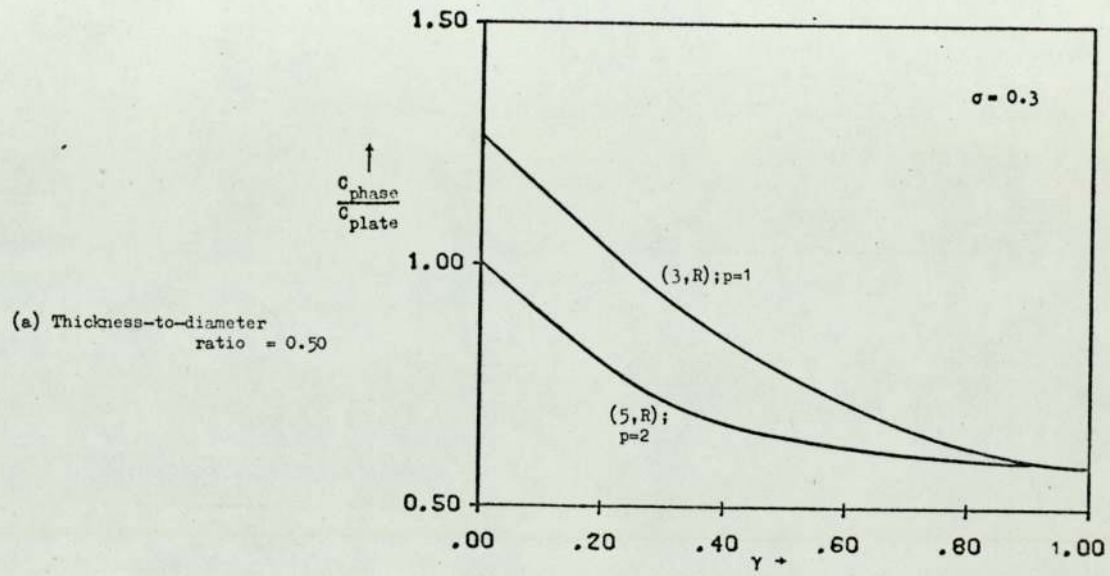

(a) Thickness-to-diameter ratio = 0.50

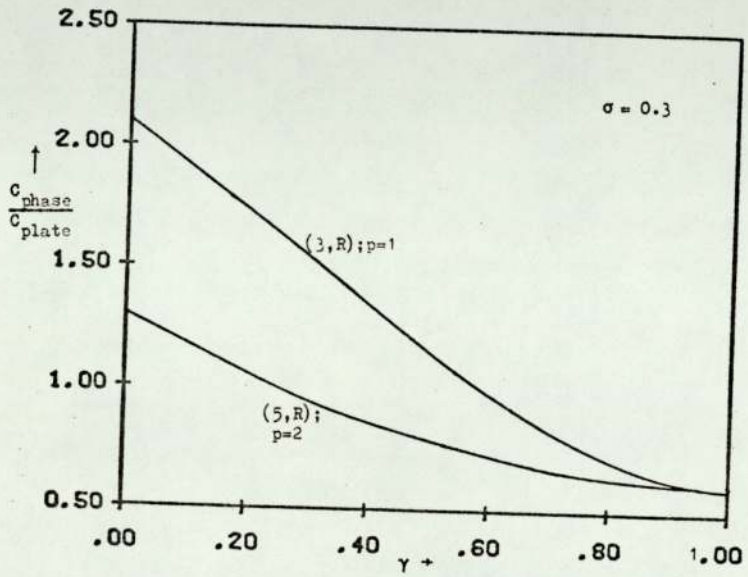

(b) Thickness-to-diameter ratio = 0.25

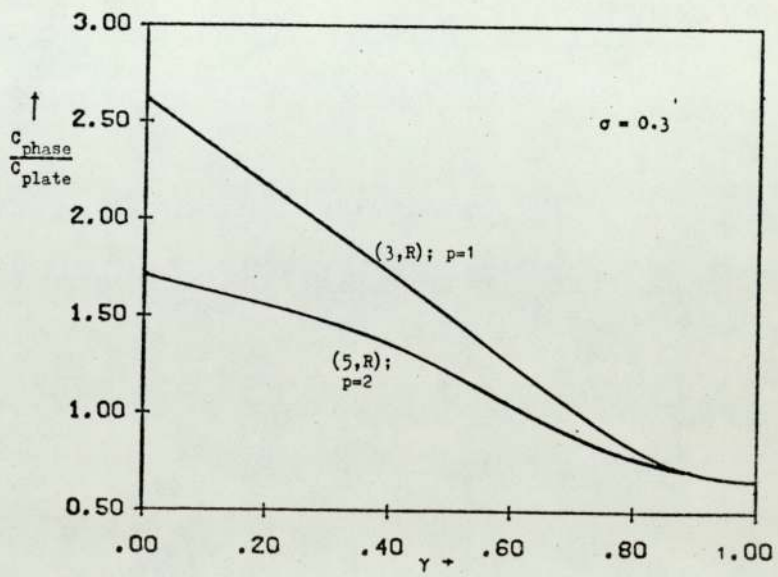

(c) Thickness-to-diameter ratio = 0.125.

Fig.4.2 The first two radial (axial shear or plate) modes, whose velocities tend, asymptotically, to $C_\delta = (K\, C_{plate}/\delta)$, as $\gamma \to 1$.

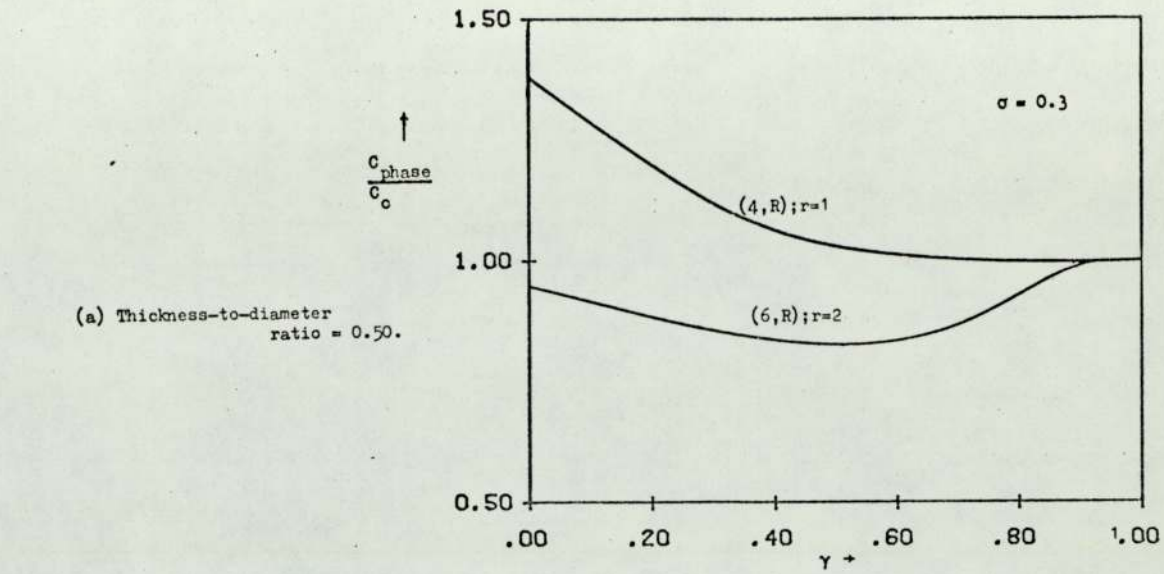

(a) Thickness-to-diameter ratio = 0.50.

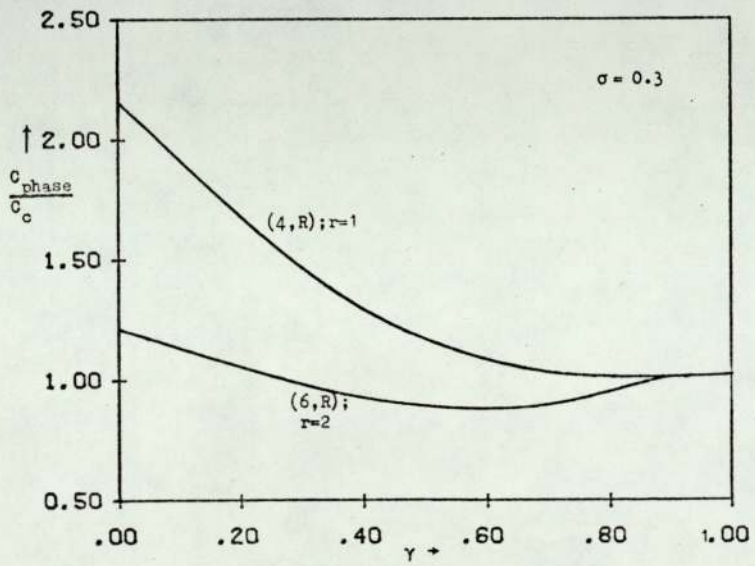

(b) Thickness-to-diameter ratio = 0.25.

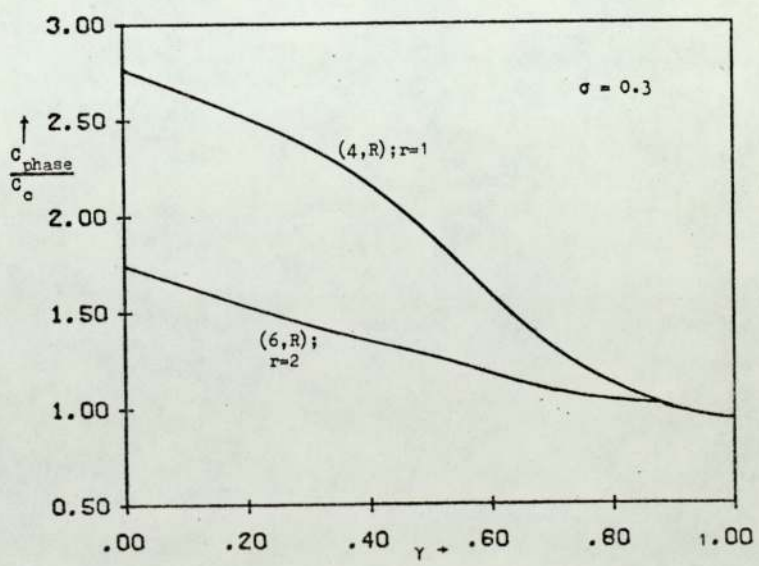

(c) Thickness-to-diameter ratio = 0.125.

Fig.4.3 The first two pure radial(Compressional) modes, whose velocities tend, asymptotically, to $(K/\lambda\delta\sqrt{c})$, as $\gamma \to 1$.

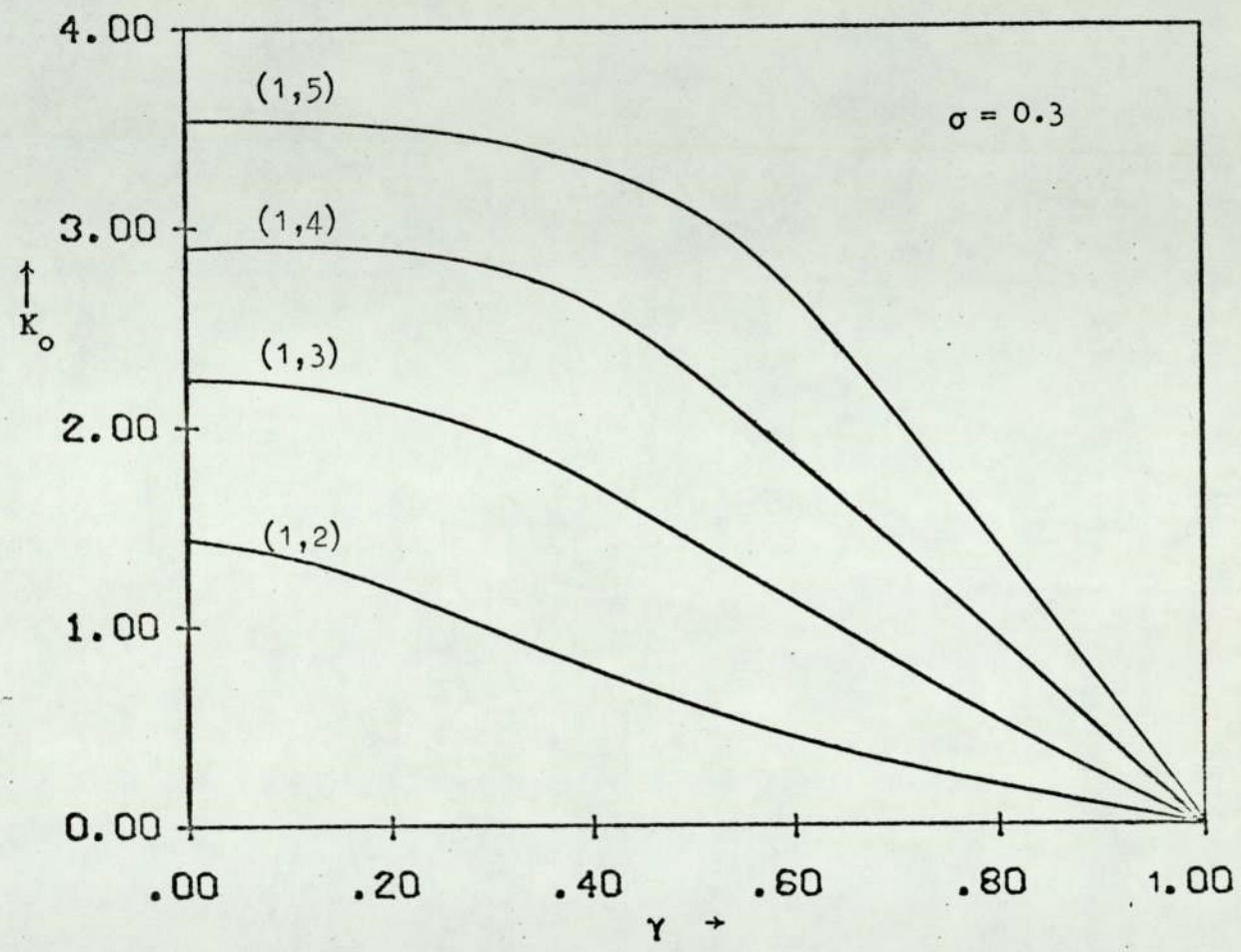

Fig.4.4 The first four flexural (Compound) modes for $\eta = 2.0$, which go to zero frequency as γ approaches the shell region. For $\gamma \to 1$, these modes become less dependent on σ.

two sets of finite frequency modes in cylindrical shells. Figs.4.5 show the variation of K_o values of first set of finite frequency modes, namely, (1,R),(1,1),(2,2) and (2,3), with γ, for σ =0.3 and for various η's. These modes are less dependent on Poisson's ratio in the shell region.

The lowest mode in this series is (1,R), as given by eqn.(4.5.21a) for the shell, and this can be easily excited by a radial drive, while all the other modes of this first set require a tangential or an angular drive. The experiments confirmed that the first set of n=0,1,2,3,..., shell modes have the thick disk counterparts of (1,R),(1,1),(2,2),(2,3), ...,etc., modes, respectively. The (1,R) disk radial mode frequency is greater than that of the (1,1) mode and the curves cross at a low γ value as the frequencies move to the corresponding shell values. The crossover occurs for all values of σ , the position, for σ =0.3, being γ =0.259,0.275, and 0.266 for η =2,4 and 8, respectively.

The variation of the second set of finite frequency shell modes, with γ, is illustrated in Figs.4.6, for different thickness-to-diameter ratios. These modes have different dependence on η and vary enormously with γ and η . The lowest mode of this second set, for $\gamma \to 1$, is again a radial mode (2,R), for η =2.0, as given by eqn.(4.5.21b). All these modes can be observed experimentally by radial drive alone. The second set of n=0,1,2,3,...,etc., shell modes have their thick disk counterparts as (2,R),(2,1),(3,2),(3,3),...,etc., modes, respectively. The slow transformation of these modes, for $\gamma \to 1$, from finite frequencies to asymptotic (infinite) frequencies, as $\eta \to \infty$, is evident from Fig.4.6(c), in which all the modes are gradually moving to infinite frequency values as $\gamma \to 1$. This indicates that the second set of finite frequency modes of a cylindrical shell move to the corresponding asymptotic modes of a thin ring.

It may be interesting to study the extensional vibrations of thin

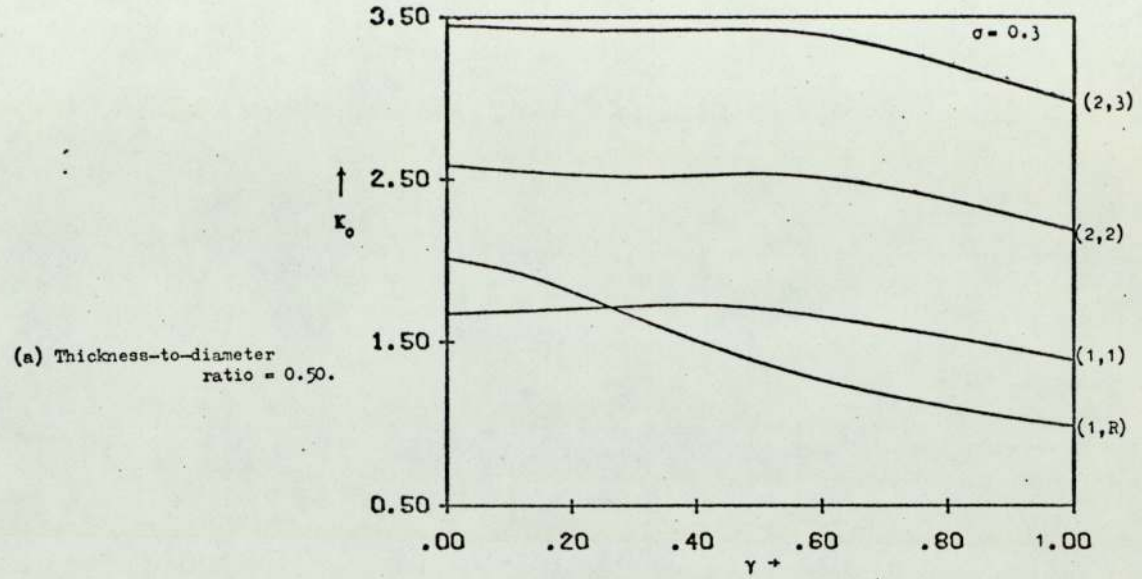

(a) Thickness-to-diameter ratio = 0.50.

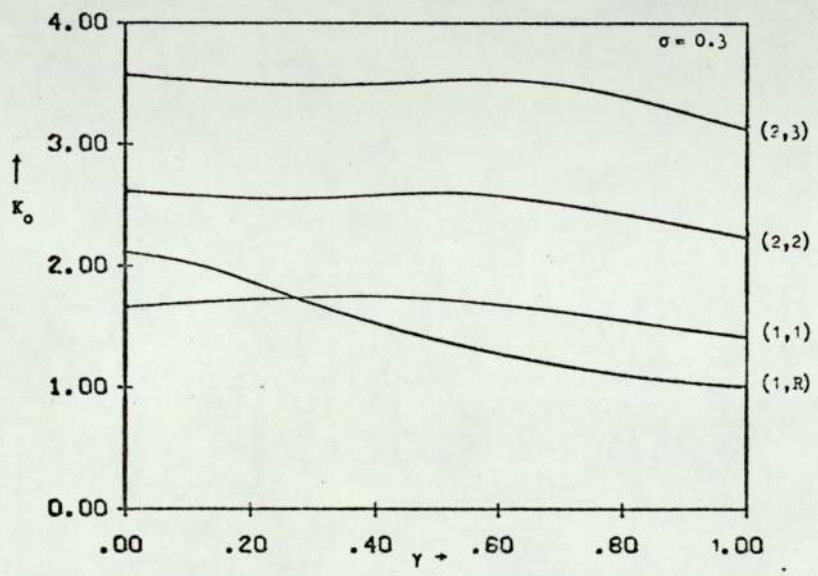

(b) Thickness-to-diameter ratio = 0.25.

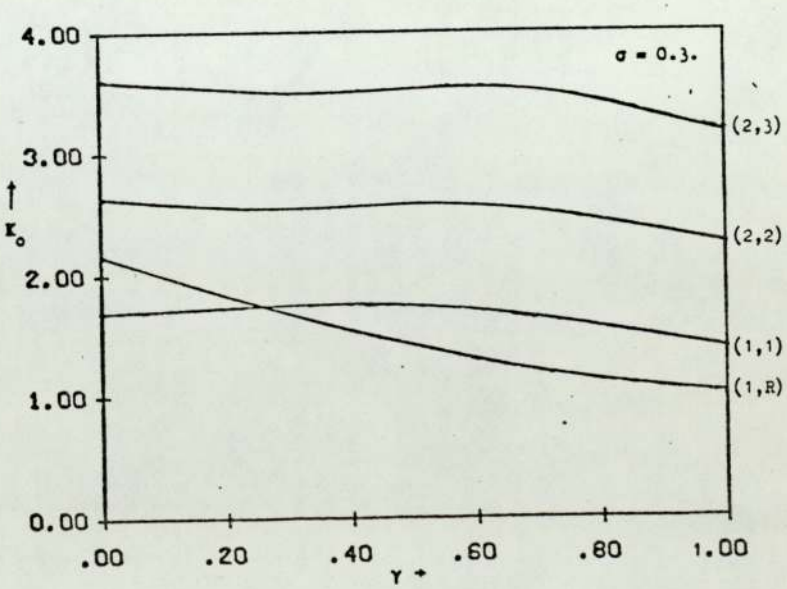

(c) Thickness-to-diameter ratio = 0.125.

Fig.4.5 A typical family of first finite frequency modes for various η's. These modes become less dependent on σ as γ → 1.

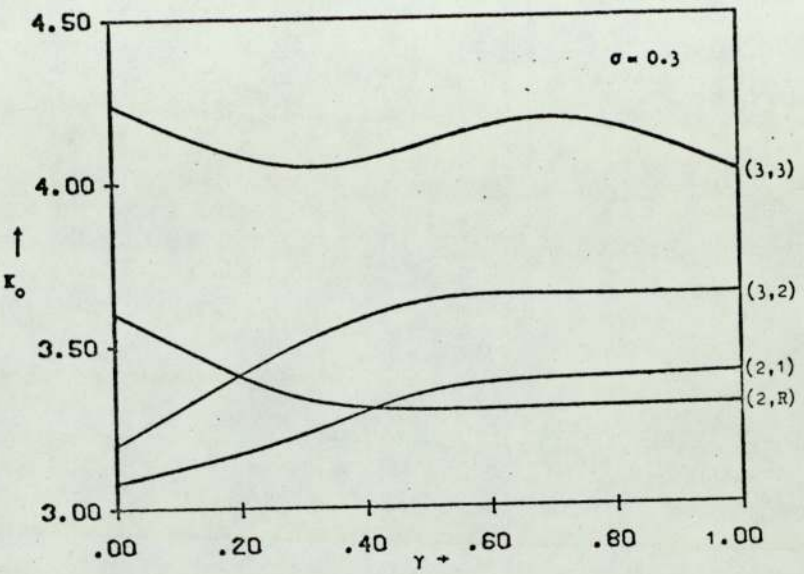

(a) Thickness-to-diameter ratio = 0.50.

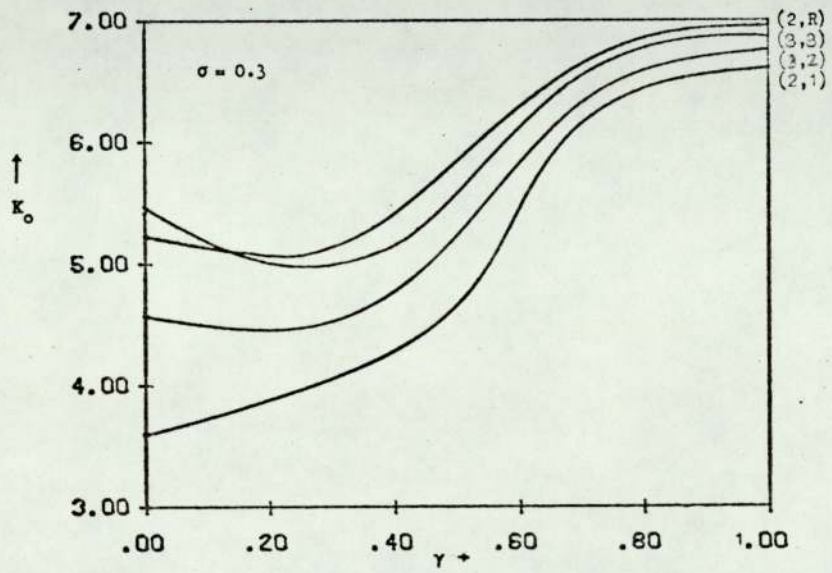

(b) Thickness-to-diameter ratio = 0.25.

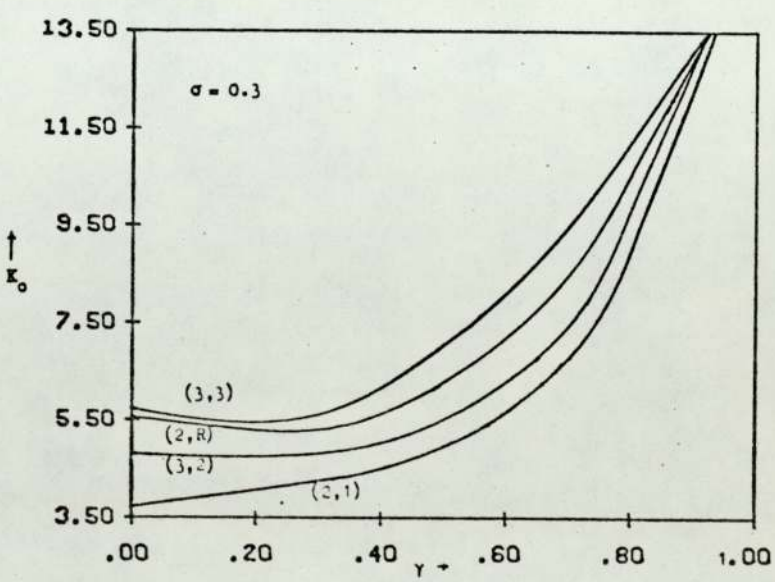

(c) Thickness-to-diameter ratio = 0.125.

Fig.4.6 The second set of finite frequency modes of cylindrical shells for a wide range of thickness-to-diameter ratios. Notice that the finite frequency modes tend to asymptotic modes, for $\eta \to \infty$.

cylindrical shells, given by eqn.(4.5.20). The two roots of this equation, as given by eqns.(4.5.21a) and (4.5.21b), are the K_{1R} and K_{2R} modes of the shell, respectively. The K values for the corresponding radial modes of a thick annular disk can be obtained from the frequency eqn.(4.3.6). Then, the following ratios of K values can be obtained from eqns.(4.5.21):

$$\frac{K_{1R}}{K^s_{1R}} = \frac{K_{1R}(1+\gamma)}{2\left[1 + \frac{\pi^2\eta^2\sigma^2(1+\gamma)^2}{\{16 - \pi^2\eta^2(1+\gamma)^2\}}\right]^{\frac{1}{2}}} \tag{4.6.3}$$

$$\frac{K_{2R}}{K^s_{2R}} = \frac{2K_{2R}}{\pi\eta\left[1 - \frac{16\,\sigma^2}{\{16 - \pi^2\eta^2(1+\gamma)^2\}}\right]^{\frac{1}{2}}} \tag{4.6.4}$$

The above equations were used to investigate the departure from the corresponding radial mode frequencies of the shell as a function of σ, γ and η, and the resulting curves for various η's are plotted in Figs.4.7(a) and (b), respectively.

The higher compound modes, like pure radial and tangential modes, approach infinite frequency as $\gamma \to 1$, for each η, the asymptotic values being the solutions of eqns.(4.5.9a), (4.5.9b) and (4.5.9c) for plate, shear and compressional waves, respectively, where p, q and r are the number of nodal circles. The ways in which the limit values are approached, as $\gamma \to 1$, are shown in Figs.4.8 for the two δ(plate) modes (4,1), (5,2), Figs.4.9 for the two shear modes (3,1),(4,2) and Figs.4.10 for the two $\lambda\delta$(compressional) modes, all for various thickness-to-diameter ratios. The asymptotic values, for $\gamma \simeq 1$, are equal to $K\pi/\delta$ for δ modes, π for shear modes and $K_c\pi/\lambda\delta$ for compressional modes, where the integers p,q and r are, therefore, equal to unity. It may be interesting to note that, for $\gamma \simeq 1$, as η is increasing, the asymptotic values corresponding to the thin ring are approached, namely, π for δ(plate) and shear modes and 2π for the compressional modes.

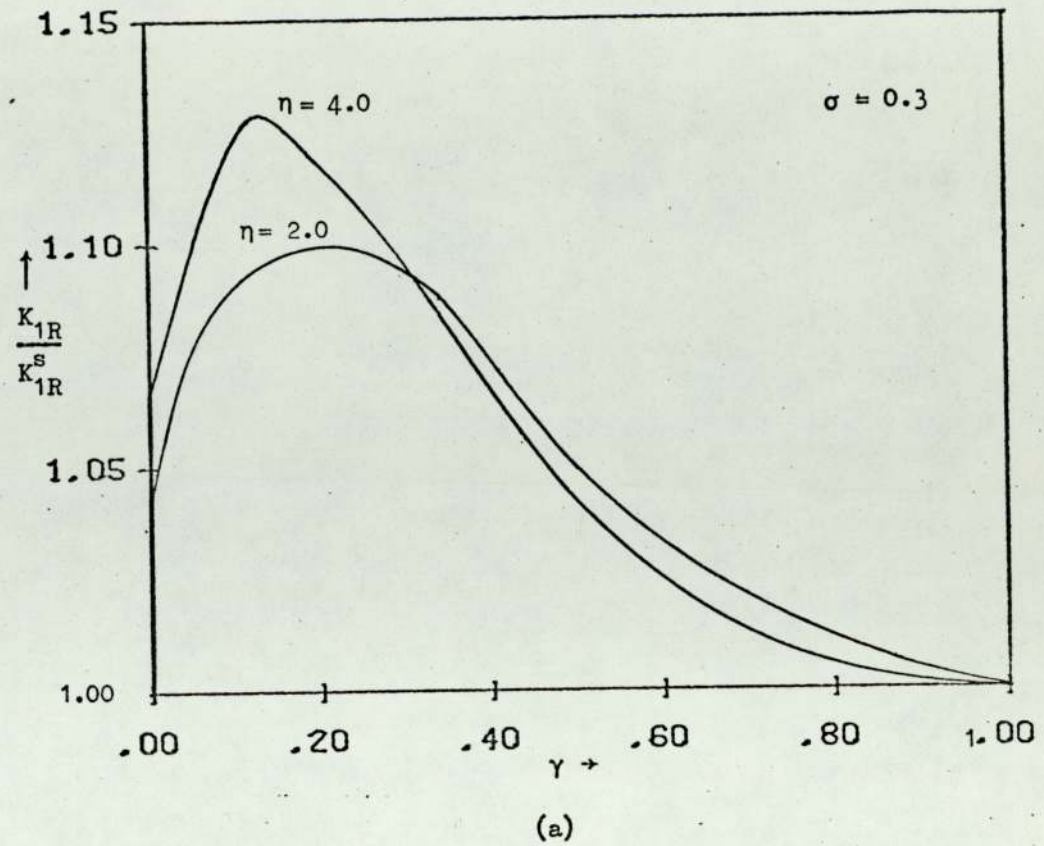

(a)

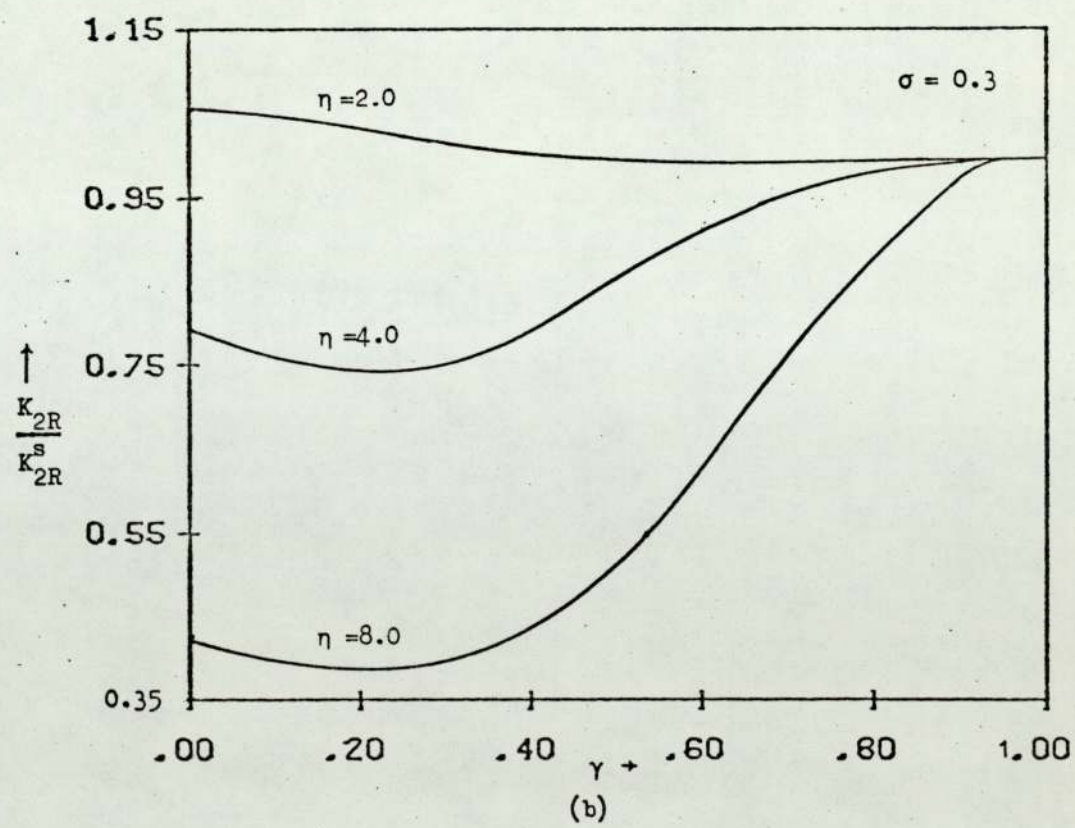

(b)

Fig.4.7 The deviation of the frequencies predicted by the shell theory for the radial modes (a) K_{1R} and (b) K_{2R}.

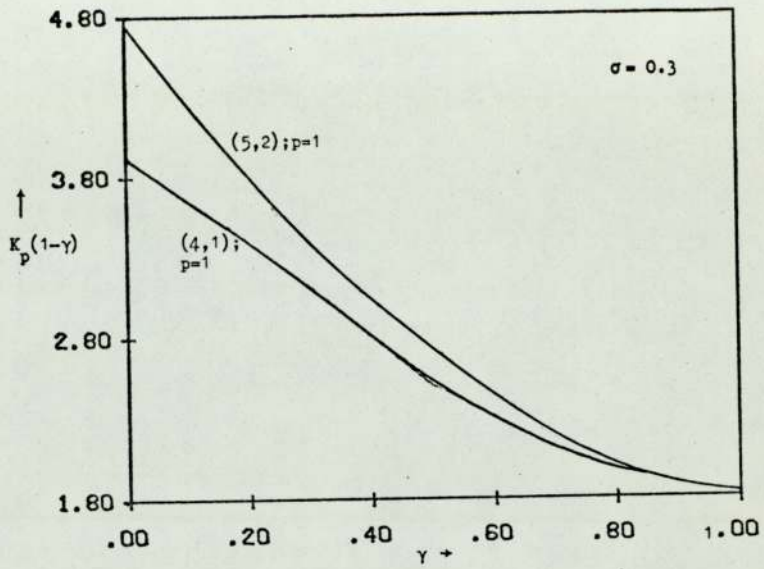

(a) Thickness-to-diameter ratio = 0.50.

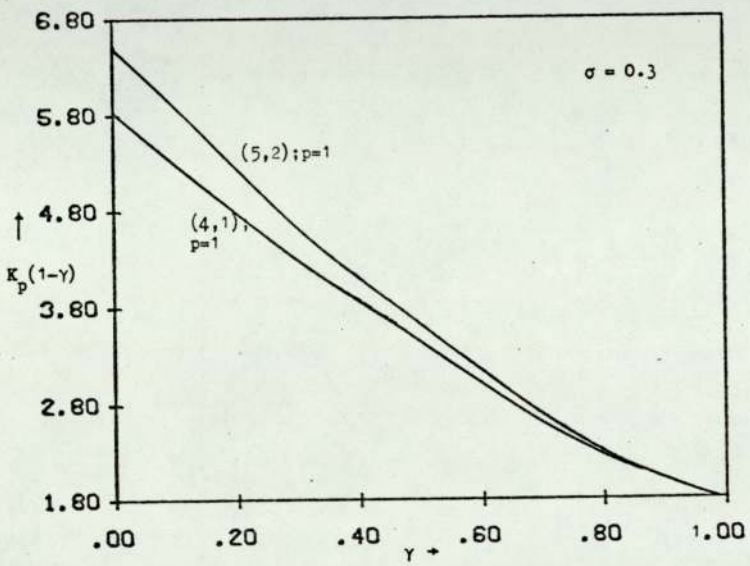

(b) Thickness-to-diameter ratio = 0.25.

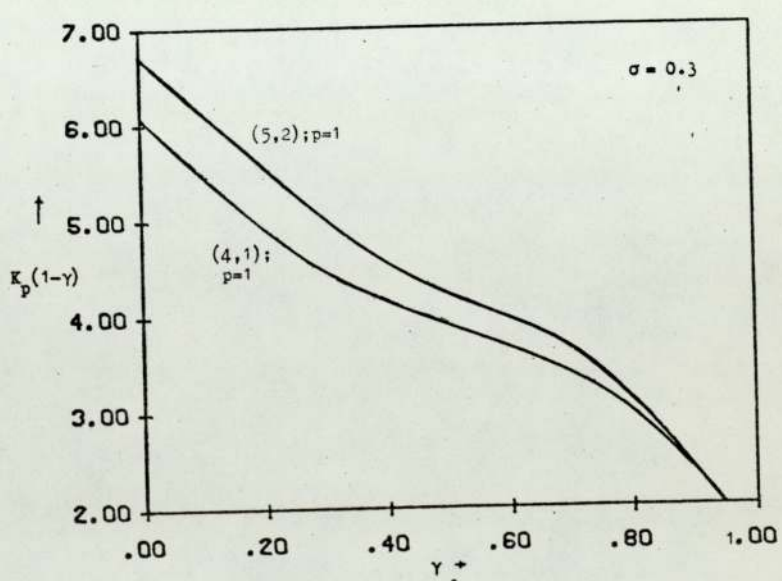

(c) Thickness-to-diameter ratio = 0.125.

Fig.4.8 The $K_p(1-\gamma)$ values for (4,1) and (5,2) plate (δ) modes, as a function of γ.

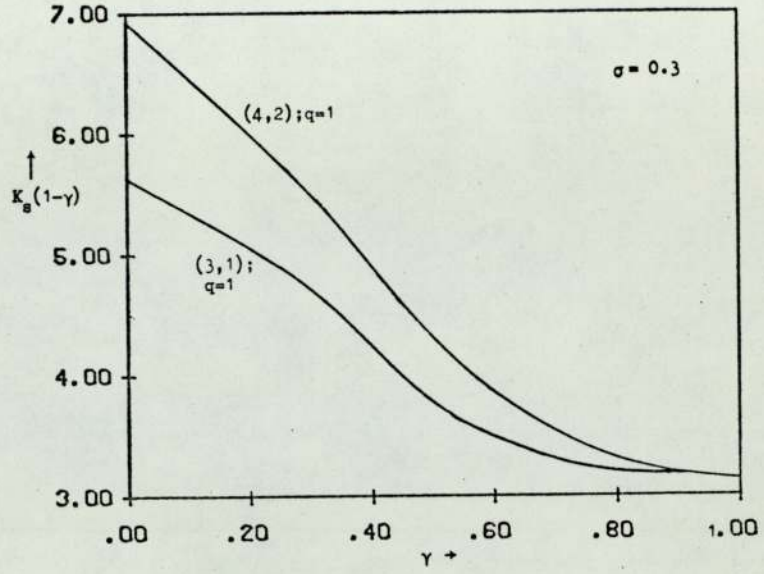

(a) Thickness-to-diameter ratio = 0.50.

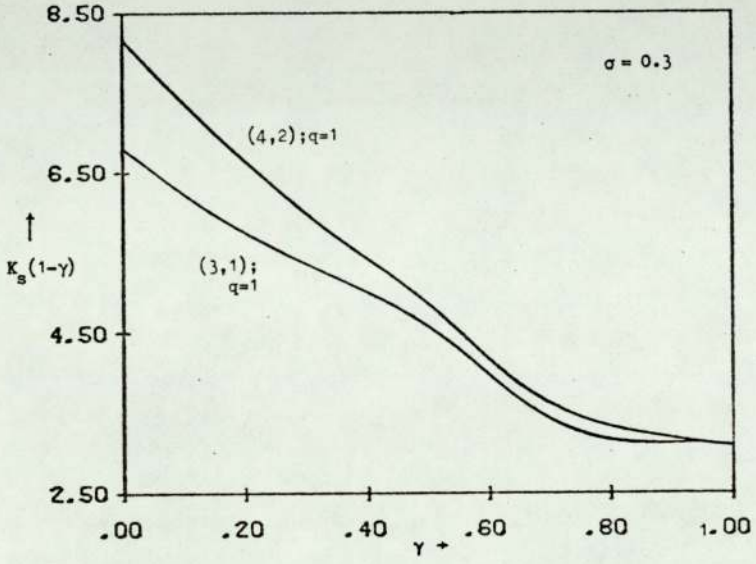

(b) Thickness-to-diameter ratio = 0.25.

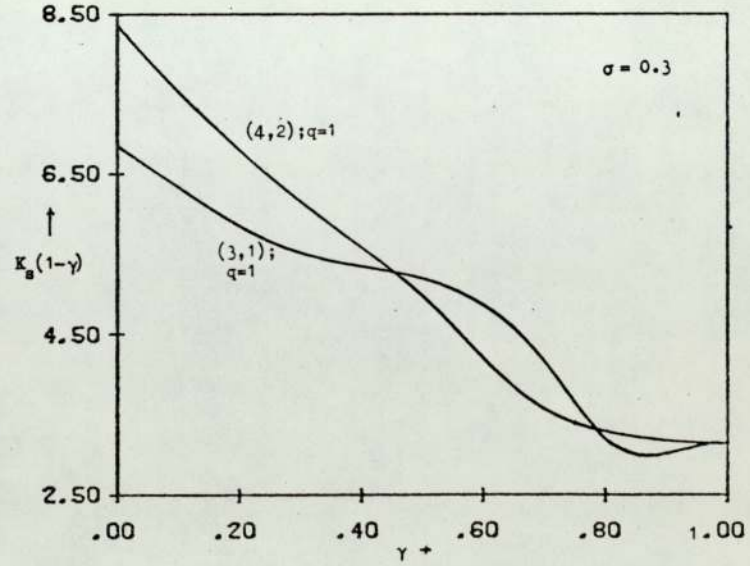

(c) Thickness-to-diameter ratio = 0.125.

Fig.4.9 The $K_s(1-\gamma)$ values for (3,1) and (4,2) shear modes, as a function of γ.

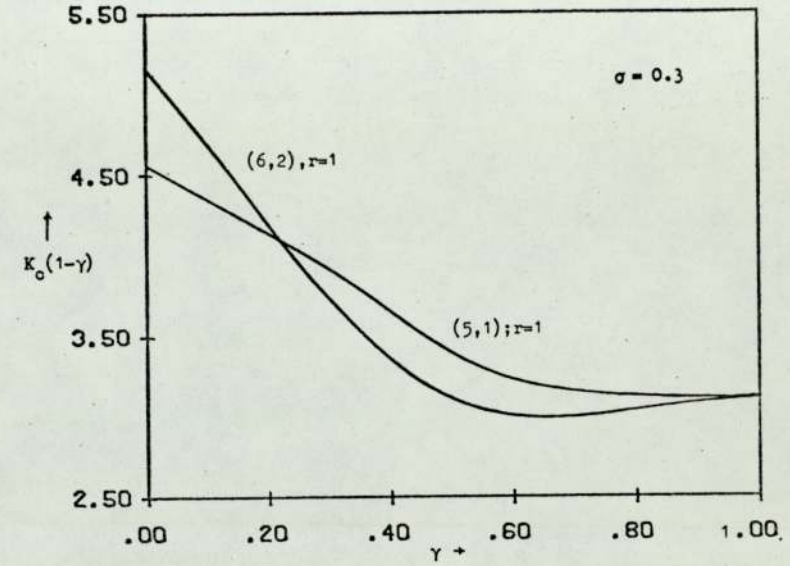

(a) Thickness-to-diameter ratio = 0.50.

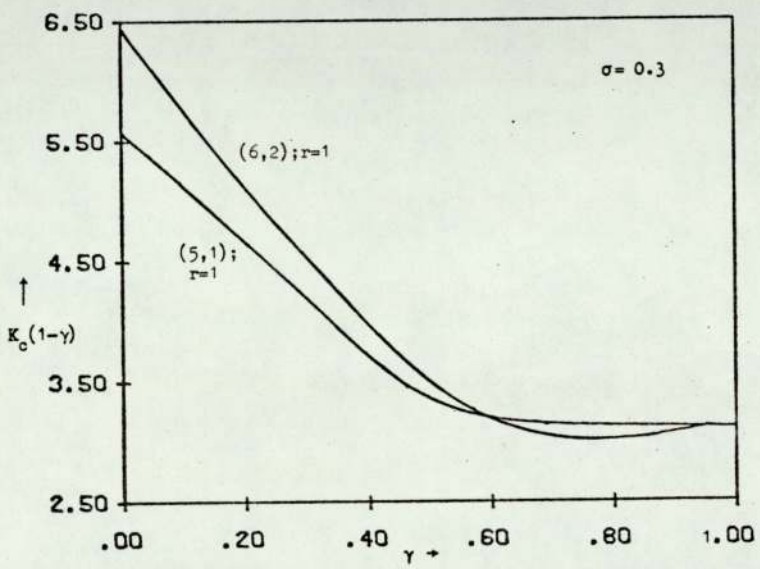

(b) Thickness-to-diameter ratio = 0.25.

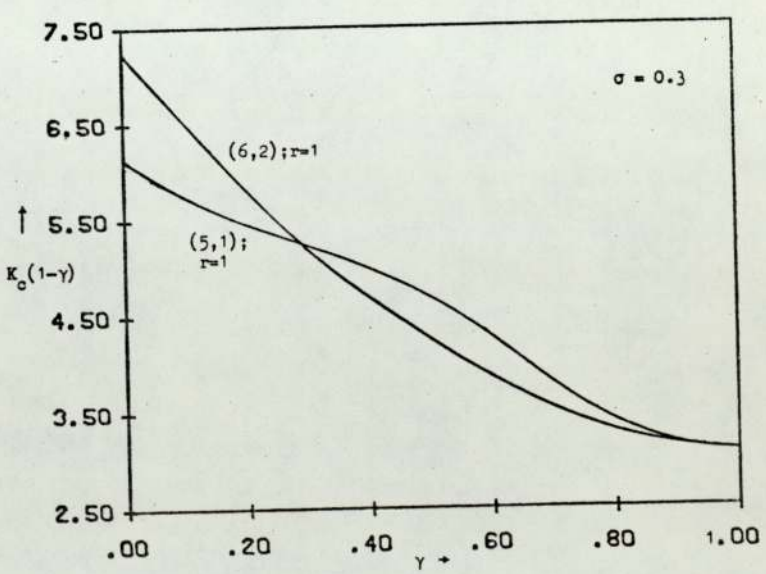

(c) Thickness-to-diameter ratio = 0.125.

Fig.4.10 The plot of $K_c(1-\gamma)$ values versus γ, for (5,1) and (6,2) compressional modes.

The variation of first finite frequency modes, (1,R),(1,1),(2,2) and (2,3), with η is shown in Figs.(4.11) for γ =0.0,0.5 and 0.9. It may be noted that the frequency variation with η for the lowest modes 1,R and 1,1 is more significant for smaller values of γ than that for γ =0.9, whereas the variation for the (2,2) and (2,3) modes are the same for all γ's. It will be noted that the K values of these modes shown in Fig.4.11(a), for γ =0.0 and $1/\eta$ =0.0, correspond to those of the thin disk modes and the K values of the modes shown in Fig.4.11(c), for γ =0.9 and $1/\eta$ =0.0, correspond to those of the ring finite frequency modes.

Fig.4.12 shows the progression of shell radial modes to ring radial modes. The designation of the modes are thus different for the shell and the ring. It may be noted from the figure that the K_{2R} and K_{3R} shell modes progress to a single mode K^T_{2R}, which is a thin ring plate mode with p=1. Similarly, K_{4R} and K_{5R} of the shell merge to the mode K^T_{3R}, which is also a plate mode of the ring, for p=2.

In Figs.4.13 and 4.14, the second finite frequency modes and the two asymptotic modes of the shell are shown for n=1 and 2, respectively. It may be noted from the figures that the modes K_{21} and K_{41} and the modes K_{32} and K_{52} of the shell progress and merge to the thin ring plate modes K^T_{31} and K^T_{42}, respectively. It may also be noted that the shear modes K_{31} and K_{42} of the shell remain same as the corresponding shear modes K^T_{21} and K^T_{32} of the ring, respectively.

Other higher compound modes of the shell were investigated for γ=0.9, σ =0.3 and the results are tabulated in Table 4.7, for η =2.0, 4.0 and 8.0, which predicts the wave velocities C_{phase}/C_p, for δ(plate) modes, C_{phase}/C_s, for shear modes and C_{phase}/C_c, for compressional modes. The lowest mode is the (3,1) which heads the shear mode series (3,1), (4,2),(4,3),(4,4),...,etc., and the higher modes are the δ(plate) mode series (4,1),(5,2),(5,3),(5,4),...,etc., and the compressional mode

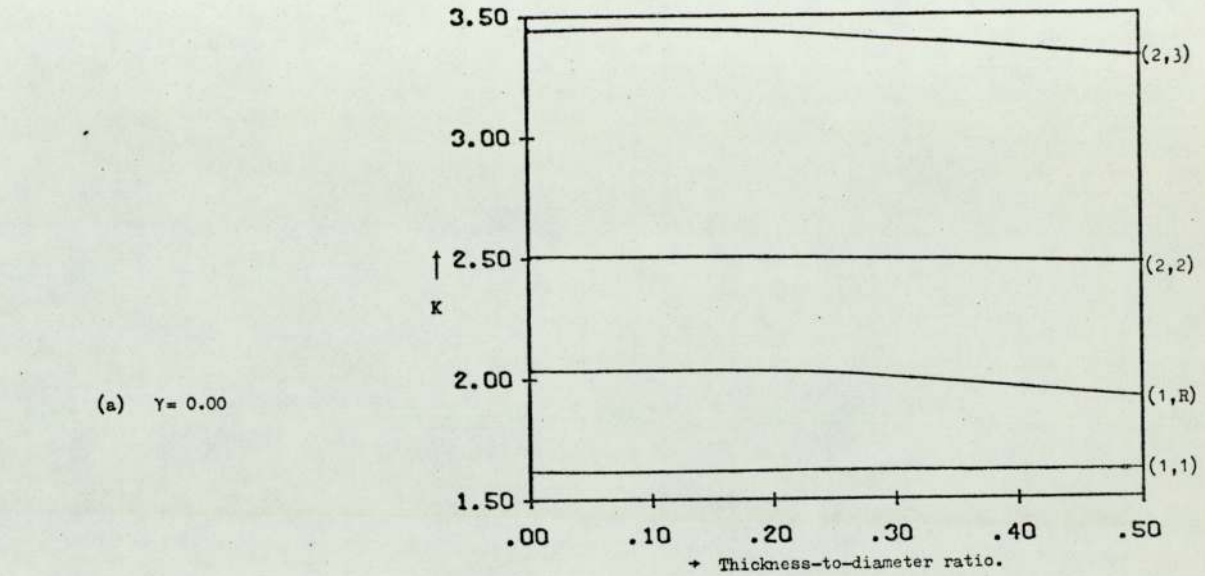

(a) $\gamma = 0.00$

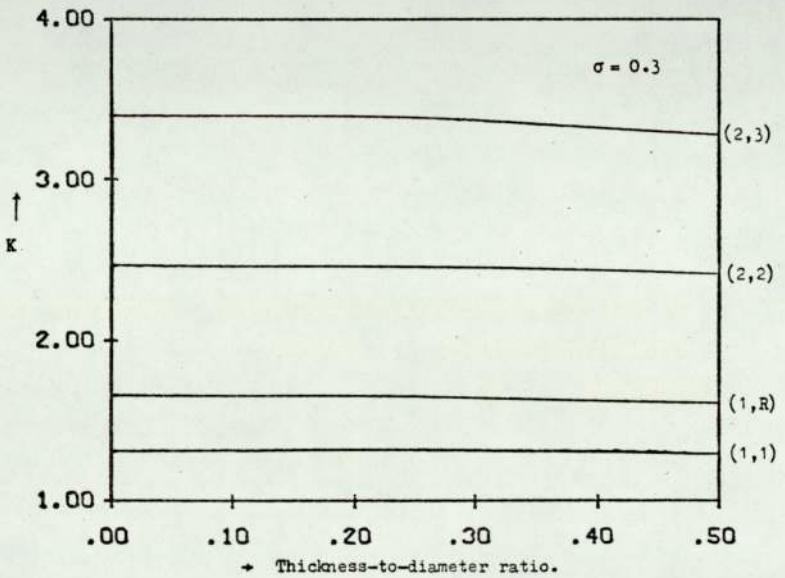

(b) $\gamma = 0.50$.

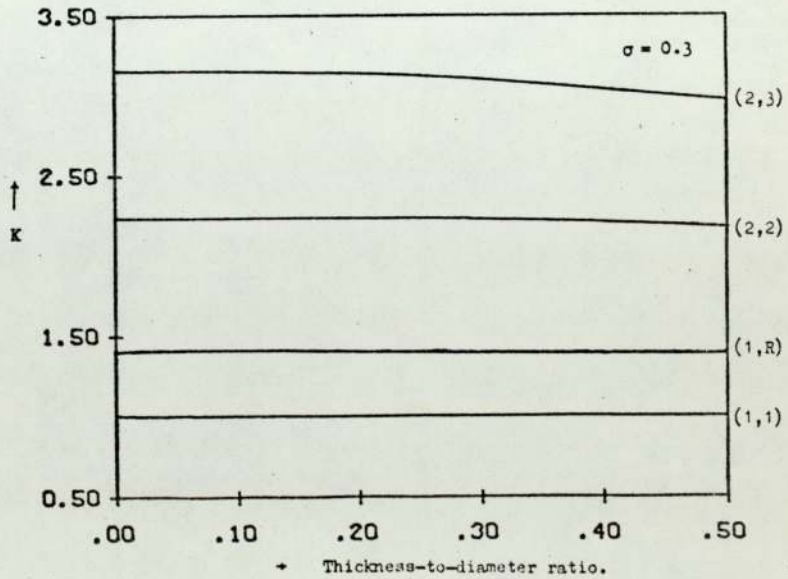

(c) $\gamma = 0.90$.

Fig.4.11 The variation of first set of finite frequency modes with thickness-to-diameter ratio, for $\sigma = 0.30$.

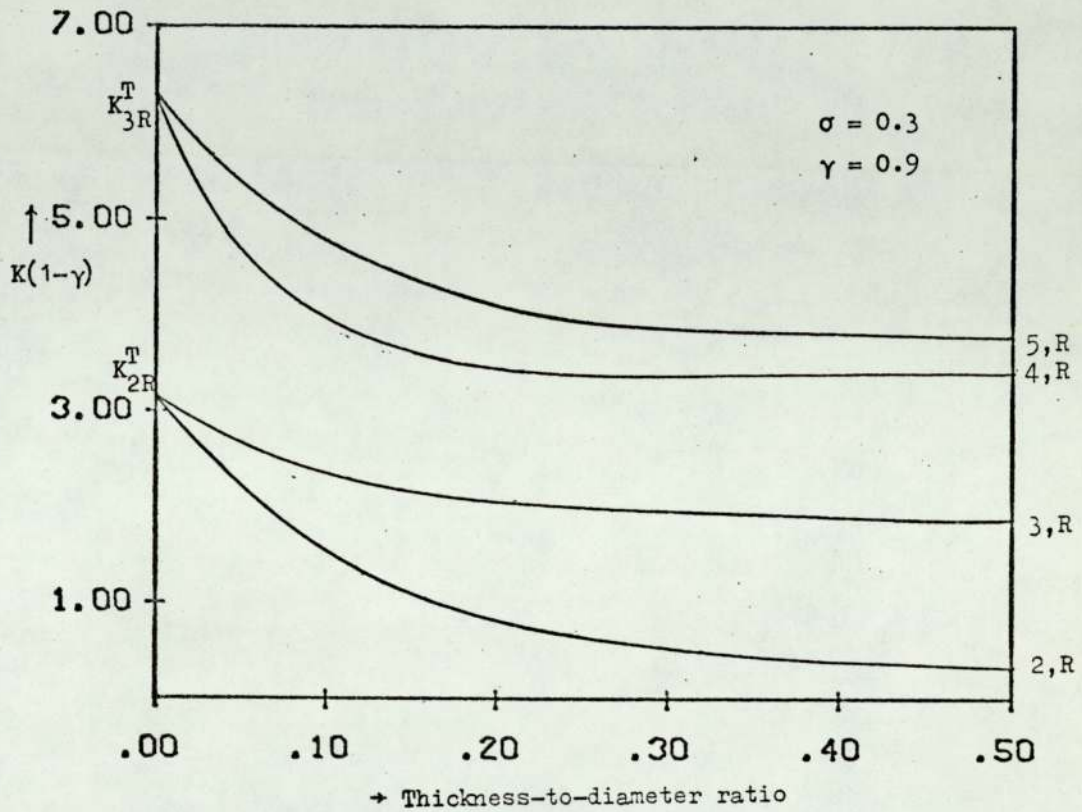

Fig.4.12 The variation of higher radial modes with thickness-to-diameter ratio. Notice that the two modes K_{2R} and K_{3R} of shell merge to a single mode K^T_{2R} of ring. Similarly, K_{4R} and K_{5R} progress to K^T_{3R}.

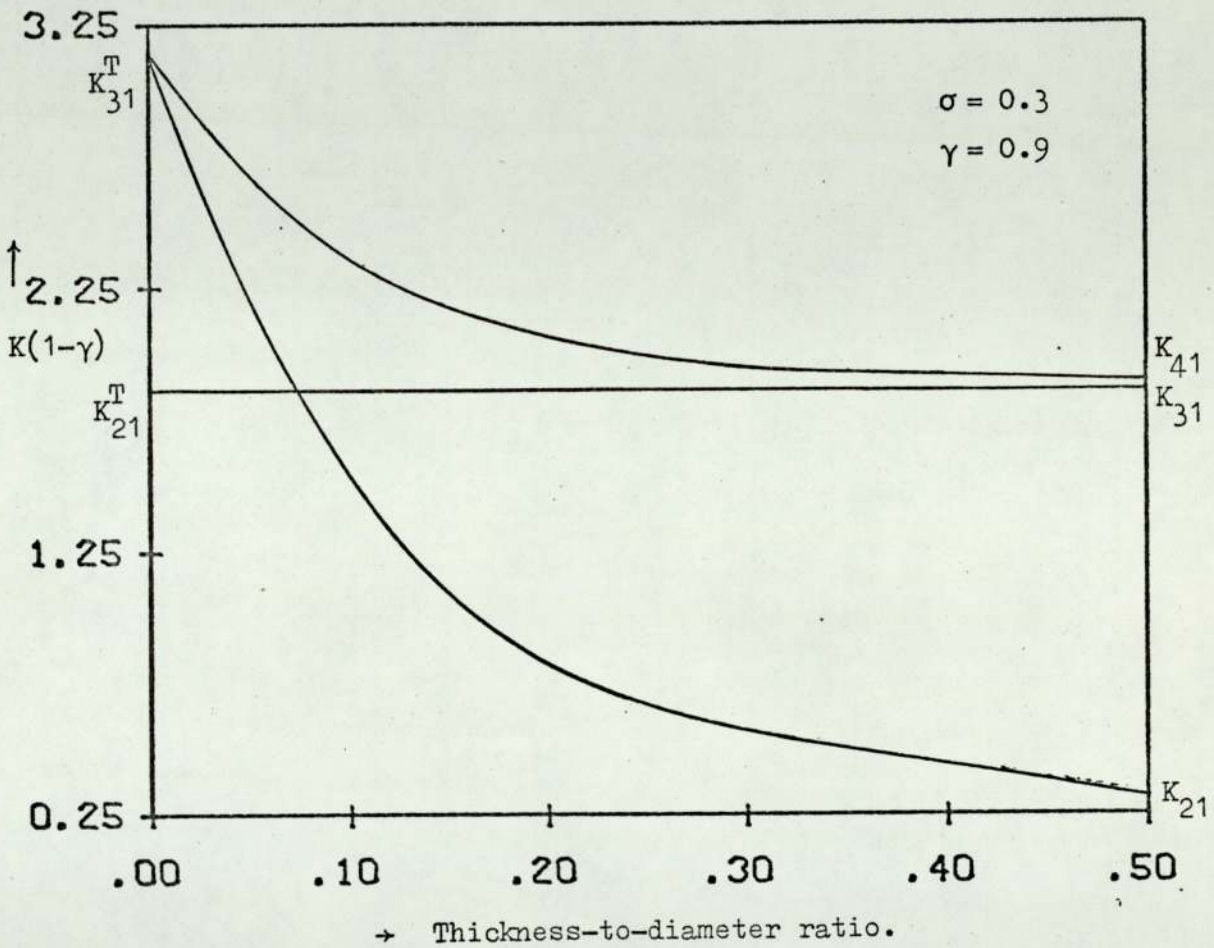

Fig.4.13 The variation of higher compound modes for n=1. This illustrates that the shell modes (2,1) and (4,1) tend to a single mode K_{31}^T of ring, but the shear mode (3,1) remains the same and becomes the K_{21}^T ring mode.

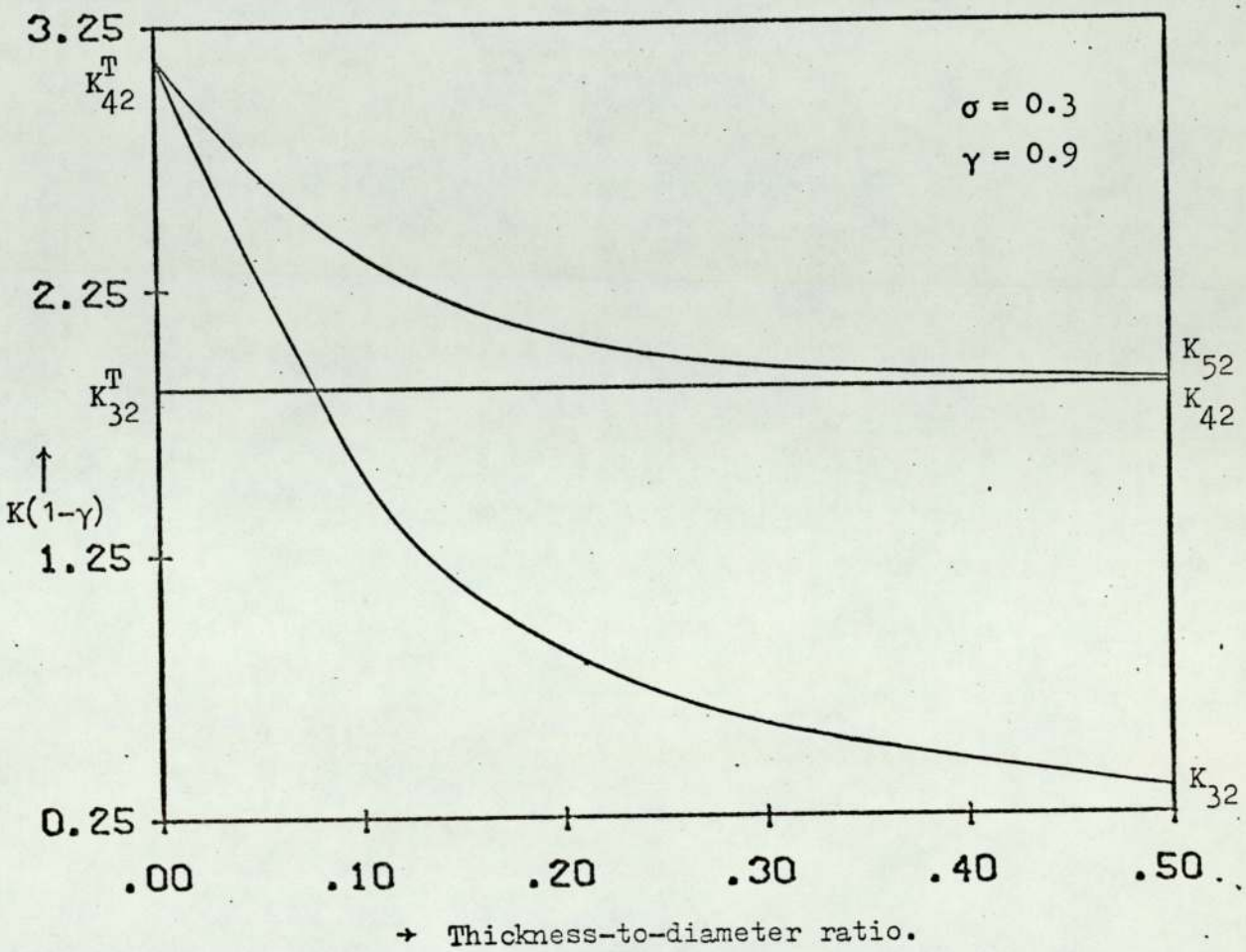

Fig.4.14 The variation of $K(1-\gamma)$ values, with thickness-to-diameter ratio, for higher compound modes for n=2. The modes K_{32} and K_{52} of the shell move to ring mode K^T_{42} and the shell mode K_{42} moves to ring mode K^T_{32}.

n \ m	2	3	4	5	6	7	8	9
1	Finite	S1.00392(1)	P0.600092(1)	C0.99867(1)	S (2)	P (2)	S (3)	P(3)
2			S1.00983(1)	P0.60191(1)	C0.99467(1)	S (2)	P (2)	S(3)
3	frequency		S1.01622(1)	P0.60523(1)	C0.98902(1)	S (2)	P (2)	S(3)
4	modes		S1.02127(1)	P0.61178(1)	C0.98253(1)	S (2)	P (2)	S(3)

(a) Thickness-to-diameter ratio = 0.50.

n \ m	2	3	4	5	6	7	8	9
1	Finite	S1.00394(1)	P0.62456(1)	C0.99840(1)	S (2)	P (2)	S (3)	P(3)
2			S1.00939(1)	P0.62567(1)	C0.99460(1)	S (2)	P (2)	S(3)
3	frequency		S1.01820(1)	P0.62770(1)	C0.98919(1)	S (2)	P (2)	S(3)
4	modes		S1.02993(1)	P0.63070(1)	C0.98293(1)	S (2)	P (2)	S(3)

(b) Thickness-to-diameter ratio = 0.25.

n \ m	2	3	4	5	6	7	8	9
1	Finite	S1.00395(1)	P0.71246(1)	C1.00261(1)	S (2)	P (2)	S (3)	P(3)
2			S1.00944(1)	P0.71345(1)	C0.99897(1)	S (2)	P (2)	S(3)
3	frequency		S1.01844(1)	P0.71506(1)	C0.99382(1)	S (2)	P (2)	S(3)
4	modes		S1.03075(1)	P0.71738(1)	C0.98786(1)	S (2)	P (2)	S(3)

(c) Thickness-to-diameter ratio = 0.125.

Table 4.7 Wave velocities for a cylindrical shell. $\gamma = 0.90$, $\sigma = 0.30$.

series (5,1),(6,2),(6,3),(6,4),...,etc. The prefix letter gives the wave type and the suffix number, the number of nodal circles. Thus, the (7,1) thick disk mode with six nodal circles becomes the q=2 shell plate (δ) mode, four circles having been lost. The variation of the wave velocity ratios from unity is small for shear and compressional modes. This indicates that the velocity of the shear waves in a shell is almost the same as that in a thin ring. It also changes slightly with n, the number of nodal diameters and with the Poisson's ratio. It may be noted that the departure of the plate velocity ratio from unity is very large. This is because, the velocity ratio for δ (plate) modes is equal to K/δ for a cylindrical shell and the ratio approaches unity for a thin ring, since $\delta \to K$ as $1/\eta \to 0.0$. For example, the (7,1) shell mode progresses to $(5,1)^T$ ring plate mode as η increases and the velocity ratio thus increases to unity.

CHAPTER 5

VIBRATION SPECTRA OF HOLLOW CYLINDERS

5.1 Introduction

In chapters 3 and 4, the in plane vibrations of annular rings and thick annular disks were investigated. This chapter is concerned with the study of free vibrations in hollow cylinders and rods, as special cases of the theory developed in chapter 4 for a thick disk with a central hole.

The free vibrations of an isotropic infinite solid cylinder have been investigated by Pochhammer[39] and Chree[40], on the basis of the linear theory of elasticity. The corresponding vibrations of hollow cylinders have been analysed by means of various approximate shell theories, starting from Love's first approximation[8] and including the contributions of Lin and Morgan[41], Naghdi and Cooper[42] and Mirsky and Hermann[43,44], which take into account the shear deformation and rotatory inertia on the frequencies of thick shells. All these theories are limited to first few modes only. Further, these theories do not provide accurate results for hollow cylinders of large wall-thickness. The accuracy and the validity of the shell theories to the hollow cylinders can be largely extended, only by comparison with an exact solution of three dimensional eigenvalue problem. Such solutions for axisymmetric and asymmetric modes of vibration have been given by Bassett[45], McFadden[46], Hermann and Mirsky[47], Gazis[23] and McNiven, Shah and Sackmann[28]. Redwood and Lamb[48] have given a detailed account of compressional wave propagation in isotropic elastic solid cylinders.

In this chapter, the vibrations of an infinite hollow cylinder are investigated as a special case of a thick annular disk, when $\eta = 0$. The frequency equations for the axisymmetric and asymmetric modes are derived from the corresponding frequency equation (4.2.3) of chapter 4

and are shown to be identical to those derived by Gazis[23,26] from the linear theory of elasticity. The vibrations of various special cases, such as thin rods and cylindrical shells, are also investigated. It is shown that, when $\eta=0$, eqn.(4.2.3) breaks down into a product of two determinants, one for the nonaxisymmetric (plane strain) vibrations and the other for the longitudinal shear vibrations of an infinite hollow cylinder. These two vibrations exist as uncoupled modes when $\eta=0$. The eigenvalues obtained from the solution of the frequency equations are designated by K^{I}_{mn}, where the superscript I denotes 'infinite rod' case and this notation is used in order to differentiate between the rod and thick disk modes. One-to-one correspondence is also established between the infinite solid cylinder modes and the thin cylindrical shell modes. It is also shown that a simple transformation of the material modulus yields the plane stress results of an annular ring from the plane strain results of an infinite hollow cylinder.

Table 5.1 shows the classification of various infinite hollow cylinder modes, where the superscripts I and LI refer to plane strain and longitudinal shear vibrations. There is one series each of pure torsional, pure radial and pure axial(longitudinal) shear modes, for n=0. In addition, there is one series of flexural modes, which approach zero frequency, one series of finite frequency modes and one series each of compound shear and compound compressional modes which approach infinite frequency as $\gamma \to 1$, all belonging to plane strain vibrations. The modes belonging to longitudinal shear vibrations consist of one series each of finite frequency modes and asymptotic modes.

5.2 Spectra of Rods

There has been considerable interest shown in the study of free vibrations of rods[31,33,49]. In this section, the theory developed in chapter 2 is applied to the vibrations of rods and the numerical results thus obtained are compared with those of the theories due to Rayleigh[19],

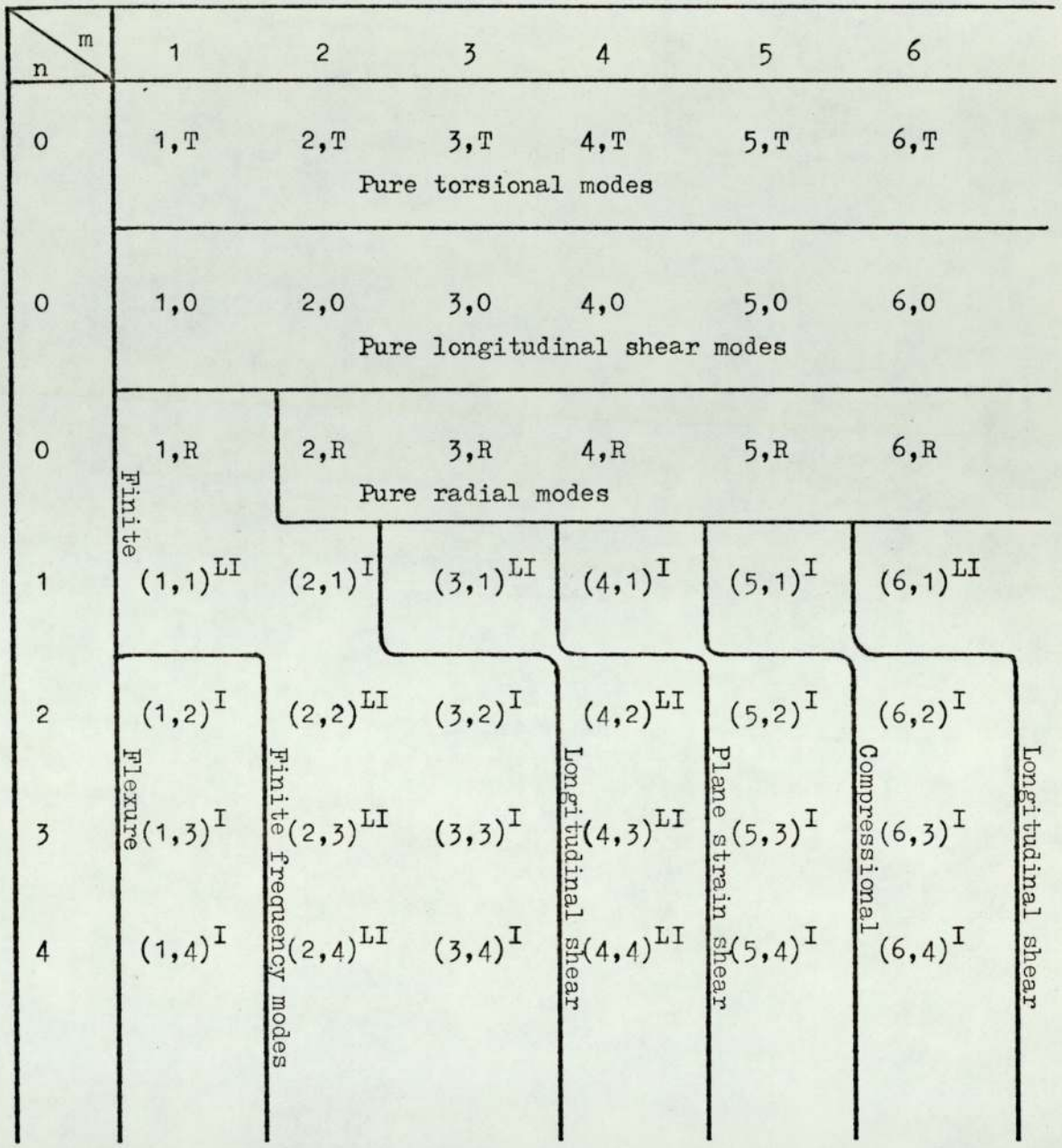

I → Plane strain vibrations; LI → Longitudinal shear vibrations.

Table 5.1. Classification of Infinite hollow cylinder modes.

Pochhammer-Chree[39,40], Lucey[12] and with the experiment. The agreement between the theoretical and the experimental results is remarkably good over a wide range of length-to-diameter ratios of the rods.

It may be interesting to derive the classical formula for the longitudinal vibration of a rod from the frequency equation(2.2.16), derived in Chapter 2, for the thick disk radial modes. When the diameter of the rod is much smaller than its length, i.e., when $\eta << 1$, the wavenumbers $\delta << 1$ and $\bar{\lambda}\delta << 1$. For $x << 1$, we have $M_1(x) \simeq 2$. Substituting this in eqn.(2.2.16) and simplifying, yields

$$(\delta^2 - \bar{\lambda}^2\delta^2)\left[K^2\theta^2\{\frac{K^2}{c} - (\delta^2 + \bar{\lambda}^2\delta^2)\} + \delta^2(\bar{\lambda}^2\delta^2)\right] = 0 \qquad (5.2.1)$$

Since, $(\delta^2 - \bar{\lambda}^2\delta^2) \neq 0$, this equation simplifies to

$$K^2\theta^2\{\frac{K^2}{c} - (\delta^2 + \bar{\lambda}^2\delta^2)\} = -\delta^2(\bar{\lambda}^2\delta^2) \qquad (5.2.2)$$

Substituting for δ and $\lambda\delta$, from eqns.(2.2.7) and simplifying, the above equation reduces to

$$K^c = \frac{\pi\eta}{2}\sqrt{(1 - \sigma^2)} \quad , \qquad (5.2.3)$$

which is the first longitudinal mode of vibration of a thin rod[8] and the superscript c refers to the classical formula. The above equation can be rewritten in the form

$$f^c\lambda = C_0 \quad , \qquad (5.2.4)$$

which is the classical formula for the longitudinal vibrations of a thin rod, where C_0 is the longitudinal velocity, f is the frequency of longitudinal vibration and λ is the wavelength given by $\lambda = 2l/p$, where l and p are the length and the number of half wavelengths of the rod, respectively.

The Rayleigh's[50] correction formula for the frequencies of longitudinal vibration of isotropic rods is given by

$$K^R = K^c\left[1 - \left(\frac{p\pi\sigma\eta}{4}\right)^2\right] \quad , \qquad (5.2.5)$$

where the superscript R refers to the Rayleigh's formula. The above equation can be rewritten, as

$$f^R\lambda = C_0\left[1 - \frac{k_1^2}{4}\left(\frac{d}{\lambda}\right)^2\right] \qquad (5.2.6)$$

where $k_1 = \pi\sigma$ and $d = 2a$, is the diameter of the rod.

Lucey's[12] correction formula for the fundamental frequency of the longitudinal resonance of an elastic rod is given by

$$K^L = K^c\left[1 - \frac{(1-\sigma^2)}{12}\left(\frac{\pi\eta}{K^T}\right)^2\right]^{\frac{1}{2}} \qquad (5.2.7)$$

where the superscript L and T refer to Lucey and thin disk theories, respectively. The above equation can also be written in the form

$$f^L\lambda = C_0\left[1 - \frac{k_2^2}{3\lambda^2}\right]^{\frac{1}{2}} \qquad (5.2.8)$$

where $k_2 = \frac{C_0}{f^T}$ and f^T is the corresponding thin disk radial mode frequency.

Pochhammer-Chree[39,40] have given exact solution for the natural frequencies of longitudinal resonance in elastic rods. The frequency equation is repeated here

$$\left[\frac{p^2\pi^2\eta^2}{2} - (K^p\theta)^2\right]^2 M_1(\nu_1) + \nu_1^2 p^2\pi^2\eta^2 M_1(\nu_2) - 2(\nu_1 K^p\theta)^2 = 0 \qquad (5.2.9)$$

where $$\nu_1 = \sqrt{\frac{K^2}{c} - \left(\frac{p\pi\eta}{2}\right)^2} \quad , \quad \nu_2 = \sqrt{K^2\theta^2 - \left(\frac{p\pi\eta}{2}\right)^2} \quad , \qquad (5.2.10)$$

and $K^p = \frac{2\pi f^p a}{c_p}$, is the solution of the above equation, and the superscript p refers to Pochhammer-Chree theory.

Fig.5.1 shows the plot of $f\lambda$ versus d^2/λ^2 , as obtained from various theories given by eqns.(5.2.3) to (5.2.9), for the longitudinal resonance of an aluminium rod with diameter of 1.9 cms and various

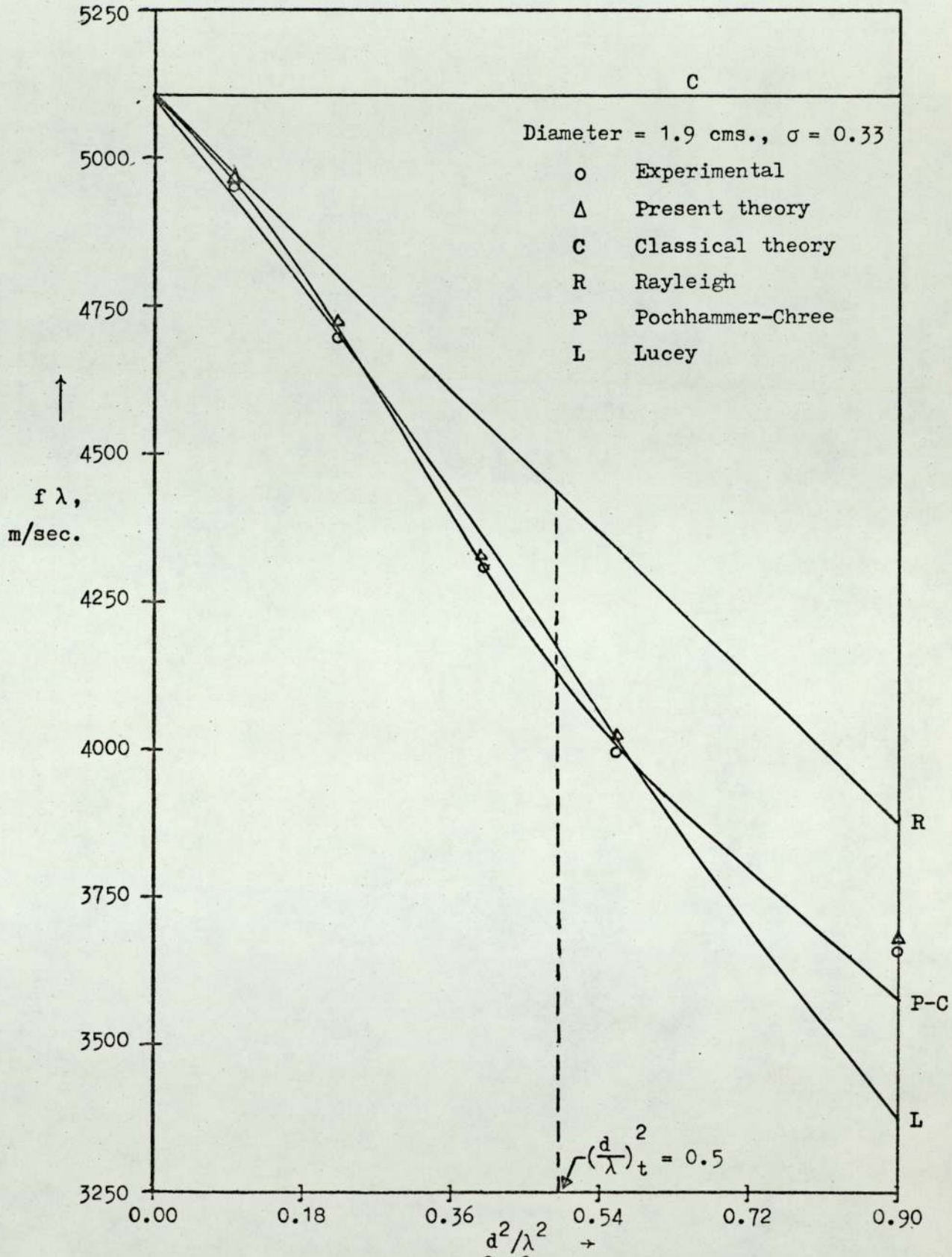

Fig. 5.1 The graph of $f\lambda$ versus d^2/λ^2 for the longitudinal vibration of an aluminium rod. A fair agreement between the present theory and the experiment could be noticed. The point $(d/\lambda)^2_t = 0.5$, corresponds to the transition from the rod to thick disk.

lengths. These results are also compared with those of the present theory given by eqn.(2.2.16) and the experiment. It may be noted from the figure that the theoretical frequencies of longitudinal vibrations of a rod, as obtained from the present theory, closely agree with those predicted by the exact theory due to Pochhammer-Chree and the experiment, over a range of rod lengths. However, the deviation of the Pochhammer-Chree, Lucey and Rayleigh's results from the experimental frequencies is significant when the diameter of the rod becomes comparable with its length i.e., when the transition from rod to thick disk takes place at $(d/\lambda)_t^2 = 0.5$. This is evident from Fig.5.1, which shows that, for $(d/\lambda)^2 > 0.5$, the frequencies predicted by Rayleigh's and Pochhammer-Chree theories differ considerably from the experimental results.

The spectrum as found experimentally for the aluminium rod of diameter 1.9 cms, when excited radially, consisted of various non-axisymmetric vibrations as well as the first two radial vibrations observed in the thick aluminium disk. The plot of the experimental frequency values versus thickness-to-diameter ratio is given in Fig.5.2, for the first two radial vibrations (1,R) and (2,R) and the first eight nonaxisymmetric vibrations (1,1) to (1,8). These results are in close agreement with McMahon's[16] results, who gave the experimental data for an aluminium rod for lower order modes (viz, (1,R),(1,1),(1,2) and (1,3)) only.

5.3 Plane Strain Vibrations of Infinite Hollow Cylinders

For infinite hollow cylinders, $\eta = 0$ and γ is finite, and hence the wavenumbers δ and $\lambda\delta$ of eqns.(2.2.7) reduce to

$$\delta = K^I\Theta \quad \text{and} \quad \overline{\lambda}\delta = K^I/\sqrt{c} \tag{5.3.1}$$

where $\overline{\lambda}\delta$ is real, $\overline{\lambda}^2\delta^2 = -\lambda^2\delta^2$ and the superscript I refers to the infinite rod case. Then, the elements X_{33}, X_{34}, X_{63} and X_{64} of the frequency equation (4.2.3), of thick annular disk reduce to

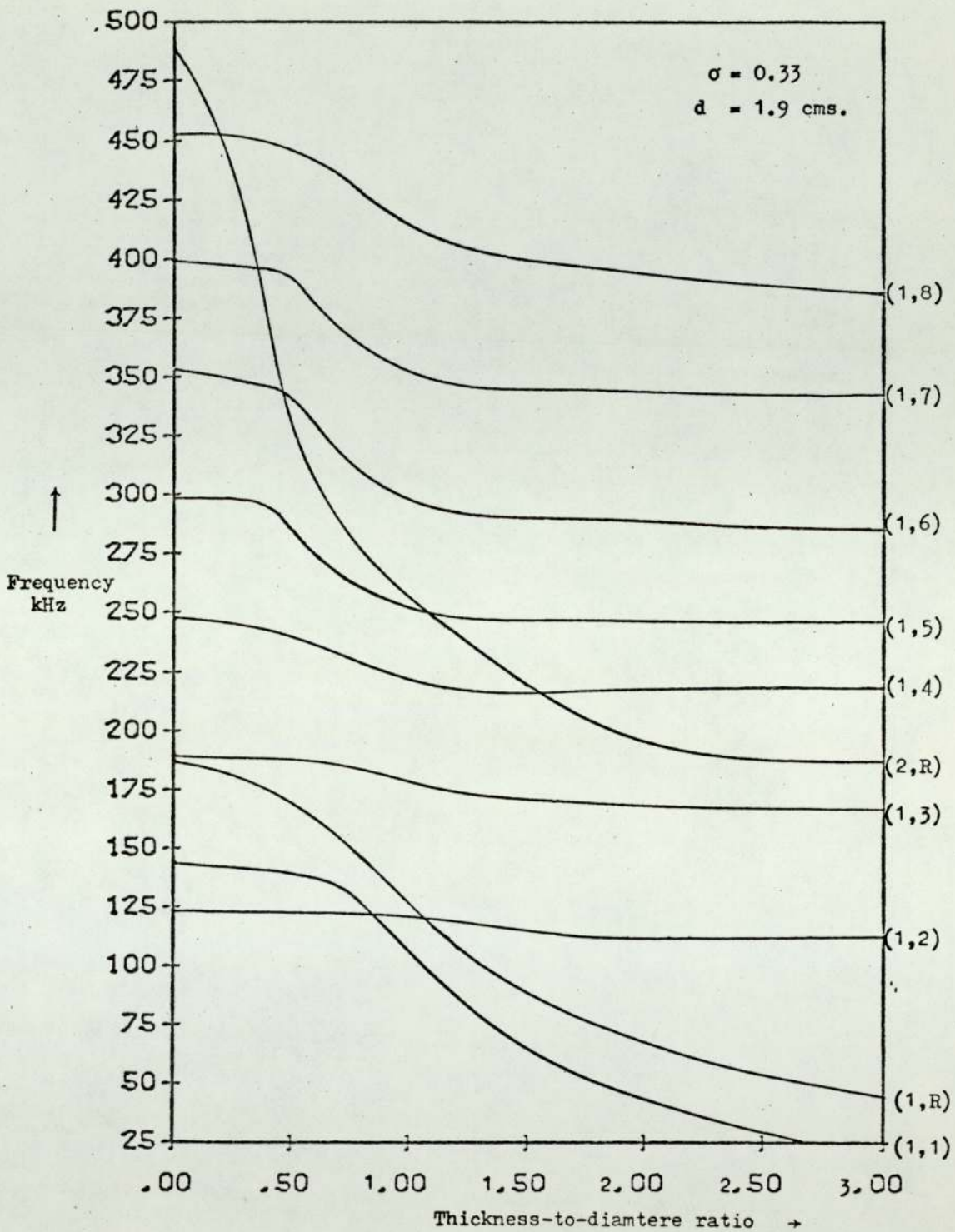

Fig.5.2 The plot of measured frequencies versus thickness-to-diameter ratio for various modes of an aluminium rod. Notice that the frequencies of the modes (1,1), (1,R), and (2,R) vary quite considerably over the range shown.

$$X_{33} = 0 \quad , \qquad X_{34} = 0$$
$$X_{63} = 0 \quad \text{and} \qquad X_{64} = 0 \tag{5.3.2}$$

Substituting eqns.(5.3.1) and (5.3.2) into eqn.(4.2.3) and simplifying, yields

$$D_5 \cdot D_6 = 0 \tag{5.3.3}$$

where

$$D_5 = \begin{vmatrix} X_{13} & X_{14} & X_{15} & X_{16} \\ X_{23} & X_{24} & X_{25} & X_{26} \\ X_{43} & X_{44} & X_{45} & X_{46} \\ X_{53} & X_{54} & X_{55} & X_{56} \end{vmatrix} \tag{5.3.4}$$

and

$$D_6 = \begin{vmatrix} X_{31} & X_{32} \\ X_{61} & X_{62} \end{vmatrix} \tag{5.3.5}$$

where

$$X_{13} = J_n(K_c^I)\{M_n(K_c^I) - n(n+1) + (K^I\Theta)^2/2\}$$
$$X_{14} = Y_n(K_c^I)\{L_n(K_c^I) - n(n+1) + (K^I\Theta)^2/2\}$$
$$X_{15} = n\, J_n(K^I\Theta)\{M_n(K^I\Theta) - (n+1)\}$$
$$X_{16} = n\, Y_n(K^I\Theta)\{L_n(K^I\Theta) - (n+1)\}$$
$$X_{23} = n\, J_n(K_c^I)\{M_n(K_c^I) - (n+1)\}$$
$$X_{24} = n\, Y_n(K_c^I)\{L_n(K_c^I) - (n+1)\}$$
$$X_{25} = J_n(K^I\Theta)\{M_n(K^I\Theta) - n(n+1) + (K^I\Theta)^2/2\}$$
$$X_{26} = Y_n(K^I\Theta)\{L_n(K^I\Theta) - n(n+1) + (K^I\Theta)^2/2\}$$
$$X_{43} = J_n(\gamma K_c^I)\{M_n(\gamma K_c^I) - n(n+1) + \gamma^2(K^I\Theta)^2/2\}$$
$$X_{44} = Y_n(\gamma K_c^I)\{L_n(\gamma K_c^I) - n(n+1) + \gamma^2(K^I\Theta)^2/2\}$$
$$X_{45} = n\, J_n(K^I\gamma\Theta)\{M_n(K^I\gamma\Theta) - (n+1)\}$$
$$X_{46} = n\, Y_n(K^I\gamma\Theta)\{L_n(K^I\gamma\Theta) - (n+1)\}$$
$$X_{53} = n\, J_n(\gamma K_c^I)\{M_n(\gamma K_c^I) - (n+1)\}$$
$$X_{54} = n\, Y_n(\gamma K_c^I)\{L_n(\gamma K_c^I) - (n+1)\} \tag{5.3.6}$$

$$X_{55} = J_n(K^I\gamma\theta)\{M_n(K^I\gamma\theta) - n(n+1) + \gamma^2(K^I\theta)^2/2\}$$

$$X_{56} = Y_n(K^I\gamma\theta)\{L_n(K^I\gamma\theta) - n(n+1) + \gamma^2(K^I\theta)^2/2\}$$

and

$$X_{31} = J_n(K^{LI}\theta)\{M_n(K^{LI}\theta) - n\}, \quad X_{32} = Y_n(K^{LI}\theta)\{L_n(K^{LI}\theta) - n\} \tag{5.3.7}$$

$$X_{61} = J_n(K^{LI}\gamma\theta)\{M_n(K^{LI}\gamma\theta) - n\}, \quad X_{62} = Y_n(K^{LI}\gamma\theta)\{L_n(K^{LI}\gamma\theta) - n\}$$

where $K_c^I = K^I/\sqrt{c} = \omega a/C_c$, and C_c is the compressional (bulk) velocity. Then, the frequency equation

$$D_5 = 0 \tag{5.3.8}$$

corresponds to the nonaxisymmetric vibrations of an infinite hollow cylinder. A frequency equation equivalent to eqn.(5.3.8) has been given by Gazis[23] for an infinite hollow cylinder, who also derived simplified equations for thin cylindrical shells and infinite rods. It may be noted that a transformation of the material modulus from bulk to plate reduces eqn.(5.3.8)of plane strain vibrations to eqn.(3.2.1) of plane stress vibrations of an annular ring. That is, if K_c^I is replaced by K^T, eqn.(5.3.8) reduces to eqn.(3.2.1).

The case

$$D_6 = 0 \tag{5.3.9}$$

corresponds to 'longitudinal shear vibrations', which will be considered in the next section.

For axisymmetric vibrations of an infinite hollow cylinder, n is set to zero and eqn.(5.3.8) breaks down into the following product

$$\begin{vmatrix} Y_{13} & Y_{14} \\ Y_{43} & Y_{44} \end{vmatrix} \times \begin{vmatrix} Y_{25} & Y_{26} \\ Y_{55} & Y_{56} \end{vmatrix} = 0 \tag{5.3.10}$$

where

$$Y_{13} = J_1(K_c^I)\{M_1(K_c^I) - 2/c\theta^2\}, \quad Y_{14} = Y_1(K_c^I)\{L_1(K_c^I) - 2/c\theta^2\}, \tag{5.3.11}$$

$$Y_{43} = J_1(\gamma K_c^I)\{M_1(\gamma K_c^I) - 2/c\theta^2\}, \quad Y_{44} = Y_1(\gamma K_c^I)\{L_1(\gamma K_c^I) - 2/c\theta^2\}$$

and

$$Y_{25} = J_1(K^I\Theta)\{M_1(K^I\Theta) - 2\}, \quad Y_{26} = Y_1(K^I\Theta)\{L_1(K^I\Theta) - 2\},$$
$$Y_{55} = J_1(K^I\gamma\Theta)\{M_1(K^I\gamma\Theta) - 2\}, \quad Y_{56} = Y_1(K^I\gamma\Theta)\{L_1(K^I\gamma\Theta) - 2\} \tag{5.3.12}$$

Eqn.(5.3.10) is satisfied if and only if

$$\begin{vmatrix} Y_{13} & Y_{14} \\ Y_{43} & Y_{44} \end{vmatrix} = 0 \tag{5.3.13a}$$

or

$$\begin{vmatrix} Y_{25} & Y_{26} \\ Y_{55} & Y_{56} \end{vmatrix} = 0 \tag{5.3.13b}$$

It may be noted that eqns.(5.3.13a) and (5.3.13b) correspond to the axisymmetric extensional and shear (torsional) vibrations, respectively, and they are essentially uncoupled. For a given n, σ and γ, the numerical computation of the roots of the frequency equations (5.3.8) and (5.3.13) is carried out using the procedure described in Chapter 2 (section 2.3). The cut off freqencies of some of the symmetric and antisymmetric modes are given in Appendix A.5, for $\sigma = 0.3$ and $n = 0, 1$ and 2. These values can also be found in reference 51.

5.3.1 Infinite Rods

For an infinite rod, $\eta = 0$ and $\gamma = 0$. As $\gamma \to 0$, $Y_n(\gamma K_c^I) \to \infty$ and $Y_n(K^I\gamma\Theta) \to \infty$. Thus, dividing the elements X_{i4}, $i = 1,2,4,5$, by $Y_n(\gamma K_c^I)$ and the elements X_{5j}, $j = 3,4,5,6$, by $Y_n(K^I\gamma\Theta)$, the frequency equation (5.3.8) reduces to

$$\begin{vmatrix} X_{13} & X_{15} \\ X_{23} & X_{25} \end{vmatrix} = 0 \tag{5.3.14}$$

which is the frequency equation for nonaxisymmetric vibrations of an infinite solid cylinder[16], where the elements of the above determinant are given by eqns.(5.3.6). Putting n=0 in eqn.(5.3.14) yields

$$X_{13} \cdot X_{25} = 0 \tag{5.3.15}$$

which is satisfied, if

$$X_{11} = \{ M_1(K_c^I) - 2/c\theta^2 \} = 0 \qquad (5.3.16)$$

or $$X_{25} = \{ M_1(K^I\theta) - 2 \} = 0 \qquad (5.3.17)$$

where eqns.(5.3.16) and (5.3.17) are the frequency equations for the radial[33,39] and torsional[8] modes of vibration, respectively. It may be noted that eqns.(5.3.14), (5.3.16) and (5.3.17) are identical in form to those obtained by Onoe[9] and Holland[10] for a thin disk (see section 3.4), except that K is replaced by K_c^I , where $K_c^I = K^I/\sqrt{c}$. Eqn.(5.3.16) is a well known Pochhammer-Chree equation for longitudinal vibrations in an infinite rod, which can be derived from eqn.(5.2.9) by setting $\eta=0$. Further, it is interesting to note that the frequencies of the torsional modes are the same for an infinite rod as for a thin disk[16], since eqn. (5.3.17) is same as the thin disk torsional mode frequency equation[8].

5.3.2 Thin Cylindrical Shells

The physical parameters for a thin cylindrical shell are $\eta=0$ and $\gamma\to1$. It is observed that as $\gamma\to1$, $K^I\to\infty$, and using this assumption in eqn.(5.3.4), the frequency equation for nonaxisymmetric vibrations becomes

$$\begin{vmatrix} J_n(K_c^I) & Y_n(K_c^I) \\ J_n(\gamma K_c^I) & Y_n(\gamma K_c^I) \end{vmatrix} \times \begin{vmatrix} J_n(K^I\theta) & Y_n(K^I\theta) \\ J_n(K^I\gamma\theta) & Y_n(K^I\gamma\theta) \end{vmatrix} = 0 \qquad (5.3.18)$$

Substituting the asymptotic expansions of eqns.(4.5.5), valid for large argument values of Bessel functions, in eqns.(5.3.18) and simplifying yields the frequency equation for high frequency modes of an infinite cylindrical shell, as

$$\sin K^I\theta(1-\gamma).\ \sin K_c^I(1-\gamma) = 0 \qquad (5.3.19)$$

which is satisfied if

$$\sin K^I\theta(1-\gamma)= 0, \text{ i.e., } K^I\theta(1-\gamma)= p\pi\ , \ p =1,2,3,\ldots \qquad (5.3.20a)$$

or $$\sin K_c^I(1-\gamma)= 0\ , \text{ i.e., } K_c^I(1-\gamma)= q\pi\ , \ q =1,2,3,\ldots \qquad (5.3.20b)$$

These equations show that the high frequency nonaxisymmetric vibrations

of a thin cylindrical shell are effectively of pure shear or pure compressional waves, respectively.

Similarly, it can be shown that the frequency equation for the high frequency axisymmetric extensional vibrations of the thin cylindrical shell can be obtained[23] from eqn.(5.3.13a), as

$$\{\sin K_c^I(1-\gamma) - \frac{(7-15\sigma)(1-\gamma)}{8\gamma K_c^I(1-\sigma)} \cos K_c^I(1-\gamma)\} = 0 \qquad (5.3.21)$$

whose solution is given by

$$K_c^I = \frac{q\pi}{(1-\gamma)}\left[1 + \frac{(7-15\sigma)(1-\gamma)^2}{8q^2\pi^2\gamma^2(1-\sigma)}\right], \quad q = 1,2,3,..,\text{etc.}, \qquad (5.3.22)$$

and the frequency equation for the higher order axisymmetric shear vibrations can be obtained from eqn.(5.3.13b), as

$$\{\sin K^I\Theta(1-\gamma) - \frac{15(1-\gamma)}{8K^I\gamma\Theta} \cos K^I\Theta(1-\gamma)\} = 0 \qquad (5.3.23)$$

whose solution is given by

$$K^I\Theta = \frac{p\pi}{(1-\gamma)}\left[1 + \frac{15(1-\gamma)^2}{8p^2\pi^2\gamma^2}\right], \quad p = 1,2,3,..,\text{etc.}, \qquad (5.3.24)$$

It may be noted that eqns.(5.3.21) and (5.3.23) do not predict the lowest flexural and extensional modes of the infinite cylindrical shell, for which the assumption, that $K^I \to \infty$ as $\gamma \to 1$, is not valid. However, eqns.(5.3.21) to (5.3.24) describe all the higher axisymmetric extensional and shear vibrations which tend, for $\gamma \to 1$, to the simple thickness-stretch and thickness-shear modes, respectively, of an infinite cylindrical shell, whose frequencies are given by

$$K_c^I = \frac{q\pi}{(1-\gamma)} \quad , \qquad (5.3.25a)$$

and

$$K^I\Theta = \frac{p\pi}{(1-\gamma)} \qquad (5.3.25b)$$

The flexural modes tend to zero frequency and the extensional modes tend to finite frequencies, as $\gamma \to 1$. For an infinite shell, γ can be written as $\gamma = (1-d\gamma)$ such that $d\gamma \to 0$ as $\gamma \to 1$. Then, using this

value of γ and the truncated Taylor series expansion of Bessel functions involving γ, in the elements of the frequency equation (5.3.8) and simplifying, yields, for $\gamma \to 1$

$$\left[(K^I)^2 - \frac{4(1-\gamma)^2 n^2 (n^2-1)^2}{3(1+\gamma)^4 (n^2+1)}\right]\left[(K^I)^2 - \frac{4(n^2+1)}{(1+\gamma)^2}\right]\{J_n(K_c^I)Y_{n-1}(K_c^I) - J_{n-1}(K_c^I)Y_n(K_c^I)\}\{J_n(K^I\theta)Y_{n-1}(K^I\theta) - J_{n-1}(K^I\theta)Y_n(K^I\theta)\} = 0 \tag{5.3.26}$$

Then, using the Gray and Mathew's theorem for Bessel functions, the above equation reduces to

$$\left[(K^I)^2 - \frac{4(1-\gamma)^2 n^2 (n^2-1)^2}{3(1+\gamma)^4 (n^2+1)}\right] = 0 \text{ , i.e., } K^I = \frac{2(1-\gamma)\, n(n^2-1)}{(1+\gamma)^2\sqrt{3(n^2+1)}} \text{ , } n>1 \tag{5.3.27}$$

or

$$\left[(K^I)^2 - \frac{4(n^2+1)}{(1+\gamma)^2}\right] = 0 \text{ , i.e., } K^I = \frac{2}{(1+\gamma)}\sqrt{(n^2+1)} \tag{5.3.28}$$

It may be ascertained that eqns.(5.3.27) and (5.3.28) are the frequency equations of the flexural and extensional modes of an infinite cylindrical shell, respectively.

The frequency equation for the lowest two radial vibrations of a cylindrical shell was derived in Chapter 4 and the two modes are given by the roots of eqn.(4.5.20). For a thin cylindrical shell, when $\eta \to 0$, the two roots of the eqn.(4.5.20) are given by

$$K = \frac{\pi\eta}{2}\sqrt{(1-\sigma^2)} \qquad \text{and} \quad K = \frac{2}{(1+\gamma)} \tag{5.3.29}$$

For an infinite cylindrical shell, $\eta = 0$ and hence the first root given by the above equation will be equal to zero. Hence, the lowest radial mode for an infinite cylindrical shell, for $\gamma \to 1$, is given by

$$K_{1R}^I = \frac{2}{(1+\gamma)} \tag{5.3.30}$$

It may be noted that the above equation can also be derived from eqn. (5.3.13a) for $\gamma \to 1$ and from eqn.(5.3.28) by setting n=0. Thus, the

second and higher radial modes progress to high frequency compressional modes given by eqn.(5.3.25a) and all the tangential modes of the infinite cylindrical shell tend to high frequency shear modes given by eqn. (5.3.25b).

5.4 Longitudinal Shear Vibrations

It was pointed out in the previous section that the frequency equation

$$D_6 = \begin{vmatrix} X_{31} & X_{32} \\ X_{61} & X_{62} \end{vmatrix} = 0 \qquad (5.4.1)$$

corresponds to the longitudinal shear vibrations of an infinite hollow cylinder, where the elements of the above determinant are given by eqns. (5.3.7). These are the vibrations for which the particle displacement is purely axial. It may be noted, from eqn.(5.3.3), that the plane strain and the longitudinal shear vibrations in an infinite hollow cylinder are uncoupled and the frequencies of these vibrations are the cut-off frequencies. The modes of propagation, of a infinite hollow cylinder, associated with these cut-off frequencies, for n=0, are the 'radial shear' and 'axial shear' modes, respectively[33]. Further, when n=0, eqn.(5.4.1) reduces to

$$\{J_1(K^{LI}\theta)\ Y_1(K^{LI}\gamma\theta) - Y_1(K^{LI}\theta)\ J_1(K^{LI}\gamma\theta)\} = 0 \qquad (5.4.2)$$

and the modes predicted by the above equation are uncoupled with the axisymmetric extensional vibrations given by eqn.(5.3.13a).

The displacement functions for the longitudinal shear vibrations governed by the frequency equation (5.4.1), are given by

$$u_r = 0\ ,\quad u_\theta = 0,\quad \text{and}$$

$$u_z = k\{A_1\ J_n(kr) + B_1\ Y_n(kr)\}\ \cos n\theta\ \sin \omega t \qquad (5.4.3)$$

where $k = \omega/C_s$. The eigenvalues obtained from the solution of eqn. (5.4.1) are designated by K^{LI}_{mn}. Thus, one of the lowest longitudinal

shear mode (K_{11}^{LI} , m=n=1) corresponds, essentially, to a shearing of the cylinder across its diameter[26] and the higher longitudinal shear modes, which involve a number of nodal circles and nodal diameters, correspond essentially to a shearing of the hollow cylinder across its thickness.

5.4.1 Thin Rods

For thin rods, $\gamma \to 0$ and hence $Y_n(K^{LI}\gamma\theta) \to \infty$. Then, using these conditions in eqn.(5.4.1), yields the frequency equation for the longitudinal shear vibrations of an infinite solid cylinder, as

$$\{M_n(K^{LI}\theta) - n\} = 0 \qquad (5.4.4)$$

When n=0, this equation becomes

$$J_1(K^{LI}\theta) = 0 \qquad (5.4.5)$$

The frequencies corresponding to eqns.(5.4.4) and (5.4.5) are the cut-off frequencies and are independent of σ, the Poisson's ratio.

5.4.2 Thin Cylindrical Shells

For a thin cylindrical shell, $\gamma \to 1$ and it is observed for few modes that $K^{LI}\theta \to \infty$ as $\gamma \to 1$. Using this condition and the asymptotic expansions of Bessel functions, in eqn.(5.4.1), one can obtain the frequency equation for the longitudinal shear vibrations of a thin cylindrical shell, as

$$\left[\sin K^{LI}\theta(1-\gamma) - \frac{(4n^2+3)(1-\gamma)}{8K^{LI}\gamma\theta} \cos K^{LI}\theta(1-\gamma)\right] = 0 \qquad (5.4.6)$$

whose frequencies are given by

$$K^{LI}\theta \simeq \frac{q\pi}{(1-\gamma)}\left[1 + \frac{(4n^2+3)(1-\gamma)^2}{8q^2\pi^2\gamma^2}\right], \quad q = 1,2,3,\ldots \qquad (5.4.7)$$

The above equations are valid for asymptotic modes, whose frequencies tend to infinity as $\gamma \to 1$, but, they do not predict the lowest mode, for which $K^{LI}\theta$ is finite. However, when $\gamma \simeq 1$, all second and higher modes tend to the simple thickness-shear modes, whose frequencies are given by

$$K^{LI}_{\theta} = \frac{q\pi}{(1-\gamma)} \quad , \quad q = 1,2,3,\ldots \tag{5.4.8}$$

The lowest longitudinal shear mode, for $n \geq 1$, tends to finite frequency, as $\gamma \to 1$. For this case, γ can be written as $\gamma = (1 - d\gamma)$. Substituting this value of γ and the corresponding truncated Taylor's series expansion of Bessel functions involving γ, in the elements of the frequency equation (5.4.1) and simplifying, yields the frequency of the lowest longitudinal shear vibration, as

$$K^{LI}_{\theta} = \frac{2n}{(1+\gamma)} \quad , \quad n \geq 1 \tag{5.4.9}$$

The frequencies of the first and second modes, given by eqns.(5.4.9) and (5.4.8) for $\gamma=0.9$ and $\sigma=0.3$ are shown in Figs.5.8 and 5.9, respectively, for $n = 1$ and 2.

5.5 Discussion

The plot of $K^{I}_{c}(1-\gamma)$ versus γ is shown in Fig.5.3 for the first two asymptotic modes K^{I}_{2R} and K^{I}_{3R} given by eqn.(5.3.13a), for two different values of Poisson's ratio, in order to illustrate the effect of σ on the nature of the transition from infinite cylindrical shell frequencies to the infinite rod frequencies. The ratio of the phase velocity to the compressional velocity of these waves is given by

$$\frac{C_{phase}}{C_{c}} = \frac{K^{I}_{c}(1-\gamma)}{p\pi} \quad ; \quad p = 1,2,3,\ldots \tag{5.5.1}$$

From Fig.5.3, it may be seen that the limiting values approached for $\gamma \simeq 1$, are π and 2π for K^{I}_{2R} and K^{I}_{3R}, respectively, which establishes that the waves travel with the compressional velocity, as given by eqn. (5.5.1), and are not dispersive.

Fig.5.3 also indicates that the frequency of these asymptotic modes, given by eqn.(5.3.22) for an infinite cylindrical shell of thickness (a-b), deviates, but little, from the corresponding frequency of a thin ring of the same thickness, even for large values of γ. This can be noticed from Figs.3.3 and 5.3. Also, it may be noted that this

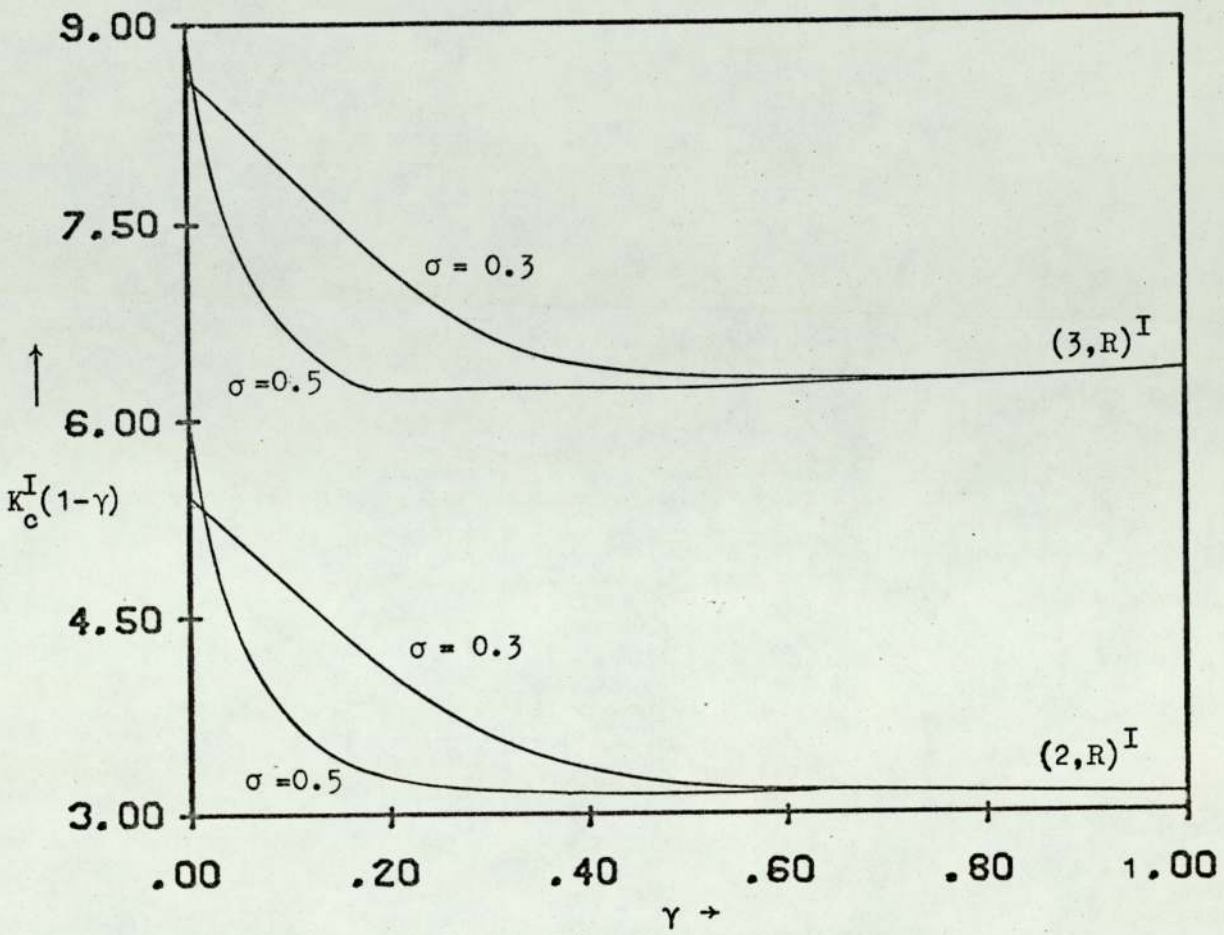

Fig.5.3 The plot of $K_c^I(1-\gamma)$ versus γ for pure extensional modes $(2,R)^I$ and $(3,R)^I$, for various σ's. The figure shows that the transformation of thin cylindrical shell frequencies to the Pochhammer frequencies of rods.

deviation is less pronounced for the higher modes than for the lower modes. However, these remarks do not apply to the lowest extensional mode K^{I}_{1R}, whose frequency remains finite for $\gamma \to 1$.

The lowest mode of the radial mode series in a shell is (1,R), as given by eqn.(4.5.20), but, for an infinite cylindrical shell, the frequency of this mode tends to zero, for $\eta = 0$, as given by eqn.(5.3.29), for all γ's. Fig.5.4(a) shows the variation of K_{1R} over a wide range of thickness-to-diameter ratios, for different γ's. The frequency of the second radial mode (2,R) is given by eqn.(4.5.20) for the cylindrical shell, but this transforms itself to the first mode, K^{I}_{1R} of the radial mode series, for an infinite cylindrical shell, as given by eqn.(5.3.30). Fig.5.4(b) illustrates the variation of $K_{2R}(1-\gamma)$ with thickness-to-diameter ratio, for various γ's. It may be noted that, for $\gamma = 0.9$, the frequency of the (2,R) mode, which has an asymptotic value given by eqn.(3.4.15a) for a thin ring, progresses to a finite frequency value, given by eqn.(5.3.30), for a thin cylindrical shell.

For an infinite hollow cylinder, there is only one series of finite frequencies in plane strain vibrations, as in the case of an annular ring. The lowest mode in this series, for $\gamma \to 1$, is again $(1,R)^{I}$. The frequency of this mode is greater than that of $(2,1)^{I}$ mode for lower values of γ, but these two progress, respectively, to K=1 and $K=\sqrt{2}$ thin cylindrical shell values, as given by eqn.(5.3.28), crossing each other. This crossover occurs at a specific value, which is dependent on σ. Fig.5.5 illustrates the variation of the frequencies of the first three finite frequency modes $(1,R)^{I}$, $(2,1)^{I}$ and $(3,2)^{I}$, with γ. The undulations in the curves, similar to that observed in the plot of K_0 values with γ in Fig.3.5 for finite frequency modes of annular rings, can be noticed here for all the modes except $(1,R)^{I}$ mode. For modes with larger n, the increase in frequency values, for $\gamma \to 1$, is rather significant. It may be noted, from eqns.(3.4.10) and (5.3.28),

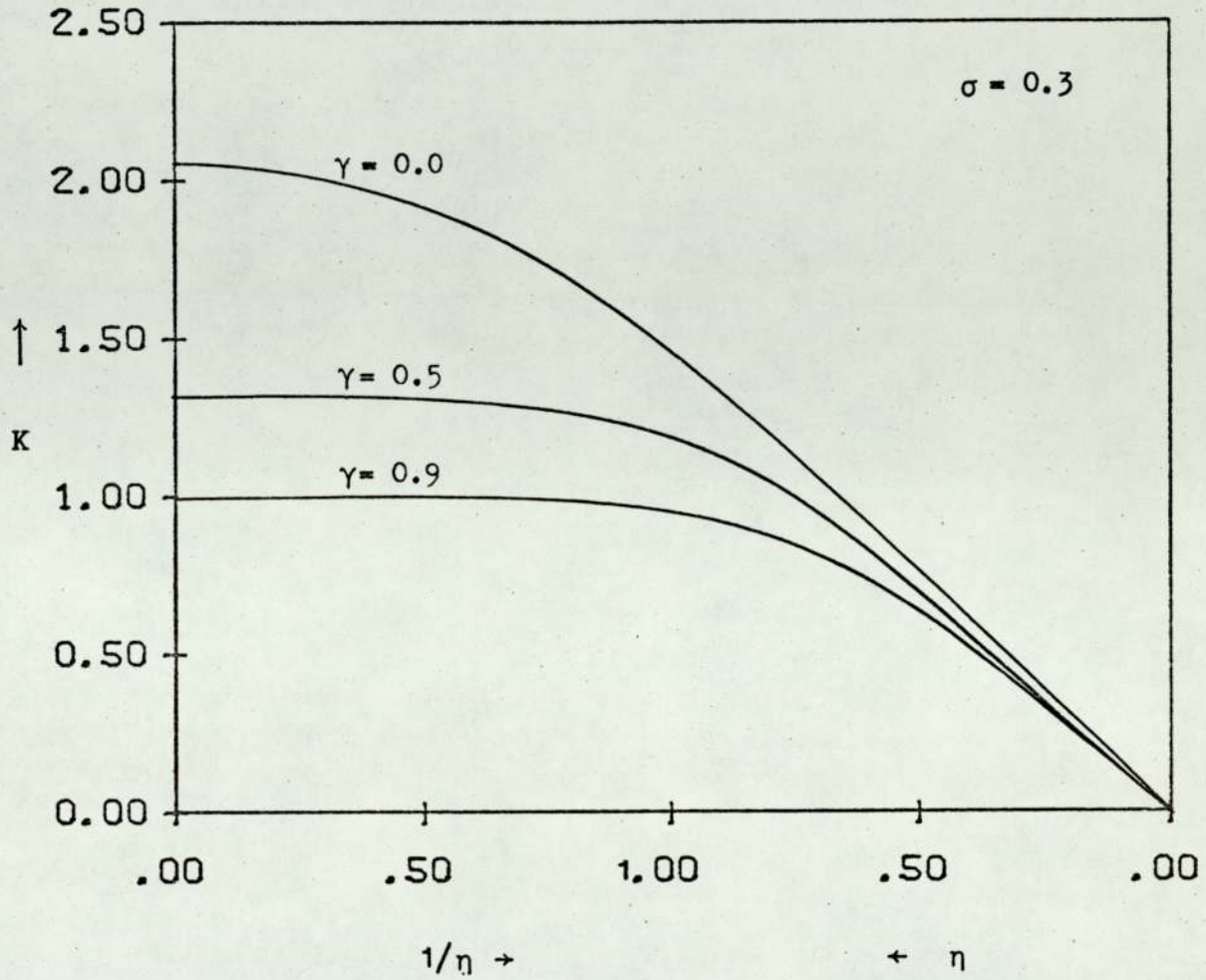

Fig.5.4(a) The graph of K_{1R} versus thickness-to-diameter ratio, for different γ's. Notice that the finite frequency annular ring radial mode tends to zero frequency for infinite hollow cylinder, for all γ's.

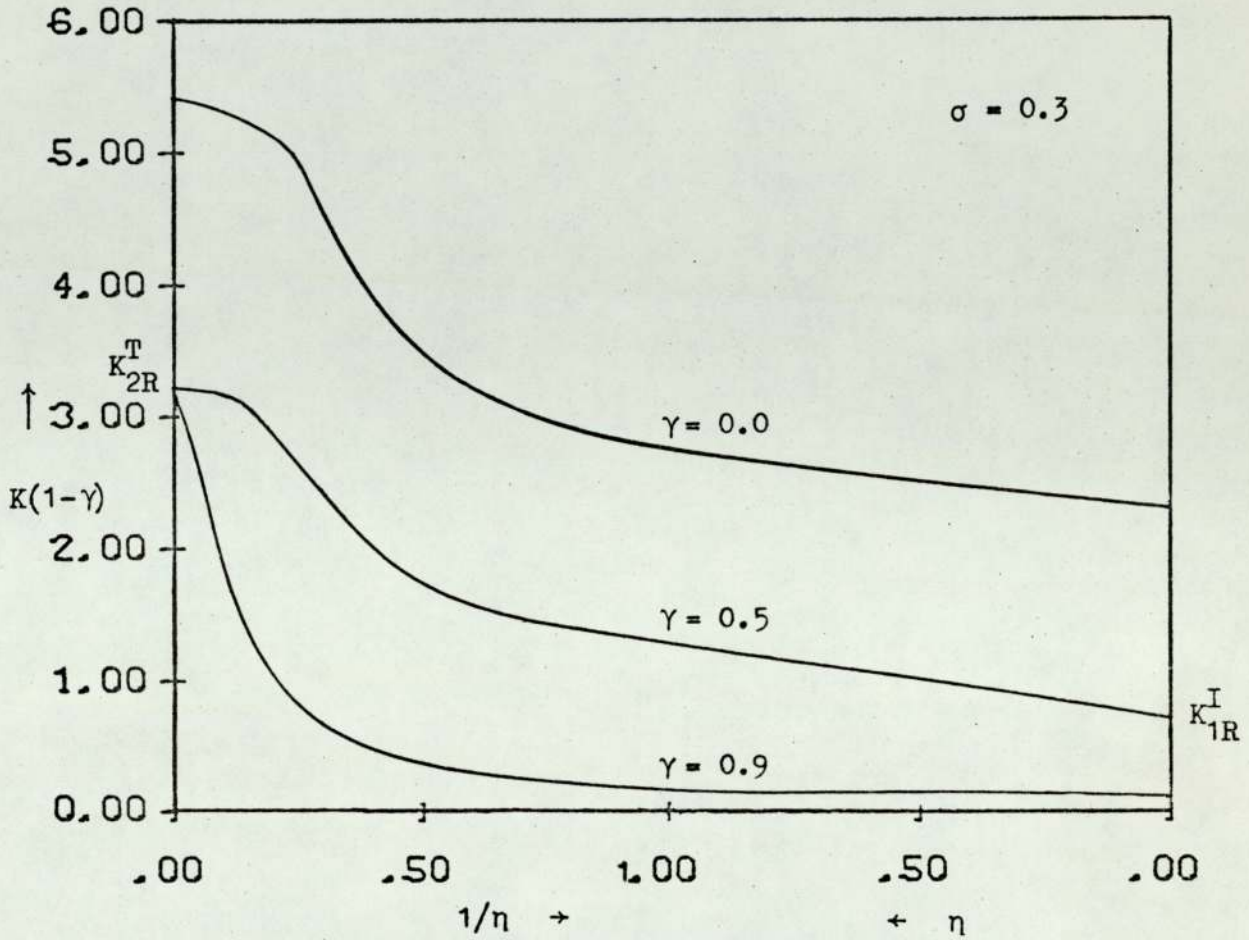

Fig.5.4(b) The graph of K(1-γ) values versus thickness-to-diameter ratio for second radial mode, for various γ's. Notice that, for γ = 0.9, the infinite frequency radial mode of an annular ring transforms to a finite frequency extensional mode of a thin cylindrical shell.

that, in thin rings, K_0^T is independent of Poisson's ratio whereas in the case of infinite shells, K^I is independent of σ. This implies that the finite frequency modes in thin rings propagate with rod velocity and in infinite shells, they propagate with plate velocity.

However, eqn.(5.3.28) does not describe the flexural modes, similar to those found in a thin ring. The lowest mode for n=1 is the flexural mode which degenerates to a zero frequency, as $\eta \to 0$, for all γ's, as in the case of a thin ring. But, this is not true for $n > 1$, as for the case n=2, the frequency of the lowest flexural mode decreases monotonically with increasing γ, from a finite Pochhammer frequency for $\gamma=0$ to a zero frequency for $\gamma=1$.

The nonaxisymmetric (plane strain) modes of a thin cylindrical shell, which, like pure extensional and shear modes, tend to infinite frequency as $\gamma \to 1$, the asymptotic values are being the solutions of eqns.(5.3.20a) and (5.3.20b), for shear and compressional waves, respectively. Fig.5.6 shows the plot of $K^I\Theta(1-\gamma)$ versus γ, for (4,1) and (5,2) shear modes. It may be noted from the figure that the limiting values approached as $\gamma \to 1$, for both the modes is π, showing that these modes travel with shear velocity. Similarly, the compressional modes $(5,1)^I$ and $(6,2)^I$ progress to an asymptotic value π, for $\gamma \to 1$, as shown in Fig.5.7. Thus, these two modes propagate with the compressional velocity, as $\gamma \to 1$.

The longitudinal shear vibrations, which exist as uncoupled with the plane strain (nonaxisymmetric) vibrations for an infinite hollow cylinder, classify into two types of modes for $n > 0$, as the frequencies transform from those of an infinite rod to those of a thin cylindrical shell. For $n > 0$, the first set of modes remain as finite frequency modes as $\gamma \to 1$, while the second set of modes tend to infinite shear frequencies. Fig.5.8 shows the variation of the frequencies of the finite frequency modes $(1,1)^{LI}$ and $(2,2)^{LI}$, with γ, in which

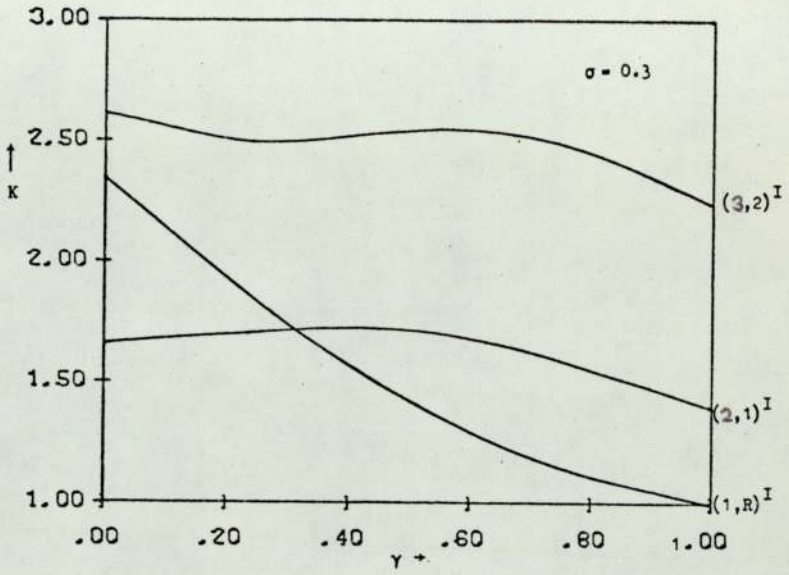

Fig.5.5 The variation of finite frequency modes with γ. The crossover for the modes $(1,R)^I$ and $(2,1)^I$, which is characteristic of Poisson's ratio, occurs at $\gamma = 0.3038$ for $\sigma = 0.3$.

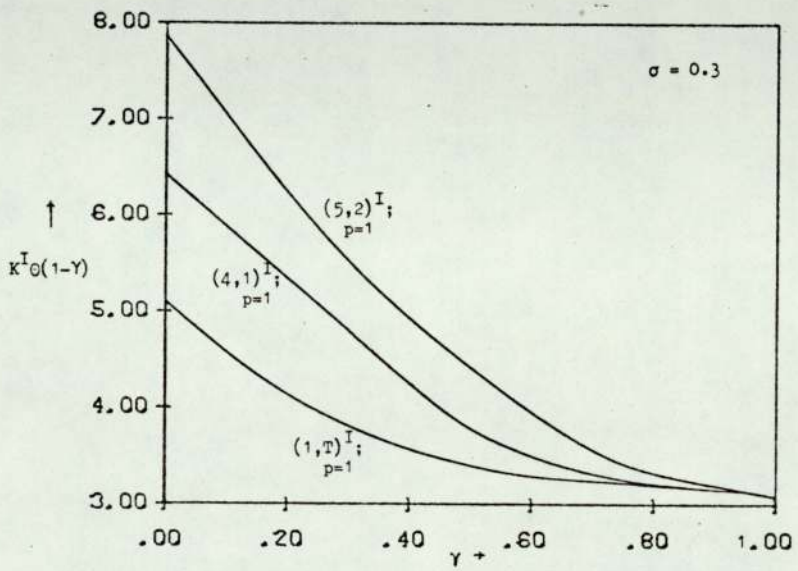

Fig.5.6 The $K^I\Theta(1-\gamma)$ values for $(4,1)^I$, $(5,2)^I$ shear modes and $(1,T)^I$ pure torsional mode, plotted as a function of γ. The asymptotic value reached for all modes, as $\gamma \to 1$, is π.

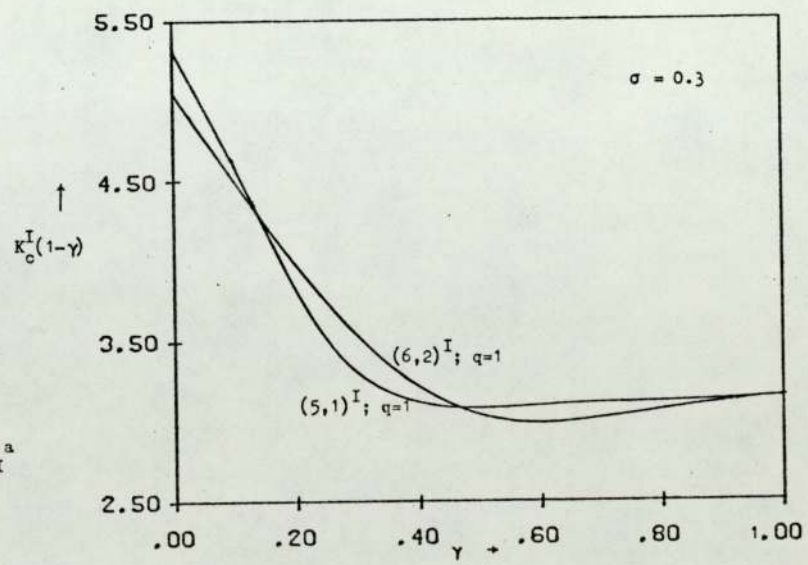

Fig.5.7 The plot of $K_c^I(1-\gamma)$ values as a function of γ for modes $(5,1)^I$ and $(6,2)^I$. The limiting value reached as $\gamma \to 1$ is π establishing that these modes belong to the compound compressional mode series.

the limiting value attained as $\gamma \to 1$ is given by eqn.(5.4.9). Those modes $(3,1)^{LI}$ and $(4,2)^{LI}$, which tend to infinite frequencies, as given by eqn.(5.4.8) for $\gamma \to 1$, is shown in Fig.5.9. However, for n=0, all the modes including the lowest will tend to infinite frequency as shown in Fig.5.9.

The correspondence between the thin ring modes and the infinite shell modes, is shown in Fig.5.10 for the symmetric modes and Fig.5.11 for the antisymmetric modes, for $\sigma = 0.3$. It may be noticed from Fig.5.10, that the (2,R) and (3,R) shell modes progress to $(2,R)^{T}$ for a thin ring and to $(1,R)^{I}$ and $(1,0)^{LI}$ modes, respectively, for the infinite cylindrical shell. Similar feature is observed for the (4,R) and (5,R) shell modes. Fig.5.11 shows the finite frequency and high frequency shell modes and their thin ring and infinite shell counterparts.

To summarise, this chapter describes the transition from the vibrations of an infinite cylindrical shell to the Pochhammer vibrations of an infinite solid cylinder and the following results may be of particular interest:

(a) The plane strain extensional and shear modes of an infinite hollow cylinder exist as uncoupled in the case of axisymmetric motion. All the shear modes progress to the corresponding infinite frequency modes of a thin shell, for $\gamma \to 1$, as in the case of a thin ring and they tend asymptotically to the Pochhammer modes as $\gamma \to 0$. Among the radial modes, all the modes except the lowest one have similar properties with γ, as the shear modes. For all these modes, this amounts to a rise in frequency as γ increases from 0.0 to 1.0. The lowest extensional mode tends to a finite frequency mode for $\gamma \to 1$ and to the corresponding Pochhammer mode for $\gamma \to 0$. In any case, the frequency of a cylindrical shell mode, for a given γ, differs, but little, from that of the corresponding mode of an annular ring of same γ, even for the values of γ's of the order of 0.5.

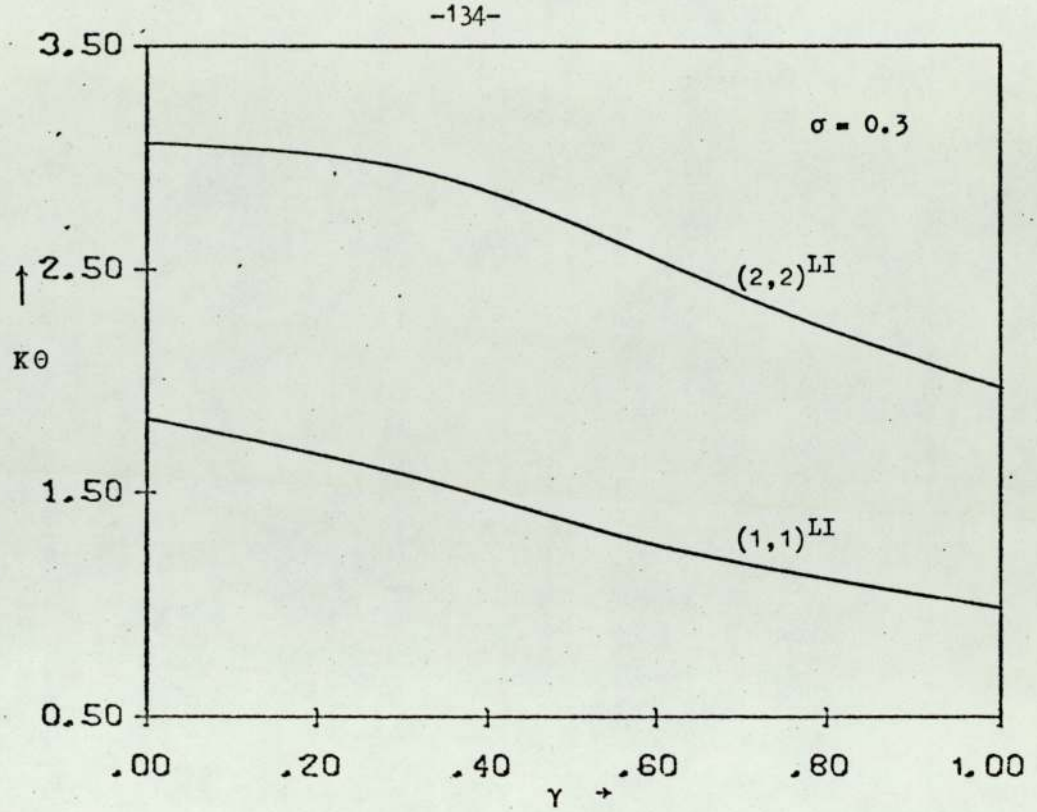

Fig.5.8 The graph of KΘ versus γ for finite frequency longitudinal shear modes. These modes progress, as γ→1, to 1:2 ratio.

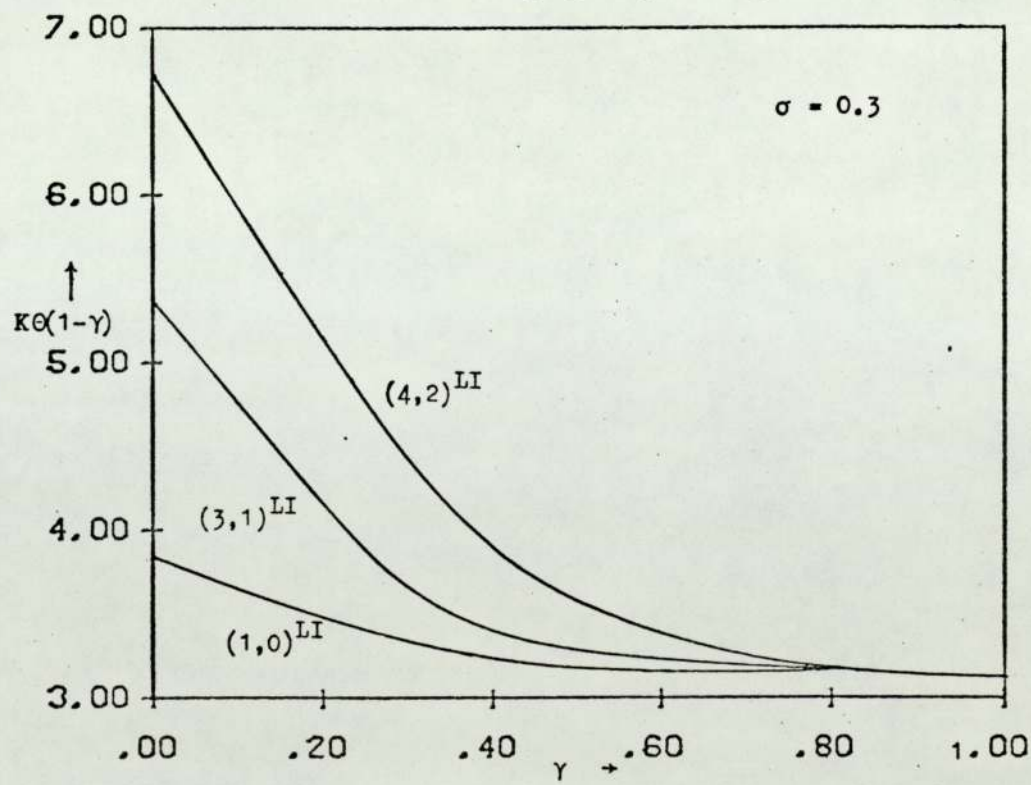

Fig.5.9 The plot of KΘ(1-γ) versus γ for higher longitudinal shear modes. The asymptotic value reached, as γ→1, for all these modes is π.

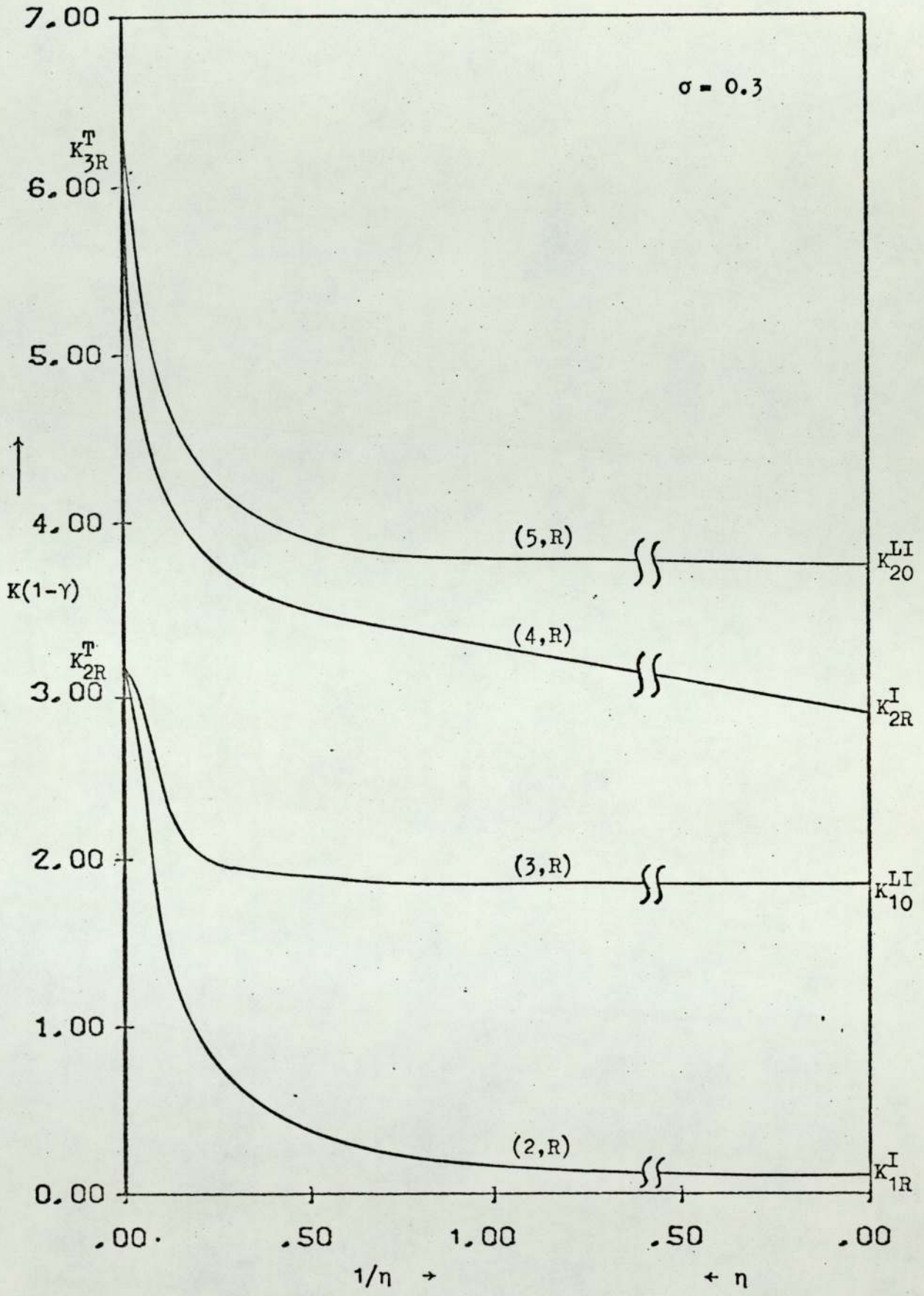

Fig.5.10 The K(1-γ) values plotted as a function of η, for γ=0.9, for (2,R), (3,R), (4,R) and (5,R) modes of the thick annular disk. Notice the transformation of these modes to the corresponding symmetric plane strain and longitudinal shear vibrations.

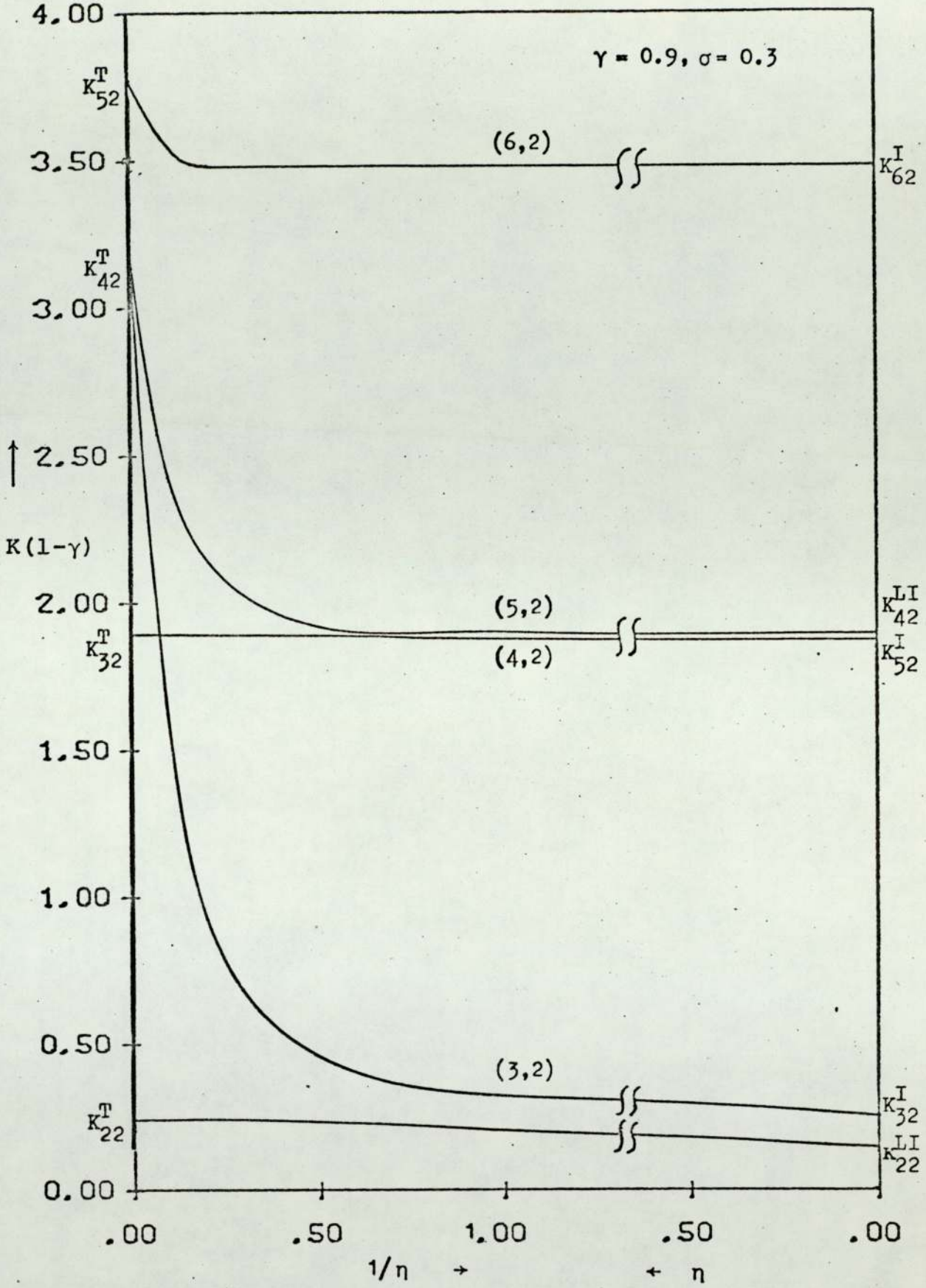

Fig.5.11 The plot of K(1-γ) values versus η, for higher modes for n=2. Notice the transformation of thick annular disk modes to the corresponding thin annular ring and cylindrical shell modes.

(b) The extensional and shear modes are always coupled in the case of non-axisymmetric motion. Also, for $\eta = 0$, these non-axisymmetric (plane strain) modes are uncoupled with the longitudinal shear modes. The two lowest modes of plane strain vibrations for $n > 1$, progress to a flexural and a finite frequency mode series, respectively, as $\gamma \to 1$. However, for $n=1$, the flexural mode always has a zero frequency for all γ's and hence the lowest mode tends to finite frequency as $\gamma \to 1$. All the higher modes, will tend, for $\gamma \to 1$, to either pure extensional (Compressional) or shear mode series.

(c) The longitudinal shear vibrations, which are uncoupled with the plane strain vibrations, are the vibrations which involve only axial displacements. Among the longitudinal shear vibrations, for $n > 0$, the lowest mode tends to a finite frequency mode series, as $\gamma \to 1$. All the higher modes tend to shear frequencies as $\gamma \to 1$. However, for $n=0$, all the modes progress to pure shear modes as γ increases.

CHAPTER 6

PERFORMANCE OF TUNING FORK RESONATOR IN VARIOUS GAS ENVIRONMENTS

6.1 Introduction

A remote acoustic resonator, in the form of solid thermometer (integral probe), has been succesfully employed[1,5] in the measurement of temperature. It is a specially designed tuning fork on the end of a long line and operates at high frequencies. The principal object here is to develop a compact version of such a system, employing a tuning fork, whose lowest natural frequency of flexural vibration is used for the measurement of gas parameters. The system used is an aluminium tuning fork, shown in Fig.6.1, made from a 1" x 1" x 1½" block, aluminium being chosen for its low density and low internal friction. The fork is sufficiently large to enable good machining accuracy, particularly of the gap between the tines, to be obtained. The resonant frequency of the lowest flexural mode of vibration, is of the order of 8 kHz. The internal friction of aluminium at this frequency is of the order of 10^{-4} and the losses measured can, therefore, be attributed to the gas.

The method of determining the resonant frequency and the losses in the resonator is similar to that employed in the measurement of temperature[52]. An electronic system (transmitter) is constructed, which generates bursts of oscillations and these oscillations are applied to the transducer to excite the lowest resonance in the tuning fork. The decrement signal received from the resonator is, in its nature, at the natural resonant frequency. Direct measurements of this frequency and the losses, were made. Thus, the drive frequency need only be sufficiently close to the resonant frequency for a good decrement to be produced. The decrement signal is converted into square pulses in the receiver in order to measure the period of the gate, of ten decrement pulses, generated once in every transmitted burst. This provides an

accurate measurement of the frequency variation with the gas pressure. The performance of the tuning fork resonator in various gas environments and under various pressures are also investigated for different slot widths between the tines of the fork.

6.2 Frequency and Q factor of the Resonator

The tuning fork resonator shown in Fig.6.1 may be regarded as a rectangular bar clamped at one end. The natural frequencies of resonance are given by[53]

$$f_n = \frac{\pi}{2}\left(\frac{\beta_n}{L}\right)^2 k_g C_0 \qquad (6.2.1)$$

where L = length of fork, k_g = the radius of gyration which is $h/\sqrt{12}$ for a bar of rectangular cross-section, $C_0 = \sqrt{E/\rho}$, the rod velocity (velocity of sound in material), β_n = factor determining the overtones, whose values are given by $\beta_1 = 0.597$, $\beta_2 = 1.494$, $\beta_3 = 2.50$ etc. It may be noted that, for large n, $\beta_n \simeq (n-\frac{1}{2})$. Thus, the ratio of the frequencies of overtones to the fundamental resonant frequency is given by

$$\frac{f_n}{f_1} = \left(\frac{\beta_n}{\beta_1}\right)^2 , \qquad n > 1 \qquad (6.2.2)$$

which shows that the fundamental frequency is well isolated from the overtones.

For the aluminium tuning fork used in the measurements (Fig.6.1), the dimensions are h = 1.27 cms., C_0 = 5100 m/sec., L = 3.81 cms. The calculated fundamental frequency of the resonator is 7.211 kHz. The measured frequency of the fundamental resonance is 7.9 kHz.

In the analysis of the tuning fork resonator where the effect of gas vibrations in the narrow gap between the tines is to be studied, a simple model which can be readily analysed is shown in Fig.6.2. The vibration is idealised to the two masses oscillating without rotation increasing and decreasing the air gap. All the mass is considered to be in the masses and all the stiffness in the spring. Any stiffness

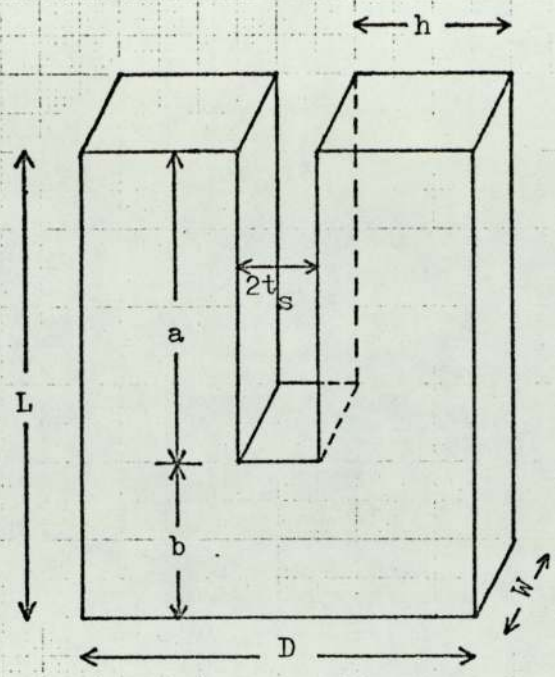

L : Length of fork = $1\frac{1}{2}$"

W : Width of tine = 1"

h : Thickness of tine = 0.48"

b : Length of base = $\frac{1}{2}$"

D : Width of bar = 1"

$2t_s$: Slot width = 0.04"

a : Length of tine = 1"

Fig.6.1 Geometrical form of Tuning fork Resonator

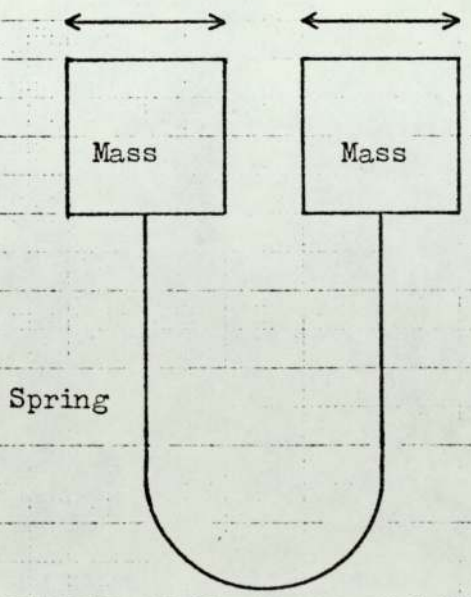

Fig.6.2 Lumped impedance model of Tuning fork Resonator.

arising from the gas in the gap will add to the stiffness of the spring which increases the frequency, because the relation between the stiffness and the frequency is given by[53]

$$\omega^2 = S/m \qquad (6.2.3)$$

where S and m are the stiffness and the mass of the spring, respectively. Treating m as constant, the relation between the added stiffness δS due to the gas pressure between the tines, and the change in the frequency δf can be obtained, by differentiating eqn.(6.2.1), as

$$(\delta f/f) = \tfrac{1}{2} (\delta S/S) \qquad (6.2.4)$$

The added stiffness due to the gas in the gap is calculated in Appendix A.6.1, by regarding the tuning fork as a lumped impedance model. Thus, eqn.(6.2.4) predicts that 1% change in the stiffness changes the frequency by $\frac{1}{2}$ %.

The 'Q' factor of the resonator is given by

$$Q = 2\pi f \times \frac{\text{Energy stored in the fork}}{\text{Power dissipated from the fork}} \qquad (6.2.5)$$

where f is the resonator frequency. The stored energy is lost at a rate proportional to itself. Then, the amplitude of the n^{th} pulse of the exponential echo decrement is given by

$$A_n = A_0 \exp(-n\pi/Q) \quad , \qquad (6.2.6)$$

where A_0 and A_n are the amplitudes of two decrement oscillations n periods apart and Q is the 'Q' factor of the resonator. Then, Q can be determined by measuring A_0 and A_n and it may be noted from eqn.(6.2.6) that Q = n, when the decrement amplitude (A_n) falls to 1/23 of the initial value, A_0.

It is now shown that the Q factor of the resonator is proportional to the half slot-width 't_s' between the tines of the tuning fork shown in Fig.6.1. The piston vibration of the tines pumps the gas in and out of the gap between the tines of the fork. Then, the inertia effect of the gas between tines of the fork yields

$$\text{Energy stored} = \tfrac{1}{2} m C^2 \quad , \qquad (6.2.7)$$

$$\text{Power dissipated} = \frac{1}{2}\left(\frac{16aW\eta_v}{6t_s}\right) C^2 \quad ,$$

where m is the mass of the tine, C is the velocity, a, W and t_s are the dimensions of the tine and η_v is the viscosity of the gas. Then, substituting eqns.(6.2.7) into eqn.(6.2.5), yields

$$Q = k_1 \cdot t_s \qquad (6.2.8)$$

and

$$Q = \frac{k_2}{\eta_v}$$

where k_1 and k_2 are constants of proportionality. Thus, the 'Q' factor is inversely proportional to the viscosity of the gas and directly proportional to the gap between the tines of the fork.

6.3 Electronic System

This section describes the electronic system developed for the measurement of pressure. The functions of the electronic system are: (a) To generate a burst of oscillations, from a variable frequency oscillator, which drives the mechanical resonator (tuning fork) through a magnetostrictive transducer and (b) to measure the frequency of the decrement of the signal received from the resonator through the same transducer.

The block diagram of the experimental arrangement used to measure the pressure is shown in Fig.6.3. In this section, the transmitter which generates the burst of oscillations and the receiver which measures the frequency of the decrement of the resonator, are described.

6.3.1 Transmitter

The function of the transmitter is to generate a burst of oscillations with sufficient duration to allow the tuning fork resonator to approach the maximum amplitude of oscillation and with a sufficient

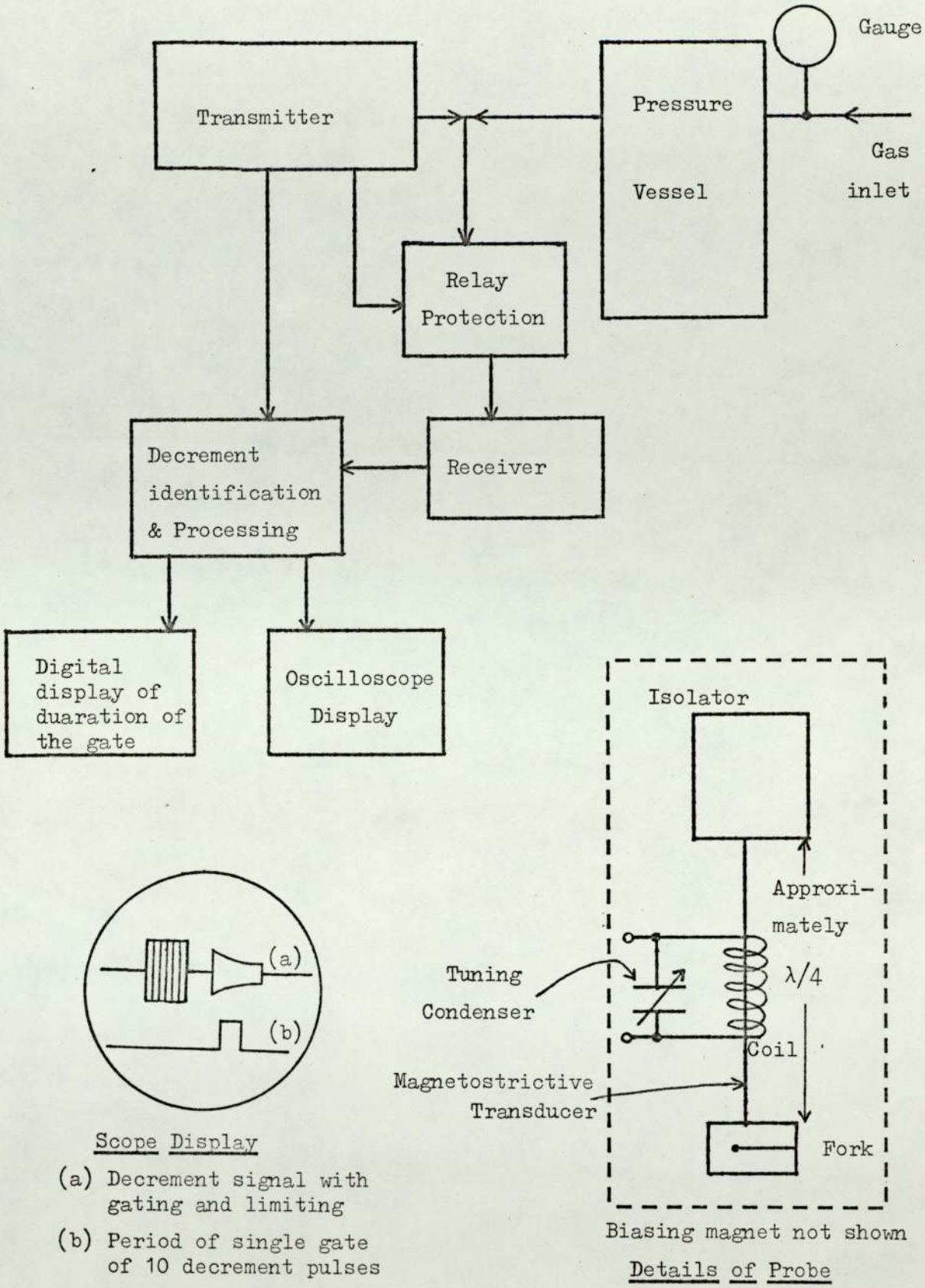

Fig.6.3 The experimental arrangement used for the measurement of gas parameters.

repetition interval to allow the amplitude of the resonator to fall to at least $1/23^{rd}$ of its maximum amplitude. The block diagram of the transmitter is shown in Fig.6.4. The fundamental frequency of fork's flexural resonances has been used for all the measurements. It was found that this resonant frequency is about 8 kHz for the aluminium tuning fork used in the experiments. A variable frequency oscillator is used to produce the transmitted burst of oscillations at a frequency of 8 kHz. The low frequency oscillations (p.r.f), which determines the number of transmitted bursts per second, is derived from the output of the variable frequency oscillator by an arrangement consisting of a Schmitt trigger, divide circuits and a D type flip-flop, as shown in Fig.6.4. This ensures that the p.r.f and drive frequencies are always in synchronism. The waveforms at various points of Fig.6.4 are shown in Fig.6.5. The waveforms at A and B which produce the low frequency oscillations and the high frequency oscillations at points C, are fed to a NAND gate. The output from the NAND gate will then be the required burst of oscillations as shown by waveform D. The power amplifier produces a burst of high voltage transmitter pulses of -15 V to +5 V amplitude, as shown by waveform E in Fig.6.5. These transmitter pulses are then used to drive the magnetostrictive transducer inserted in a coil, which in turn drives the tuning fork resonator connected to one end of the transducer, as shown in Fig.6.3. The circuit diagram of the power amplifier is shown in Fig.A.6.1. Transistors T_1 and T_2 are used for power amplification and the transistor T_3 is used to generate sufficient current in the coil to bias the magnetostrictive transducer. It may be noted from the figure that one end of the coil is connected to the output of the power amplifier, the other end of which is connected to the positive variable power supply line. Because of the short length of the transducer line used, this electromagnetic bias was more practical than the use of a magnet. In particular, final adjust-

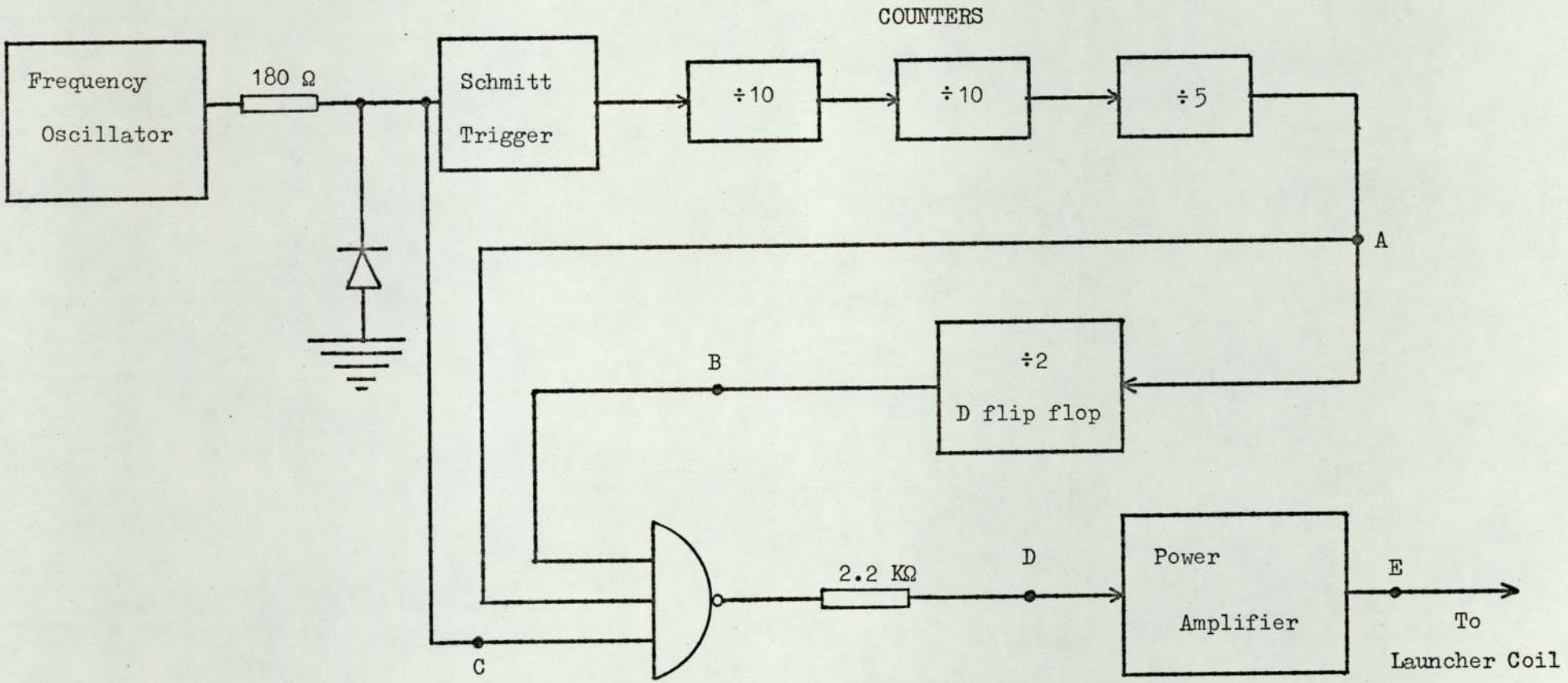

Fig.6.4 Block Diagram of the Transmitter

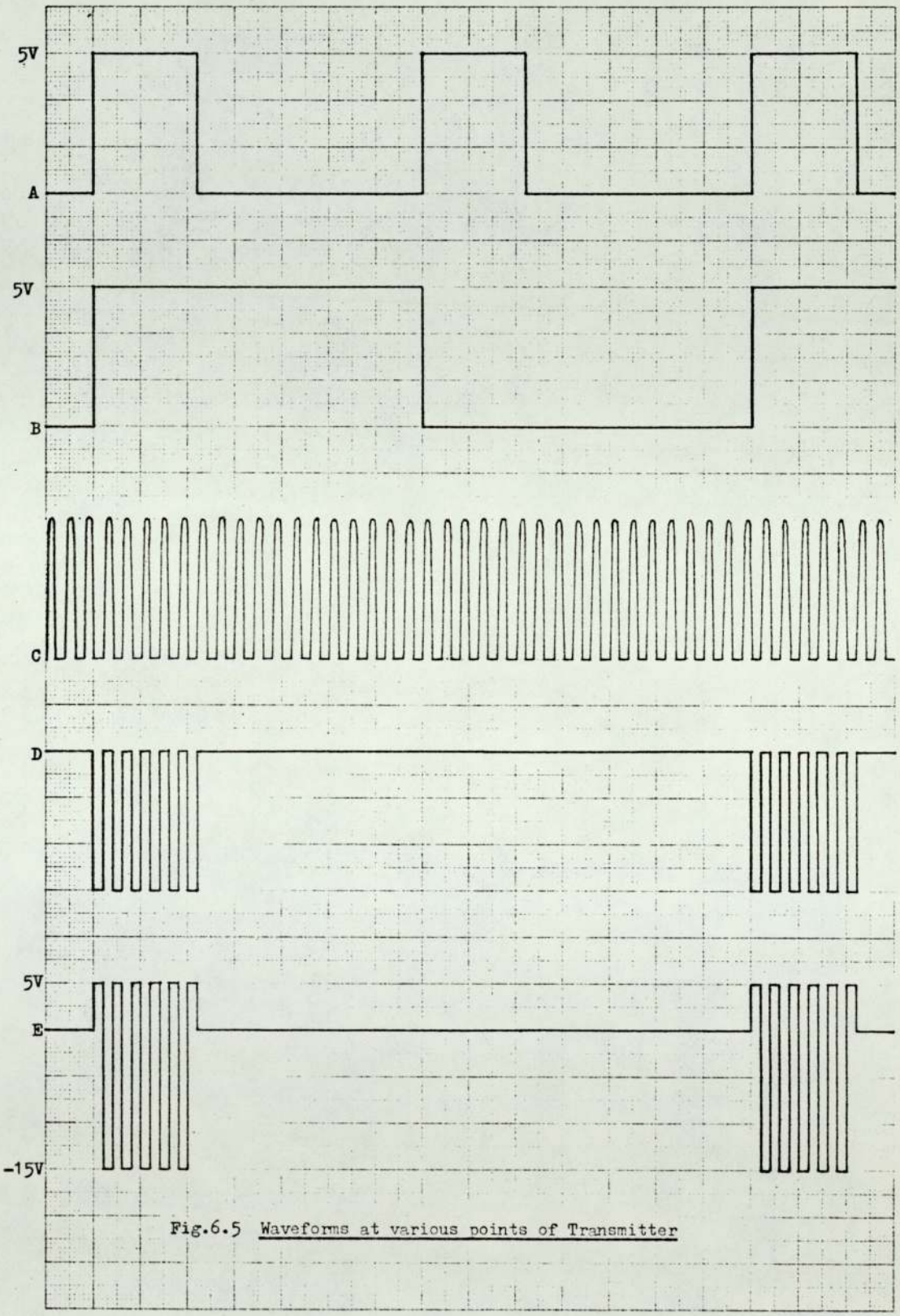

Fig.6.5 Waveforms at various points of Transmitter

ment, when the unit was inside the pressure vessel, could be made. This arrangement gives a maximum amplitude of the signal received from the resonator. This method of obtaining the required burst of transmitter pulses, gives very stable signals, even as the frequency is changed, as it is self synchronised.

6.3.2 Receiver

The block diagram of the receiver is shown in Fig.6.6. The function of the receiver is to amplify and process the received echo signal and to measure the frequency or in this case, the period of the decrement. This is carried out by using ten selected oscillations of the decrement to produce a gate of precisely ten periods duration. The echo pattern is shown by waveform EP in Fig.6.7, which consists of the transmitted burst followed by the transients and the decrement. Thus, processing of the echo signal involves generation of square pulses for TTL circuit operation and sampling of the echo decrement to provide pulses for the reset of the counter and to form a gate of ten pulses.

The receiver basically consists of an open collector reed relay compatible with TTL circuits, monostables generating a control signal for the relay, decrement amplifier, variable gain amplifier with d.c. shift, zero-crossing detector, decrement sampling and divide circuits to generate a gate of ten decrement pulses. The circuit diagrams of some units are given in Appendix A.6 and the waveforms at various points of the receiver are shown in Fig.6.7.

Relay arrangement

The signal on the transducer is comprised of the transmitted burst, the transients and the echo decrement. In order to limit the saturation of the amplifiers and the comparator (zero-crossing detector), a relay arrangement is employed to suppress the transmitted burst and the transients. The control signal for the relay is the output of M_2 shown by M_{2Q} in Fig.6.7. The control signal is derived

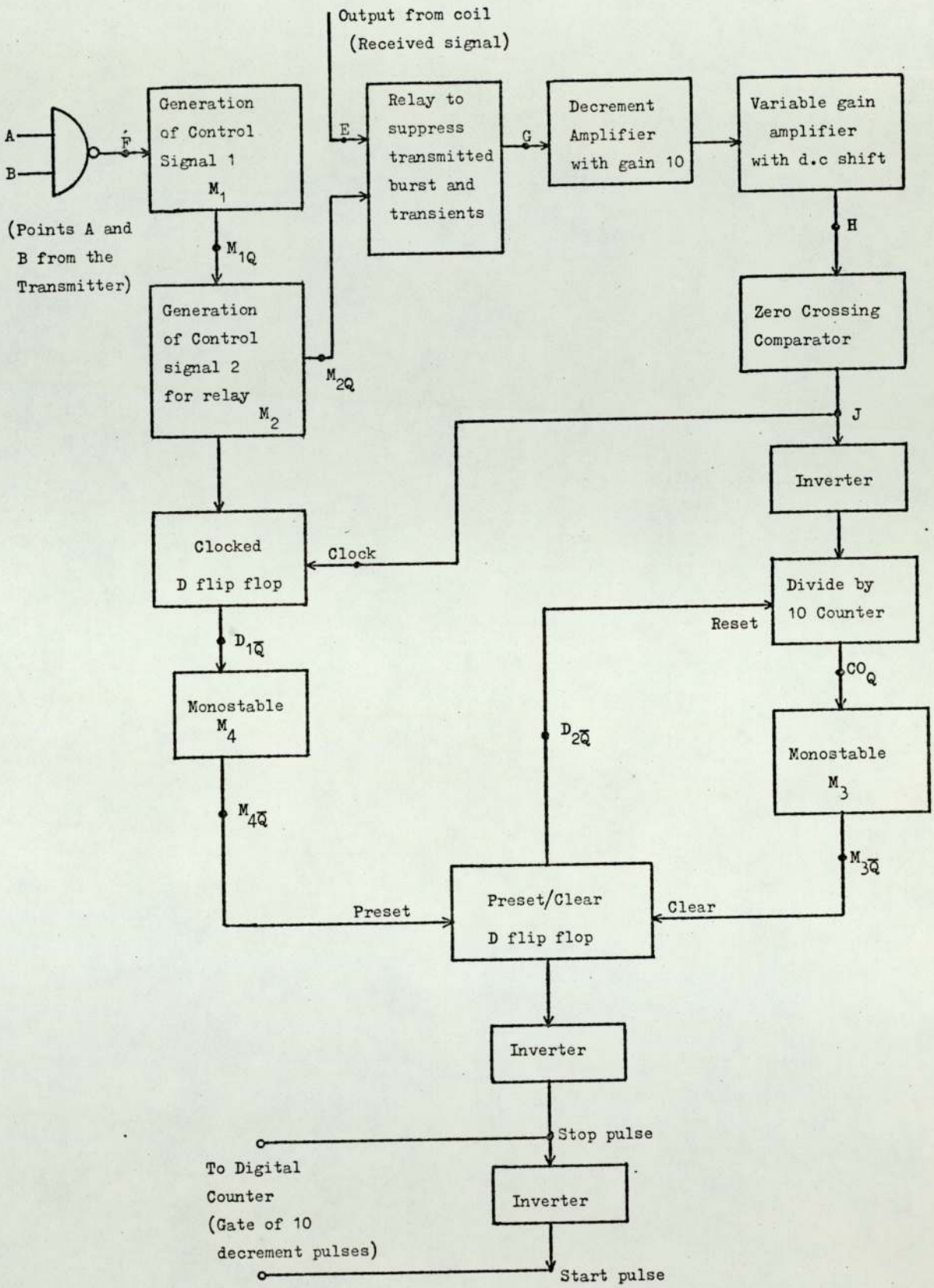

Fig.6.6 Block Diagram of Receiver

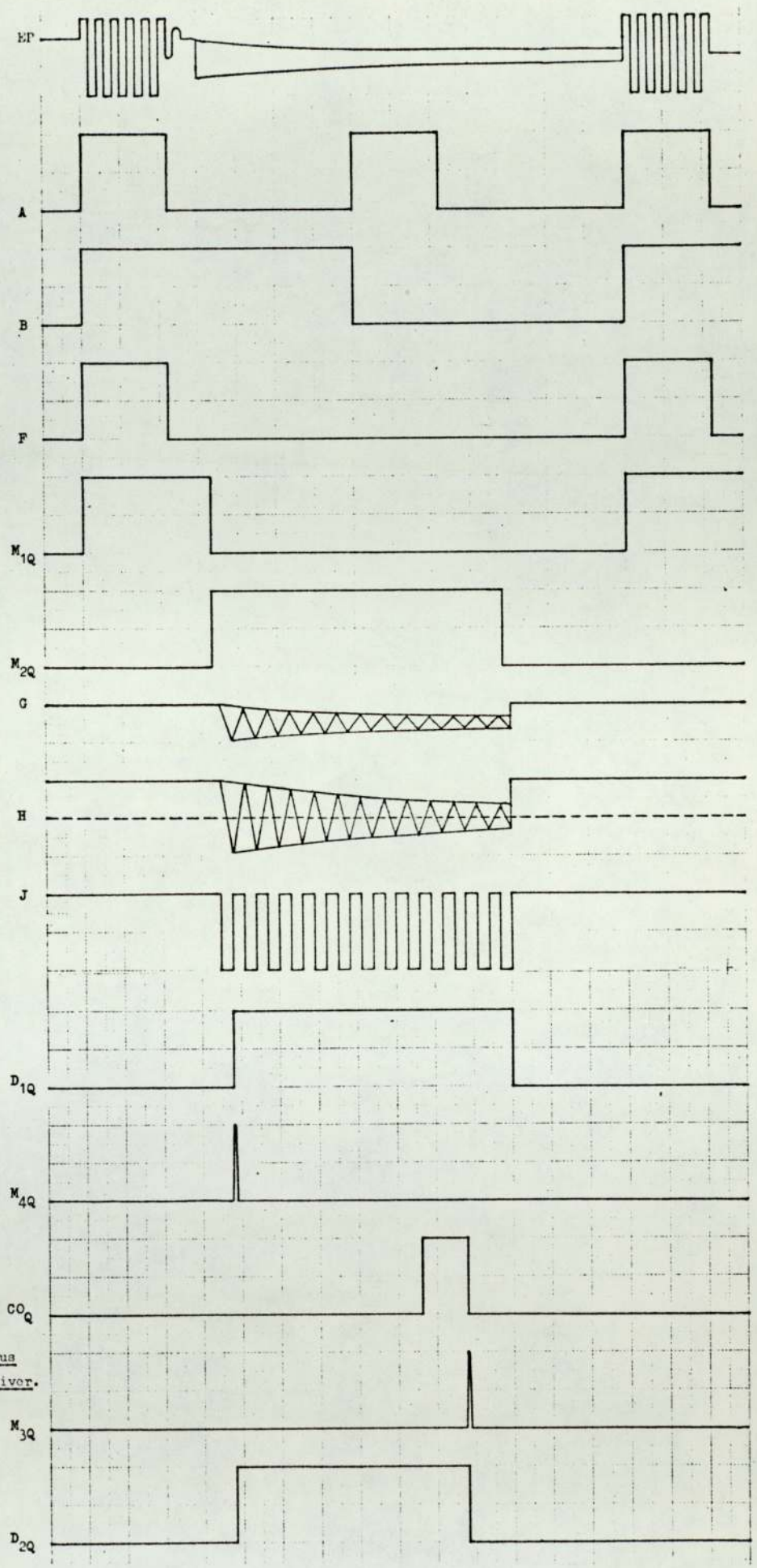

Fig.6.7 Waveforms at various points of the Receiver.

from the signals A and B of the transmitter (shown in Fig.6.5) using two monostables M_1 and M_2. Both the monostables give a flexible arrangement to vary the width of their output pulses by means of a potentiometer, the former to suppress as many transient pulses as needed and the latter to select as many decrement pulses as required. The reed relay is a switch and operates direct from the TTL output as shown in Fig.A.6.2. During the period of the transmitted burst and the transients, the input to relay is in '0' state and the relay is shorted thus suppressing the transmitted pulses and the transients. The output of the relay, then, consists of weak decrement pulses only, as shown in Fig.6.7 by the waveform G.

Decrement amplifier

The output of the relay is then amplified to obtain a sufficient echo signal amplitude for the zero crossing comparator. The amplification is done in two stages with a first stage gain of 10, the second stage being a variable gain amplifier. The first stage also acts as a buffer between the relay output and the input of the second stage. The second stage has an additional facility to shift the d.c. level of the relay output before amplification, in order to drive the zero crossing comparator. This is required because the decrement was asymmetric about the zero level, which may be due to the asymmetry in the transmitted burst and the e.m.f induced by the demagnetisation of the line driving the resonator. The output of the second amplifier is shown by waveform H.

Zero crossing comparator

The zero crossing comparator (LM 306) is used to convert the amplified decrement signal into square pulses. It gives a TTL compatible digital output when the input signal amplitude goes through the zero level. The comparator has a strobe facility which can be used to activate the comparator, only for the required period. The output of

the comparator is shown by the waveform J.

Decrement sampling and counting

The transmitted burst and the transients in the received signal were suppressed in order to obtain the true decrement. Since there is some delay in the relay operation, the output of mono M_2 is not in synchronism with the output of comparator C_1. The two outputs are then synchronised in flip-flop D_1, such that the output of D_1 consists of an integral number of comparator output pulses. The comparator output is fed to a divide-by-ten counter which is reset to start counting only when the output of D_1 goes from the 0 to 1 state. The resetting of the counter is done by the output D_{2Q} of the preset/clear D flip-flop D_2, as shown in Fig.A.6.2. The output of the counter CO is shown by waveform CO_Q in Fig.6.7. The negative going edges of outputs $D_{1\bar{Q}}$ and CO_Q trigger monostables M_4 and M_3, respectively, whose outputs M_{4Q} and M_{3Q} are shown in Fig.6.7. The outputs $M_{4\bar{Q}}$ and $M_{3\bar{Q}}$ of these monostables are then used to preset/clear the D flip-flop D_2, which generates a gate of ten pulses of the decrement. The output D_{2Q} is also shown in Fig.6.7. The duration of the gate is measured by the digital counter as shown in Fig.A.6.2. This gives the frequency of the decrement and provides a better calibration against the pressure.

6.4 Experimental Apparatus

The apparatus, for the measurement of gas parameters such as pressure and viscosity, consists of (a) a probe which is fed by the transmitted burst of oscillations from the electronic system, (b) a pressure vessel into which the probe is located and a pressure gauge.

6.4.1 Probe

The probe consists of an isolator, a magnetostrictive transducer, a driving coil and the tuning fork resonator, as shown in Fig.6.3. The probe, as a whole, is to be located inside the pressure vessel which contains the gas whose effect on the natural frequency of the resonator,

is to be investigated. In addition, a permanent magnet may be incorporated to polarise the magnetostrictive line which increases the decrement amplitude.

The isolator, consisting of a two inch long steel cylinder of one inch diameter, can be regarded as a solid termination to the line. The standing waves will result in the overall system having a slightly different natural frequency from that of the fork alone. The driving line, assumed lossless will present a reactance, to the fork, of $-j Z_0 \cot \theta$ where Z_0 is the impedance of the line, $\theta = 2\pi l/\lambda$, and l and λ are the length of the line and the wavelength, respectively. Between l=0 and $\lambda/4$, the reactance will represent a stiffness, increasing the natural frequency of the fork, and between $\lambda/4$ and $\lambda/2$, a mass, decreasing the frequency. The $\lambda/2$ value must be avoided as it, in effect, represents the whole of the isolator attached to the point of contact. In practice, the line length was chosen to be about $\lambda/4$ giving zero reactive load.

The magnetostrictive transducer used is a short telcoseal line and a coil of about 2000 turns of fine wire is wound on this line. The length of the magnetostrictive line was chosen to be of quarter-wavelength (15.5 cms.) between the isolator and the resonator. The transmitter output, which is fed to the coil, produces a varying magnetic field. The magnetostrictive transducer converts this magnetic field into mechanical energy which drives the resonator. The same launcher coil acts as the receiver of the signal from the resonator. A permanent field in the coil, due to the current generated from the transistor T_3 in Fig.A.6.1, polarises the transducer and sets up a bias condition on the transducer. Depending on the position of the coil, this bias condition either aids or opposes the magnetostrictive action. Maximum signal was obtained from the resonator when the coil was resting either on the isolator or on the tuning fork. Later, it was observed that the

permanent magnet aided the magnetostrictive action and resulted in maximum signal. A decade switched capacitor is connected in parallel with the coil, to tune the resonance to the driving frequency.

The resonator is basically an aluminium block which has a deep narrow slot cut as shown in Fig.6.1. The dimensions of the tuning fork resonator are also shown in the figure. The tuning fork is driven by the magnetostrictive line which is recessed into the base or one of the tines of the fork and sealed with araldite to give a good acoustic joint. The coupling can be adjusted by changing the point at which the line joins the fork or by changing the diameter of the line. In all measurements, the fork was driven at right angles to the plane of the tines.

The resonator vibrates upon receiving energy from the transducer and the stored energy in the resonator decays exponentially at its natural frequency. The resonant frequency of the tuning fork is proportional to the velocity of sound in the material (aluminium) and is also a function of the fork's shape and dimensions. For a given shape $\omega a/C$ is a constant, which depends, to some extent, on Poisson's ratio depending on the particular type of velocity chosen for C, where 'a' is a scaling dimension. The measurements of the decrement amplitude enable the measurement of Q where Q^{-1} represents the losses in the resonator. When the tuning fork is in the presurre vessel, the smaller the width of the slot between the tines, the larger will be the inertia added to the system due to the gas pressure in the slot. The inertia also increases with the pressure of the gas between the tines. The resonant frequency of the fork, which is proportional to the inertia, thus increases as the pressure in the vessel is increased.

6.4.2 The Pressure Vessel and the Gauge

The pressure vessel was constructed to withstand pressures upto 250 psi. It was made of brass to ensure that no magnetic interaction

occurs between the vessel and the probe. The length of the vessel was made about 65 cms., to enable the measurement of gas parameters, to be carried out with a longer magnetostrictive line (transducer) between the resonator and the isolator. The diameter of the vessel was made about 10 cms. The cover (lid) for the vessel was designed to allow the maximum pressure of 250 psi to be reached when the probe is inside the vessel. To anchor the isolator of the probe into the lid, a vice type wooden clamp is provided. Provision is also made for locating the electrical terminals of the driving coil outside the cover.

The pressure gauge used has a dial which has been calibrated upto 250 psi and each division is 5 psi. The pressure vessel and the gauge can be seen in the photograph of the experimental set up (Fig.6.8). Further details about the probe and the pressure vessel are given in the undergraduate project report[54].

6.5 Measurements

To investigate the effect of the gas parameters on the performance of the tuning fork, the experimental arrangement is set up, together with all the associated equipment, as shown in Fig.6.8. The digital counter is used to measure the duration of the gate of ten pulses, generated from the decrement pulses and an oscilloscope is used in order to display the decrement and to enable its resonance to be detected. At resonance, the decrement from the resonator will have a maximum amplitude and the decay will always be at the natural frequency of the resonator. For all measurements, the lowest flexural resonant mode was investigated, by driving the fork at right angles to the tines. Precaution was taken to suppress the standing waves in the pressure vessel.

6.5.1 The Effect of Pressure on the Resonator Frequency

The effect of the pressure on the performance of the tuning fork resonator can be investigated by measuring the resonator frequency for various gas pressures. To determine the natural frequency of the

Fig.6.8 Photograph of the experimental arrangement used to measure the gas parameters.

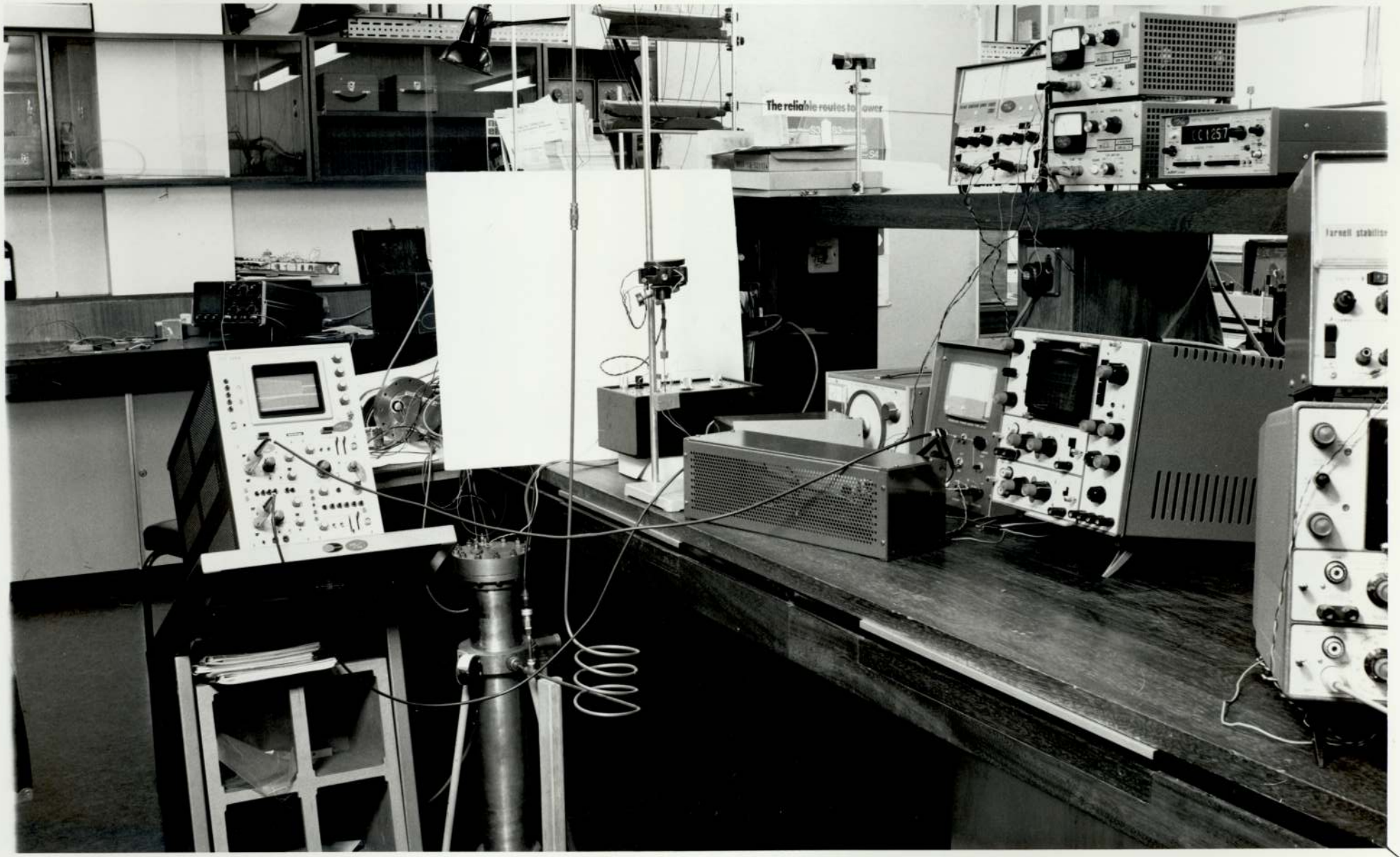

resonator, the duration of the gate of ten decrement pulses was measured on the digital counter shown in Fig.6.8, for various pressures in the vessel.

The tuning fork resonator was excited, by the transmitter output, using the magnetostrictive transducer. The resonance of the fork was detected by observation, of the echo decrement signal received from the resonator, on the oscilloscope. The position of the coil on the transducer, the tuning capacitance and the driving frequency are adjusted to maximise the amplitude of the decrement. After these initial adjustments, the probe is placed inside the pressure vessel by clamping the isolator in the vice type clamp. The vessel was then pressurised at the highest pressure available, namely 250 psi, and the effect of pressure on the decrement was observed. The period of the gate of ten pulses was measured on the digital counter, for pressures from 230 psi to 0 psi in steps of 10 psi, and the pressure was measured each time on the calibrated pressure gauge. The graph of this period is plotted as a function of pressure as shown in Fig.6.9. The two graphs in the figure represent the measurements taken on two different tuning forks of slot widths of 0.040 and 0.015 inches, respectively.

6.5.2 Measurement of Losses

The losses in the resonator, which change with pressure, occur in many ways, due to, (a) the internal friction in the resonator material, (b) the energy lost in the coupling of the magnetostrictive line to the resonator, (c) the acoustic radiation, (d) the viscous losses and (e) the thermal losses[6]. The losses (a) and (b) can be calculated by measuring the appropriate Q factors; namely 'material Q' in the former and the 'coupling Q' in the latter; designated by Q_m and Q_c, respectively. For a given line, Q_c is constant and is independent of pressure. The Q_m for aluminium resonator is very large and, therfore, the losses can be taken as negligible. The losses (Q^{-1}) can be

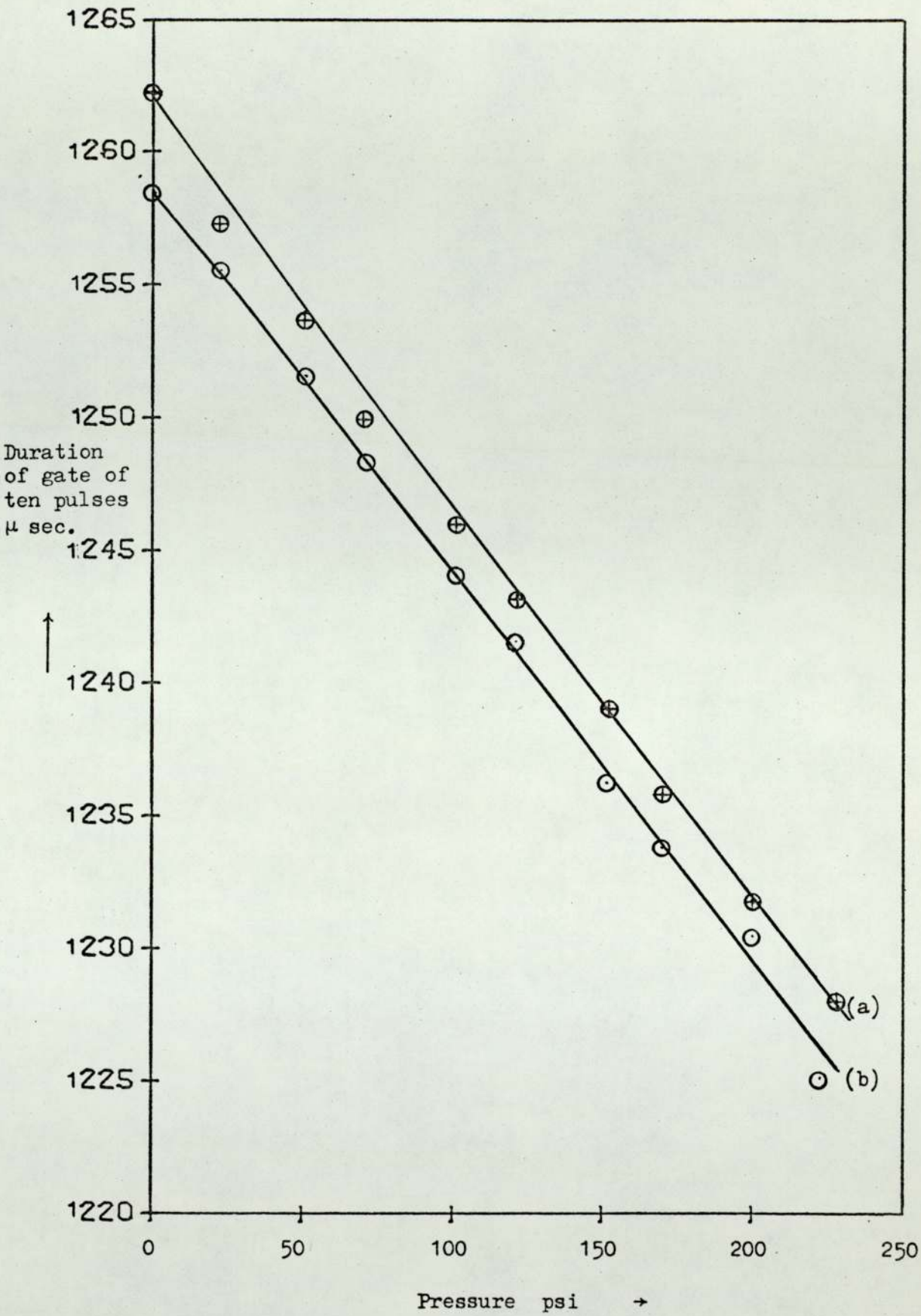

Fig.6.9 Graph of duration of ten decrement pulses versus Pressure
(a) Tuning fork with large slot width (0.04 in.)
(b) Tuning fork with small slot width (0.015 in.)

calculated by noting the amplitudes A_0 and A_n of two decrement pulses n periods apart and using the formula

$$Q^{-1} = \frac{\ln(A_0/A_n)}{n\pi} \qquad (6.5.1)$$

Equation (6.5.1), which can be derived from eqn.(6.2.6), gives the expression for Q^{-1}, the losses. The amplitudes A_0 and A_n, the number of pulses n and the pressure were measured at intervals of 10 psi from 230 psi to 0 psi, as before. The plot of Q^{-1} versus pressure is shown in Fig.6.10. The two graphs correspond to the same two tuning forks considered in the previous section.

6.6 Discussion

It can be noticed from Fig.6.9 that the tuning fork with a smaller slot width between the tines, vibrates at a higher frequency than that of the fork with a larger gap between the tines. This is because, the smaller the width between the fork's tines, the larger will be the stiffness added to the system. This is explained by eqn.(A.6.11). Also, note that the two forks were made from identical aluminium blocks.

The figure also shows that the resonant frequency of a given tuning fork increases with pressure. This is expected, because, the increase in pressure results in an increase in the stiffness which, in turn, produces an increase in the resonant frequency. This is explained by eqn.(6.2.4).

The behaviour of energy losses in the resonator with the change in pressure can be explained by viscous losses, thermal losses, material losses, coupling losses and acoustic radiation. The coupling losses remain constant with pressure and the material losses are negligible. The thermal and viscous losses increase with pressure because of the increase of gas density with pressure. From Fig.6.10, it may be seen that the energy losses are large at higher pressure. In the figure, a peculiar change in the losses, may also be noticed at high pressures.

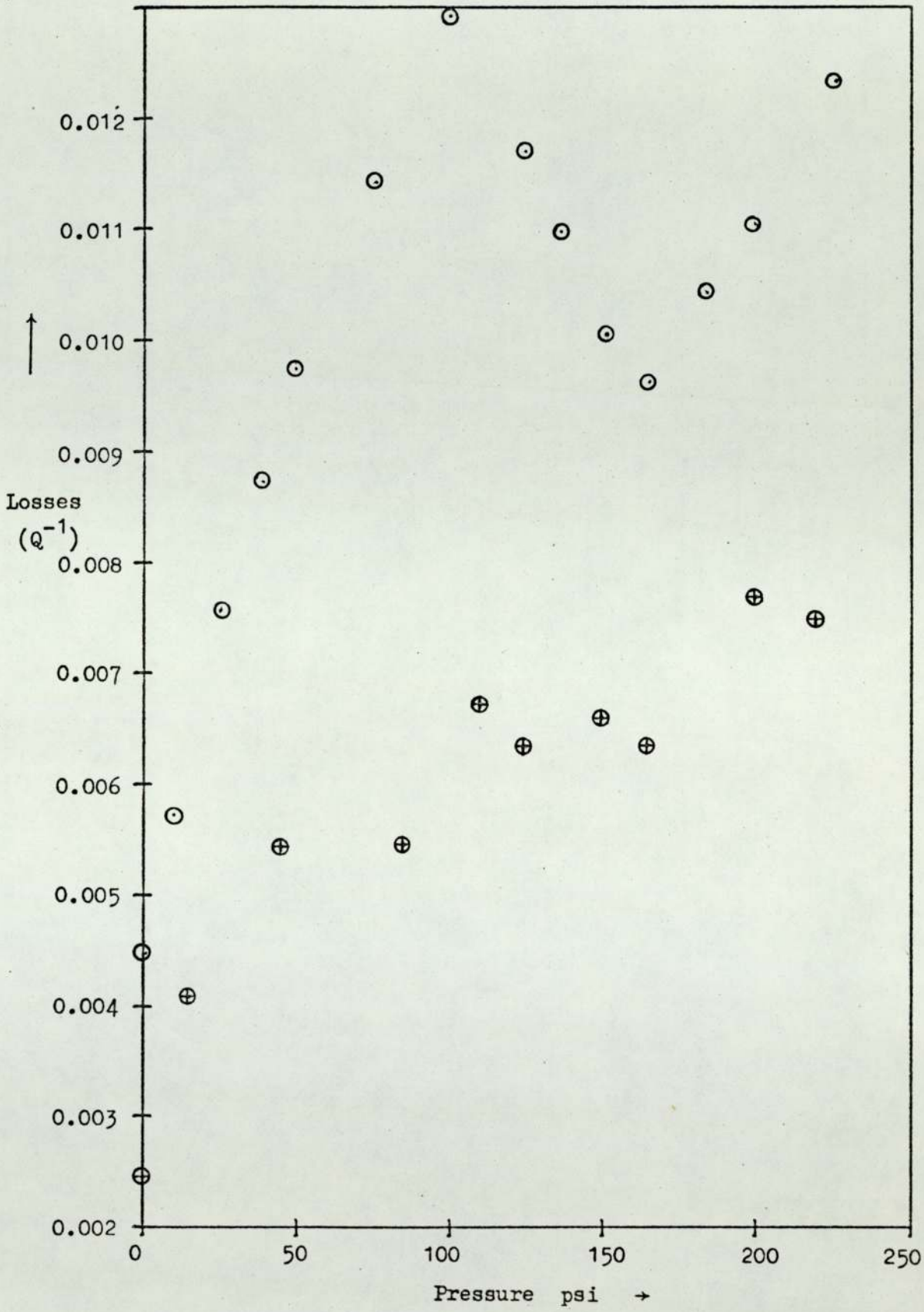

Fig.6.10 Graph showing the variation of losses with pressure.

⊙ Tuning fork with small slot width

⊕ Tuning fork with large slot width.

This may be due to acoustic radiation. Reverberations in the chamber may be one of the factors causing this peculiar change in losses. The phenomena is so complex that further investigation was not pursued. However, the suggestions for further work in this area are given in Chapter 8.

CHAPTER 7

THE SPECTRA OF DISK-SHAFT RESONATORS

7.1 Introduction

The vibrations in disks and rods were investigated in previous Chapters. This chapter deals with the vibration spectra of disk-shaft system shown in Fig.7.1. This structure resembles, to some extent, the turbine disk in turbomachinery and hence it is of interest to study the spectra of its in plane vibrations.

The solution for the flexural vibrations of uniformly loaded circular and rectangular plates with various boundary conditions was given by Berger[56]. Later, Berger's equations have been applied to obtain the frequency equations for flexural vibrations of clamped[57,58] and simply supported[58] circular plates with concentric rigid mass. The frequency equations for the critical speeds associated with backward and forward whirling modes of a rotating shaft-disk system were given by Eshleman and Eubanks[59]. Vogel and Skinner[60] have derived frequency determinants for various combinations of boundary conditions with the flexural (transverse) vibrations of uniform annular plates. Recently, the axisymmetric (flexural) vibrations of circular plates with a single circular step thickness has been analysed by Juarez[61].

In this chapter, an attempt is made to obtain the solution for axisymmetric (radial and torsional) and non-axisymmetric (Compound) vibrations of the disk-shaft system shown in Fig.7.1. Various theories are proposed to deal with the vibration problems associated with different shaft lengths. The resonant spectra were obtained for disk-shaft resonators of various disk and shaft dimensions.

7.2 Proposed Theory

In this section, three types of theory are proposed to deal with the problem of non-axisymmetric vibrations of a disk-shaft resonator, for varying shaft lengths and disk diameters. The disk-shaft system can

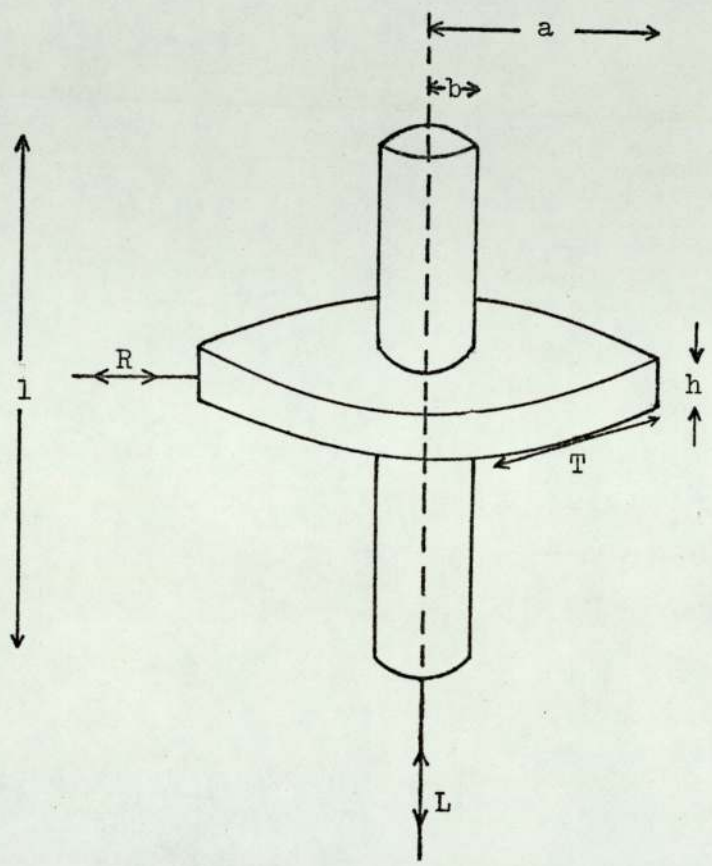

a = Disk radius ,
b = Shaft radius,
h = Disk thickness ,
l = Shaft length.

R — Radial drive; L — Longitudinal drive ; and
T — Tangential drive.

Fig.7.1 Geometrical form of a Disk-shaft resonator.

be treated as, either (a) a disk with a rigid centre or (b) a thick disk inside a thick annular disk for shaft lengths smaller than its diameter or (c) a shaft inside an annular plate.

7.2.1 Disk with a Concentric Rigidity

In this section, the disk-shaft resonator shown in Fig.7.1 is regarded as an annular plate with a free edge at r=a and the edge at r=b being rigid (clamped). The frequency equations and their numerical solutions, for flexural vibrations of an annular plate clamped at centre, are given by Gontkevich[62] and Raju[63], respectively. The frequency equations for the non-axisymmetric (compound) and axisymmetric (radial and tangential) vibrations of this structure, are derived here, using the annular ring theory given in chapter 3.

The radial and tangential displacements ξ_r and ξ_θ are given by eqns.(A.3.4) in Appendix A.3.1. The boundary conditions at the free edge r=a, are

$$\begin{aligned} T_{rr} &= 0 \text{ at } r=a \\ T_{r\theta} &= 0 \text{ at } r=a \end{aligned} \qquad (7.2.1)$$

and at the clamped edge r=b, are

$$\begin{aligned} \xi_r &= 0 \text{ at } r=b \\ \xi_\theta &= 0 \text{ at } r=b \end{aligned} \qquad (7.2.2)$$

The expressions for T_{rr} and $T_{r\theta}$ are also given in Appendix A.3.1, by eqns.(A.3.6). Thus, substituting eqns.(A.3.4) and (A.3.6) into eqns. (7.2.1) and (7.2.2) and simplifying, yields the compound mode frequency equation, formed by the determinant of the amplitude constants, as

$$|a_{ij}| = 0 , \quad i,j = 1 \text{ to } 4, \qquad (7.2.3)$$

where the elements in the first two rows of the above determinant are given by the first eight elements of eqns.(3.2.2), by replacing K^T by K and

$$
\begin{aligned}
a_{31} &= J_n(K\gamma)\{M_n(K\gamma) - n\} \quad , \\
a_{32} &= Y_n(K\gamma)\{L_n(K\gamma) - n\} \quad , \\
a_{33} &= n\, J_n(K\gamma\theta) \quad , \\
a_{34} &= n\, Y_n(K\gamma\theta) \quad , \\
a_{41} &= n\, J_n(K\gamma) \quad , \\
a_{42} &= n\, Y_n(K\gamma) \quad , \\
a_{43} &= J_n(K\gamma\theta)\{M_n(K\gamma\theta) - n\} \quad , \\
a_{44} &= Y_n(K\gamma\theta)\{L_n(K\gamma\theta) - n\}
\end{aligned}
\tag{7.2.4}
$$

Putting n=0 in eqn.(7.2.3) and simplifying yields the radial mode frequency equation, as

$$
\begin{vmatrix} b_{11} & b_{12} \\ b_{31} & b_{32} \end{vmatrix} = 0 \quad , \tag{7.2.5}
$$

and the tangential mode frequency equation as

$$
\begin{vmatrix} b_{23} & b_{24} \\ b_{43} & b_{44} \end{vmatrix} = 0 \quad , \tag{7.2.6}
$$

where

$$
\begin{aligned}
b_{11} &= J_1(K)\{M_1(K) - (1-\sigma)\} \quad , \\
b_{12} &= Y_1(K)\{L_1(K) - (1-\sigma)\} \quad , \\
b_{31} &= J_1(K\gamma) \quad , \\
b_{32} &= Y_1(K\gamma) \quad , \\
b_{23} &= J_1(K\theta)\{M_1(K\theta) - 2\} \quad , \\
b_{24} &= Y_1(K\theta)\{L_1(K\theta) - 2\} \quad , \\
b_{43} &= J_1(K\gamma\theta) \quad , \\
b_{44} &= Y_1(K\gamma\theta) \quad .
\end{aligned}
\tag{7.2.7}
$$

7.2.2 Thick Disk inside a Thick Annular Plate

The disk-shaft with shaft length smaller than its diameter, can be treated as a thick disk inside a thick annular plate. Thus, the thick disk theory of chapter 2 and the theory developed in chapter 4 for thick annular plates, could be used in order to obtain the compound mode frequency equation of this structure. Then, the boundary conditions at the free edge r=a, for this system, will be

$$\begin{aligned} T_{rr_2} &= 0 \quad , \\ T_{r\theta_2} &= 0 \quad , \\ T_{rz_2} &= 0 \end{aligned} \tag{7.2.8a}$$

and the continuity conditions at r=b, will be

$$\begin{aligned} T_{rr_1} &= T_{rr_2} \quad , \\ T_{r\theta_1} &= T_{r\theta_2} \\ T_{rz_1} &= T_{rz_2} \\ \xi_{r_1} &= \xi_{r_2} \\ \xi_{\theta_1} &= \xi_{\theta_2} \\ \xi_{z_1} &= \xi_{z_2} \end{aligned} \tag{7.2.8b}$$

where the suffices 1 and 2 refer to the thick disk and the thick annular plate, respectively. The stress resulatants T_{rr_1}, $T_{r\theta_1}$, and T_{rz_1} for the thick disk and T_{rr_2}, $T_{r\theta_2}$, and T_{rz_2} for the thick annular plate, are given by

$$\begin{aligned} T_{rr_i} &= \frac{h_i E}{(1+\sigma)(1-2\sigma)} \left[(1-\sigma) \frac{\partial \xi_{r_i}}{\partial r} + \frac{\sigma}{r} \left(\xi_{r_i} + \frac{\partial \xi_{\theta_i}}{\partial \theta} \right) + \frac{2\sigma}{h_i} \xi_{z_i} \right] \\ T_{r\theta_i} &= \frac{h_i E}{2(1+\sigma)} \left[\frac{\partial \xi_{\theta_i}}{\partial r} - \frac{\xi_{\theta_i}}{r} + \frac{1}{r} \frac{\partial \xi_{ri}}{\partial \theta} \right] \end{aligned} \tag{7.2.9}$$

$$T_{rz_i} = \frac{h_i^2 E}{\pi^2(1+\sigma)} \frac{\partial \xi_{z_i}}{\partial r}$$

where i=1,2 and h_i = 1, for i=1,
= h, for i=2.

The displacement functions for the thick disk and the thick annular plate are given by

$$\xi_{r_1} = \left[A_1 \frac{dJ_n(\alpha_1 r)}{dr} + B_1 \frac{dI_n(\beta_1 r)}{dr} + \frac{nC_1}{r} J_n(\nu_1 r) \right] \cos n\theta$$

$$\xi_{\theta_1} = -\left[\frac{nA_1}{r} J_n(\alpha_1 r) + \frac{nB_1}{r} I_n(\beta_1 r) + C_1 \frac{dJ_n(\nu_1 r)}{dr} \right] \sin n\theta$$

$$\xi_{z_1} = \left[A_1 \phi_1 J_n(\alpha_1 r) - B_1 \phi_2 I_n(\beta_1 r) \right] \cos n\theta \qquad (7.2.10)$$

$$\xi_{r_2} = \left[A_2 \frac{dJ_n(\alpha_2 r)}{dr} + A_3 \frac{dY_n(\alpha_2 r)}{dr} + B_2 \frac{dI_n(\beta_2 r)}{dr} + B_3 \frac{dK_n(\beta_2 r)}{dr} + \frac{nC_2}{r} J_n(\nu_2 r) + \frac{nC_3}{r} Y_n(\nu_2 r) \right] \cos n\theta$$

$$\xi_{\theta_2} = -\left[\frac{nA_2}{r} J_n(\alpha_2 r) + \frac{nA_3}{r} Y_n(\alpha_2 r) + \frac{nB_2}{r} I_n(\beta_2 r) + \frac{nB_3}{r} K_n(\beta_2 r) + C_2 \frac{dJ_n(\nu_2 r)}{dr} + C_3 \frac{dY_n(\nu_2 r)}{dr} \right] \sin n\theta$$

$$\xi_{z_2} = \left[A_2 \phi_3 J_n(\alpha_2 r) + A_3 \phi_3 Y_n(\alpha_2 r) - B_2 \phi_4 I_n(\beta_2 r) - B_3 \phi_4 K_n(\beta_2 r) \right] \cos n\theta$$

where $$\phi_1 = \frac{(1-\sigma)}{b\ \eta_1 \sigma} \left[\delta_1^2 - \frac{K^2\gamma^2}{c} \right] ,$$

$$\phi_2 = \frac{(1-\sigma)}{b\ \eta_1 \sigma} \left[\lambda_1^2 \delta_1^2 + \frac{K^2\gamma^2}{c} \right] , \qquad (7.2.11)$$

$$\phi_3 = \frac{(1-\sigma)}{a\ \eta_2 \sigma} \left[\delta_2^2 - \frac{K^2}{c} \right] ,$$

$$\phi_4 = \frac{(1-\sigma)}{a\ \eta_2 \sigma} \left[\lambda_2^2 \delta_2^2 + \frac{K^2}{c} \right] ,$$

$$\gamma = \frac{b}{a} \ , \quad \eta_1 = \frac{2b}{l} \ , \quad \eta_2 = \frac{2a}{h} \ , \tag{7.2.12a}$$

and the wavenumbers are given by

$$\delta_1 = \alpha_1 b \ , \quad \lambda_1\delta_1 = \beta_1 b \ , \ \delta_2 = \alpha_2 a \ , \quad \lambda_2\delta_2 = \beta_2 a \ , \ K\Theta = \nu_2 a, \quad K\gamma\Theta = \nu_1 b \ , \tag{7.2.12b}$$

where

$$\delta_i = \frac{\pi \eta_i}{2} \sqrt{\frac{G_i(\psi_i+1)}{(1-\sigma)}} \ ,$$

$$\lambda_i\delta_i = \frac{\pi \eta_i}{2} \sqrt{\frac{G_i(\psi_i-1)}{(1-\sigma)}}$$

$$G_i = \left[\frac{2K_i^2 (3-4\sigma)}{\pi^2 \eta_i^2 (1-\sigma)} - 1 \right] \tag{7.2.12c}$$

$$\psi_i = \left[1 + \frac{4(G_i+1)(1-\sigma)^2}{G_i^2 (3-4\sigma)} \{ 1 - \frac{2(G_i+1)(1-\sigma)}{c\,(3-4\sigma)} \} \right]^{\frac{1}{2}}$$

where $i=1,2$ and $K_i = K\gamma$, for $i=1$,
$= K$, for $i=2$.

Substituting eqns.(7.2.9) to (7.2.12) into eqns.(7.2.8) and simplifying, yields the frequency equation for compound modes of vibration, as

$$|X_{ij}| = 0 \ ; \ i,j = 1 \text{ to } 9 \tag{7.2.13}$$

where

$$X_{11} = 0 \ ,$$

$$X_{12} = - J_n(\delta_2) \{ M_n(\delta_2) - n(n+1) + \frac{K^2\Theta^2}{2} \} \ ,$$

$$X_{13} = - Y_n(\delta_2) \{ L_n(\delta_2) - n(n+1) + \frac{K^2\Theta^2}{2} \} \ ,$$

$$X_{14} = 0 \ ,$$

$$X_{15} = - I_n(\lambda_2\delta_2) \{ N_n(\lambda_2\delta_2) - n(n+1) + \frac{K^2\Theta^2}{2} \} \ ,$$

$$X_{16} = K_n(\lambda_2\delta_2) \{ P_n(\lambda_2\delta_2) + n(n+1) - \frac{K^2\Theta^2}{2} \} \ ,$$

$$X_{17} = 0 \ ,$$

$$X_{18} = n\, J_n(K\Theta)\,\{ M_n(K\Theta) - (n+1)\} \quad ,$$

$$X_{19} = n\, Y_n(K\Theta)\,\{ L_n(K\Theta) - (n+1)\}$$

$$X_{21} = 0 \quad ,$$

$$X_{22} = - n\, J_n(\delta_2)\,\{ M_n(\delta_2) - (n+1)\} \quad ,$$

$$X_{23} = - n\, Y_n(\delta_2)\,\{ L_n(\delta_2) - (n+1)\} \quad ,$$

$$X_{24} = 0 \quad ,$$

$$X_{25} = - n\, I_n(\lambda_2\delta_2)\,\{ N_n(\lambda_2\delta_2) - (n+1)\} \quad ,$$

$$X_{26} = n\, K_n(\lambda_2\delta_2)\,\{ P_n(\lambda_2\delta_2) + (n+1)\} \quad ,$$

$$X_{27} = 0 \quad ,$$

$$X_{28} = J_n(K\Theta)\,\{ M_n(K\Theta) - n(n+1) + \frac{K^2\Theta^2}{2}\} \quad ,$$

$$X_{29} = Y_n(K\Theta)\,\{ L_n(K\Theta) - n(n+1) + \frac{K^2\Theta^2}{2}\} \quad ,$$

$$X_{31} = 0 \quad ,$$

$$X_{32} = (\delta_2^2 - \frac{K^2}{c})\, J_n(\delta_2)\,\{ M_n(\delta_2) - n\} \quad ,$$

$$X_{33} = (\delta_2^2 - \frac{K^2}{c})\, Y_n(\delta_2)\,\{ L_n(\delta_2) - n\} \quad ,$$

$$X_{34} = 0 \quad ,$$

$$X_{35} = - (\lambda_2^2\delta_2^2 + \frac{K^2}{c})\, I_n(\lambda_2\delta_2)\,\{ N_n(\lambda_2\delta_2) - n\} \quad ,$$

$$X_{36} = (\lambda_2^2\delta_2^2 + \frac{K^2}{c})\, K_n(\lambda_2\delta_2)\,\{ P_n(\lambda_2\delta_2) + n\} \quad ,$$

$$X_{37} = 0 \quad ,$$

$$X_{38} = 0 \quad ,$$

$$X_{39} = 0 \quad ,$$

$$X_{41} = -\frac{\gamma\eta_2}{\eta_1} J_n(\delta_1)\{M_n(\delta_1) - n(n+1) + \frac{(K\gamma\theta)^2}{2}\} ,$$

$$X_{42} = J_n(\gamma\delta_2)\{M_n(\gamma\delta_2) - n(n+1) + \frac{(K\gamma\theta)^2}{2}\} ,$$

$$X_{43} = Y_n(\gamma\delta_2)\{L_n(\gamma\delta_2) - n(n+1) + \frac{(K\gamma\theta)^2}{2}\} ,$$

$$X_{44} = -\frac{\gamma\eta_2}{\eta_1} I_n(\lambda_1\delta_1)\{N_n(\lambda_1\delta_1) - n(n+1) + \frac{(K\gamma\theta)^2}{2}\} ,$$

$$X_{45} = I_n(\gamma\lambda_2\delta_2)\{N_n(\gamma\lambda_2\delta_2) - n(n+1) + \frac{(K\gamma\theta)^2}{2}\} ,$$

$$X_{46} = -K_n(\gamma\lambda_2\delta_2)\{P_n(\gamma\lambda_2\delta_2) + n(n+1) - \frac{(K\gamma\theta)^2}{2}\} ,$$

$$X_{47} = \frac{\gamma\eta_2}{\eta_1} n J_n(K\gamma\theta)\{M_n(K\gamma\theta) - (n+1)\} ,$$

$$X_{48} = -n J_n(K\gamma\theta)\{M_n(K\gamma\theta) - (n+1)\} ,$$

$$X_{49} = -n Y_n(K\gamma\theta)\{L_n(K\gamma\theta) - (n+1)\} ,$$

$$X_{51} = -\frac{\gamma\eta_2}{\eta_1} n J_n(\delta_1)\{M_n(\delta_1) - (n+1)\} ,$$

$$X_{52} = n J_n(\gamma\delta_2)\{M_n(\gamma\delta_2) - (n+1)\} ,$$

$$X_{53} = n Y_n(\gamma\delta_2)\{L_n(\gamma\delta_2) - (n+1)\} ,$$

$$X_{54} = -\frac{\gamma\eta_2}{\eta_1} n I_n(\lambda_1\delta_1)\{N_n(\lambda_1\delta_1) - (n+1)\} ,$$

$$X_{55} = n I_n(\gamma\lambda_2\delta_2)\{N_n(\gamma\lambda_2\delta_2) - (n+1)\} ,$$

$$X_{56} = -n K_n(\gamma\lambda_2\delta_2)\{P_n(\gamma\lambda_2\delta_2) + (n+1)\} ,$$

$$X_{57} = \frac{\gamma\eta_2}{\eta_1} J_n(K\gamma\theta)\{M_n(K\gamma\theta) - n(n+1) + \frac{(K\gamma\theta)^2}{2}\} ,$$

$$X_{58} = -J_n(K\gamma\theta)\{M_n(K\gamma\theta) - n(n+1) + \frac{(K\gamma\theta)^2}{2}\} ,$$

$$X_{59} = -Y_n(K\gamma\theta)\{L_n(K\gamma\theta) - n(n+1) + \frac{(K\gamma\theta)^2}{2}\} ,$$

$$X_{61} = (\frac{\eta_2}{\eta_1})^2 (\delta_1^2 - \frac{K^2\gamma^2}{c}) J_n(\delta_1)\{M_n(\delta_1) - n\} ,$$

$$X_{62} = -(\delta_2^2 - \frac{K^2}{c}) J_n(\gamma\delta_2)\{M_n(\gamma\delta_2) - n\} ,$$

$$X_{63} = -\left(\delta_2^2 - \frac{K^2}{c}\right) Y_n(\gamma\delta_2)\{L_n(\gamma\delta_2) - n\} \quad ,$$

$$X_{64} = -\left(\frac{\eta_2}{\eta_1}\right)^2 \left(\lambda_1^2\delta_1^2 + \frac{K^2\gamma^2}{c}\right) I_n(\lambda_1\delta_1)\{N_n(\lambda_1\delta_1) - n\} \quad ,$$

$$X_{65} = \left(\lambda_2^2\delta_2^2 + \frac{K^2}{c}\right) I_n(\gamma\lambda_2\delta_2)\{N_n(\gamma\lambda_2\delta_2) - n\} \quad ,$$

$$X_{66} = -\left(\lambda_2^2\delta_2^2 + \frac{K^2}{c}\right) K_n(\gamma\lambda_2\delta_2)\{P_n(\gamma\lambda_2\delta_2) + n\} \quad ,$$

$$X_{67} = 0 \quad ,$$

$$X_{68} = 0 \quad ,$$

$$X_{69} = 0 \quad ,$$

$$X_{71} = J_n(\delta_1)\{M_n(\delta_1) - n\} \quad ,$$

$$X_{72} = -J_n(\gamma\delta_2)\{M_n(\gamma\delta_2) - n\} \quad ,$$

$$X_{73} = -Y_n(\gamma\delta_2)\{L_n(\gamma\delta_2) - n\} \quad ,$$

$$X_{74} = I_n(\lambda_1\delta_1)\{N_n(\lambda_1\delta_1) - n\} \quad ,$$

$$X_{75} = -I_n(\gamma\lambda_2\delta_2)\{N_n(\gamma\lambda_2\delta_2) - n\} \quad ,$$

$$X_{76} = K_n(\gamma\lambda_2\delta_2)\{P_n(\gamma\lambda_2\delta_2) + n\} \quad ,$$

$$X_{77} = n\, J_n(K\gamma\Theta) \quad ,$$

$$X_{78} = -n\, J_n(K\gamma\Theta) \quad ,$$

$$X_{79} = -n\, Y_n(K\gamma\Theta) \quad ,$$

$$X_{81} = -n\, J_n(\delta_1) \quad ,$$

$$X_{82} = n\, J_n(\gamma\delta_2) \quad ,$$

$$X_{83} = n\, Y_n(\gamma\delta_2) \quad ,$$

$$X_{84} = -n\, I_n(\lambda_1\delta_1) \quad ,$$

$$X_{85} = n\, I_n(\gamma \lambda_2 \delta_2) \quad ,$$

$$X_{86} = n\, K_n(\gamma \lambda_2 \delta_2) \quad ,$$

$$X_{87} = -\, J_n(K\gamma\theta)\{\, M_n(K\gamma\theta) - n\} \quad ,$$

$$X_{88} = J_n(K\gamma\theta)\,\{M_n(K\gamma\theta) - n\} \quad ,$$

$$X_{89} = Y_n(K\gamma\theta)\,\{L_n(K\gamma\theta) - n\} \quad ,$$

(7.2.14)

$$X_{91} = \frac{1}{\gamma \eta_1}\left(\delta_1^2 - \frac{K^2\gamma^2}{c}\right) J_n(\delta_1) \quad ,$$

$$X_{92} = -\frac{1}{\eta_2}\left(\delta_2^2 - \frac{K^2}{c}\right) J_n(\gamma\, \delta_2) \quad ,$$

$$X_{93} = -\frac{1}{\eta_2}\left(\delta_2^2 - \frac{K^2}{c}\right) Y_n(\gamma\, \delta_2) \quad ,$$

$$X_{94} = -\frac{1}{\gamma \eta_1}\left(\lambda_1^2\delta_1^2 + \frac{K^2\gamma^2}{c}\right) I_n(\lambda_1 \delta_1) \quad ,$$

$$X_{95} = \frac{1}{\eta_2}\left(\lambda_2^2\delta_2^2 + \frac{K^2}{c}\right) I_n(\gamma \lambda_2 \delta_2) \quad ,$$

$$X_{96} = \frac{1}{\eta_2}\left(\lambda_2^2\delta_2^2 + \frac{K^2}{c}\right) K_n(\gamma \lambda_2 \delta_2) \quad ,$$

$$X_{97} = 0 \quad ,$$

$$X_{98} = 0 \quad ,$$

$$X_{99} = 0 \quad .$$

Putting n=0, in eqn.(7.2.13), yields the radial mode frequency equation, as

$$\begin{vmatrix} Y_{11} & Y_{12} & Y_{13} & Y_{14} & Y_{15} & Y_{16} \\ Y_{31} & Y_{32} & Y_{33} & Y_{34} & Y_{35} & Y_{36} \\ Y_{41} & Y_{42} & Y_{43} & Y_{44} & Y_{45} & Y_{46} \\ Y_{61} & Y_{62} & Y_{63} & Y_{64} & Y_{65} & Y_{66} \\ Y_{71} & Y_{72} & Y_{73} & Y_{74} & Y_{75} & Y_{76} \\ Y_{91} & Y_{92} & Y_{93} & Y_{94} & Y_{95} & Y_{96} \end{vmatrix} = 0 \qquad (7.2.15)$$

and the tangential mode frequency equation as

$$\begin{vmatrix} Y_{27} & Y_{28} & Y_{29} \\ Y_{57} & Y_{58} & Y_{59} \\ Y_{87} & Y_{88} & Y_{89} \end{vmatrix} = 0 \qquad (7.2.16)$$

where the elements Y_{ij} ; i,j = 1 to 9, can be obtained by setting n=0 in the corresponding elements given by eqns.(7.2.14).

7.2.3 Shaft inside an Annular Plate

When the shaft length is larger than its diameter, the disk-shaft resonator may be regarded as a shaft inside a thin annular plate. In this case, the disk thickness h is taken as small compared to its diameter 2a, so that the theory developed in chapter 3 for the annular rings could be used, along with the Gazis's[26] three-dimensional theory applicable to solid cylinders, to obtain the compound mode frequency equation of this structure.

The boundary conditions for this case, will be

$$\begin{aligned} T_{rr_4} &= 0 \text{ at } r=a \ , \\ T_{r\theta_4} &= 0 \text{ at } r=a \ , \\ T_{rz_3} &= 0 \text{ at } r=b \ , \end{aligned} \qquad (7.2.17a)$$

and the continuity conditions at r=b, will be

$$\begin{aligned} T_{rr_3} &= T_{rr_4} \ , \\ T_{r\theta_3} &= T_{r\theta_4} \ , \\ \xi_{r_3} &= \xi_{r_4} \ , \\ \xi_{\theta_3} &= \xi_{\theta_4} \ , \end{aligned} \qquad (7.2.17b)$$

where the suffices 3 and 4 refer to the shaft and the thin annular

plate, respectively.

The stress resultants for the solid cylinder and the annular plate are given by

$$T_{rr_3} = \text{Bulk Modulus} \times \left[\frac{\partial \xi_{r_3}}{\partial r} + \frac{\sigma}{(1-\sigma)} \frac{1}{r} \left(\xi_{r_3} + \frac{\partial \xi_{\theta_3}}{\partial \theta} \right) + \frac{\sigma}{(1-\sigma)} \frac{\partial \xi_{z_3}}{\partial z} \right]$$

$$T_{rr_4} = \text{Plate Modulus} \times \left[\frac{\partial \xi_{r_4}}{\partial r} + \frac{\sigma}{r} \left(\xi_{r_4} + \frac{\partial \xi_{\theta_4}}{\partial \theta} \right) \right]$$

$$T_{r\theta_3} = \text{Shear Modulus} \times \left[\frac{\partial \xi_{\theta_3}}{\partial r} - \frac{\xi_{\theta_3}}{r} + \frac{1}{r} \frac{\partial \xi_{r_3}}{\partial \theta} \right] \qquad (7.2.18)$$

$$T_{r\theta_4} = \text{Shear Modulus} \times \left[\frac{\partial \xi_{\theta_4}}{\partial r} - \frac{\xi_{\theta_4}}{r} + \frac{1}{r} \frac{\partial \xi_{r_4}}{\partial \theta} \right]$$

$$T_{rz_3} = \text{Shear Modulus} \times \left[\frac{\partial \xi_{r_3}}{\partial z} + \frac{\partial \xi_{z_3}}{\partial r} \right]$$

The displacement functions for the shaft and the annular plate are given by

$$\xi_{r_3} = \{ A_1 \frac{dJ_n(\alpha_3 r)}{dr} + \frac{n}{r} B_1 J_n(\beta_3 r) + \zeta C_1 J_{n+1}(\beta_3 r) \} \cos n\theta \cos(\omega t + \zeta z)$$

$$\xi_{\theta_3} = \{ -\frac{n}{r} A_1 J_n(\alpha_3 r) + \zeta C_1 J_{n+1}(\beta_3 r) - B_1 \frac{dJ_n(\beta_3 r)}{dr} \} \sin n\theta \cos(\omega t + \zeta z)$$

$$\xi_{z_3} = \left[-\zeta A_1 J_n(\alpha_3 r) - C_1 \{ \frac{dJ_{n+1}(\beta_3 r)}{dr} + \frac{(n+1)}{r} J_{n+1}(\beta_3 r) \} \right] \cos n\theta \sin(\omega t + \zeta z) \qquad (7.2.19)$$

$$\xi_{r_4} = \{ A_2 \frac{dJ_n(hr)}{dr} + A_3 \frac{dY_n(hr)}{dr} + \frac{nB_2}{r} J_n(kr) + \frac{nB_3}{r} Y_n(kr) \} \cos n\theta$$

$$\xi_{\theta_4} = -\{ \frac{nA_2}{r} J_n(hr) + \frac{nA_3}{r} Y_n(hr) + B_2 \frac{dJ_n(kr)}{dr} + B_3 \frac{dY_n(kr)}{dr} \} \sin n\theta$$

where

$$\delta_3^2 = \alpha_3^2 b^2 = \left(\frac{K^2 \gamma^2}{c} - \zeta^2 b^2 \right), \quad \lambda_3^2 \delta_3^2 = \beta_3^2 b^2 = \left(K^2 \gamma^2 \theta^2 - \zeta^2 b^2 \right), \qquad (7.2.20)$$

$\zeta = \frac{p\pi}{l}$, $p=1,2,3,\ldots$; is the longitudinal wavenumber, $k = \frac{\omega}{C_s}$ and $h = \frac{\omega}{C_p}$, are the shear and plate wavenumbers, respectively. Let $\zeta b = \nu_3$.

Then, substituting eqns.(7.2.18) to (7.2.20) into eqns.(7.2.17) and simplifying, yields the frequency equation for compound modes of vibration, as

$$| X_{ij} | = 0 \quad ; \quad i,j = 1 \text{ to } 7, \tag{7.2.21}$$

where

$$X_{11} = 0 \ ,$$

$$X_{12} = - J_n(K) \{ M_n(K) - n(n+1) + \frac{(K\Theta)^2}{2} \} \ ,$$

$$X_{13} = - Y_n(K) \{ L_n(K) - n(n+1) + \frac{(K\Theta)^2}{2} \} \ ,$$

$$X_{14} = 0 \ ,$$

$$X_{15} = n \, J_n(K\Theta) \{ M_n(K\Theta) - (n+1) \} \ ,$$

$$X_{16} = n \, Y_n(K\Theta) \{ L_n(K\Theta) - (n+1) \} \ ,$$

$$X_{17} = 0 \ ,$$

$$X_{21} = 0 \ ,$$

$$X_{22} = - n \, J_n(K) \{ M_n(K) - (n+1) \} \ ,$$

$$X_{23} = - n \, Y_n(K) \{ L_n(K) - (n+1) \} \ ,$$

$$X_{24} = 0 \ ,$$

$$X_{25} = J_n(K\Theta) \{ M_n(K\Theta) - n(n+1) + \frac{(K\Theta)^2}{2} \} \ ,$$

$$X_{26} = Y_n(K\Theta) \{ L_n(K\Theta) - n(n+1) + \frac{(K\Theta)^2}{2} \} \ ,$$

$$X_{27} = 0 \ ,$$

$$X_{31} = - 2 \nu_3 \, Z_n(\mu_3) \{ d_1 \, W_n(\mu_3) - n(2d_1 - 1) \}$$

$$X_{32} = 0 \ ,$$

$$X_{33} = 0 \ ,$$

$$X_{34} = -\, n\ \nu_3\ Z_n(\mu_4) \quad ,$$

$$X_{35} = 0 \quad ,$$

$$X_{36} = 0 \quad ,$$

$$X_{37} = \frac{Z_n(\mu_4)}{\lambda_3 \delta_3}\left[\{\nu_3^2 - \lambda_3^2\delta_3^2\}\, W_n(\mu_4) - n(2\nu_3^2 - \lambda_3^2\delta_3^2)\right] \quad ,$$

$$X_{41} = -\, Z_n(\mu_3)\{d_1\, W_n(\mu_3) - n(n+2d_1-1) + \frac{(\delta_3^2 - \nu_3^2)}{2}\} \quad ,$$

$$X_{42} = J_n(K\gamma)\{M_n(K\gamma) - n(n+1) + \frac{(K\gamma\theta)^2}{2}\} \quad ,$$

$$X_{43} = Y_n(K\gamma)\{L_n(K\gamma) - n(n+1) + \frac{(K\gamma\theta)^2}{2}\} \quad ,$$

$$X_{44} = n\, Z_n(\mu_4)\{d_2\, W_n(\mu_4) - (2nd_2 - n + 1)\} \quad ,$$

$$X_{45} = -\, n\, J_n(K\gamma\theta)\{M_n(K\gamma\theta) - (n+1)\} \quad ,$$

$$X_{46} = -\, n\, Y_n(K\gamma\theta)\{L_n(K\gamma\theta) - (n+1)\} \quad ,$$

$$X_{47} = \frac{\nu_3\, Z_n(\mu_4)}{\mu_4}\{(n+1)\, W_n(\mu_4) - 2n(n+1) + (\lambda_3\delta_3)^2\} \quad , \qquad (7.2.22)$$

$$X_{51} = -\, n\, Z_n(\mu_3)\{d_1\, W_n(\mu_3) - (2nd_1 - n+1)\} \quad ,$$

$$X_{52} = n\, J_n(K\gamma)\{M_n(K\gamma) - (n+1)\} \quad ,$$

$$X_{53} = n\, Y_n(K\gamma)\{L_n(K\gamma) - (n+1)\} \quad ,$$

$$X_{54} = Z_n(\mu_4)\{d_2\, W_n(\mu_4) - n(n-1+2d_2) + \frac{(\lambda_3\delta_3)^2}{2}\} \quad ,$$

$$X_{55} = -\, J_n(K\gamma\theta)\{M_n(K\gamma\theta) - n(n+1) + \frac{(K\gamma\theta)^2}{2}\} \quad ,$$

$$X_{56} = -\, Y_n(K\gamma\theta)\{L_n(K\gamma\theta) - n(n+1) + \frac{(K\gamma\theta)^2}{2}\} \quad ,$$

$$X_{57} = \frac{\nu_3\, Z_n(\mu_4)}{\mu_4}\{(n+1)\, W_n(\mu_4) - 2n(n+1) + \frac{(\lambda_3\delta_3)^2}{2}\} \quad ,$$

$$X_{61} = Z_n(\mu_3)\{W_n(\mu_3) - n\} \quad ,$$

$$X_{62} = - J_n(K\gamma)\{ M_n(K\gamma) - n\} \quad ,$$

$$X_{63} = - Y_n(K\gamma)\{ L_n(K\gamma) - n\} \quad ,$$

$$X_{64} = n\, Z_n(\mu_4) \quad ,$$

$$X_{65} = - n\, J_n(K\gamma\theta) \quad ,$$

$$X_{66} = - n\, Y_n(K\gamma\theta) \quad ,$$

$$X_{67} = - \nu_3 \frac{Z_n(\mu_4)}{\mu_4}\{W_n(\mu_4) - 2n\} \quad ,$$

$$X_{71} = - n\, Z_n(\mu_3) \quad ,$$

$$X_{72} = n\, J_n(K\gamma) \quad ,$$

$$X_{73} = n\, Y_n(K\gamma) \quad ,$$

$$X_{74} = - Z_n(\mu_4)\{ W_n(\mu_4) - n\} \quad ,$$

$$X_{75} = J_n(K\gamma\theta)\{ M_n(K\gamma\theta) - n\} \quad ,$$

$$X_{76} = Y_n(K\gamma\theta)\{ L_n(K\gamma\theta) - n\} \quad ,$$

$$X_{77} = - \nu_3 \frac{Z_n(\mu_4)}{\mu_4}\{ W_n(\mu_4) - 2n\} \quad ,$$

where $\mu_3 = \delta_3$ or $\overline{\delta}_3$, $\mu_4 = \lambda_3\delta_3$ or $\overline{\lambda_3\delta_3}$, $\overline{\delta}_3^2 = - \delta_3^2$, $(\overline{\lambda_3\delta_3})^2 = - \lambda_3^2\delta_3^2$, $\overline{\delta}_3$ and $\overline{\lambda_3\delta_3}$ are real, Z = J or I and $W_n(x) = x\, Z_{n-1}(x)/Z_n(x)$. The proper selection of Bessel functions[26] to be used, depending on whether the wavenumbers δ_3 and $\lambda_3\delta_3$, as given by eqns.(7.2.20), are real or imaginary, is shown in Table 7.1. In Table 7.1, the values of the parameters d_1 and d_2 are also given. These parameters are used to take into account the differences in the recursive and differentiation formulae between the different kinds of Bessel functions.

If n is set equal to zero, eqn.(7.2.21) reduces to

Range of the magnitude of wavenumbers	Bessel functions used		Values of constants	
	$Z_n(\mu_3)$	$Z_n(\mu_4)$	d_1	d_2
$\nu_3 < \frac{K\gamma}{\sqrt{c}}$	$J_n(\delta_3)$	$J_n(\lambda_3\delta_3)$	1	1
$\frac{K\gamma}{\sqrt{c}} < \nu_3 < K\gamma\Theta$	$I_n(\overline{\delta_3})$	$J_n(\lambda_3\delta_3)$	-1	1
$K\gamma\Theta < \nu_3$	$I_n(\overline{\delta_3})$	$I_n(\overline{\lambda_3\delta_3})$	-1	-1

Table 7.1 Selection of Bessel Functions.

$$\begin{vmatrix} Y_{11} & Y_{12} & Y_{13} & Y_{17} \\ Y_{31} & Y_{32} & Y_{33} & Y_{37} \\ Y_{41} & Y_{42} & Y_{43} & Y_{47} \\ Y_{61} & Y_{62} & Y_{63} & Y_{67} \end{vmatrix} = 0 \qquad (7.2.23)$$

or

$$\begin{vmatrix} Y_{24} & Y_{25} & Y_{26} \\ Y_{54} & Y_{55} & Y_{56} \\ Y_{74} & Y_{75} & Y_{76} \end{vmatrix} = 0 \qquad (7.2.24)$$

where the elements Y_{ij} ; i,j = 1 to 7, can be obtained from the elements of eqns.(7.2.22) by putting n=0. It may be noted that eqns. (7.2.23) and (7.2.24) correspond to radial and torsional modes of vibration .

7.3 Experimental Resonant Spectra

The specimens of the resonator, in the form of disk-shafts with various disk thicknesses and shaft lengths, were cut from the same aluminium rod of diameter 7.6 cms. and length 10cms. The ratio γ of the shaft diameter 2b to the disk diameter 2a was varied by machining the disk (outer) diameter for most of the experiments. But, for the disk-shaft of a shorter shaft length of 1.27 cms., the ratio γ was changed by machining the shaft diameter. For each disk-shaft, the frequencies of various resonances were noted by driving (a) radially into the disk, (b) longitudinally into the shaft and (c) tangentially (or angularly) to the disk. All the resonances were measured by the crossover method described in Appendix A.2.2. The resonant spectra obtained in various drives, for shaft lengths progressing from 10 cms. to 1 cm. in intervals of 1 cm., has been tabulated in Tables 7.2 to 7.4 for three disk-shafts of different γ. Tables 7.5 to 7.7 provide the spectra of resonances obtained for various γ's for disk-shafts of

Frequencies in kHz.												
l = 5 cms.			l = 4 cms.		l = 3.5 cms.		l = 3 cms.		l = 2 cms.		l = 1 cm.	
R	L	T	R	L	R	L	R	L	R	L	R	L
32.24	8.51	19.67	32.19	10.42	32.21	10.68	31.93	10.89	32.18	11.68	31.45	12.25
33.87	36.84	32.10	47.71	38.38	43.63	39.10	47.39	39.93	47.73	42.21	47.73	43.42
46.57	46.26	35.57	47.86	47.90	47.88	48.17	48.19	48.33	48.49	48.54	48.29	48.94
47.73	54.86	46.48	61.87	68.48	48.19	77.26	49.36	82.70	61.98	85.24	61.90	82.54
55.26	75.97	47.54	63.98	80.39	61.99	81.70	61.66	88.49	75.45	114.26	75.40	122.39
56.43	98.22	56.34	75.37	113.38	68.66	121.18	75.13	126.33	78.16	128.99	77.43	162.64
61.99	121.97	57.70	88.39	127.23	75.47	129.33	88.24	132.10	88.46	153.00	88.40	185.00
75.41	146.36	61.79	90.90	133.38	78.60	136.84	91.55	145.65	90.12	159.84	90.67	199.66
88.39	159.39	68.59	101.21	160.48	88.55	159.06	101.06	161.14	99.27	171.90	101.24	234.70
88.55		75.20	103.48	165.34	91.30	173.06	103.48	174.64	101.35	181.87	102.30	236.60
101.42		78.12	113.81	171.95	101.39	173.40	113.69		104.24	189.76	113.76	
104.26		88.18	117.22	186.03	103.58		117.47		113.98	213.98	117.10	
113.95		92.49	121.29	200.26	109.58		121.22		117.15	220.36	120.70	
117.45		93.24	126.31		113.95		126.25		121.30		126.12	
121.65		99.47	127.08		117.48		132.14		126.41		138.79	
126.58		101.01	138.73		121.47		138.70		131.07		142.92	
137.90		104.03	139.86		126.44		142.99		138.89		151.17	
138.48		113.70	142.93		129.36		151.30		139.95		152.98	
140.86		117.37	151.20		138.88		162.76		143.09		163.49	
120.3		120.36							151.39			
		121.59							159.38			
		126.06							163.73			
									166.61			

Table 7.2 The natural frequencies of resonance of disk-shaft system observed in (a) radial (R), (b) longitudinal (L) and (c) tangential(T) drives. Ratio of shaft-diameter-to-disk diameter = 0.25, Disk diameter(2a) = 7.6 cms., Shaft diameter(2b) = 1.9 cms., Disk thickness = 0.754 cm., Poisson's ratio = 0.33, and l = Shaft length.

Frequencies in kHz.												
l = 10 cms.			l = 9 cms.		l = 8 cms.			l = 7 cms.			l = 6 cms.	
R	L	T	R	L	R	L	T	R	L	T	R	L
7.55	25.56	7.47	9.12	26.75	11.27	12.57	11.27	14.19	36.66	14.18	18.38	42.77
30.57	26.50	21.58	35.33	28.49	41.02	32.18	25.78	47.47	69.25	28.51	53.98	79.28
55.48	50.32	30.62	60.21	55.33	75.95	61.76	41.08	76.09	97.58	47.51	76.18	103.07
75.92	74.37	48.16	75.90	81.51	86.09	89.94	58.78	96.61	117.60	65.81	104.81	119.72
92.13	93.95	55.85	77.34	108.15	89.89	110.69	65.37	97.58	131.43	69.79	108.79	128.77
104.13	105.15	71.08	81.69	121.39	104.07	111.86	76.01	104.34	160.03	76.31	115.04	143.58
104.99	119.27	76.12	98.96	133.33	104.57	124.56	86.29	110.34	167.59	96.69	117.63	157.53
109.37	124.23	76.48	104.00	143.07	111.75	144.01	89.91	114.85	185.18	97.61	128.32	158.54
114.18	134.26	92.24	108.04	157.72	125.80	158.42	93.21	117.63	194.70	103.80	144.65	171.37
114.62	151.51	103.48	114.66	162.29	128.32	159.83	104.92	128.88	201.21	110.47	146.15	182.26
124.33	157.05	104.41	116.32	168.73	143.80	173.10	111.81	135.71	212.95	116.64	152.45	199.31
128.47	159.95	114.31	120.91	169.03	147.77	181.15	115.52	137.14	234.96	117.45	162.43	205.76
133.76	160.35	116.19	128.06	182.63	152.12	195.05	125.68	153.52	238.90	128.08	163.58	212.91
136.56	173.38	128.03	133.19	190.03	156.12	201.50	128.13	154.74	248.70	135.59	169.76	219.46
138.80	180.02	133.31	141.16	204.82	167.22	207.23	131.90	159.51	259.99	137.23	177.40	228.61
150.24	192.17	136.63	152.63	213.82	172.05	220.34	147.95	165.87	281.13	152.52	184.42	239.85
151.66	196.91	159.50	162.16	217.97	177.25	233.96	152.38	170.09	289.55	158.36	204.18	242.69
155.38	202.19	160.79	162.45	225.02	180.78	244.53	158.09	180.47		165.90	205.43	258.02
164.73	212.25	164.01	171.02	235.10	191.34	247.25	161.56	191.86		177.40	208.03	
173.85	220.49	173.81	177.29		197.01	256.29	167.39	203.03		180.68	212.83	
176.20	231.22	177.62	179.94		202.39	274.69	172.20	207.97		202.86	216.05	
177.91	239.86	180.68	182.68		209.91		177.27	234.38		208.15	228.81	
181.89	241.52	201.26	186.47		227.96		180.91	238.36		213.95	237.43	
193.34	247.55	212.76	192.04		235.55		191.60	245.66		222.96	254.64	
196.87	262.22	226.71	196.10		242.44		196.63	248.46		227.14	254.64	
203.43	268.92		201.73		248.09		203.79	253.14		229.34		
213.45			207.56				216.18	261.97		234.40		
213.75			209.67				226.86	274.69		245.64		

Table 7.3 Resonant spectra of aluminium disk-shaft system ; Y = 0.5, 2a = 3.8 cms; 2b = 1.9 cms; h = 0.4 cm; σ = 0.33.

Frequencies in kHz.												
l = 5 cms.			l = 4 cms.			l = 3 cms.		l = 2 cms.		l = 1 cm.		
R	L	T	R	L	T	R	L	R	L	R	L	T
24.25	27.20	24.35	33.87	27.65	34.26	48.20	28.41	61.23	29.78	67.64	32.18	68.20
59.09	50.87	36.34	62.84	62.61	44.07	75.32	80.26	75.23	97.12	72.30	84.88	71.99
75.58	91.20	59.67	75.43	105.20	66.84	80.41	114.27	97.11	117.42	102.06	101.48	101.09
85.27	106.30	75.31	97.10	109.42	70.62	102.63	116.04	101.87	143.04	110.07	104.71	111.34
104.50	120.98	85.79	102.98	125.34	95.72	102.93	143.59	125.29	159.96	125.95	163.89	125.29
106.36	143.85	86.52	109.34	159.17	99.36	109.60	160.38	127.15	168.78	137.14	164.40	137.03
115.31	159.54	102.76	127.41	160.75	107.16	115.46	161.51	142.87	184.31	151.17	204.35	137.43
121.41	162.38	106.01	134.65	182.94	110.54	115.71	187.79	149.97	218.56	163.08	251.43	148.99
127.07	189.10	110.13	146.30	164.50	111.13	127.15	217.30	156.72	267.07	169.70	272.89	153.57
143.83	199.65	111.90	152.42		112.14	128.48	236.02	157.73	267.35	173.59	286.93	162.78
152.39	203.67	116.63	157.24		115.57	143.56		167.80		191.19	319.20	169.38
154.85	209.56	121.31	164.23		125.03	147.53		177.37		199.06		190.43
178.50	221.64	127.55	169.63		135.01	150.09		193.47		204.29		193.57
183.93	229.23	127.73	175.92		138.42	159.27		203.77		211.59		195.83
188.73	237.74	137.60	190.22		156.40	161.61		207.41		216.12		212.24
197.78		155.52			160.20	163.82		221.08		222.63		215.78
202.54		157.98			164.91	175.74		226.86		246.71		227.80
205.02		161.83			176.00	178.67		246.58		256.47		229.66
222.97		176.06				182.61		247.08		262.23		247.11
229.37		183.96				191.61		261.11		276.24		257.08
240.39		186.88				194.91		274.13		287.93		258.82
241.94		196.26				200.42				291.20		267.64
247.24		217.32				226.70				299.08		275.91
						234.72						287.91
						235.74						290.78
						244.21						

Table 7.3 (Contd.); Y = 0.5, 2a = 3.8 cms; 2b = 1.9 cms; h = 0.4 cm; σ = 0.33.

Frequencies in kHz.												
l = 10 cms.			l = 9 cms.		l = 8 cms.			l = 6 cms.		l = 5 cms.		
R	L	T	R	L	R	L	T	R	L	R	L	T
7.86	25.53	7.91	9.48	28.17	44.75	31.76	11.67	19.05	41.92	26.32	51.60	26.44
32.58	48.26	28.25	37.92	30.84	80.63	58.94	34.33	63.97	73.42	77.74	83.33	49.68
62.50	74.50	32.61	70.72	52.91	90.93	90.84	44.83	106.94	95.25	103.94	104.51	77.89
74.76	100.19	56.88	81.79	81.61	103.70	116.07	69.17	110.37	113.60	113.59	129.38	103.83
89.55	115.23	62.52	97.10	88.92	106.76	132.59	80.96	112.57	140.60	129.44	157.88	107.69
107.21	132.69	85.77	106.98	106.73	112.87	151.48	90.97	128.74	151.37	143.54	159.45	113.58
115.27	142.16	89.85	123.67	123.50	132.37	156.32	103.93	145.84	158.48	152.47	162.49	127.02
122.18	156.15	106.39	127.68	141.29	139.44	160.50	106.24	151.40	180.30	157.25	167.67	143.50
125.48	157.72	106.54	129.66	149.09	149.89	179.52	113.30	155.64	184.57	167.88	192.43	151.36
137.22	159.85	114.56	142.70	158.10	154.11	183.44	129.71	158.75	199.31	172.31	206.34	154.32
142.17	160.89	122.30	149.19	171.74	160.35	196.12	131.43	161.90	211.37	180.90	210.10	156.29
144.94	163.98	137.15	153.58	167.64	169.84	206.09	132.41	172.56	216.40	189.19	223.52	167.82
155.45	179.53	143.01	156.64	189.71	179.67	209.11	139.44	179.13	233.78	204.68	239.69	172.85
162.64	182.23	144.69	168.37	189.09	191.32	214.21	149.47	184.02	237.77	210.07	242.70	180.36
163.23	193.00	153.21	170.94	193.95	195.85	222.39	153.32	198.85	258.07	211.98	256.29	188.10
168.77	195.74	162.65	171.07	194.10	195.94	231.83	162.53	201.82	242.44	222.80	266.92	204.79
171.35	202.16	164.66	171.58	199.60	204.61	240.46	169.82	207.24	249.86	231.58	269.27	210.50
182.26	218.56	168.82	182.89	212.73	208.58	247.95	173.69	211.32		252.56	282.28	211.28
194.69	220.35	171.57	192.22	213.40	213.94	256.04	182.83	225.80		252.82	289.94	231.92
195.73	223.72	182.23	199.47	216.42	229.34	270.90	189.62	231.89		260.54	323.44	239.64
205.15	231.10	184.60	210.09	228.52	237.10	269.38	192.66	234.02		262.12	331.79	257.50
209.11	239.47	194.84	212.29	233.35	245.82	280.44	202.93	241.30		269.88	338.37	259.30
221.50	249.11	195.02	216.17	235.05	247.71	303.37	205.21	246.08		271.25		261.60
234.47		204.95	225.12	244.09	267.04	320.28	208.90			285.02		272.28
241.84		209.13	228.34	247.57	269.05		214.04			290.57		291.82
247.40		212.21	238.53	251.19	281.49		224.91			291.71		293.78
254.36		223.96	239.69	258.67	291.49		229.52			295.55		316.13
261.03		229.19	249.61	260.82	306.53		235.48			296.22		317.03

Table 7.4 The resonant frequencies of disk-shaft system; $\gamma = 0.7$, $2a = 2.71$ cms; $2b = 1.9$ cms; $h = 0.4$ cm; $\sigma = 0.33$.

Frequencies in kHz.										
l = 4 cms.			l = 3 cms.			l = 2 cms.			l = 1 cm.	
R	L	T	R	L	T	R	L	T	R	L
37.49	64.52	37.67	55.53	83.48	56.30	87.93	93.58	88.83	99.20	84.38
64.55	94.57	58.26	83.33	92.43	74.73	104.04	112.23	101.37	102.58	119.16
92.17	119.02	64.62	102.83	143.70	83.33	112.77	157.55	103.27	138.50	138.64
99.42	140.94	92.40	116.31	160.95	102.71	125.06	163.98	112.61	150.24	161.87
112.65	158.36	99.03	124.85	167.67	106.46	149.50	184.69	125.64	153.13	188.64
114.33	159.41	99.35	149.80	170.58	116.29	151.28	203.15	150.43	188.24	217.92
136.12	180.16	113.07	151.67	201.81	124.91	164.16	220.16	165.53	199.99	218.38
140.81	199.92	114.48	156.36	219.90	151.87	169.14	221.70	178.61	207.82	236.98
146.12	227.38	128.78	167.93	251.28	152.98	178.67	232.91	186.23	222.59	250.17
152.29	235.25	136.36	190.08	252.19	156.19	188.64	235.37	190.98	237.31	251.39
161.11	250.52	140.43	201.53	264.55	167.92	203.49	260.96	204.30	238.47	
171.59	293.62	145.30	208.46	265.50	170.11	213.01	264.01	216.63	253.37	
183.46	300.30	152.48	216.39	291.28	172.92	223.57	300.22	233.28	255.00	
184.04	323.73	161.29	222.25	296.91	186.37	228.27	321.32	234.76	270.37	
186.15	329.31	162.39	246.03	311.89	187.78	233.54	338.77	251.38	280.90	
198.51		181.11	253.84	330.39	201.31	234.98	344.44	252.61	286.82	
218.64		183.49	256.40	348.52	202.65	252.08		264.71	294.56	
225.84		188.64	262.10	359.12	208.83	256.70		267.97	320.27	
237.24		192.80	264.23		217.59	262.32		272.40	318.69	
239.78		198.47	272.10		222.59	264.69		286.31	351.35	
252.99		214.03	287.30		224.83	272.33		301.16	352.56	
258.49		217.84	305.40		230.15	287.73		314.28	353.70	
264.96		219.42	316.53		252.48	301.20		318.19	384.97	
285.89		227.05	320.42		254.97	322.02		313.89		
292.68		238.56	325.66		256.92	328.45		323.31		
300.32			326.32		264.78	348.64		344.43		
316.13			328.10		272.91	350.99		350.96		
317.03			340.60		279.01	368.07				

Table 7.4 (Contd.), Y = 0.7; 2a = 2.72 cms; 2b = 1.9 cms; h = 0.4 cm; σ = 0.33

Frequencies in kHz.						
2a =6.31cms, γ =0.3			2a =4.76cms, γ =0.4			2a =3.15cms, γ =0.6
R	L	T	R	L	T	R
20.75	8.51	16.54	22.98	16.44	22.99	25.63
40.30	38.53	20.78	48.54	51.54	31.20	125.92
50.72	50.65	28.56	51.50	69.94	48.16	138.45
57.52	61.93	39.39	56.31	83.27	55.79	167.86
61.96	85.93	40.22	75.63	94.57	75.54	187.94
74.55	90.59	57.82	78.55	99.87	82.39	196.56
90.71	93.90	61.93	83.40	140.59	92.33	196.87
94.96	100.31	70.37	94.48	157.24	98.85	206.87
106.36	102.72	74.46	99.55	158.07	107.33	209.80
110.59	105.99		107.66	159.42	119.66	211.02
118.00	110.58		120.59	163.79	124.22	
121.67	119.38		123.74	184.64	140.21	
122.41	121.48		141.06	201.41	145.10	
129.94	129.79		148.26	208.45	149.26	
137.32	134.79		161.68	208.82	158.52	
142.13	136.87		163.60		158.93	
152.15	145.27		181.91		160.66	
167.49	148.89		190.43		163.35	
	156.64		192.43		177.13	
			201.78		181.10	
			222.04		186.05	
			223.62		191.92	
					200.92	

Table 7.5. The resonant spectra of a disk-shaft of length 5 cms, for different γ's. 2b = 1.9 cms; h =0.45 cms.

Frequencies in kHz								
2a=6.31 cms, γ =0.3			2a=4.76 cms, γ =0.4			2a=3.16 cms, γ =0.6		
R	L	T	R	L	T	R	L	T
27.85	23.34	27.72	31.46	21.81	31.48	36.25	61.66	36.26
39.63	47.06	36.87	54.72	62.98	39.63	64.51	64.54	50.48
56.48	56.47	39.46	62.98	79.32	54.60	80.04	114.50	79.91
57.42	70.15	44.62	77.75	85.73	55.09	86.64	127.47	86.71
69.48	99.46	57.38	83.94	119.06	62.92	104.27	157.97	104.92
70.07	120.72	69.25	99.16	158.31	77.44	113.54	165.18	119.26
74.29	147.14	74.08	120.10	159.67	84.05	124.09	175.74	123.08
90.37	159.97	84.32	124.75	162.12	85.70	127.47	188.36	127.39
105.92	175.53	90.10	140.74	185.33	91.35	143.43	220.86	130.38
109.70	185.40	93.51	143.91	204.08	91.93	148.23	226.64	143.16
121.26	204.84	105.79	149.62		98.95	154.15	227.69	148.31
122.27		109.57	158.87		100.99	172.49	238.96	154.29
136.52		111.19	160.96		119.84	175.40	249.53	172.19
138.18		112.28	181.52		122.98	184.31		183.69
141.47		115.29	189.56		131.28	188.91		188.92
147.03		118.35	194.12		140.66	192.49		196.63
151.50		120.74	198.53		140.99	212.88		212.79
167.20		122.12	201.74		143.81	226.94		226.99
172.07		135.85	204.12		149.50	228.87		
175.04		138.03	220.80		157.44	242.23		
181.15		141.36	224.80		158.73			
185.93		150.81			160.60			
190.21		154.55			180.53			
196.60		166.50			185.43			
					189.99			
					194.12			

Table 7.6 Resonant spectra of aluminium disk-shaft of shaft length 4 cms., 2b = 1.9 cms., h = 0.65 cm., σ = 0.33.

Frequencies in kHz							
2b=2.28cms, Y=0.3		2b=3.8cms, Y=0.5		2b=5.31cms, Y=0.7		2b=6.8cms, Y=0.9	
R	L	R	L	R	L	R	L
33.80	26.94	38.68	8.72	30.30	16.89	32.97	19.51
47.93	62.09	53.12	38.46	38.05	35.93	38.62	59.79
49.98	100.84	55.32	61.10	56.24	56.44	50.41	98.54
58.49	125.66	64.88	106.91	57.84	83.26	50.96	122.43
62.02	167.76	70.59	108.72	73.12	109.90	66.50	125.51
75.13	172.60	76.88	136.12	78.39	140.86	81.24	142.39
78.97	197.59	85.42	175.57	85.66	165.32	84.04	165.47
88.22	205.88	89.09	183.74	94.19	166.67	94.68	167.58
92.11	230.68	101.57	190.23	97.29	192.23	95.41	188.39
101.17	263.72	106.89	211.05	98.15	204.19	103.53	197.61
102.27	275.87	114.43		103.24	204.53	105.12	211.05
113.89		115.01		108.24	218.19	109.40	223.60
118.55		121.72		108.56		119.75	240.67
120.42		126.57		117.01		122.35	248.41
125.56		139.29		118.46		122.96	
126.20		142.27		121.55		136.69	
139.37		144.96		124.91		138.98	
142.85		148.77		125.60		141.60	
		152.01		129.78		143.35	
		161.36		135.51			
		164.36		141.34			
		166.90		150.54			
		170.06		152.96			
		176.81		153.41			
		179.41		164.75			
		189.23		171.42			
		196.99		172.97			
		199.34		176.75			

Table 7.7 The resonant spectrum of aluminium disk-shaft system of shaft length 1.27 cms., 2a=7.6 cms., h=0.4 cm., σ = 0.33.

shaft lengths 5 cms., 4 cms., and 1.27 cms., respectively.

A radial drive, by fixing the line radially into the disk of the disk-shaft, excited all the radial and compound modes of the disk-shaft, for which the radial component is large. It was found that the radial drive also excites the longitudinal modes of the shaft. A longitudinal drive, by fixing the line into the shaft of the disk-shaft resonator, enabled the excitation of all the longitudinal modes of the shaft together with the radial modes of the disk-shaft system. A tangential or an angular drive, which can be obtained by driving the disk of the specimen at an angle, excited all the torsional and compound modes which, mainly, have shear component. A probe of fine wire was used as a receiver to identify the modes such as (1,2), (1,3) etc.

7.4 Discussion

The measured resonant frequencies for disk-shafts of various dimensions were tabulated in section 7.3. The frequencies which are common to both longitudinal and radial drives, may correspond to either radial modes or longitudinal modes. Of these, the frequencies which are tightly coupled in longitudinal drive and loosely coupled in radial drive were identified to be longitudinal modes. Those frequencies which are tightly coupled in radial drive and loosely coupled in the longitudinal drive were identified to be the radial modes of the disk-shaft resonator, while the nonaxisymmetric (compound) modes appear in both the angular and radial drives. These features can be noticed in Tables 7.2 to 7.7 of section 7.3.

The variation of the lowest radial mode frequency, with the shaft length has been studied in greater detail for different Υ's of the disk-shaft system. The plot of $(2a\, f_{1RS})$ versus shaft length is shown in Fig.7.2, for different Υ's. The frequency is found to increase as the shaft length is increased, initially, but, it starts decreasing after reaching a peak value. This might be due to the energy coupling from

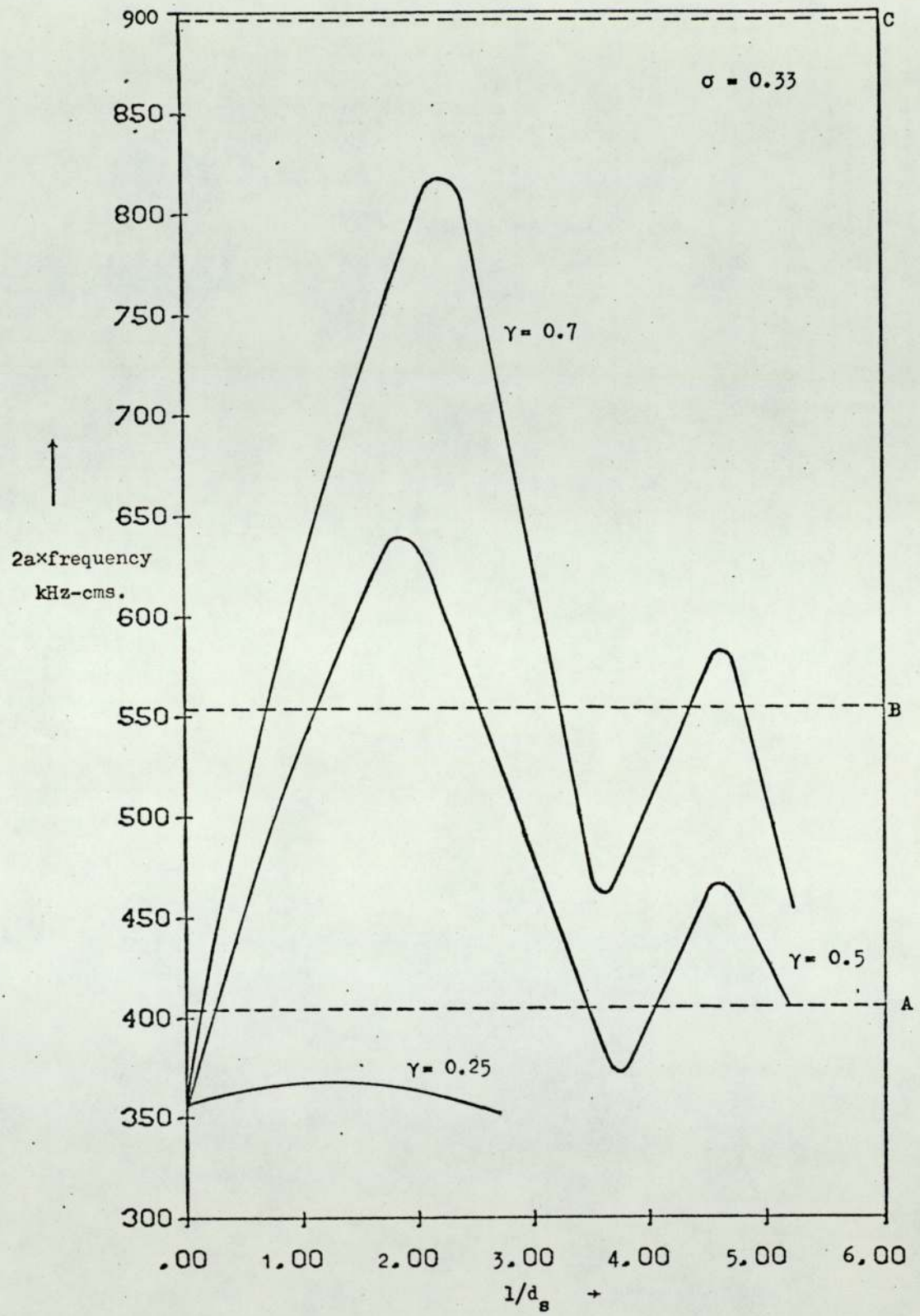

Fig.7.2 The graph of the measured frequency × 2a versus $1/d_s$ for the radial mode of a disk-shaft resonator of disk diameter 2a, shaft diameter d_s and length l, for $\gamma = 0.25$, 0.5 and 0.7. Lines A, B and C represent the values predicted by the theory for the disk with a rigid centre, for $\gamma = 0.25, 0.5$ and 0.7, respy.

the disk into the shaft. It may be noted from the figure that this peak frequency value for higher γ's is attained at larger shaft lengths. It may also be interesting to note that, for lower γ's (i.e., when the disk diameter is large), the variation of shaft length has less effect on frequency. But, as the disk diameter is reduced, the effect of the shaft length on the frequency becomes very significant. The dotted lines A, B and C in the figure represent the frequencies predicted by the theory developed in section 7.2.1 for the annular plate with a rigid centre. The corresponding frequencies of an annular plate, with the inner boundary free, are very low.

The numerical solution of the radial mode frequency equation (7.2.5) of a disk with a rigid centre, predicts that the frequency increases with γ, whereas, for an annular plate with a free inner boundary, the frequency of the lowest radial mode decreases as γ increases. This variation of frequency with γ is shown in Figs.7.3(a) and 7.3(b), for the first two radial modes. Notice that the figure show the plot of $K(1-\gamma)$ versus γ.

The plot of $(2af_{1RS})$ versus γ is shown in Fig.7.4, for different shaft lengths, for the first radial mode together with the theoretical values given by eqn.(7.2.5) for a disk with a rigid centre. For lower values of γ, the theory represents the correct direction of frequency variation. For smaller shaft lengths, the deviation of the frequency from the rigid centre value is quite considerable, showing that the stiffness offered by the shaft is dependent on the length of the shaft.

It is of particular interest to study the longitudinal resonances which appear in both the radial and longitudinal drives of the disk-shaft resonator. The plot of $(1/f)$ versus shaft length, where f is the frequency of the first longitudinal mode, is shown in Fig.7.5 for various γ's. The intercept on the X axis for each γ represents the rigidity offered by the disk. The inverse of the frequency of the

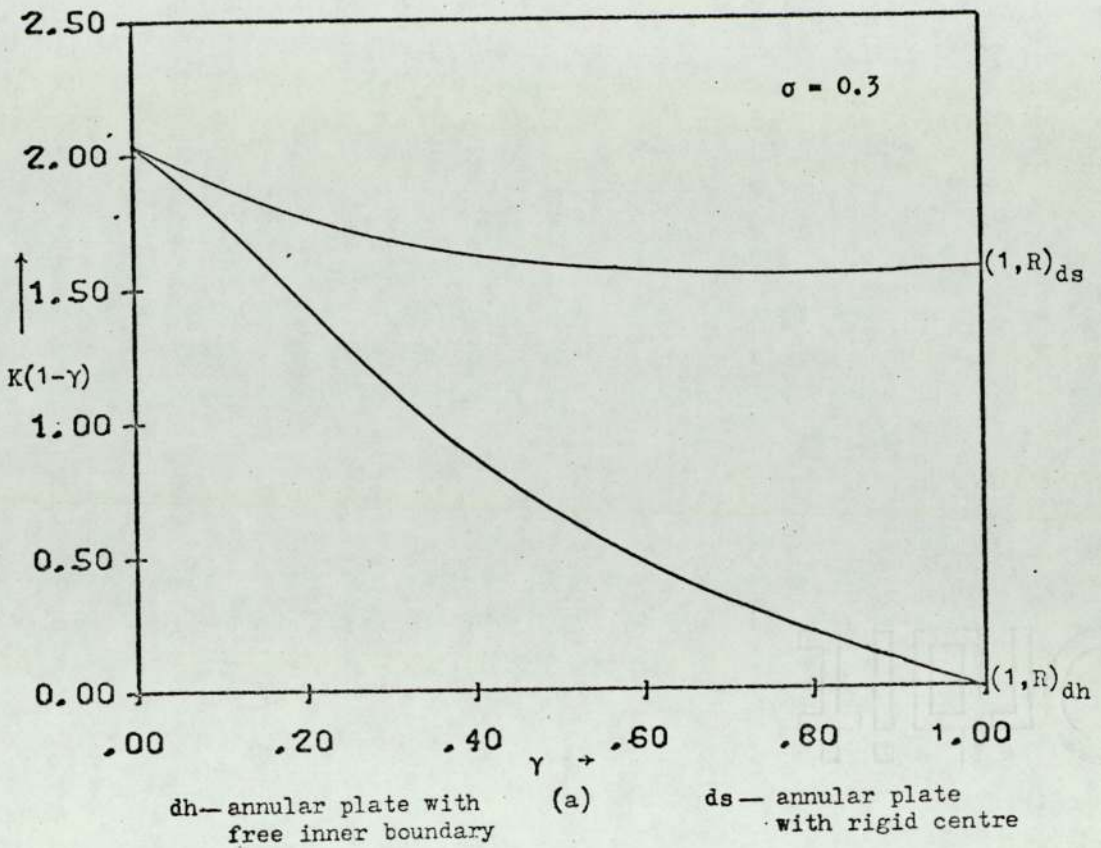

dh— annular plate with free inner boundary

(a)

ds— annular plate with rigid centre

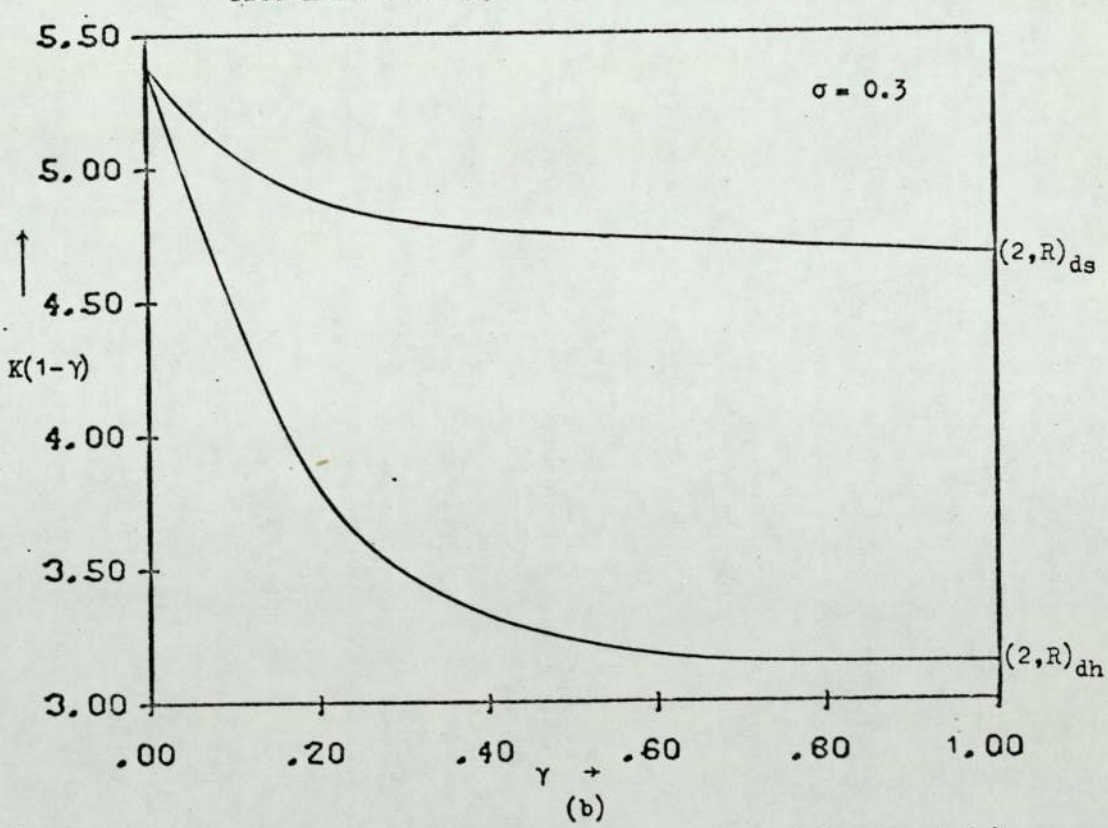

(b)

Fig.7.3 These graphs show the variation with γ, of (a) K_{1R} and (b) K_{2R} radial mode frequencies of an annular plate with free inner boundary(dh) and a disk with a rigid centre(ds).

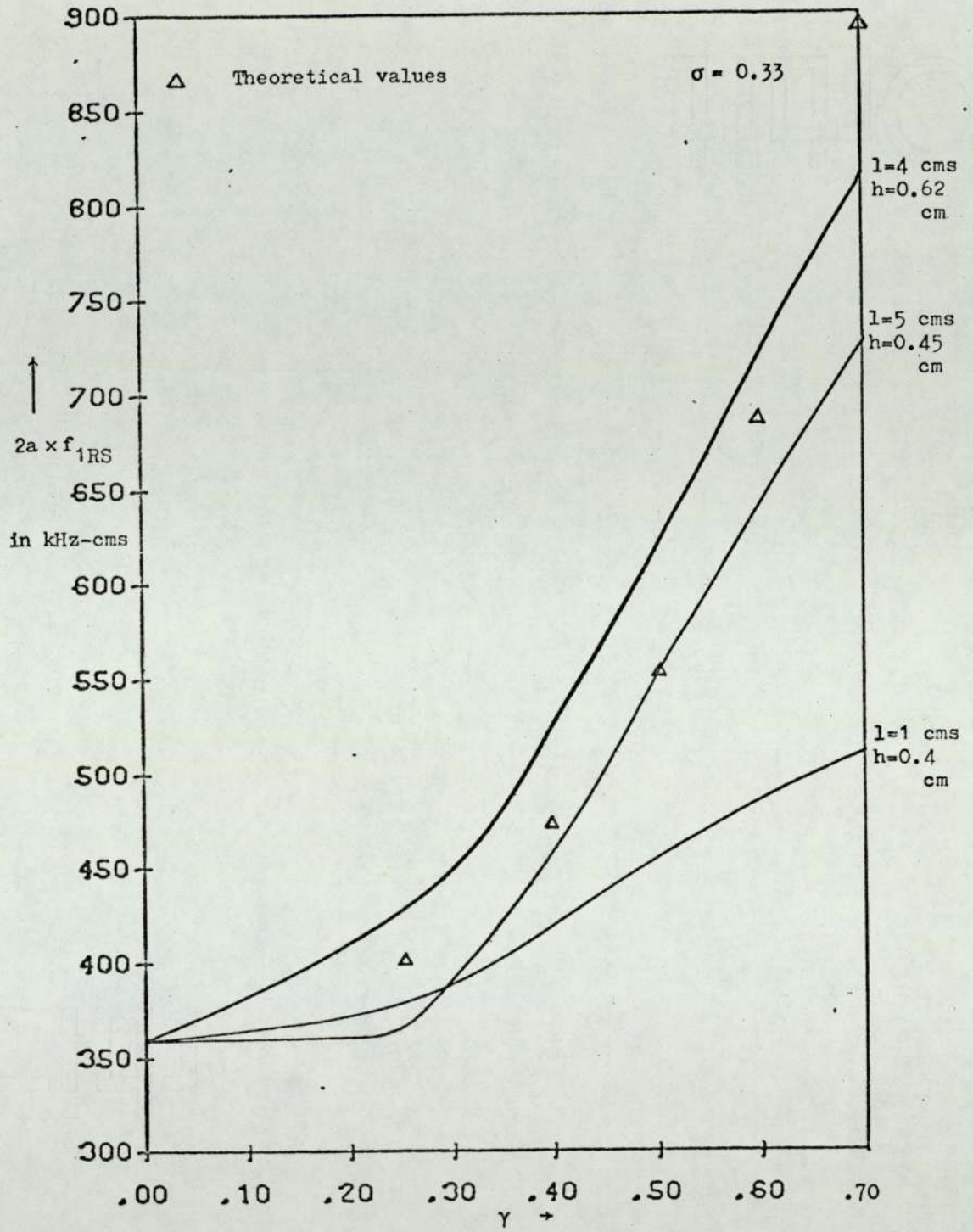

Fig.7.4 This gives the variation of measured frequency with γ. Each curve is for a disk-shaft of different shaft lengths. Notice that the frequency is dependent on the shaft length.

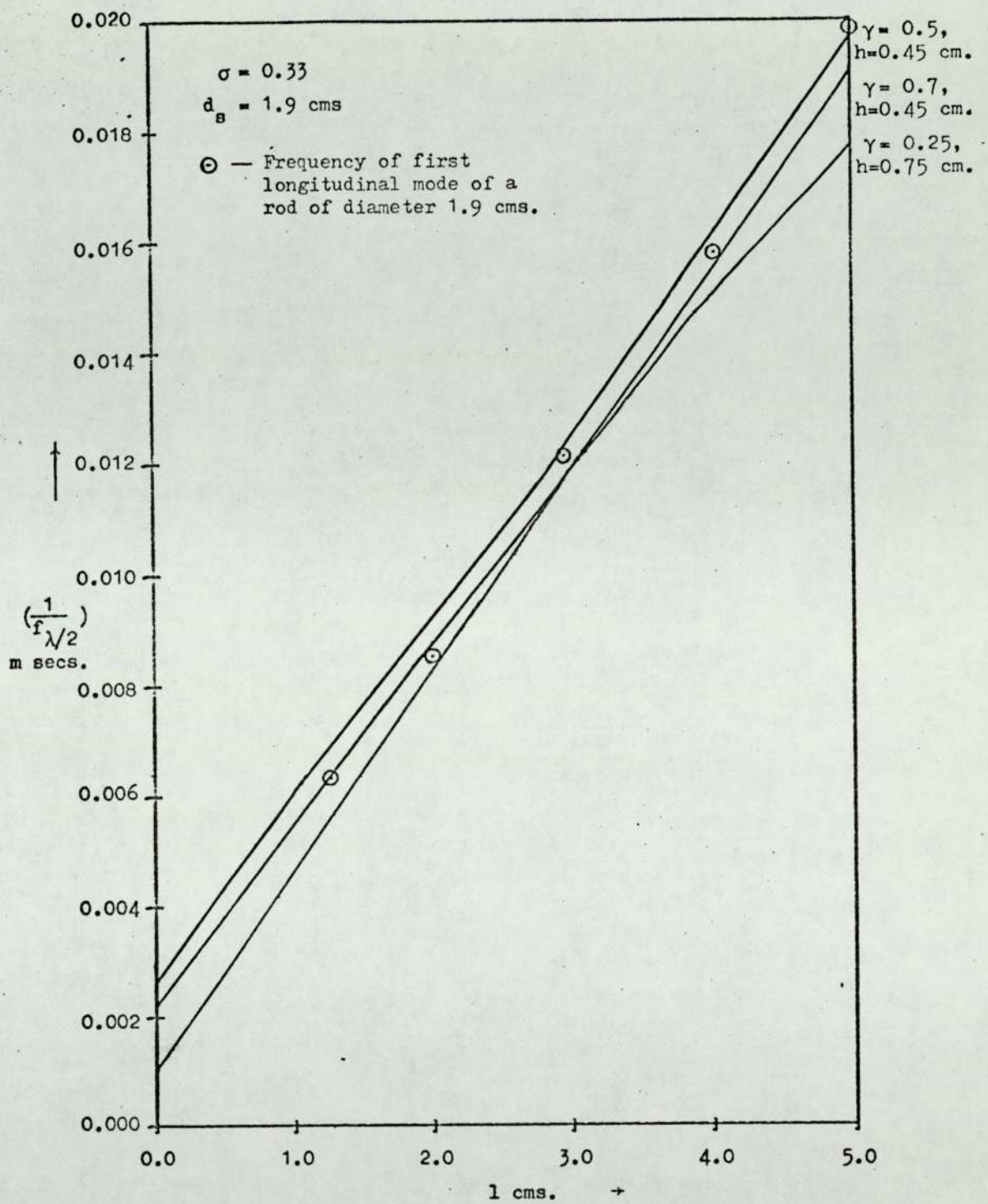

Fig.7.5 The plot of $(1/f_{\lambda/2})$ versus shaft length l, for various γ's, to illustrate the change in the longitudinal mode frequency due to the disk on the centre of the shaft. Notice that the slope of each curve gives the longitudinal velocity for the corresponding γ.

longitudinal resonance, for each γ , may be proportional to the sum of the shaft length and the corresponding intercept on the X axis, the constant of proportionality (slope) being the longitudinal velocity. The corresponding results of the first longitudinal resonance of the rod, are also shown in the figure by circles.

In the experiments carried out on the disk-shaft resonators, it was possible to identify the lower order non-axisymmetric (Compound) vibrations, using a probe of fine wire. Figs.7.6(a) and (b) show the plot of (2af) versus γ for modes (1,2) and (1,3), respectively. The frequency of these modes increases initially with γ, reaching a peak value, which is different for different modes, and then the frequency decreases with increasing γ. This maximum value of the frequency occurs at γ=0.6 and 0.7, for the modes (1,2) and (1,3), respectively. It may be seen from these figures that the variation of the frequencies of these modes is highly dependent on the length of the shaft and is of the same nature for both the modes. However, for smaller shaft lengths, the frequency variation with γ is very large.

The suggestions for further work in this area are given in the next chapter.

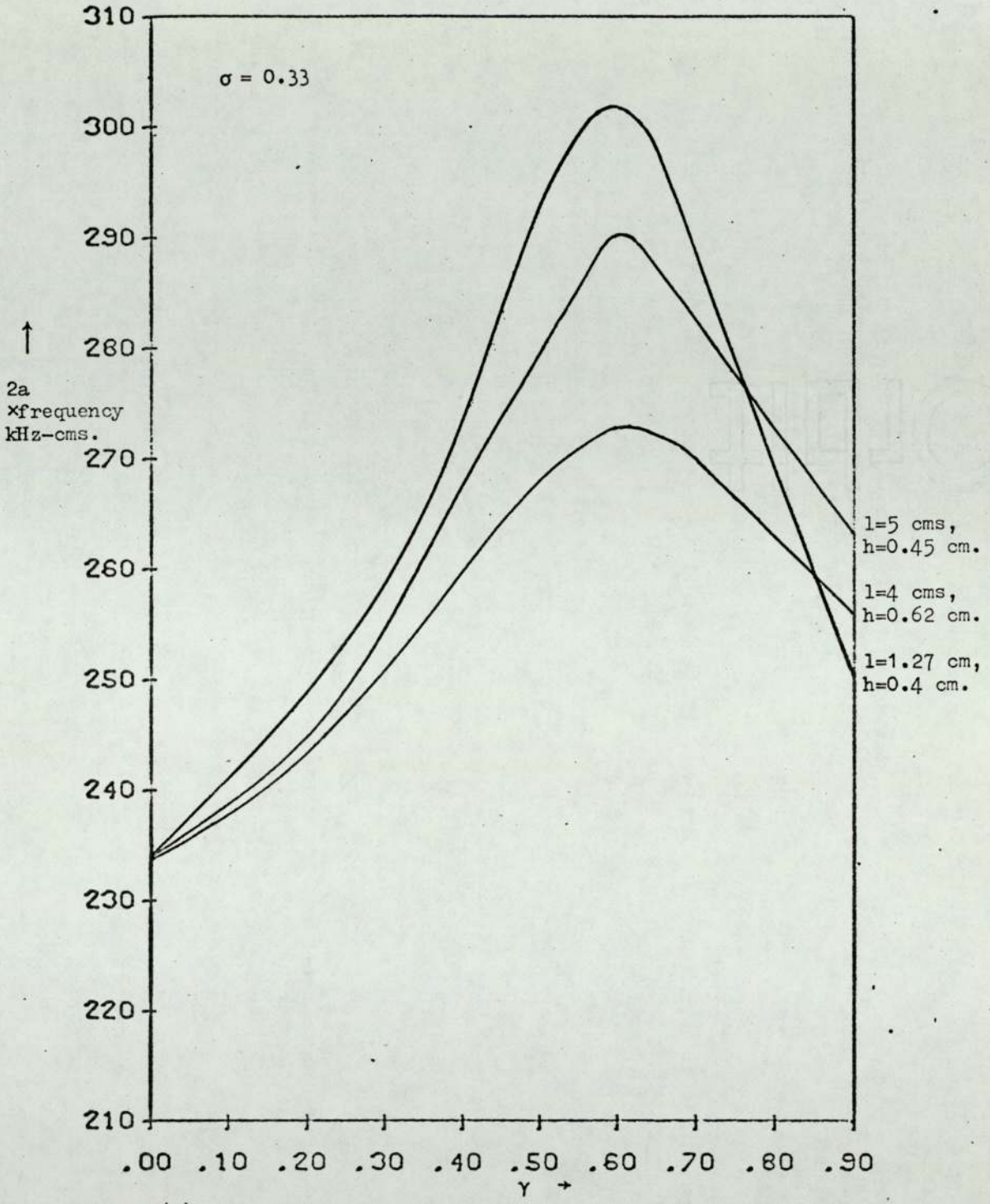

Fig.7.6(a) The plot of the measured frequency versus γ, for the non-axisymmetric mode (1,2). The peak value is reached at $\gamma = 0.6$.

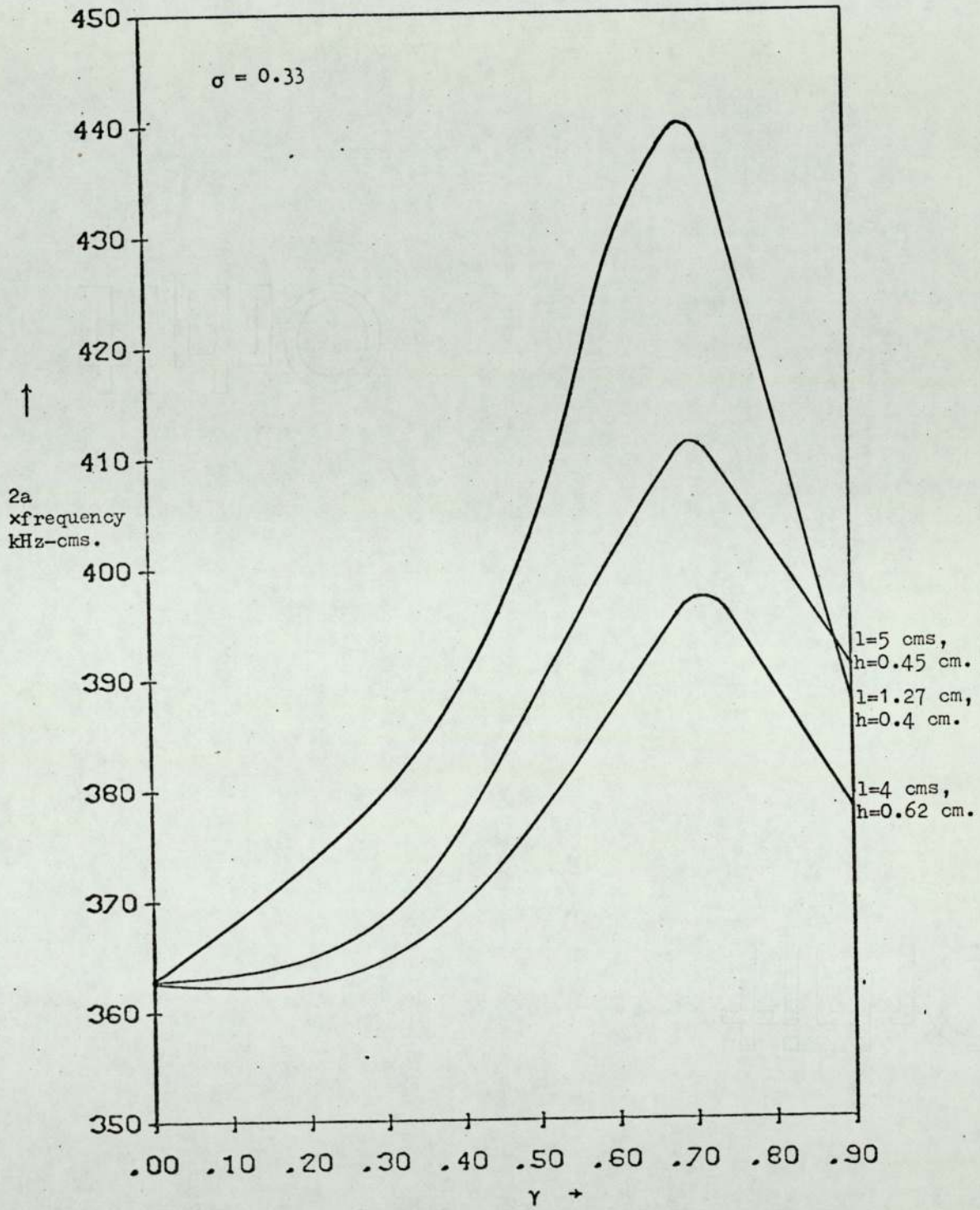

Fig.7.6(b) The plot of 2af versus γ, for the mode (1,3). Notice that the peak value for this mode is reached for $\gamma = 0.7$.

CHAPTER 8

SUGGESTIONS FOR FURTHER WORK

One of the limiting cases obtained by simplifying the thick annular disk compound mode frequency equation (4.2.3) is that of a hollow cylinder. For this case, γ is finite and $\eta \to 0$ and the wave-numbers δ and $\lambda\delta$ of eqns.(4.5.6) reduce to

$$\delta = \sqrt{K^2\Theta^2 + \frac{\pi^2\eta^2}{\Theta^2}} \quad \text{and} \quad \bar{\lambda}\delta = \sqrt{\frac{K^2}{c} - \frac{\pi^2\eta^2}{\Theta^2}} \tag{8.1}$$

It may be interesting to evaluate the numerical solutions of eqn. (4.2.3), using eqns.(8.1) given above, for several modes of vibration in hollow cylinders, for $\eta < 2.0$ and γ between 0.0 to 1.0 and compare these results with the experiments and with those of other workers[26,33,64,66]. It may be useful to establish one-to-one correspondence between the solid cylinder and cylindrical shell modes. The plane strain vibrations and the longitudinal shear vibrations, which were uncoupled in the case of an infinite hollow cylinder, exist as coupled modes in hollow cylinders. It may, therefore, be of more value to study the effect of this coupling on the frequencies of the hollow cylinder modes. The results for axisymmetric vibrations of hollow cylinders can be obtained by the numerical solution of eqns. (4.3.6) and (4.3.7), using eqn.(8.1), for $\eta < 2.0$ and γ in the range 0.0 to 1.0.

Some further investigations into the performance of tuning forks in gas environments would be:

(a) Investigation with tuning forks of various tine widths,

(b) Study of the frequency variation of higher modes, with pressure,

(c) Investigation with a wide range of gases and temperatures, and

(d) Application to pressure measurement.

Further work in disk-shaft resonators can be aimed at:

(a) Obtaining numerical solutions of the frequency equations derived

in chapter 7 for disk-shafts of various shaft lengths and comparing them with the experimental data given in section 7.3.

(b) Identifying and classifying all the resonances observed in disk-shaft resonators of various disk and shaft dimensions, and

(c) studying the variation of resonant frequencies of the disk-shaft resonator with various disk and shaft dimensions.

REFERENCES

1. Bell, J.F.W.: 'A solid acoustic thermometer', Ultrasonics, Vol.6, 1968, pp.11-14.
2. Ambati, G.: 'Experimental and numerical studies of radial and contour extensional modes in elastic disks', M.Sc. Thesis, University of Aston, U.K., 1973.
3. Kolsky, H.: 'Stress waves in solids', Dover, 1963.
4. Pelmore, J.M. : 'Internal friction and high temperature measurements on refractory materials', Ph.D. Thesis, University of Aston, 1975.
5. Seth, T.N. : 'Ultrasonic pyrometer for industrial applications', Ph.D. Thesis, University of Aston, 1974.
6. Waygood, R. : 'A study of the behaviour of a resonant flexurally vibrating clamped disc close to a fixed disc', M.Sc. Thesis, University of Aston, 1974.
7. Ambati, G., Bell, J.F.W. and Sharp, J.C.K. : 'In plane vibrations of annular rings', (Accepted for publication), Journal of Sound and Vibration, 1976.
8. Love, A.E.H. : 'The mathematical theory of elasticity', Fourth edition, Cambridge University Press, 1927.
9. Onoe, M. : 'Contour vibrations of isotropic circular plates', J. Acoust. Soc. Am., Vol.28, No.6, 1956, pp.1158-1162.
10. Holland, R. : 'Numerical studies of elastic-disk contour modes lacking axial symmetry', J. Acoust. Soc. Am., Vol.40, No.5, 1966, pp.1051-1057.
11. Mosley, D.S. : 'Contribution to the theory of radial extensional vibrations in thin disks', J. Acoust. Soc. Am., Vol.32, No.8, Aug. 1960, pp.991-995.
12. Lucey, G.K. : 'Resonant and antiresonant frequencies of thick disks and thick rods', J. Acoust. Soc. Am., Vol.43, No.6, 1968, pp.1324-1328.

13. Baerwald, H. : 'Electrical admittance of a circular ferroelectric disk', TR No.3, ONR Contract No. NOR 1055(00), Brush Labs., Cleveland, Ohio, Jan 1955.

14. Rasband, S.N. : 'Resonant vibrations of free cylinders and disks', J. Acoust. Soc. Am., Vol.57,No.4, 1975, pp.899-905.

15. Martincek, G. : 'The determination of Poisson's ratio and the dynamic modulus of elasticity from the frequencies of the natural vibration in thick circular plates', J. Sound and Vibration, Vol.2, Part 2, 1965, pp.116-127.

16. Mc Mahon, G. : 'Experimental study of the vibration of solid isotropic elastic cylinders', J. Acoust. Soc. Am., Vol.36, 1964, pp.85-92.

17. Meitzler, A.H., O'Bryan, H.M. and Tiersten, H.F. : 'Definition and measurement of radial mode coupling factors in piezoelectric ceramic materials with large variations in Poisson's ratio', IEEE Trans. Sonics and Ultrasonics, Vol. SU-20, No.3, 1973, pp.233-239.

18. Sharp, J.C.K. : 'A theoretical and experimental investigation into the spectra of selected resonators', Ph.D. Thesis, University of Aston, 1974.

19. Rayleigh, Lord : 'On the free vibrations of an infinite plate of homogeneous isotropic elastic matter', Proc. London Math. Soc., Vol.20, 1889, pp.225-234.

20. Poisson, S.D. : 'Memoire sur l'equilibre et le mouvement des corps elastiques', Memoire de l'Academic de Paris, Vol.8, 1829.

21. Buckens, F. : 'Influence of the relative radial thickness of a ring on its natural frequencies', J. Acoust. Soc. Am., Vol.22, No.1, July 1950, pp.437-443.

22. Stephenson, C.V. : 'Radial vibrations in short, hollow cylinders of Barium titanate', J. Acoust. Soc. Am., Vol.28, No.1, Jan 1956, pp.51-56.

23. Gazis, D.C. : 'Exact analysis of the plane-strain vibrations of thick-walled hollow cylinders', J. Acoust. Soc. Am., Vol.30, No.8, Aug 1958, pp.786-794.

24. Gray, A. and Mathews, G.B. : 'A treatise on Bessel functions', London, 1895, pp.13-16.

25. Hoppe, R. : J. F. Math. (Crelle), Bd.73, 1871, pp.158.

26. Gazis, D.C. : 'Three-dimensional investigation of the propagation of waves in hollow circular cylinders. I. Analytical foundation', J. Acoust. Soc. Am., Vol.31, No.5, May 1959, pp.568-573.

27. Mirsky, I. : 'Vibrations of orthotropic, thick, cylindrical shells', J. Acoust. Soc. Am., Vol.36, No.1, 1964, pp.41-51.

28. Mc Niven, H.D., Shah, A.H. and Sackman, J.L. : 'Axially symmetric waves in hollow, elastic rods: Part I', J. Acoust. Soc. Am., Vol.40, No.4, 1966, pp.784-792.

29. Mc Niven, H.D., Shah, A.H. and Sackman, J.L. : 'Axially symmetric waves in hollow, elastic rods: Part II', Ibid, No.5, pp.1073-1076.

30. Arnold, R.N. and Warburton, G.B. : 'Flexural vibrations of the walls of thin cylindrical shells having freely supported ends', Proc. Roy. Soc. A197, 1949, pp.238-256.

31. Mindlin, R.D. and Mc Niven, H.D. : 'Axially symmetric waves in elastic rods', J. Appl. Mech., March 1960, pp.145-151.

32. Zemanek, J. and Rudnick, I. : 'Attenuation and dispersion of elastic waves in a cylindrical bar', J. Acoust. Soc. Am., Vol.33, No.10, Oct 1961, pp.1283-1288.

33. Zemanek, J. : 'An experimental and theoretical investigation of elastic wave propagation in cylinder', J. Acoust. Soc. Am., Vol.51, No.1 (Part 2), 1972, pp.265-283.

34. Shaw, E.A.G. : 'On the resonant vibrations of thick Barium titanate disks', J. Acoust. Soc. Am., Vol.28, No.1, 1956, pp.38-50.

35. Kane, T.R. and Mindlin, R.D. : 'High frequency extensional

vibrations of plates', J. Appl. Mech., June 1956, pp.277-283.

36. Watson, G.N. : 'A treatise on the theory of Bessel functions', Second edition, Cambridge University Press, 1962.

37. Ghosh, J. : 'Longitudinal vibrations of a hollow cylinder', Bull. Calcutta Mathematical Society, Vol.14, No.1, 1923-24, pp.31-40.

38. Gustafsson, D.G. and Kane, T.R. : 'Axially symmetric extensional vibrations of a circular disk with a concentric hole', J. Appl. Mech., Dec. 1959, pp.541-545.

39. Pochhammer, L. : 'Uber die Fortpflanzungsgeschwindigkeiten kleiner Schwingungen in einem unbegrenzten isotropen Kreiszylinder', J.f.d reine u. angew. Math., Vol. 81, 1876, pp.324-336 (German).

40. Chree, C. : 'The equations of an isotropic elastic solid in polar and cylindrical coordinates - their solutions and applications', Trans. Cambridge Phil. Soc., Vol. 14, 1889, pp.250-369.

41. Lin, T.C. and Morgan, G.W. : 'A study of the axisymmetric vibrations of cylindrical shells as affected by rotary inertia and transverse shear', J. Appl. Mech., Vol. 23, 1956, pp.255-261.

42. Naghdi, P.M. and Cooper, R.M. : 'Propagation of elastic waves in Cylindrical shells, including the effects of transverse shear and rotary inertia', J. Acoust. Soc. Am., Vol. 28, 1956, pp.56-63.

43. Mirsky, I. and Herrmann, G. : 'Axially symmetric motions of thick cylindrical shells', J. Appl. Mech., Vol. 25, 1958, pp.97-102.

44. Mirsky, I. and Herrmann, G. : 'Non-axially symmetric motions of cylindrical shells', J. Acoust. Soc. Am., Vol. 29, 1957, pp.1116-1123.

45. Bassett, A.B. : 'Shell analysis by exact theory', Proc. London Math. Soc., Vol. 21, 1891, pp.53-58.

46. McFadden, J.A. : 'Radial vibrations of thick-walled hollow cylinders', J. Acoust. Soc. Am., Vol. 26, 1954, pp.714-715.

47. Herrmann, G. and Mirsky, I. : 'Three-dimensional and shell-theory analysis of axially symmetric motions of cylinders', J. Appl. Mech.,

Vol. 23, 1956, pp.563-568.

48. Redwood, M. and Lamb, J. : 'On the propagation of high-frequency compressional waves in isotropic cylinders', Proc. Phys. Soc. B70, 1957, pp.136-143.

49. Mindlin, R.D. and Herrmann, G. : 'A one-dimensional theory of compressional waves in an elastic rod', Proc. of the first U.S. National Congress of Applied Mechanics, 1950, pp.187-191.

50. Rayleigh, Lord. : 'Theory of sound', Vol. 1, Mac Millan and Company, London, 1894.

51. Armenakas, A.E., Gazis, D.C. and Herrmann, G. : 'Free vibrations of circular cylindrical shells', Pergamon Press, First edition, 1969.

52. Bell, J.F.W. : 'Ultrasonic thermometry using resonance techniques', 5th Symposium on Temperature, Washington, D.C., 1971, pp.709-713.

53. Morse, P.M. : 'Vibration and Sound', Mcgraw Hill, Second edition, 1948.

54. Broadbent, I., et al. : 'Investigation into the performance of high frequency tuning forks in various gas environments', B.Sc. project report, Univ. of Aston, 1973.

55. Singh, B.R. and Nandeeswaraiah, N.S. : 'Vibration analysis of turbine disc in its plane', J. of Sci. Engg. Research, Vol. 1, July 1957, pp.157-160.

56. Berger, H.M. : 'A new approach to the analysis of large deflections of plates', J. Appl. Mech., Dec. 1955, pp.465-472.

57. Sugiyama, K. : 'Unsymmetrical vibration of circular diaphragm with concentric rigid part at the centre', J. Acoust. Soc. Japan, Vol. 23, No. 6, 1967, pp.425-432.

58. Chiang, D.C. and Chen, S.S.H. : 'Large amplitude vibration of a circular plate with concentric rigid mass', J. Appl. Mech., June 1972, pp.577-583.

59. Eshleman, R.L. and Eubanks, R.A. : 'On the critical speeds of a

continuous shaft-disk system', J. of Engg. for Industry, Trans. A.S.M.E., Nov. 1967, pp.645-652.

60. Vogel, S.M. and Skinner, D.W. : 'Natural frequencies of transversely vibrating uniform annular plates', J. Appl. Mech., Trans. A.S.M.E., Dec. 1965, pp.926-931.

61. Gallego Juarez, J.A. : 'Axisymmetric vibrations of circular plates with stepped thickness', J. of Sound and vibration, Vol.26, 1973, pp.411-416.

62. Gontkevich, V.S. : 'Natural vibrations of plates and shells', A.P. Filippov, ed., Nauk Dumka (Kiev), 1964, (Translated by Lockheed Missiles and Space Company (Sunnyvale, California).

63. Raju, P.N. : 'Vibrations of annular plates', J. Aeron. Soc. India, Vol. 14, No.2, May 1962, pp.37-52.

64. Gazis, D.C. : 'Three-dimensional investigation of the propagation of waves in hollow circular cylinders, Part II - Numerical results', J. Acoust. Soc. Am., Vol. 31, No.5, May 1959, pp.573-578.

65. Kaye, G.W.C. and Laby, T.H. : 'Tables of physical and chemical constants', Longmans, 1958.

66. Hutchinson, J.R. : 'Axisymmetric vibrations of a free finite-length rod', J. Acoust. Soc. Am., Vol. 51, No.1, 1972, pp.233-240.

67. Chladni, E.E.F. : 'Entdeckungen uber der theorie des klanges', Leipzig, 1787.

68. Ravenhall, F.W. and Som, A.K. : 'Some recent observations on Chladni's figures', Acustica, Vol. 29, 1973, pp.14-21.

69. Timoshenko, S.P. : 'Theory of plates and shells', McGraw Hill Book Company, U.S.A., 1959.

70. Redwood, M. : 'Mechanical waveguides', Pergamon Press, London, 1960.

71 Stephens, R.W.B. and Bate, A.E. : 'Acoustics and vibrational Physics', Edward Arnold (Publishers) Ltd., London, Second edition, 1966.

APPENDIX A.2.1

THEORY OF CONTOUR VIBRATIONS IN THICK DISKS

The disks with planar isotropy, in particular, are considered here. There are two basic types of vibration: (a) flexural[67,68] and (b) contour extensional (in plane) modes. Here, the method to obtain the frequency equations for contour vibrations in thick disks, is described. Lucey[12] has defined a boundary between a thick disk and a thick rod. He classified the cylinder as a thick disk, if its length is smaller than its radius and as a thick rod, if its radius is smaller than its length. This classification has been used in this development.

Consider a disk of diameter 2a and thickness h placed with its axis along the Z axis and with the centre of the disk at the origin, as shown in Fig.A.2. For contour vibrations in the disk, the components of displacement in cylindrical coordinates r, θ , z, may be taken as

$$u_r = \xi_r (r,\theta,t)$$
$$u_\theta = \xi_\theta (r,\theta,t) \qquad \text{(A.2.1)}$$
and $$u_z = \sin (p\pi z/h)\ \xi_z (r,\theta,t)$$

where ξ_r , ξ_θ represent the amplitudes of uniform distribution of radial and tangential displacements, across the thickness, ξ_z is the amplitude of the sinusoidal distribution of axial displacement corresponding to thickness-stretch modes and p=1 represents coupling of contour vibrations with first thickness mode, p=2 represents the coupling with second thickness mode and so on.

It may be noted that the radial and tangential components of displacement has been taken as uniformly distributed across the disk thickness direction, as in the case of generalised plane stress theory, whereas the distribution of the axial component over the thickness direction has been taken as sinusoidal, as in the rod theory. It is assumed that the sine distribution behaves as a linear distribution for disk thicknesses smaller than its diameter, which is normally the case

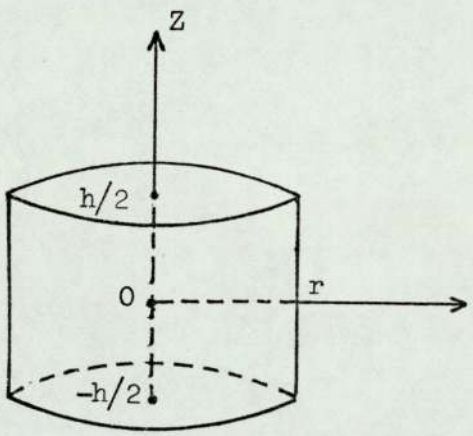

r = Disk radius ; h = Disk thickness.

Fig.A.2 A thick disk and its co-ordinate system.

with thick disks, and hence this theory provides fairly accurate results over the disk range of thickness-to-diameter ratios. However, for the rod range of thickness-to-diameter ratios, this theory yields only approximate results, because, the distributions of u_r and u_θ over thickness direction will be sinusoidal in the case of cylinders, whereas they are assumed to be uniformly distributed in this theory.

The stresses acting on the flat and cylindrical surfaces are defined as[35]

$$T_{rr} = \int_{-h/2}^{h/2} \sigma_r \, dz \quad ; \quad T_{zz} = \int_{-h/2}^{h/2} \sigma_z \, dz \quad ;$$

$$T_{zr} = \int_{-h/2}^{h/2} \sigma_{zr} \cdot z \cdot dz \quad ; \quad T_{z\theta} = \int_{-h/2}^{h/2} \sigma_z \cdot z \cdot dz \qquad \text{(A.2.2)}$$

$$T_{r\theta} = \int_{-h/2}^{h/2} \sigma_{r\theta} \, dz \quad ; \quad \text{and} \quad T_{\theta\theta} = \int_{-h/2}^{h/2} \sigma_\theta \, dz \quad ,$$

where σ_r , σ_z , σ_θ etc., are the usual components of stress[69,70]. These are related to the displacements ξ_r, ξ_θ and ξ_z by

$$T_{rr} = h \times \text{Bulk Modulus} \left[\frac{\partial \xi_r}{\partial r} + \frac{\sigma}{(1-\sigma)} \frac{1}{r} \left(\xi_r + \frac{\partial \xi_\theta}{\partial \theta} \right) + \frac{2\sigma}{h(1-\sigma)} \xi_z \right]$$

$$T_{zz} = h \times \text{Bulk Modulus} \left[\frac{2}{h} \xi_z + \frac{\sigma}{(1-\sigma)} \left(\frac{\partial \xi_r}{\partial r} + \frac{\xi_r}{r} + \frac{1}{r} \frac{\partial \xi_\theta}{\partial \theta} \right) \right]$$

$$T_{\theta\theta} = h \times \text{Bulk Modulus} \left[\frac{1}{r} \left(\xi_r + \frac{\partial \xi_\theta}{\partial \theta} \right) + \frac{\sigma}{(1-\sigma)} \frac{\partial \xi_r}{\partial r} + \frac{2\sigma}{h(1-\sigma)} \xi_z \right] \qquad \text{(A.2.3)}$$

$$T_{zr} = \frac{2h^2}{\pi^2} \times \text{Shear Modulus} \times \frac{\partial \xi_z}{\partial r} \quad , \quad T_{z\theta} = \frac{2h^2}{\pi^2} \times \text{Shear Modulus} \times \frac{1}{r} \frac{\partial \xi_z}{\partial \theta}$$

$$\text{and} \quad T_{r\theta} = h \times \text{Shear Modulus} \left[\frac{\partial \xi_\theta}{\partial r} - \frac{\xi_\theta}{r} + \frac{1}{r} \frac{\partial \xi_r}{\partial \theta} \right]$$

Using the above equations and considering the case of p=1, without loss of generality, the three dimensional equations of motion[8,70] can be expressed in terms of dilatation Δ and rotation $\tilde{\omega}$ as

$$\left[(1-\sigma)\frac{\partial \Delta}{\partial r} - \frac{(1-2\sigma)}{r}\frac{\partial \tilde{\omega}}{\partial \theta} + \frac{2\sigma}{h}\frac{\partial \xi_z}{\partial r}\right] = -\frac{\rho\omega^2(1+\sigma)(1-2\sigma)}{E}\xi_r$$

$$\left[\frac{(1-\sigma)}{r}\frac{\partial \Delta}{\partial \theta} + (1-2\sigma)\frac{\partial \tilde{\omega}}{\partial r} + \frac{2\sigma}{h}\frac{1}{r}\frac{\partial \xi_z}{\partial \theta}\right] = -\frac{\rho\omega^2(1+\sigma)(1-2\sigma)}{E}\xi_\theta \qquad \text{(A.2.4)}$$

and

$$\left[\frac{h(1-2\sigma)}{2}\nabla^2\xi_z - \frac{\pi^2}{2}\sigma\Delta - \frac{\pi^2(1-\sigma)\xi_z}{h}\right] = -\frac{\rho h\omega^2(1+\sigma)(1-2\sigma)}{E}\xi_z$$

where $$\nabla^2 = \left[\frac{\partial^2}{\partial r^2} + \frac{1}{r}\frac{\partial}{\partial r} + \frac{1}{r^2}\frac{\partial^2}{\partial \theta^2}\right] \qquad \text{(A.2.5)}$$

$$\Delta = \left[\frac{\partial \xi_r}{\partial r} + \frac{\xi_r}{r} + \frac{1}{r}\frac{\partial \xi_\theta}{\partial \theta}\right]; \quad \tilde{\omega} = \frac{1}{2}\left[\frac{\partial \xi_\theta}{\partial r} + \frac{\xi_\theta}{r} - \frac{1}{r}\frac{\partial \xi_r}{\partial \theta}\right] \qquad \text{(A.2.6)}$$

It may be noted that the coupling of the contour modes with only the first thickness mode has been taken in this case, which gives fairly accurate results, even for higher modes, for disk range of thickness-to-diameter ratios. But, for the rod range of thickness-to-diameter ratios, this theory is approximately valid for low frequency modes only, due to the coupling of higher contour modes with higher thickness modes. The above equations of motion can be simplified into the form,

$$\left[(1-\sigma)\nabla^2\Delta + \frac{2\sigma}{h}\nabla^2\xi_z + \frac{\rho\omega^2(1+\sigma)(1-2\sigma)}{E}\Delta\right] = 0 \ ,$$

$$(\nabla^2 + \nu^2)\tilde{\omega} = 0 \ , \qquad \text{(A.2.7)}$$

and

$$\left[\frac{E}{2\rho(1+\sigma)}\nabla^2\xi_z + \{\omega^2 - \frac{\pi^2 E(1-\sigma)}{4\rho h^2(1+\sigma)(1-2\sigma)}\}\xi_z - \frac{\pi^2 E\sigma}{4\rho h(1+\sigma)(1-2\sigma)}\Delta\right] = 0,$$

where $\nu^2 = \frac{2\omega^2\rho(1+\sigma)}{E}$. The above three dimensional equations of motion can be reduced to the equivalent two dimensional equations, by eliminating ξ_z between the first and the third of eqns.(A.2.7). Then, the Helmholtz equations which must be satisfied by the dilatation Δ and the rotation $\tilde{\omega}$, become

$$(\nabla^2 + \alpha^2)(\nabla^2 - \beta^2)\Delta = 0 \ , \qquad \text{(A.2.8a)}$$

and

$$(\nabla^2 + \nu^2)\tilde{\omega} = 0 \ , \qquad \text{(A.2.8b)}$$

where
$$\alpha^2 = \frac{\pi^2 G}{h^2(1-\sigma)} (1+\psi) \quad ,$$

$$\beta^2 = \frac{\pi^2 G}{h^2(1-\sigma)} (\psi - 1) \quad ,$$

$$\nu^2 = \frac{2\omega^2\rho(1+\sigma)}{E} \quad , \qquad \text{(A.2.9)}$$

$$\psi = \left[1 + \frac{4(G+1)(1-\sigma)^2}{G^2(3-4\sigma)} \{1 - \frac{2(G+1)(1-2\sigma)}{(1-\sigma)(3-4\sigma)}\}\right]^{\frac{1}{2}} \quad ,$$

and
$$G = \left[\frac{\omega^2 h^2 \rho(1+\sigma)(3-4\sigma)}{2\pi^2 E} - 1\right] \quad .$$

The solutions of equations(A.2.8) in polar coordinates are given by

$$\Delta = \{A_1 J_n(\alpha r) + A_2 Y_n(\alpha r) + B_1 I_n(\beta r) + B_2 K_n(\beta r)\} \cos n\theta$$
$$\text{and } \tilde{\omega} = \left[C_1 J_n(\nu r) + C_2 Y_n(\nu r)\right] \sin n\theta \qquad \text{(A.2.10)}$$

where J_n and Y_n are the Bessel functions of the first and second kinds, respectively and I_n and K_n are the modified Bessel functions of the first and second kinds, respectively. In the absence of singularities at the origin, the coefficients A_2, B_2 and C_2 are taken as equal to zero. Hence, Δ and $\tilde{\omega}$ are given by

$$\Delta = \{A_1 J_n(\alpha r) + B_1 I_n(\beta r)\} \cos n\theta$$
$$\text{and} \quad \tilde{\omega} = C_1 J_n(\nu r) \sin n\theta \quad , \qquad \text{(A.2.11)}$$

where the coefficients A_1 and B_1 indicate the magnitude of the dilatational components of the displacement and the coefficient C_1 indicates the magnitude of the shear component of the displacement.

To determine the displacement functions ξ_r and ξ_θ associated with the dilatation and the rotation, let us consider eqn.(A.2.6) which defines Δ and $\tilde{\omega}$ in terms of ξ_r and ξ_θ.

If we assume that ξ_r and ξ_θ can be expressed in the form, using separation of variables, as

$$\xi_r = \xi_{rn} \cos n\theta$$

and $$\xi_\theta = \xi_{\theta n} \sin n\theta \quad , \tag{A.2.12}$$

where ξ_{rn} and $\xi_{\theta n}$ are functions of 'r' alone, then the substitution of this and the eqns.(A.2.11) for Δ and $\tilde{\omega}$ into eqns.(A.2.6), leads to the following differential equations in ξ_{rn} and $\xi_{\theta n}$.

$$\left[\frac{\xi_{rn}}{r} + \frac{d\,\xi_{rn}}{dr} + \frac{n\,\xi_{\theta n}}{r}\right] = A_1\, J_n(\alpha r) + B_1\, I_n(\beta r) \quad ,$$

and $$\left[\frac{\xi_{\theta n}}{r} + \frac{d\,\xi_{\theta n}}{dr} + \frac{n\,\xi_{rn}}{r}\right] = C_1\, J_n(\nu r) \quad .$$

The above equations are solved for ξ_{rn} and $\xi_{\theta n}$, which when substituted into eqns.(A.2.12) leads to the following displacement functions

$$\xi_r = \left[A_1 \frac{dJ_n(\alpha r)}{dr} + B_1 \frac{dI_n(\beta r)}{dr} + \frac{nC_1}{r} J_n(\nu r)\right] \cos n\theta$$

$$\xi_\theta = -\left[\frac{nA_1}{r} J_n(\alpha r) + \frac{nB_1}{r} I_n(\beta r) + C_1 \frac{dJ_n(\nu r)}{dr}\right] \sin n\theta \quad , \tag{A.2.13}$$

where n is known as the angular index or the circumferential order.

The above displacement functions can also be derived by noting that

$$\xi_r = \left(\frac{\partial \Delta}{\partial r} + \frac{1}{r}\frac{\partial \tilde{\omega}}{\partial \theta}\right)$$

and $$\xi_\theta = \left(\frac{1}{r}\frac{\partial \Delta}{\partial \theta} - \frac{\partial \tilde{\omega}}{\partial r}\right) \tag{A.2.14}$$

The expression for ξ_z can then be obtained from eqns.(A.2.7), (A.2.8), (A.2.11) and (A.2.14), as

$$\xi_z = \{A_1 \phi_1 J_n(\alpha r) - B_1 \phi_2 I_n(\beta r)\} \cos n\theta \tag{A.2.15}$$

where

$$\phi_1 = \frac{h(1-\sigma)}{2\sigma}\left[\alpha^2 - \frac{\omega^2 \rho (1+\sigma)(1-2\sigma)}{E(1-\sigma)}\right] \quad ,$$

and $$\phi_2 = \frac{h(1-\sigma)}{2\sigma}\left[\beta^2 + \frac{\omega^2 \rho (1+\sigma)(1-2\sigma)}{E(1-\sigma)}\right] \quad . \tag{A.2.16}$$

APPENDIX A.2.2

THE ACOUSTIC SPECTRUM ANALYSER

An electronic acoustic spectrum analyser was designed and constructed, to measure the resonant spectrum of a solid specimen by the pulse-echo technique. Basically, the system generates a repetitive burst of high frequency oscillations with variable burst length to excite various resonances in the specimen. The block diagram and the circuit diagram of the system are shown in Figs.A.2.1 and A.2.2, respectively.

The components of the system are:

(a) A variable high frequency voltage controlled oscillator covering 0.8 - 620 kHz in three ranges.

(b) A repetition rate oscillator with the repetition rate of the burst variable from 10 m secs. to 0.26 secs.

(c) A burst length controller with a facility to change the number of oscillations in the burst.

(d) A gating circuitry to synchronise the high frequency and low frequency oscillations.

(e) An output circuit to amplify the burst of oscillations to 30 V peak-to-peak.

The high frequency and repetition rate oscillators, each consist of a pair of cross coupled monostable multivibrators, whose period can be controlled by means of a potentiometer and ganged capacitors. Another monostable with a potentiometer is used at the output of the repetition rate oscillator, to control the burst length. The synchronisation between the low frequency and high frequency oscillations is done through a D flip-flop to ensure that the start of high frequency oscillations coincides with the rising edge of the low frequency oscillator output. The complementary waveforms are derived using NAND gates as shown in Fig.A.2.2. The waveforms at various points are shown in Fig.A.2.3. The output circuit constructed is a push pull transistor

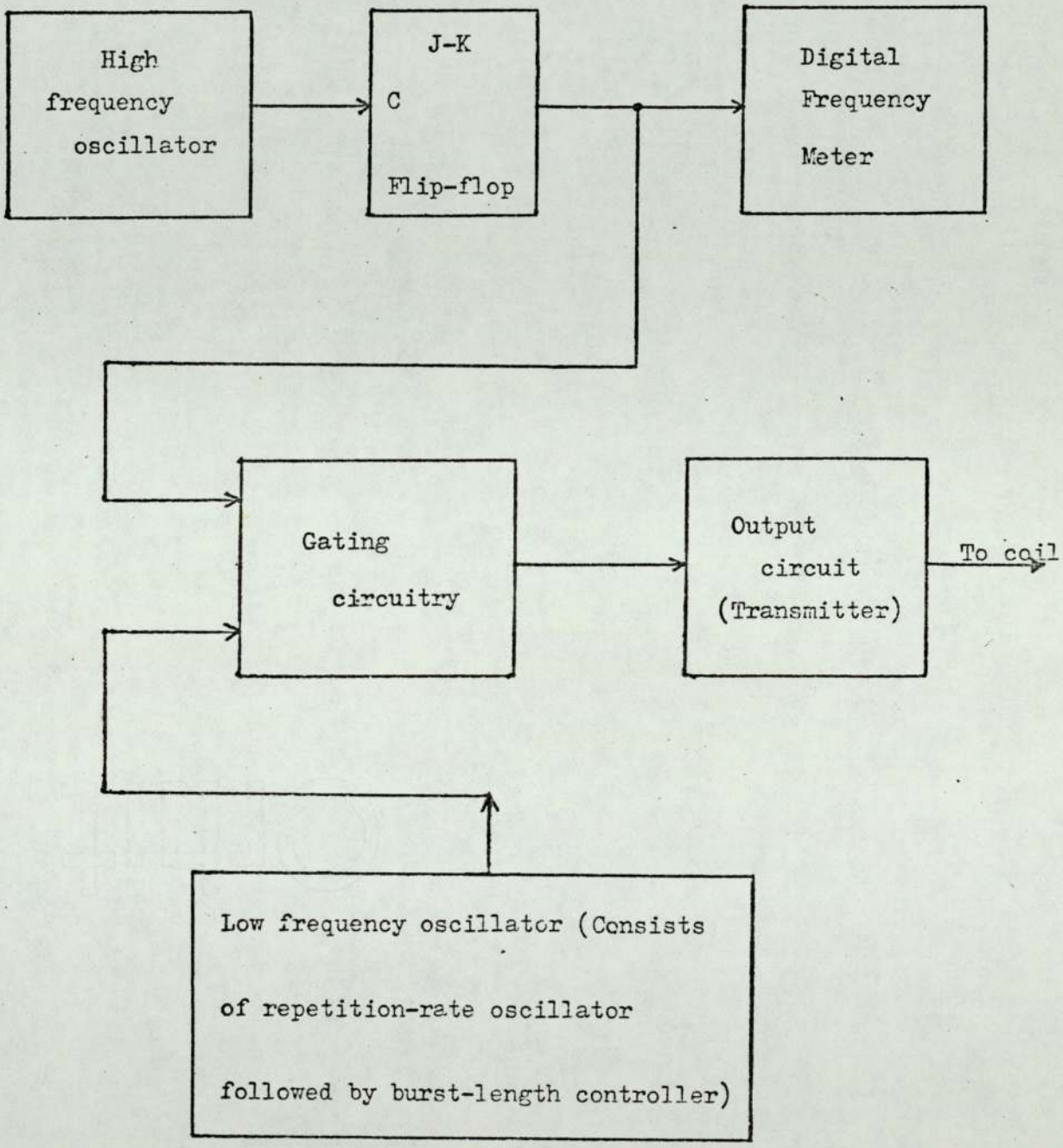

Fig.A.2.1 Block Diagram of Acoustic Spectrum Analyser.

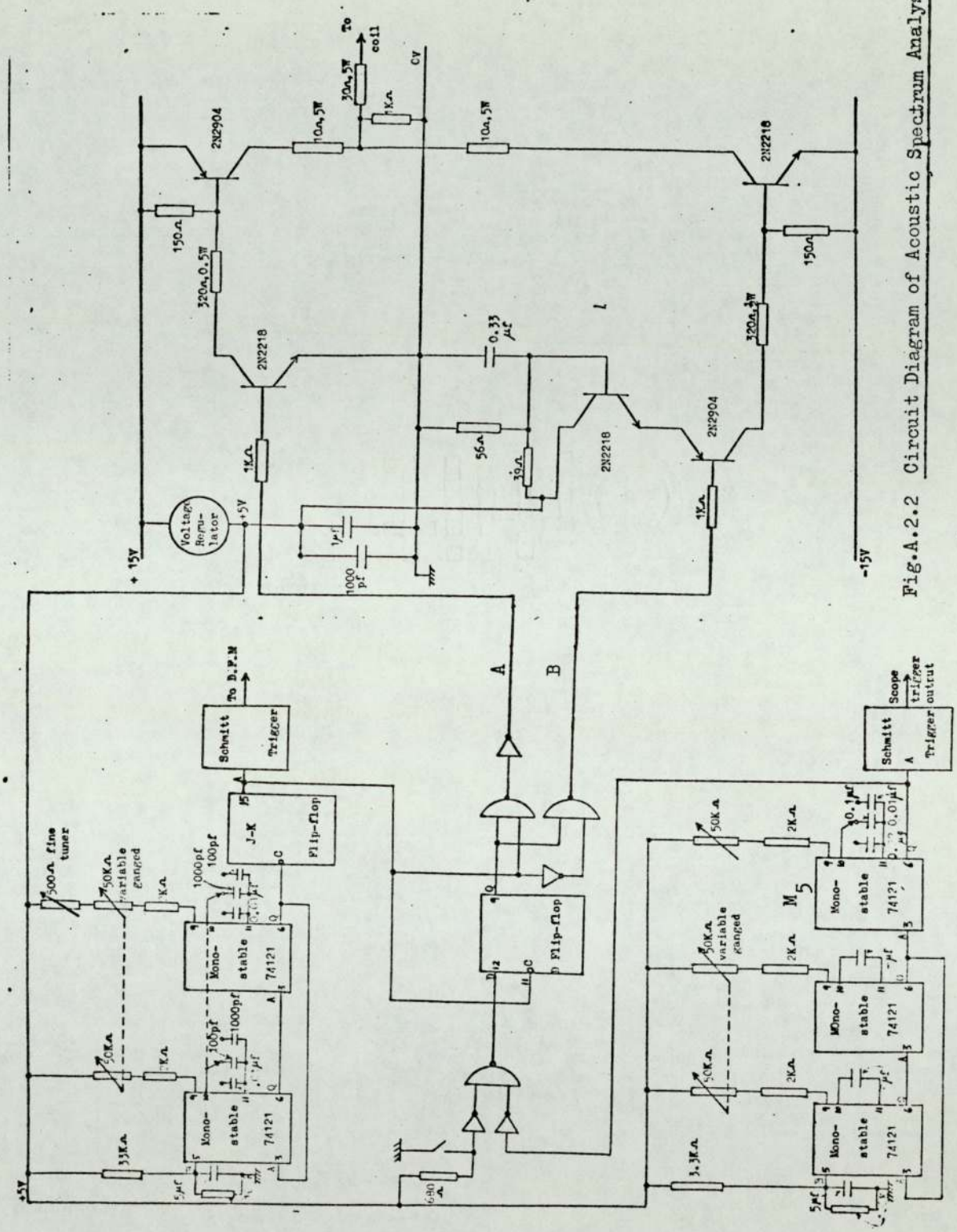

Fig.A.2.2 Circuit Diagram of Acoustic Spectrum Analyser.

Fig.A.2.3

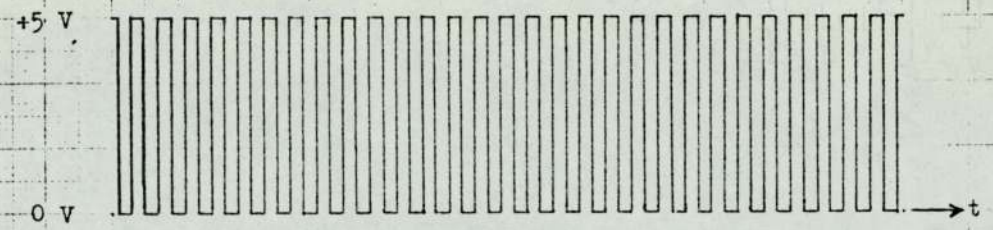

(a) Output of the high frequency oscillator.

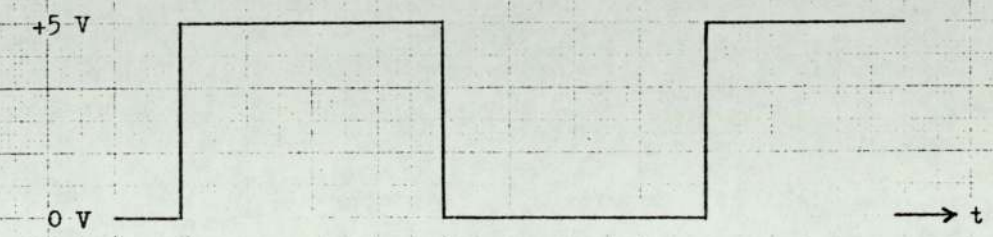

(b) Output of the repetition rate oscillator.

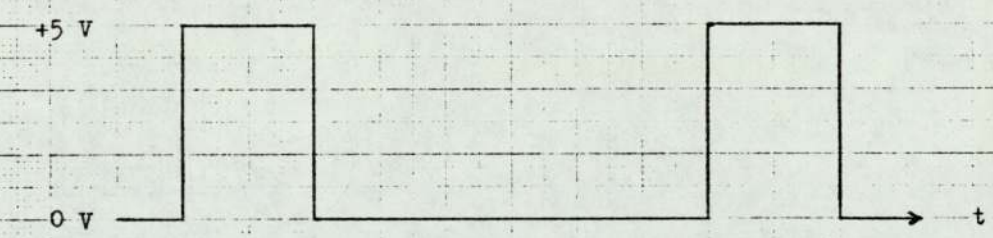

(c) Output of the low frequency oscillator(Input to D flip-flop)

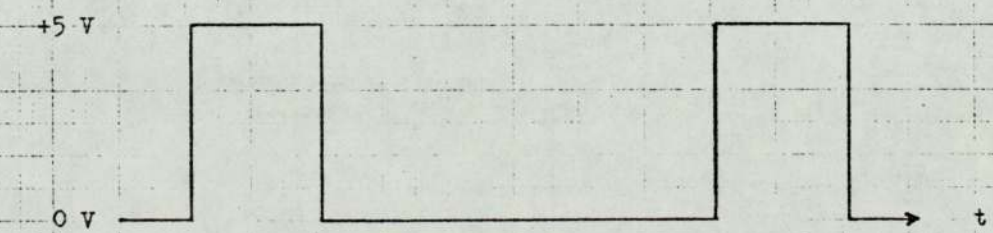

(d) Output of D flip-flop.

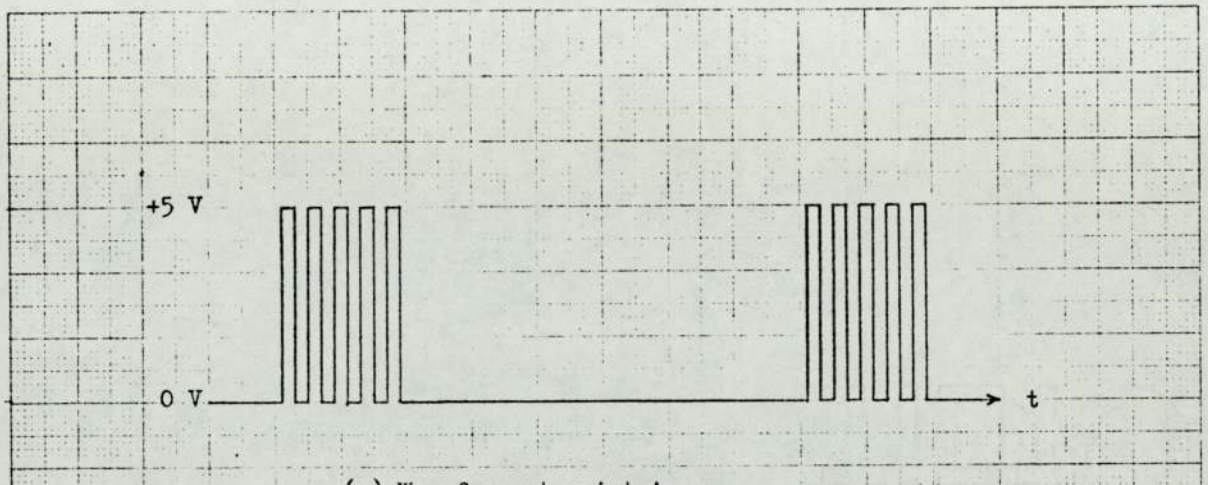

(e) Waveform at point A.

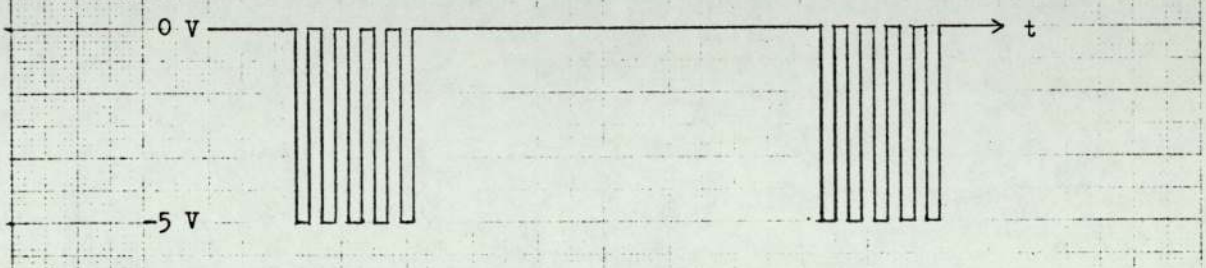

(f) Waveform at point B.

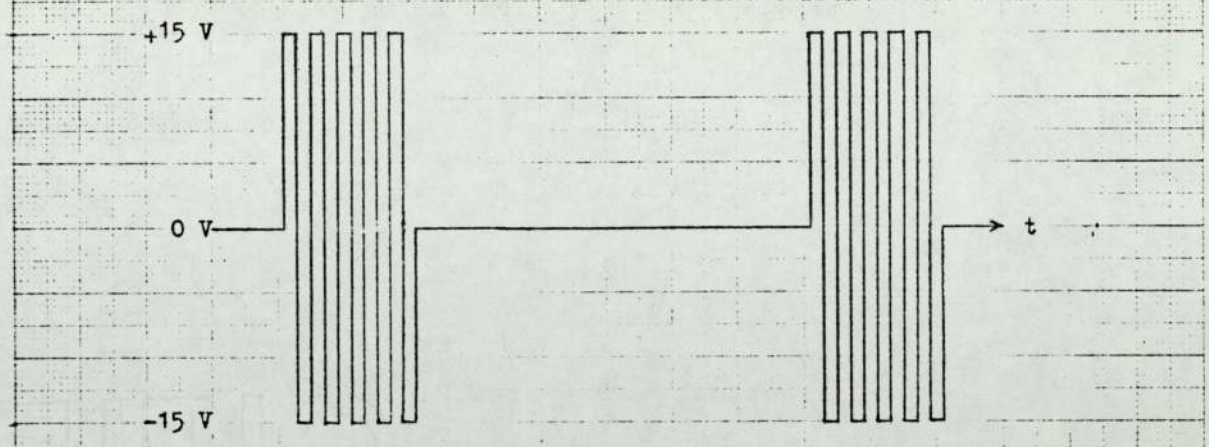

(g) Output of the transmitter(output circuit).

Fig.A.2.3 Waveforms at various points of the Spectrum Analyser.

arrangement to give an output of 30 V peak-to-peak. A digital frequency meter reads the oscillator frequency.

A pulse-echo technique, originally developed by Bell[1] for ultrasonic thermometry, has been used to measure the resonant spectrum of the specimen. The block diagram of the experimental arrangement used to measure the resonant spectrum is shown in Fig.A.2.4. A photograph of the equipment is given in Fig.A.2.5. Basically the resonant spectrum is obtained by driving the resonator with a long thin wire fixed radially or at an angle to the periphery of the disk resonator. A burst of longitudinal oscillations, from the output of the transmitter, is transmitted up the magnetostrictive line through a coil, which must introduce sufficient delay to separate the signal returned from that transmitted. The line, in the coil, which acts as a transducer, converts the electrical pulses into mechanical energy to drive the resonator. If the line is lossless, the number of oscillations to crossover, from one resonator to another resonator of same shape, but different dimensions, will be in the same ratio from fundamental to overtones. The coil is matched to the transmitter by the decade capacitance box, which puts capacity in parallel with the coil. Under these conditions- the absence of standing waves- the wire presents a purely resistive load to the resonator, which, while limiting the sharpness of resonance, has no effect on the resonant frequencies. The structure of the signal returned from the resonator, due to periodical excitation by the acoustic signal sent, enables the resonant condition to be identified very precisely. At resonance, the transmitted frequency is equal to the decrement frequency, and a well defined crossover is obtained. The sensitivity of this crossover method renders very small changes in resonant frequency detectable. A typical picture of the echo returned from the resonator is shown in Fig.A.2.6.

The resonators considered here are solids having cylindrical

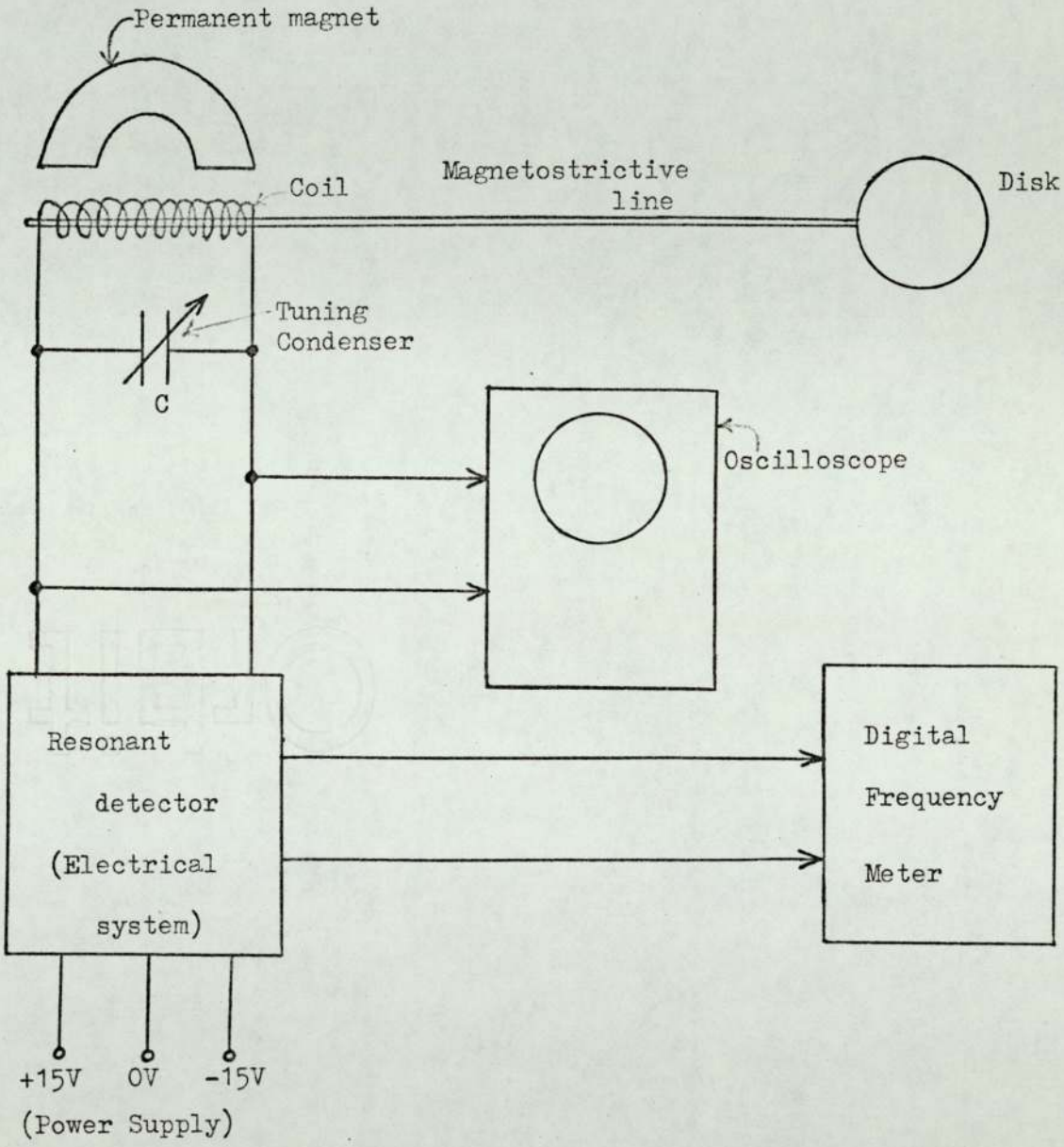

Fig.A.2.4 Block Diagram of the Experimental Arrangement used to Measure the Resonant Spectrum of the Specimen.

Fig.A.2.5 The photograph of the experimental arrangement used to measure the resonant spectra of the specimen.

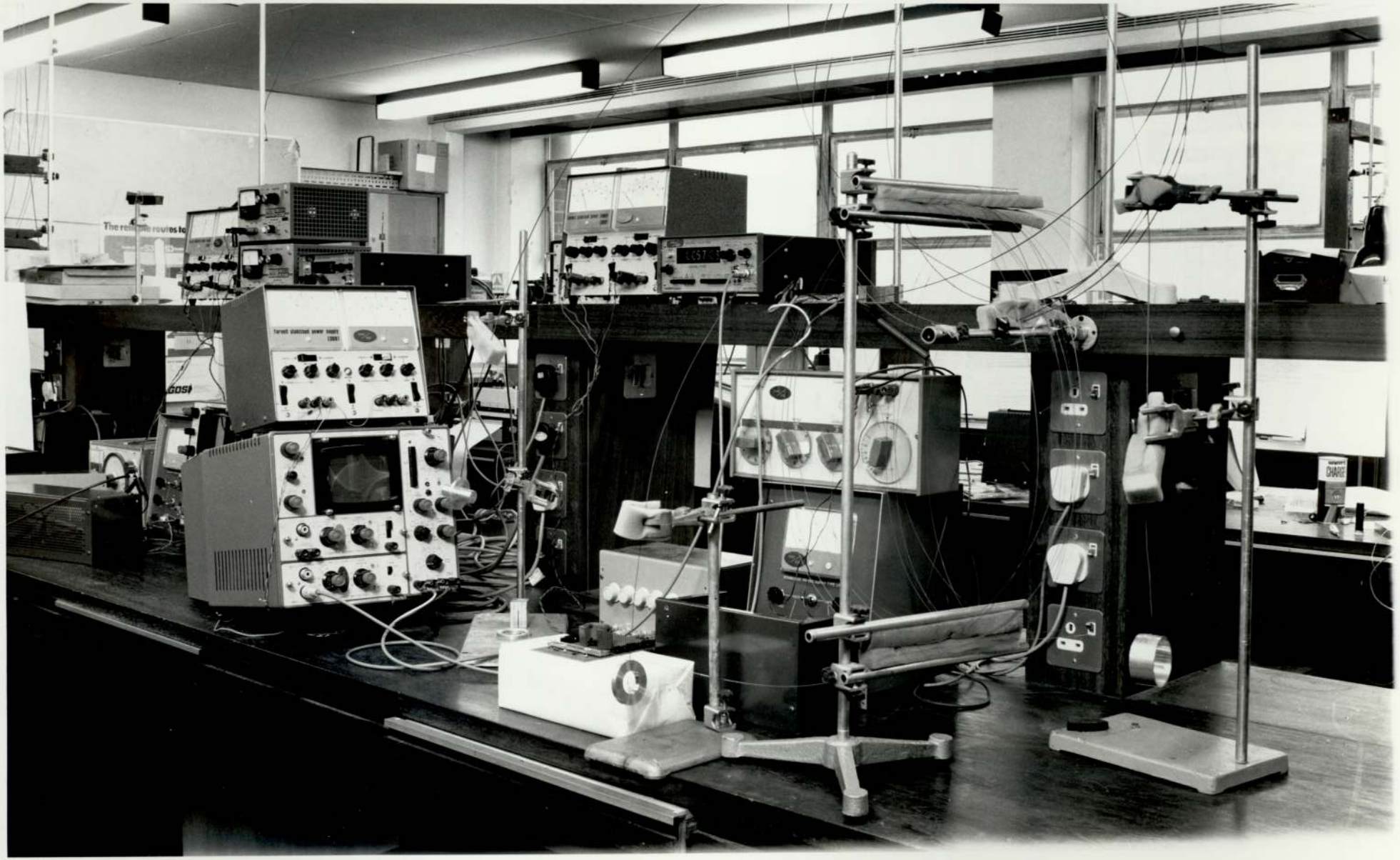

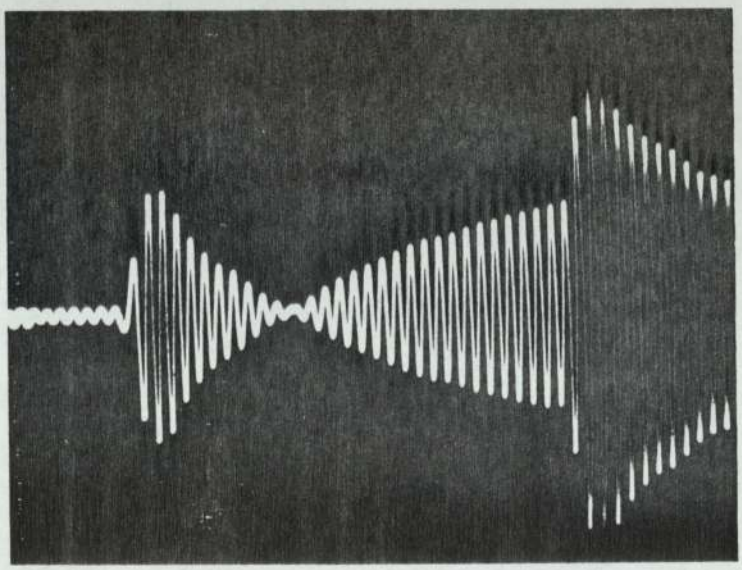

Fig.A.2.6 A typical picture of the echo signal received from the resonator.

geometry. The degree of coupling to a particular resonance depends on the direction of vibration at the point of drive. There are, mainly, four types of drive techniques used for the measurement of the resonant spectra of resonators of various shapes. They are:

(1) Radial drive: The resonator is driven by fixing the line radially into the periphery. This drive gives a good coupling if the radial component is large. This drive was found to excite (a) radial and compound modes in disks, annular rings and thick annular disks. (b) transverse and longitudinal vibrations in rods, and (c) radial, compound and longitudinal resonances in disk-shaft system. In disk-shaft resonators, the radial resonances will be strongly coupled and the longitudinal resonances are loosely coupled in this drive.

(2) Tangential or angular drive: In this drive, the line is fixed at an angle to the periphery of the resonator, giving good coupling for shear modes. This drive excites (a) tangential and compound modes in disks and annular disks, (b) torsional modes in rods and (c) (c) tangential and compound modes in disk-shaft system.

(3) Longitudinal or axial drive: The line is fixed longitudinally into the resonator. This drive technique excites (a) longitudinal modes in rods, (b) flexure modes in disks, and (c) longitudinal and radial modes in disk-shaft system. The longitudinal modes will be strongly coupled and the radial modes will be loosely coupled in the disk-shaft resonator.

(4) Double drive: The two ends of the line (through the coil) are fixed at diametrically opposite points of the resonator. This was found to excite higher modes in disk resonators, giving a greater degree of coupling. When two frequencies of a resonator are close together, this drive at different points can, by phasing, suppress one mode in favour of the other.

The above drive techniques are illustrated in Fig.A.2.7.

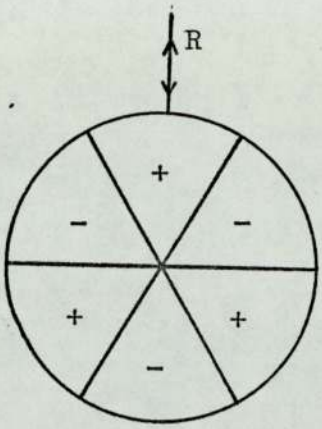

Radial drive which excites (1,R), (1,1),(1,2),(1,3),...,etc., modes.

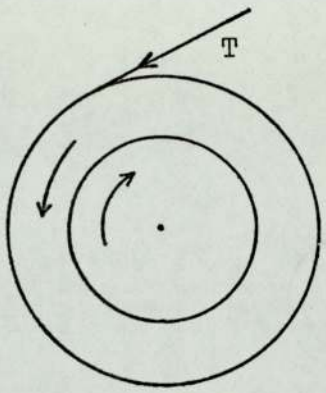

Tangential drive which excites (1,T),(2,T),(2,2),(2,3), (2,4),...,etc., modes.

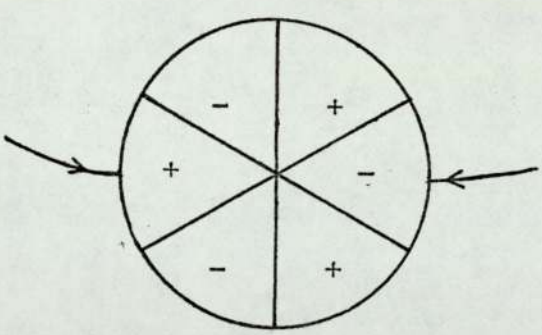

Double drive which excites (1,R) mode, but suppresses the adjacent (1,3) mode.

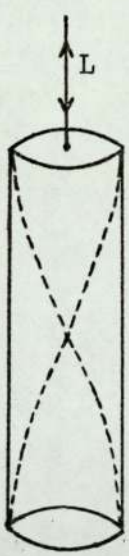

Longitudinal drive which excites $f_{\lambda/2}$, f_{λ} ,..., etc., modes.

Fig.A.2.7 Illustration of various drive techniques.

APPENDIX A.3.1

DERIVATION OF FREQUENCY EQUATION FOR ANNULAR RINGS

The differential equations for various wave motions of the resonant system are first established, in polar coordinates, for this case. A general solution of the equations of motion may be obtained by using the boundary conditions of the system, in this case, that the radial and tangential stresses must vanish at the inner and outer perimeters. The specific solutions obtained will, then, consist of simultaneous algebraic equations containing amplitude constants and the eigenvalue, which gives the frequency of the system in terms of the dimensions of the resonator and the wave velocity.

The wave equations of motion of the resonant system in terms of the dilatation Δ and the rotation $\tilde{\omega}$, are given by[8]

$$\nabla^2\Delta = \frac{1}{C_p^2}\,\frac{\partial^2\Delta}{\partial t^2} \quad ; \qquad \nabla^2\tilde{\omega} = \frac{1}{C_s^2}\,\frac{\partial^2\tilde{\omega}}{\partial t^2} \tag{A.3.1}$$

where C_p and C_s are the plate and shear velocities, respectively. The solutions of these equations of motion are given by

$$\begin{aligned} \Delta &= \{A_1\, J_n(hr) + A_2\, Y_n(hr)\} \cos n\theta \cos \omega t \\ \tilde{\omega} &= \{C_1\, J_n(kr) + C_2\, Y_n(kr)\} \sin n\theta \cos \omega t \end{aligned} \tag{A.3.2}$$

where $h = \omega/C_p$, $k = \omega/C_s$, n is the circumferential order, J and Y are the Bessel functions of first and second kind and A_1, A_2, C_1, C_2 are the amplitude constants. If required these amplitude constants can also be evaluated to obtain the eigen function of the mode expressing the components of strain or stress throughout the resonator.

The dilatation Δ and the rotation $\tilde{\omega}$ are related to the radial and tangential displacements by the following equations

$$\begin{aligned} \Delta &= \frac{\partial \xi_r}{\partial r} + \frac{1}{r}\left(\xi_r + \frac{\partial \xi_\theta}{\partial \theta}\right) \\ \tilde{\omega} &= \frac{1}{2}\left[\frac{\partial \xi_\theta}{\partial r} + \frac{1}{r}\left(\xi_\theta + \frac{\partial \xi_r}{\partial \theta}\right)\right] \end{aligned} \tag{A.3.3}$$

Then, the radial and tangential displacements ξ_r and ξ_θ can be obtained, from eqns.(A.3.2) and (A.3.3) using the procedure described in Appendix A.2.1, as

$$\xi_r = \left[A_1 \frac{dJ_n(hr)}{dr} + A_2 \frac{dY_n(hr)}{dr} + \frac{nC_1}{r} J_n(kr) + \frac{nC_2}{r} Y_n(kr) \right] \cos n\theta$$

$$\xi_\theta = -\left[\frac{nA_1}{r} J_n(hr) + \frac{nA_2}{r} Y_n(hr) + C_1 \frac{dJ_n(kr)}{dr} + C_2 \frac{dY_n(kr)}{dr} \right] \sin n\theta \qquad \text{(A.3.4)}$$

The boundary conditions for an annular ring of external radius a and internal radius b, are that the radial and tangential stresses must vanish at the inner and outer perimeters. That is,

$$T_{rr} = 0 \quad \text{at } r=a \;, \qquad T_{rr} = 0 \quad \text{at } r=b$$
$$T_{r\theta} = 0 \quad \text{at } r=a \;, \qquad T_{r\theta} = 0 \quad \text{at } r=b \qquad \text{(A.3.5)}$$

where the stress resultants T_{rr} and $T_{r\theta}$ are given by

$$T_{rr} = \text{Plate Modulus} \left[\frac{\partial \xi_r}{\partial r} + \sigma \left(\frac{\xi_r}{r} + \frac{1}{r} \frac{\partial \xi_\theta}{\partial \theta} \right) \right]$$
$$T_{r\theta} = \text{Shear Modulus} \left[\frac{\partial \xi_\theta}{\partial r} - \frac{\xi_\theta}{r} + \frac{1}{r} \frac{\partial \xi_r}{\partial \theta} \right] \qquad \text{(A.3.6)}$$

The frequency equation for the compound modes of an annular ring can then be obtained from satisfying the boundary conditions given in eqn. (A.3.5). Thus, substituting eqns.(A.3.4) and (A,3,6) in eqn.(A.3.5), yields the compound mode frequency equation, formed by the determinant of the amplitude constants.

APPENDIX A.3.2

TABLES OF K VALUES FOR ANNULAR RINGS

σ \ γ	K_{1T}					
	0.00	0.10	0.30	0.50	0.70	0.90
0.00	3.63142	3.63619	3.86805	4.81811	7.58028	22.26125
0.05	3.53947	3.54413	3.77010	4.69615	7.38823	21.69778
0.10	3.44509	3.44959	3.66955	4.57090	7.19119	21.11914
0.15	3.34802	3.35240	3.56616	4.44212	6.98860	20.52380
0.20	3.24805	3.25231	3.45968	4.30945	6.77995	19.91100
0.25	3.14492	3.14903	3.34983	4.17261	6.56468	19.27875
0.30	3.03827	3.04225	3.23624	4.03112	6.34211	18.62504
0.35	2.92776	2.93159	3.11852	3.88449	6.11144	17.94754
0.40	2.81290	2.81658	2.99618	3.73210	5.87173	17.24344
0.45	2.69314	2.69667	2.86862	3.57321	5.62180	16.50933
0.50	2.56781	2.57117	2.73512	3.40692	5.35994	15.74103

σ \ γ	K_{2T}					
	0.00	0.10	0.30	0.50	0.70	0.90
0.00	5.95189	5.98029	6.78844	9.09026	14.89933	44.45231
0.05	5.80119	5.82887	6.61654	8.86012	14.52207	43.32670
0.10	5.64646	5.67340	6.44007	8.62381	14.13474	42.17112
0.15	5.48737	5.51355	6.25863	8.38085	13.73650	40.98300
0.20	5.32353	5.34893	6.07176	8.13062	13.32636	39.75931
0.25	5.15449	5.17908	5.87895	7.87245	12.90319	38.49679
0.30	4.97971	5.00347	5.67961	7.60551	12.46567	37.19143
0.35	4.79857	4.82146	5.47301	7.32886	12.01222	35.83856
0.40	4.61032	4.63231	5.25829	7.04135	11.54097	34.43257
0.45	4.41404	4.43510	5.03442	6.74158	11.04964	32.96668
0.50	4.20862	4.22870	4.80012	6.42784	10.53541	31.43249

Table A.3.1 Tables of K values for (1,T) and (2,T) pure torsional modes; $K^T = \frac{\omega a}{c_p}$,
When $\gamma \to 1$, $K^T\Theta \simeq q\pi$; q=1,2,3,... .

σ \ γ	K^T_{2R}									
	0.0	0.1	0.2	0.3	0.4	0.5	0.6	0.7	0.8	0.9
0.00	5.33143	5.13720	4.96083	5.13733	5.65911	6.56494	8.04109	10.5918	15.7777	31.4469
0.05	5.34113	5.12543	4.93207	5.11068	5.63867	6.55021	8.03087	10.5851	15.7738	31.4452
0.10	5.35083	5.11135	4.90094	5.08281	5.61774	6.53528	8.02059	10.5784	15.7698	31.4434
0.15	5.36049	5.09462	4.86715	5.05376	5.59634	6.52017	8.01024	10.5716	15.7658	31.4416
0.20	5.37015	5.07472	4.83065	5.02354	5.57449	6.50489	7.99983	10.5649	15.7619	31.4398
0.25	5.37977	5.05112	4.79128	4.99214	5.55219	6.48945	7.98936	10.5581	15.7579	31.4381
0.30	5.38936	5.02315	4.74884	4.95956	5.52947	6.47385	7.97884	10.5513	15.7539	31.4363
0.35	5.39893	4.99999	4.70229	4.92582	5.50634	6.45811	7.96828	10.5445	15.7500	31.4345
0.40	5.40846	4.95067	4.65363	4.89094	5.48283	6.44224	7.95766	10.5377	15.7460	31.4328
0.45	5.41795	4.90390	4.60024	4.85495	5.45897	6.42625	7.94701	10.5309	15.7420	31.4310
0.50	5.42742	4.84816	4.54459	4.81790	5.43477	6.41015	7.93632	10.5240	15.7380	31.4292

σ \ γ	K^T_{3R}					
	0.0	0.1	0.3	0.5	0.7	0.9
0.00	8.53631	8.19916	9.30827	12.7067	21.0037	62.8473
0.05	8.54225	8.16927	9.29085	12.6986	21.0003	62.8465
0.10	8.54819	8.13651	9.27321	12.6909	20.9969	62.8457
0.15	8.55411	8.10047	9.25536	12.6828	20.9935	62.8448
0.20	8.56004	8.06100	9,23730	12.6752	20.9901	62.8440
0.25	8.56595	8.01765	9.21904	12.6670	20.9867	62.8431
0.30	8.57190	7.97018	9.20061	12.6593	20.9833	62.8422
0.35	8.57782	7.91818	9.18202	12.6511	20.9799	62.8413
0.40	8.58372	7.86136	9.16327	12.6434	20.9765	62.8404
0.45	8.58960	7.79944	9.14439	12.6352	20.9731	62.8396
0.50	8.59543	7.73212	9.12539	12.6274	20.9696	62.8387

Table A.3.2 Tables of K values for (2,R) and (3,R) pure radial modes of annular rings ; $K^T = \frac{\omega a}{C_p}$,

When $\gamma \to 1$, $K^T(1-\gamma) \simeq p\pi$; p=1,2,... .

Table A.3.3 Tables of K_o^T values for the first four in plane flexural modes of annular rings; $K_o^T = \frac{\omega a}{C_o}$.

When $\gamma \to 1$, $K_o^T \to \frac{2}{\sqrt{3}} \frac{(1-\gamma)}{(1+\gamma)^2} \left[\frac{n^2(n^2-1)^2}{(n^2+1)}\right]^{\frac{1}{2}}$.

γ / σ	$(K_o^T)_{12}$						
	0.0	0.1	0.3	0.5	0.7	0.9	1.0
0.00	1.6518	1.5250	0.9942	0.6003	0.3068	Numerical limitation on K evaluation	Zero frequency
0.05	1.6135	1.4952	0.9860	0.5981	0.3065		
0.10	1.5776	1.4669	0.9781	0.5961	0.3061		
0.15	1.5442	1.4403	0.9703	0.5940	0.3058		
0.20	1.5125	1.4149	0.9626	0.5921	0.3055		
0.25	1.4827	1.3908	0.9551	0.5900	0.3051		
0.30	1.4548	1.3679	0.9478	0.5880	0.3047		
0.35	1.4280	1.3458	0.9405	0.5860	0.3045		
0.40	1.4029	1.3249	0.9334	0.5841	0.3041		
0.45	1.3789	1.3049	0.9265	0.5821	0.3037		
0.50	1.3562	1.2858	0.9196	0.5801	0.3035		

γ / σ	$(K_o^T)_{13}$						
	0.0	0.1	0.3	0.5	0.7	0.9	1.0
0.00	2.5069	2.5009	2.1557	1.4537	0.8122	Numerical limitation on K evaluation	Zero frequency
0.05	2.4554	2.4499	2.1242	1.4432	0.8098		
0.10	2.4065	2.4012	2.0936	1.4329	0.8075		
0.15	2.3599	2.3549	2.0641	1.4227	0.8053		
0.20	2.3156	2.3109	2.0355	1.4126	0.8030		
0.25	2.2734	2.2691	2.0079	1.4027	0.8007		
0.30	2.2334	2.2292	1.9812	1.3930	0.7935		
0.35	2.1950	2.1911	1.9585	1.3834	0.7963		
0.40	2.1585	2.1548	1.9303	1.3740	0.7941		
0.45	2.1237	2.1201	1.9061	1.3648	0.7918		
0.50	2.0904	2.0871	1.8827	1.3557	0.7897		

γ / σ	$(K_o^T)_{14}$						
	0.0	0.1	0.3	0.5	0.7	0.9	1.0
0.00	3.2321	3.2318	3.1225	2.3821	1.4397	Numerical limitation on K evaluation	Zero frequency
0.05	3.1729	3.1728	3.0693	2.3579	1.4331		
0.10	3.1157	3.1156	3.0179	2.3342	1.4264		
0.15	3.0607	3.0605	2.9682	2.3109	1.4200		
0.20	3.0078	3.0076	2.9203	2.2882	1.4136		
0.25	2.9568	2.9567	2.8741	2.2660	1.4071		
0.30	2.9079	2.9078	2.8296	2.2443	1.4009		
0.35	2.8611	2.8611	2.7868	2.2229	1.3946		
0.40	2.8160	2.8159	2.7456	2.2019	1.3884		
0.45	2.7729	2.7728	2.7058	2.1816	1.3823		
0.50	2.7315	2.7314	2.6678	2.1617	1.3762		

γ / σ	$(K_o^T)_{15}$						
	0.0	0.1	0.3	0.5	0.7	0.9	1.0
0.00	3.9094	3.9094	3.8847	3.3107	2.1431	Numerical limitation on K evaluation	Zero frequency
0.05	3.8435	3.8434	3.8198	3.2701	2.1298		
0.10	3.7790	3.7789	3.7564	3.2303	2.1167		
0.15	3.7164	3.7164	3.6949	3.1914	2.1037		
0.20	3.6557	3.6557	3.6353	3.1534	2.0909		
0.25	3.5970	3.5970	3.5776	3.1164	2.0783		
0.30	3.5405	3.5405	3.5220	3.0803	2.0658		
0.35	3.4859	3.4859	3.4683	3.0450	2.0536		
0.40	3.4332	3.4332	3.4165	3.0106	2.0414		
0.45	3.3826	3.3826	3.3667	2.9772	2.0295		
0.50	3.3338	3.3337	3.3186	2.9446	2.0177		

Table A.3.4 Tables of K_o^T values for the first five finite frequency modes of annular rings; $K_o^T = \frac{\omega a}{C_o}$,

For $\gamma \to 1$, $K_o = \frac{2}{(1+\gamma)}\sqrt{(n^2+1)}$.

σ \ γ	$(K_o^T)_{1R}$										
	0.0	0.1	0.2	0.3	0.4	0.5	0.6	0.7	0.8	0.9	1.0
0.00	1.8412	1.8035	1.7051	1.5821	1.4618	1.3547	1.2631	1.1824	1.1134	1.0531	
0.05	1.8813	1.8395	1.7072	1.5984	1.4636	1.3599	1.2648	1.1836	1.1138	1.0532	
0.10	1.9250	1.8785	1.7589	1.6155	1.4810	1.3652	1.2676	1.1848	1.1143	1.0533	
0.15	1.9729	1.9205	1.7883	1.6332	1.4910	1.3706	1.2703	1.1861	1.1147	1.0534	
0.20	2.0254	1.9665	1.8196	1.6516	1.5012	1.3760	1.2730	1.1874	1.1152	1.0535	
0.25	2.0834	1.9962	1.8529	1.6707	1.5116	1.3816	1.2758	1.1886	1.1156	1.0537	1
0.30	2.1469	2.0720	1.8885	1.6905	1.4997	1.3872	1.2597	1.1899	1.0996	1.0537	
0.35	2.2200	2.1330	1.9265	1.7110	1.5332	1.3928	1.2814	1.1911	1.1166	1.0539	
0.40	2.3012	2.2008	1.9670	1.7326	1.5442	1.3986	1.2842	1.1925	1.1171	1.0539	
0.45	2.3940	2.2766	2.0105	1.7546	1.5555	1.4043	1.2871	1.1937	1.1176	1.0539	
0.50	2.5010	2.3621	2.0571	1.7777	1.5670	1.4101	1.2899	1.1950	1.1180	1.0541	

σ \ γ	$(K_o^T)_{11}$										
	0.0	0.1	0.2	0.3	0.4	0.5	0.6	0.7	0.8	0.9	1.0
0.00	1.7497	1.7555	1.7683	1.7770	1.7701	1.7411	1.6917	1.6285	1.5583	1.4859	
0.05	1.7424	1.7491	1.7705	1.7749	1.7723	1.7420	1.6938	1.6291	1.5603	1.4860	
0.10	1.7345	1.7418	1.7585	1.7722	1.7695	1.7426	1.6936	1.6336	1.5588	1.4860	
0.15	1.7256	1.7338	1.7525	1.7689	1.7686	1.7431	1.6943	1.6302	1.5590	1.4861	
0.20	1.7163	1.7251	1.7460	1.7651	1.7673	1.7433	1.6949	1.6308	1.5593	1.4861	
0.25	1.7062	1.7159	1.7387	1.7607	1.7657	1.7434	1.6955	1.6313	1.5595	1.4862	√2
0.30	1.6957	1.7061	1.7054	1.7558	1.7376	1.7630	1.6709	1.6317	1.5367	1.4863	
0.35	1.6825	1.6958	1.7226	1.7503	1.7612	1.7427	1.6963	1.6320	1.5600	1.4863	
0.40	1.6733	1.6851	1.7138	1.7445	1.7584	1.7445	1.6965	1.7421	1.5602	1.4863	
0.45	1.6615	1.6740	1.7045	1.7380	1.7552	1.7412	1.6966	1.6326	1.5603	1.4864	
0.50	1.6495	1.6626	1.6949	1.7313	1.7516	1.7401	1.6966	1.6329	1.5604	1.4864	

Table A.3.4 (Contd.)

$(K_o^T)_{22}$ σ \ γ	0.0	0.1	0.2	0.3	0.4	0.5	0.6	0.7	0.8	0.9	1.0
0.00	2.6839	2.6581	2.6329	2.6408	2.6545	2.6508	2.6152	2.5463	2.4533	2.3472	
0.05	2.6789	2.6477	2.6160	2.6248	2.6433	2.6449	2.6131	2.5450	2.4533	2.3472	
0.10	2.6724	2.6360	2.5979	2.6073	2.6306	2.6379	2.6104	2.5452	2.4532	2.3472	
0.15	2.6645	2.6232	2.5790	2.5887	2.6166	2.6299	2.6070	2.5442	2.4530	2.3472	
0.20	2.6551	2.6093	2.5592	2.5691	2.6015	2.6208	2.6030	2.5429	2.4527	2.3471	
0.25	2.6445	2.5945	2.5390	2.5488	2.5854	2.6108	2.5983	2.5413	2.4523	2.3471	√5
0.30	2.6324	2.5724	2.4812	2.5280	2.5305	2.5999	2.5548	2.5394	2.4156	2.3470	
0.35	2.6192	2.5623	2.4976	2.5068	2.5508	2.5883	2.5873	2.5373	2.4512	2.3469	
0.40	2.6049	2.5453	2.4767	2.4854	2.5326	2.5759	2.5810	2.5348	2.4505	2.3467	
0.45	2.5896	2.5278	2.4558	2.4639	2.5140	2.5630	2.5741	2.5321	2.4497	2.3466	
0.50	2.5735	2.5098	2.4350	2.4424	2.4951	2.5495	2.5667	2.5290	2.4487	2.3465	

$(K_o^T)_{23}$ σ \ γ	0.0	0.1	0.2	0.3	0.4	0.5	0.6	0.7	0.8	0.9	1.0
0.00	3.7174	3.7164	3.7162	3.6907	3.7005	3.7034	3.6699	3.5879	3.4651	3.3186	
0.05	3.7042	3.7035	3.7028	3.6611	3.6740	3.6870	3.6627	3.5857	3.4647	3.3186	
0.10	3.6901	3.6882	3.6881	3.6293	3.6442	3.6675	3.6534	3.5827	3.4640	3.3184	
0.15	3.6747	3.6760	3.6722	3.5959	3.6120	3.6452	3.6421	3.5786	3.4630	3.3183	
0.20	3.6577	3.6545	3.6546	3.5614	3.5781	3.6206	3.6291	3.5736	3.4616	3.3181	
0.25	3.6389	3.6407	3.6353	3.5264	3.5429	3.5943	3.6144	3.5676	3.4598	3.3178	√10
0.30	3.6184	3.6142	3.5608	3.4912	3.4553	3.5664	3.5449	3.5608	3.4067	3.3174	
0.35	3.5916	3.5939	3.5916	3.4561	3.4711	3.5372	3.5804	3.5531	3.4554	3.3170	
0.40	3.5724	3.5674	3.5675	3.4212	3.4350	3.5073	3.5616	3.5446	3.4526	3.3165	
0.45	3.5475	3.5448	3.5421	3.3867	3.3992	3.4768	3.5416	3.5353	3.4529	3.3159	
0.50	3.5214	3.5157	3.5158	3.3527	3.3637	3.4459	3.5208	3.5253	3.4462	3.3151	

$(K_o^T)_{24}$ σ \ γ	0.0	0.1	0.2	0.3	0.4	0.5	0.6	0.7	0.8	0.9	1.0
0.00	4.7906	4.7905	4.7884	4.7734	4.7679	4.7833	4.7577	4.6667	4.5148	4.3264	
0.05	4.7645	4.7644	4.7607	4.7335	4.7167	4.7479	4.7413	4.6615	4.5138	4.3263	
0.10	4.7378	4.7377	4.7321	4.6912	4.6612	4.7060	4.7200	4.6539	4.5120	4.3261	
0.15	4.7098	4.7097	4.7020	4.6470	4.6036	4.6591	4.6943	4.6440	4.5094	4.3257	
0.20	4.6798	4.6796	4.6699	4.6013	4.5454	4.6091	4.6648	4.6319	4.5059	4.3251	
0.25	4.6476	4.6474	4.6357	4.5546	4.4875	4.5570	4.6320	4.6177	4.5016	4.3243	√17
0.30	4.6133	4.6130	4.5314	4.5073	4.3650	4.5040	4.5288	4.6016	4.4301	4.3234	
0.35	4.5769	4.5766	4.5612	4.4599	4.3747	4.4508	4.5593	4.5036	4.4907	4.3224	
0.40	4.5387	4.5384	4.5215	4.4125	4.3203	4.3978	4.5204	4.5639	4.4842	4.3211	
0.45	4.4991	4.4988	4.4805	4.3654	4.2675	4.3456	4.4804	4.5128	4.4768	4.3197	
0.50	4.4584	4.4581	4.4388	4.3188	4.2162	4.2942	4.4397	4.5093	4.4688	4.3182	

Table A.3.5 Tables of $K^T\theta$ values for the five shear modes of annular rings; $K^T\theta = \frac{\omega n}{c_s}$;
When $\gamma \to 1$, $K^T\theta(1-\gamma) = p\pi$; p=1,2,3,... .

$(K^T\theta)_{21}$ σ \ γ	0.0	0.1	0.2	0.3	0.4	0.5	0.6	0.7	0.8	0.9	1.0
0.00	5.00323	5.13840	5.47108	5.91849	6.45188	7.21440	8.51500	10.9091	22.2929	31.5313	Infinity
0.05	5.13250	5.27114	5.60482	6.03127	6.51996	7.24812	8.53121	10.9169	22.8627	31.5328	
0.10	5.27361	5.41661	5.75132	6.14961	6.58704	7.28081	8.54697	10.9246	23.4791	31.5342	
0.15	5.42741	5.57616	5.91200	6.27228	6.65258	7.31245	8.56234	10.9322	24.1489	31.5357	
0.20	5.59446	5.75112	6.08838	6.39741	6.71613	7.34309	8.57732	10.9396	24.8796	31.5371	
0.25	5.77456	5.94259	6.28193	6.52189	6.77731	7.37292	8.59198	10.9468	25.6806	31.5385	
0.30	5.96529	6.15039	6.49348	6.64210	6.83587	7.40191	8.60634	10.9540	26.5626	31.5399	
0.35	6.15875	6.36959	6.72008	6.75382	6.89168	7.42996	8.62041	10.9610	27.5371	31.5412	
0.40	6.33585	6.57671	6.93615	6.85403	6.94468	7.45720	8.63424	10.9680	28.6124	31.5426	
0.45	6.46970	6.71606	7.05650	6.94099	6.99494	7.48394	8.64783	10.9749	29.7690	31.5439	
0.50	6.55275	6.77904	7.09768	7.01526	7.04256	7.50986	8.66121	10.9816	30.8029	31.5453	

$(K^T\theta)_{32}$ σ \ γ	0.0	0.1	0.2	0.3	0.4	0.5	0.6	0.7	0.8	0.9	1.0
0.00	6.78301	5.99802	5.75824	6.22580	7.04430	8.04912	9.26036	11.4401	22.2358	31.6780	Infinity
0.05	6.91678	6.15053	5.92318	6.40745	7.24256	8.19514	9.32552	11.4707	22.7937	31.6840	
0.10	7.05931	6.30670	6.09432	6.60062	7.45800	8.33860	9.38733	11.5001	23.3969	31.6901	
0.15	7.20852	6.46509	6.26969	6.80361	7.69280	8.47510	9.44585	11.5285	24.0510	31.6954	
0.20	7.36001	6.62260	6.44641	7.01352	7.94869	8.60002	9.50124	11.5561	24.7623	31.7010	
0.25	7.50727	6.77584	6.62046	7.22415	8.22754	8.71047	9.55366	11.5832	25.5379	31.7066	
0.30	7.64151	6.92050	6.78696	7.42621	8.53098	8.80573	9.60334	11.6090	26.3842	31.7121	
0.35	7.75545	7.05297	6.94082	7.60697	8.71110	8.88702	9.65049	11.6352	27.3046	31.7175	
0.40	7.84630	7.17021	7.02309	7.75592	8.72946	8.95650	9.69532	11.6601	28.2915	31.7230	
0.45	7.91629	7.27149	7.19596	7.87029	8.74654	9.01653	9.73805	11.6849	29.3001	31.7282	
0.50	7.96981	7.35740	7.29527	7.95501	8.76283	9.06835	9.77885	11.7090	30.1958	31.8276	

$(K^T\theta)_{33}$ σ \ γ	0.0	0.1	0.2	0.3	0.4	0.5	0.6	0.7	0.8	0.9	1.0
0.00	8.33184	8.16961	7.14681	6.78573	7.32996	8.51279	10.1478	12.2271	22.1512	31.9203	Infinity
0.05	8.42328	8.22636	7.30483	6.97030	7.51642	8.74250	10.3241	12.2942	22.6913	31.9332	
0.10	8.55330	8.42680	7.46354	7.16129	7.75450	9.00760	10.4916	12.3581	23.2750	31.9459	
0.15	8.68470	8.55735	7.62115	7.35186	7.98070	9.28699	10.6433	12.4189	23.9072	31.9585	
0.20	8.81301	8.68586	7.77529	7.54500	8.20987	9.58512	10.7748	12.4768	24.5926	31.9709	
0.25	8.93340	8.80633	7.92330	7.73070	8.43500	9.89040	10.8857	12.5321	25.3359	31.9832	
0.30	9.04184	8.91585	8.06264	7.90685	8.64756	10.1961	10.9787	12.5850	26.1401	31.9953	
0.35	9.13617	9.01240	8.19123	8.06987	8.83914	10.3956	11.0576	12.6357	27.0036	32.0074	
0.40	9.21642	9.09568	8.30788	8.21704	9.00336	10.3758	11.1258	12.6846	27.9130	32.0193	
0.45	9.28356	9.16672	8.41225	8.34783	9.14059	10.4199	11.1859	12.7314	28.8288	32.0310	
0.50	9.34000	9.22716	8.50481	8.46190	9.25149	10.4543	11.2398	12.7766	29.6691	32.0425	

σ \ γ	$(K^T\Theta)_{34}$									
	0.0	0.1	0.2	0.3	0.4	0.5	0.6	0.7	0.9	1.0
0.00	9.66629	9.65821	9.20147	8.04042	7.89217	8.77085	10.6223	13.1498	32.2537	Infinity
0.05	9.78451	9.77640	9.33198	8.22249	8.11351	9.01073	10.9014	13.2820	32.2762	
0.10	9.90732	9.89912	9.46398	8.40667	8.34417	9.26883	11.2092	13.4027	32.2984	
0.15	10.0317	10.0234	9.59558	8.59031	8.57845	9.53971	11.5471	13.5119	32.3203	
0.20	10.1540	10.1455	9.72434	8.77039	8.81076	9.81583	11.9155	13.6107	32.3736	
0.25	10.2704	10.2619	9.84760	8.94372	9.03570	10.0873	12.3048	13.7005	32.3634	
0.30	10.3780	10.3694	9.96307	9.10751	9.24827	10.3427	12.7662	13.7826	32.3845	
0.35	10.4749	10.4663	10.0692	9.25954	9.44439	10.5708	13.2313	13.8583	32.4054	
0.40	10.5606	10.5520	10.1652	9.39852	9.62133	10.7648	13.7294	13.9285	32.4261	
0.45	10.6356	10.6271	10.2513	9.52404	9.77807	10.9241	14.2522	13.9943	32.4465	
0.50	10.7010	10.6926	10.3280	9.63612	9.91511	11.0527	14.7882	14.0561	32.5375	

Table A.3.5 (Contd.)

σ \ γ	$(K^T\Theta)_{41}$						
	0.0	0.1	0.3	0.5	0.7	0.9	1.0
0.00	9.69640	9.92450	10.3345	13.1400	21.1873	62.8948	Infinity
0.05	9.88984	10.1551	10.3917	13.1604	21.1974	62.8968	
0.10	9.90416	10.2294	10.4497	13.1834	21.2049	62.8933	
0.15	9.91738	10.2418	10.5092	13.2098	21.2163	62.9023	
0.20	9.92958	10.2498	10.5713	13.2413	21.2308	62.9061	
0.25	9.94003	10.2569	10.6374	13.2801	21.2498	62.9113	
0.30	9.94932	10.2638	10.7094	13.3301	21.2765	62.9188	
0.35	9.95636	10.2709	10.7904	13.3981	21.3173	62.9309	
0.40	9.96234	10.2785	10.8848	13.4962	21.3878	62.9545	
0.45	9.96750	10.2873	10.9999	13.6470	21.5325	63.0207	
0.50	9.97280	10.2980	11.1473	13.8900	21.8819	63.5480	

Table A.3.6 Tables of K_p^T values for the first four plate modes of annular rings;

For $\gamma \to 1$, $K_p^T(1-\gamma) = q\pi$; q = 1,2,3,... .

σ \ γ	$(K_p^T)_{31}$										
	0.0	0.1	0.2	0.3	0.4	0.5	0.6	0.7	0.8	0.9	1.0
0.00	4.76164	4.82528	4.95803	5.17401	5.64629	6.53205	8.01006	10.5689	22.3146	31.4404	Infinity
0.05	4.64751	4.70920	4.84423	5.07977	5.58652	6.49810	7.99029	10.5573	21.7528	31.4376	
0.10	4.53076	4.58968	4.72606	4.98434	5.52821	6.46467	7.97037	10.5453	21.1763	31.4346	
0.15	4.41155	4.46668	4.60340	4.88867	5.47129	6.43127	7.94986	10.5327	20.5840	31.4315	
0.20	4.29034	4.34028	4.47615	4.79403	5.41542	6.39713	7.92813	10.5190	19.9749	31.4280	
0.25	4.16818	4.21086	4.34439	4.70199	5.35988	6.36114	7.90413	10.5035	19.3476	31.4239	
0.30	4.04743	4.07967	4.20867	4.61419	5.30337	6.32147	7.87604	10.4845	18.7013	31.4187	
0.35	3.93349	3.95083	4.07177	4.53172	5.24376	6.27508	7.84044	10.4589	18.0359	31.4113	
0.40	3.83723	3.83814	3.94851	4.45426	5.17758	6.21655	7.79031	10.4193	17.3548	31.3982	
0.45	3.77194	3.77023	3.88240	4.37936	5.09936	6.13630	7.71035	10.3445	16.6775	31.3640	
0.50	3.73851	3.74662	3.85713	4.30191	5.00071	6.01870	7.57024	10.1749	16.1150	31.1026	

σ \ γ	$(K_p^T)_{42}$						
	0.0	0.1	0.3	0.5	0.7	0.9	1.0
0.00	5.84525	5.71612	5.88908	6.59945	10.5112	31.4211	Infinity
0.05	5.74774	5.61808	5.76428	6.49842	10.4860	31.4152	
0.10	5.62634	5.52136	5.63839	6.40255	10.4604	31.4089	
0.15	5.50708	5.42765	5.51285	6.31421	10.4337	31.4017	
0.20	5.39430	5.33901	5.39002	6.23508	10.4044	31.3932	
0.25	5.29120	5.25782	5.27366	6.16518	10.3707	31.3824	
0.30	5.20292	5.18639	5.16916	6.10240	10.3293	31.3675	
0.35	5.13271	5.12648	5.08257	6.04262	10.2745	31.3442	
0.40	5.08022	5.07859	5.01735	5.97998	10.1963	31.3012	
0.45	5.01491	5.04145	4.97100	5.90683	10.0765	31.1951	
0.50	5.01152	5.01073	4.93190	5.81329	9.88633	30.7829	

σ \ γ	$(K_p^T)_{43}$						
	0.0	0.1	0.3	0.5	0.7	0.9	1.0
0.00	6.99688	6.95235	6.93993	7.22025	10.4489	31.3897	Infinity
0.05	6.87487	6.83697	6.82978	7.06447	10.4024	31.3788	
0.10	6.75641	6.72503	6.72281	6.90261	10.3576	31.3670	
0.15	6.64411	6.61892	6.62062	6.73526	10.3134	31.3534	
0.20	6.54080	6.52112	6.52495	6.56436	10.2676	31.3371	
0.25	6.44889	6.43360	6.43749	6.39696	10.2177	31.3159	
0.30	6.36945	6.35703	6.35943	6.25960	10.1597	31.2862	
0.35	6.31300	6.28974	6.29073	6.19111	10.0879	31.2400	
0.40	6.24004	6.22615	6.22890	6.16011	9.99317	31.1571	
0.45	6.17514	6.15205	6.16612	6.12769	9.86224	30.9761	
0.50	6.08201	6.03323	6.08128	6.07544	9.67666	30.4933	

σ \ γ	$(K_p^T)_{44}$						
	0.0	0.1	0.3	0.5	0.7	0.9	1.0
0.00	8.12712	8.12316	7.97596	8.22548	10.4371	31.3473	Infinity
0.05	8.00152	7.99785	7.87065	8.07791	10.3523	31.3298	
0.10	7.87986	7.87649	7.76827	7.92945	10.2777	31.3106	
0.15	7.76423	7.76112	7.66960	7.78246	10.2112	31.2887	
0.20	7.65631	7.65337	7.57473	7.64019	10.1500	31.2622	
0.25	7.55659	7.55367	7.48222	7.50665	10.08934	31.2281	
0.30	7.46325	7.46006	7.38731	7.38582	10.0261	31.1804	
0.35	7.37021	7.36619	7.27882	7.27959	9.95205	31.1077	
0.40	7.26359	7.25772	7.13645	7.18513	9.85902	30.9833	
0.45	7.11769	7.10856	6.94004	7.09304	9.73532	30.7396	
0.50	6.90477	6.89219	6.68795	6.98721	9.56565	30.2138	

APPENDIX A.4

TABLES OF K VALUES FOR THICK ANNULAR DISKS

Table A.4.1 Tables of K values for the first three flexural modes of thick annular disks ; Thickness-to-diameter ratio = 0.50.

K_{12} σ \ γ	0.0	0.1	0.3	0.5	0.7	0.9	1.0
0.00	1.65192	1.52496	0.99417	0.60031	0.30001	Numerical limitation on K evaluation	Zero frequency
0.05	1.61159	1.49359	0.98537	0.59797	0.30605		
0.10	1.56988	1.46064	0.97529	0.59486	0.30593		
0.15	1.52674	1.42604	0.96382	0.59118	0.30558		
0.20	1.48209	1.38970	0.95084	0.58666	0.30445		
0.25	1.43584	1.35149	0.93622	0.58129	0.30313		
0.30	1.38786	1.31128	0.91978	0.57496	0.30124		
0.35	1.33799	1.26891	0.90134	0.56752	0.29944		
0.40	1.28604	1.22418	0.88068	0.55880	0.29704		
0.45	1.23176	1.17682	0.85754	0.54861	0.29428		
0.50	1.17485	1.12653	0.83158	0.53671	0.29082		

K_{13} σ \ γ	0.0	0.1	0.3	0.5	0.7	0.9	1.0
0.00	2.50682	2.50097	2.15573	1.45375	0.81225	Numerical limitation on K evaluation	Zero frequency
0.05	2.45245	2.44691	2.12222	1.44235	0.80957		
0.10	2.39473	2.38955	2.08576	1.42928	0.80647		
0.15	2.33379	2.32902	2.04621	1.41435	0.80276		
0.20	2.26969	2.26532	2.00341	1.39737	0.79833		
0.25	2.20241	2.19843	1.95716	1.37813	0.79310		
0.30	2.13186	2.12827	1.90725	1.35635	0.78693		
0.35	2.05788	2.05467	1.85341	1.33174	0.77967		
0.40	1.98024	1.97740	1.79533	1.30392	0.77112		
0.45	1.89863	1.89613	1.73262	1.27247	0.76102		
0.50	1.81262	1.81045	1.66481	1.23686	0.74906		

K_{14} σ \ γ	0.0	0.1	0.3	0.5	0.7	0.9	1.0
0.00	3.23202	3.23184	3.12255	2.38210	1.43971	Numerical limitation on K evaluation	Zero frequency
0.05	3.16922	3.16905	3.06608	2.35626	1.43251		
0.10	3.10103	3.10087	3.00469	2.32744	1.42420		
0.15	3.02770	3.02755	2.93844	2.29536	1.41463		
0.20	2.94939	2.94925	2.86733	2.25973	1.40362		
0.25	2.86617	2.86604	2.79130	2.22019	1.39098		
0.30	2.77801	2.77790	2.71021	2.17637	1.37644		
0.35	2.68480	2.68469	2.62387	2.12781	1.35971		
0.40	2.58628	2.58619	2.53199	2.07400	1.34040		
0.45	2.48212	2.48204	2.43415	2.01433	1.31806		
0.50	2.37179	2.37172	2.32984	1.94807	1.29208		

Table A.4.2 Tables of K values for first set of finite frequency modes of thick annular disks.

K_{1R}

η = 2.0	σ \ γ	0.0	0.1	0.3	0.5	0.7	0.9
	0.00	1.84118	1.80347	1.58207	1.35467	1.18236	1.05312
	0.05	1.87683	1.83528	1.59561	1.35782	1.18189	1.05175
	0.10	1.90570	1.86061	1.60389	1.35680	1.17797	1.04738
	0.15	1.92610	1.87814	1.60659	1.35156	1.17059	1.04003
	0.20	1.93640	1.88655	1.60342	1.34203	1.15971	1.02965
	0.25	1.93531	1.88480	1.59411	1.32813	1.14528	1.01621
	0.30	1.92217	1.87223	1.57845	1.30978	1.12723	0.99962
	0.35	1.89694	1.84863	1.55622	1.28688	1.10548	0.97979
	0.40	1.86007	1.81416	1.52724	1.25929	1.07991	0.95660
	0.45	1.81219	1.76918	1.49132	1.22684	1.05034	0.92989
	0.50	1.75390	1.71405	1.44818	1.18926	1.01656	0.89944

η = 4.0	σ \ γ	0.0	0.1	0.3	0.5	0.7	0.9
	0.00	1.84117	1.80347	1.58207	1.35467	1.18236	1.05311
	0.05	1.87862	1.83683	1.59630	1.35814	1.18208	1.05186
	0.10	1.91379	1.86753	1.60675	1.35809	1.17873	1.04788
	0.15	1.94642	1.89531	1.61324	1.35446	1.17229	1.04119
	0.20	1.97612	1.91978	1.61553	1.34713	1.16268	1.03165
	0.25	2.00234	1.94043	1.61333	1.33598	1.14983	1.01928
	0.30	2.02429	1.95656	1.60631	1.32085	1.13362	1.00393
	0.35	2.04090	1.96727	1.59405	1.30151	1.11390	0.98551
	0.40	2.05077	1.97139	1.57607	1.27772	1.09049	0.96383
	0.45	2.05210	1.96746	1.55179	1.24915	1.06315	0.93871
	0.50	2.04271	1.96155	1.52051	1.21539	1.03158	0.90987

η = 8.0	σ \ γ	0.0	0.3	0.5	0.7	0.9
	0.00	1.84119	1.58207	1.35467	1.18236	1.05312
	0.05	1.87890	1.59641	1.35819	1.18212	1.05189
	0.10	1.91503	1.60723	1.35832	1.17888	1.04800
	0.15	1.94959	1.61436	1.35496	1.17261	1.04142
	0.20	1.98254	1.61758	1.34801	1.16324	1.03210
	0.25	2.01379	1.61663	1.33734	1.15068	1.01996
	0.30	2.04319	1.61119	1.32275	1.13481	1.00490
	0.35	2.07044	1.60086	1.30404	1.11546	0.98679
	0.40	2.09512	1.58516	1.28091	1.09244	0.96547
	0.45	2.11654	1.56348	1.25304	1.06549	0.94072
	0.50	2.13365	1.53511	1.21999	1.03428	0.91226

K_{11}

$\eta = 2.0$	σ \ γ	0.0	0.1	0.3	0.5	0.7	0.9
	0.00	1.74965	1.75553	1.77704	1.74112	1.62852	1.48589
	0.05	1.73997	1.74657	1.77219	1.73921	1.62660	1.48372
	0.10	1.72457	1.73181	1.76130	1.73144	1.61948	1.47703
	0.15	1.70358	1.731139	1.74438	1.71776	1.60717	1.46580
	0.20	1.67716	1.68544	1.72151	1.69818	1.58945	1.44996
	0.25	1.64546	1.65413	1.69279	1.67270	1.56647	1.42948
	0.30	1.60861	1.61757	1.65831	1.64135	1.53816	1.40431
	0.35	1.56670	1.57585	1.61815	1.60415	1.50447	1.37435
	0.40	1.51976	1.52900	1.57233	1.56109	1.46534	1.33950
	0.45	1.46772	1.47696	1.52081	1.51209	1.42063	1.29960
	0.50	1.41044	1.41959	1.46344	1.45699	1.37015	1.25442

$\eta = 4.0$	σ \ γ	0.0	0.1	0.3	0.5	0.7	0.9
	0.00	1.74965	1.75553	1.77704	1.74112	1.62852	1.48589
	0.05	1.74020	1.74682	1.77260	1.73970	1.62702	1.48402
	0.10	1.72549	1.73282	1.76292	1.73342	1.62114	1.47824
	0.15	1.70559	1.71361	1.74798	1.72224	1.61089	1.46851
	0.20	1.68060	1.68926	1.72777	1.70606	1.59607	1.45476
	0.25	1.65058	1.65981	1.70224	1.68479	1.57668	1.43690
	0.30	1.61556	1.62529	1.67134	1.65829	1.55255	1.41479
	0.35	1.57554	1.58568	1.63497	1.62638	1.52349	1.38825
	0.40	1.53046	1.54092	1.59299	1.58884	1.48926	1.35708
	0.45	1.48018	1.49086	1.54394	1.54579	1.44958	1.32099
	0.50	1.42480	1.43528	1.48789	1.49681	1.40404	1.27961

$\eta = 8.0$	σ \ γ	0.0	0.3	0.5	0.7	0.9
	0.00	1.74965	1.77704	1.74112	1.62852	1.48589
	0.05	1.74026	1.77268	1.73980	1.62710	1.48408
	0.10	1.72569	1.76324	1.73382	1.62148	1.47849
	0.15	1.70603	1.74871	1.72313	1.61162	1.46908
	0.20	1.68135	1.72905	1.70764	1.59743	1.45578
	0.25	1.65169	1.70419	1.68724	1.57879	1.43849
	0.30	1.61707	1.67405	1.66177	1.55556	1.41705
	0.35	1.57747	1.63851	1.63102	1.52752	1.39130
	0.40	1.53281	1.59740	1.59475	1.49443	1.36098
	0.45	1.48292	1.54989	1.55261	1.45594	1.32581
	0.50	1.42759	1.49594	1.50481	1.41164	1.28539

K_{22}

$\eta = 2.0$	σ \ γ	0.0	0.3	0.5	0.7	0.9
	0.00	2.68394	2.64329	2.65082	2.51630	2.34718
	0.05	2.67436	2.62137	2.64004	2.54070	2.34273
	0.10	2.65424	2.59126	2.61832	2.52439	2.32916
	0.15	2.62355	2.55305	2.58595	2.49726	2.30637
	0.20	2.58264	2.50670	2.54351	2.45970	2.27449
	0.25	2.53206	2.45279	2.49173	2.41233	2.23383
	0.30	2.47243	2.39175	2.43131	2.35586	2.18479
	0.35	2.40429	2.32389	2.36285	2.29096	2.12777
	0.40	2.32808	2.24935	2.28675	2.21812	2.06310
	0.45	2.24400	2.16809	2.20323	2.13767	1.99097
	0.50	2.15208	2.07988	2.11226	2.04967	1.91140

$\eta = 4.0$	σ \ γ	0.0	0.3	0.5	0.7	0.9
	0.00	2.68394	2.64077	2.65084	2.54631	2.34717
	0.05	2.67529	2.62135	2.64137	2.54239	2.34399
	0.10	2.65810	2.59375	2.62365	2.53110	2.33431
	0.15	2.63230	2.55837	2.59774	2.51234	2.31805
	0.20	2.59792	2.51553	2.56371	2.48602	2.29509
	0.25	2.55500	2.46550	2.52163	2.45202	2.26527
	0.30	2.50361	2.40848	2.47152	2.41019	2.22843
	0.35	2.44379	2.34454	2.41336	2.36034	2.18433
	0.40	2.37550	2.27366	2.34706	2.30222	2.13268
	0.45	2.29864	2.19567	2.27243	2.23549	2.07309
	0.50	2.21293	2.11024	2.18912	2.15969	2.00509

$\eta = 8.0$	σ \ γ	0.0	0.3	0.5	0.7	0.9
	0.00	2.68394	2.64077	2.65084	2.54631	2.34718
	0.05	2.67546	2.62145	2.64157	2.54264	2.34420
	0.10	2.65880	2.59415	2.62448	2.53213	2.33518
	0.15	2.63388	2.55920	2.59959	2.51471	2.32003
	0.20	2.60069	2.51688	2.56693	2.49027	2.29864
	0.25	2.55920	2.46742	2.52650	2.45864	2.27085
	0.30	2.50940	2.41096	2.47824	2.41963	2.23644
	0.35	2.45124	2.34756	2.42204	2.37295	2.19512
	0.40	2.38461	2.27714	2.35774	2.31827	2.14653
	0.45	2.30930	2.19953	2.28505	2.25513	2.09021
	0.50	2.22500	2.11439	2.20355	2.18295	2.02557

K_{23}

$\eta = 2.0$	σ \ γ	0.0	0.3	0.5	0.7	0.9
	0.00	3.71737	3.69074	3.70338	3.58778	3.31854
	0.05	3.69511	3.65377	3.67672	3.57168	3.30715
	0.10	3.65317	3.60087	3.62747	3.52661	3.27331
	0.15	3.59239	3.53440	3.55947	3.45875	3.21874
	0.20	3.51559	3.45651	3.47714	3.37499	3.14846
	0.25	3.42588	3.36884	3.38387	3.28070	3.06611
	0.30	3.32567	3.27248	3.28178	3.17821	2.97455
	0.35	3.21652	3.16807	3.17206	3.06889	2.87530
	0.40	3.09927	3.05588	3.05520	2.95318	2.76914
	0.45	2.97422	2.93577	2.93124	2.83109	2.65628
	0.50	2.84120	2.80755	2.79985	2.70222	2.53654

$\eta = 4.0$	σ \ γ	0.0	0.3	0.5	0.7	0.9
	0.00	3.71737	3.69074	3.70338	3.58789	3.31857
	0.05	3.69897	3.65620	3.68173	3.58037	3.31362
	0.10	3.66920	3.60992	3.64672	3.56104	3.29862
	0.15	3.62765	3.55296	3.59904	3.52983	3.27338
	0.20	3.57424	3.48620	3.53941	3.48675	3.23776
	0.25	3.50905	3.41023	3.46851	3.43185	3.19162
	0.30	3.43227	3.32545	3.38688	3.36521	3.13480
	0.35	3.34410	3.23201	3.29491	3.28688	3.06715
	0.40	3.24467	3.12985	3.19278	3.19683	2.98845
	0.45	3.13394	3.01870	3.08046	3.09491	2.89836
	0.50	3.01170	2.89691	2.95764	2.98077	2.79644

$\eta = 8.0$	σ \ γ	0.0	0.3	0.5	0.7	0.9
	0.00	3.71737	3.69074	3.70338	3.58789	3.31857
	0.05	3.69944	3.65647	3.68222	3.58107	3.31423
	0.10	3.67110	3.61087	3.64857	3.56391	3.30113
	0.15	3.63193	3.55482	3.60295	3.53633	3.27915
	0.20	3.58167	3.48903	3.54585	3.49825	3.24812
	0.25	3.52017	3.41401	3.47771	3.44952	3.20783
	0.30	3.44738	3.33006	3.39891	3.38996	3.15797
	0.35	3.36324	3.23730	3.30965	3.31931	3.09816
	0.40	3.26766	3.13565	3.21000	3.23722	3.02792
	0.45	3.16043	3.02483	3.09985	3.14321	2.94664
	0.50	3.04118	2.90435	2.97882	3.03660	2.85352

Table A.4.3 Tables of K values of second set of finite frequency modes of thick annular disks.

K_{2R}

η = 2.0	σ \ γ	0.0	0.1	0.3	0.5	0.7	0.9
	0.00	3.14118	3.14286	3.14287	3.14286	3.14287	3.14286
	0.05	3.15424	3.14836	3.14465	3.14343	3.14332	3.14333
	0.10	3.16983	3.16697	3.14981	3.14481	3.14459	3.14473
	0.15	3.21179	3.20186	3.15752	3.14629	3.14639	3.14703
	0.20	3.27724	3.25501	3.16614	3.14687	3.14837	3.15017
	0.25	3.36156	3.32216	3.17280	3.14516	3.14998	3.15408
	0.30	3.42967	3.38022	3.17319	3.13931	3.15051	3.15866
	0.35	3.42502	3.38783	3.16189	3.12703	3.14897	3.16377
	0.40	3.35797	3.33567	3.13340	3.10561	3.14397	3.16919
	0.45	3.25793	3.24472	3.08369	3.07206	3.13364	3.17463
	0.50	3.13783	3.12988	3.01105	3.02337	3.11550	3.17963

η = 4.0	σ \ γ	0.0	0.1	0.3	0.5	0.7	0.9
	0.00	5.33144	5.13714	5.13740	6.28571	6.28571	6.28571
	0.05	5.33278	5.12011	5.10399	6.23021	6.28254	6.28567
	0.10	5.31359	5.08824	5.05450	6.11023	6.27143	6.28540
	0.15	5.26980	5.03915	4.98769	5.96872	6.24972	6.28464
	0.20	5.20024	4.97156	4.90377	5.81637	6.21441	6.28308
	0.25	5.10626	4.88530	4.80378	5.65571	6.16246	6.28021
	0.30	4.99032	4.78089	4.68897	5.48720	6.09097	6.27538
	0.35	4.85490	4.65911	4.56036	5.31058	5.99751	6.26765
	0.40	4.70190	4.52066	4.41852	5.12516	5.88019	6.25568
	0.45	4.53250	4.36597	4.26356	4.92993	5.73763	6.23755
	0.50	4.34714	4.19504	4.09509	4.72357	5.56880	6.21043

η = 8.0	σ \ γ	0.0	0.3	0.5	0.7	0.9
	0.00	5.33144	5.13740	6.56494	10.5918	12.5714
	0.05	5.34017	5.11008	6.54818	10.5589	12.5689
	0.10	5.34633	5.08010	6.52620	10.4693	12.5689
	0.15	5.34881	5.04682	6.49720	10.3246	12.5427
	0.20	5.34613	5.00942	6.45894	10.1336	12.5140
	0.25	5.33632	4.96680	6.40875	9.90530	12.4704
	0.30	5.31690	4.91755	6.34352	9.64647	12.4073
	0.35	5.28475	4.85984	6.25985	9.36129	12.3192
	0.40	5.23613	4.79133	6.15419	9.05181	12.1992
	0.45	5.16679	4.70916	6.02300	8.71847	12.0396
	0.50	5.07208	4.60981	5.86290	8.36046	11.8315

K_{21}

η = 2.0	σ \ γ	0.0	0.3	0.5	0.7	0.9
	0.00	3.40067	3.33492	3.28439	3.25094	3.22859
	0.05	3.35949	3.32188	3.27780	3.24660	3.22532
	0.10	3.28889	3.29921	3.27124	3.24418	3.22403
	0.15	3.20860	3.26415	3.26330	3.24333	3.22469
	0.20	3.12285	3.21541	3.25216	3.24354	3.22723
	0.25	3.03263	3.15325	3.23556	3.24409	3.23158
	0.30	2.93806	3.07931	3.21031	3.23923	3.23175
	0.35	2.83896	2.99338	3.17549	3.24189	3.24476
	0.40	2.73498	2.89802	3.12680	3.23601	3.25310
	0.45	2.62562	2.79335	3.06270	3.22401	3.26209
	0.50	2.51022	2.67957	2.98162	3.20289	3.27110

η= 4.0	σ \ γ	0.0	0.3	0.5	0.7	0.9
	0.00	3.53782	4.18501	5.10135	6.33857	6.32716
	0.05	3.53592	4.15449	4.99418	6.33259	6.32515
	0.10	3.53120	4.11578	4.87974	6.31836	6.32336
	0.15	3.52184	4.06719	4.75849	6.29274	6.32153
	0.20	3.50561	4.00730	4.63061	6.25210	6.31930
	0.25	3.48003	3.93512	4.49611	6.19240	6.31619
	0.30	3.44248	3.85010	4.35481	6.11132	6.31043
	0.35	3.39046	3.75199	4.20639	5.99624	6.30422
	0.40	3.32181	3.64075	4.05034	5.84598	6.29300
	0.45	3.23495	3.51635	3.88600	5.65177	6.27581
	0.50	3.12895	3.37861	3.71245	5.66288	6.24975

η = 8.0	σ \ γ	0.0	0.3	0.5	0.7	0.9
	0.00	3.53782	4.18501	5.10135	7.71389	12.5884
	0.05	3.53706	4.15641	4.99528	7.52393	12.5849
	0.10	3.53642	4.12376	4.88358	7.32827	12.5752
	0.15	3.53508	4.08546	4.76603	7.12652	12.5573
	0.20	3.53185	4.03952	4.64238	6.91817	12.5281
	0.25	3.52489	3.98366	4.51231	6.70267	12.4842
	0.30	3.51122	3.91547	4.37542	6.47933	12.4204
	0.35	3.48582	3.83281	4.23122	6.24735	12.3325
	0.40	3.44046	3.73410	4.07908	6.00574	12.2123
	0.45	3.36503	3.61854	3.91824	5.75334	12.0524
	0.50	3.25505	3.48592	3.74773	5.48866	11.8438

K_{32}

$\eta = 2.0$	σ \ γ	0.0	0.3	0.5	0.7	0.9
	0.00	3.67944	3.77831	3.66966	3.55828	3.47660
	0.05	3.57112	3.74175	3.64616	3.54186	3.46367
	0.10	3.46209	3.68994	3.62277	3.53175	3.45672
	0.15	3.35794	3.62407	3.59733	3.52721	3.45570
	0.20	3.25376	3.54631	3.56692	3.52691	3.46029
	0.25	3.15443	3.45856	3.52831	3.52899	3.46997
	0.30	3.05547	3.36113	3.48369	3.48391	3.48595
	0.35	2.96992	3.25764	3.41671	3.53034	3.50124
	0.40	2.88411	3.14542	3.34044	3.52360	3.52107
	0.45	2.70474	3.02532	3.24930	3.50714	3.54232
	0.50	2.52533	2.89691	3.14284	3.47683	3.56374

$\eta = 4.0$	σ \ γ	0.0	0.3	0.5	0.7	0.9
	0.00	4.79633	4.40232	5.69159	6.50153	6.45728
	0.05	4.76364	4.41259	5.63792	6.48760	6.44957
	0.10	4.72071	4.41218	5.55671	6.46497	6.44347
	0.15	4.66435	4.39675	5.45250	6.42971	6.43869
	0.20	4.59292	4.36269	5.33001	6.37757	6.43485
	0.25	4.50320	4.30781	5.19266	6.30432	6.43136
	0.30	4.39727	4.23156	5.04254	6.20702	6.42526
	0.35	4.27514	4.13462	4.88073	6.08092	6.42193
	0.40	4.13770	4.01827	4.70762	5.92667	6.41326
	0.45	3.98568	3.88384	4.52305	5.74322	6.39914
	0.50	3.81942	3.73230	4.32641	5.53097	6.37628

$\eta = 8.0$	σ \ γ	0.0	0.3	0.5	0.7	0.9
	0.00	4.79634	4.40232	5.69159	8.08961	12.6543
	0.05	4.76645	4.41546	5.64725	7.90537	12.6477
	0.10	4.73325	4.42517	5.59040	7.71353	12.6357
	0.15	4.69389	4.42880	5.51808	7.51382	12.6159
	0.20	4.64477	4.42290	5.42807	7.30582	12.5853
	0.25	4.58168	4.40300	5.31932	7.08902	12.5402
	0.30	4.50028	4.36384	5.19199	6.86278	12.4753
	0.35	4.39760	4.30018	5.04692	6.62628	12.3865
	0.40	4.27276	4.20844	4.88505	6.37854	12.2652
	0.45	4.12690	4.08810	4.70706	6.11832	12.1039
	0.50	3.96176	3.94115	4.51306	5.84409	11.8934

K_{33}

$\eta = 2.0$	σ \ γ	0.0	0.3	0.5	0.7	0.9
	0.00	4.27432	4.44519	4.20732	4.01314	3.85464
	0.05	4.25375	4.25869	4.16528	3.98063	3.83223
	0.10	4.23396	4.19217	4.12900	3.99074	3.82895
	0.15	4.20542	4.11531	4.09183	3.99544	3.84165
	0.20	4.16637	4.02914	4.04719	4.01251	3.86648
	0.25	4.11601	3.93446	3.99052	4.02888	3.89877
	0.30	4.05074	3.83162	3.91608	4.03252	3.92770
	0.35	3.96511	3.72059	3.83277	4.03997	3.97363
	0.40	3.86204	3.60105	3.73068	4.02621	4.01223
	0.45	3.74098	3.47240	3.61326	3.99427	4.04967
	0.50	3.60258	3.33381	3.48059	3.94027	4.08422

$\eta = 4.0$	σ \ γ	0.0	0.3	0.5	0.7	0.9
	0.00	5.86758	4.79823	6.01945	6.76335	6.66851
	0.05	5.79838	4.80194	6.01001	6.73734	6.65192
	0.10	5.70968	4.79246	5.95562	6.70272	6.63947
	0.15	5.60102	4.76526	5.85900	6.65472	6.63085
	0.20	5.47403	4.71738	5.73138	6.58859	6.62556
	0.25	5.33101	4.64776	5.58214	6.50034	6.62285
	0.30	5.17392	4.55681	5.41677	6.38775	6.61971
	0.35	5.00411	4.44576	5.23806	6.24822	6.62048
	0.40	4.82227	4.31602	5.04722	6.08300	6.61725
	0.45	4.62851	4.16873	4.84446	5.89207	6.60909
	0.50	4.42242	4.00456	4.62930	5.67583	6.59198

$\eta = 8.0$	σ \ γ	0.0	0.3	0.5	0.7	0.9
	0.00	5.86758	4.79823	6.01945	8.64581	12.7634
	0.05	5.80460	4.80403	6.02849	8.47243	12.7520
	0.10	5.73457	4.80225	6.03469	8.28732	12.7360
	0.15	5.65445	4.78964	6.03435	8.09063	12.7131
	0.20	5.56111	4.76301	6.02848	7.88235	12.6802
	0.25	5.45187	4.71945	5.99170	7.66225	12.6333
	0.30	5.32498	4.65659	5.92920	7.42988	12.5668
	0.35	5.17976	4.57280	5.81500	7.18460	12.4766
	0.40	5.01626	4.46721	5.64353	6.92549	12.3535
	0.45	4.83486	4.33954	5.43428	6.65136	12.1899
	0.50	4.63578	4.18984	5.20135	6.36065	11.9762

Table A.4.4 Tables of K values for a pure radial(plate or axial shear) and compound shear modes.

K_{3R}

η = 2.0	σ \ γ	0.0	0.3	0.5	0.7	0.9
	0.00	4.14970	4.59359	5.50581	8.07677	22.4449
	0.05	4.10268	4.52159	5.41184	7.90336	21.8878
	0.10	4.05114	4.45211	5.31546	7.72563	21.3160
	0.15	3.99725	4.38585	5.21656	7.54319	20.7283
	0.20	3.94806	4.32071	5.11498	7.35561	20.1232
	0.25	3.92518	4.25747	5.01056	7.16240	19.4991
	0.30	3.99327	4.19789	4.90301	6.96295	18.8540
	0.35	4.26176	4.14297	4.79192	6.75651	18.1857
	0.40	4.63864	4.09211	4.67667	6.54220	17.4914
	0.45	4.52615	4.04230	4.55633	6.31886	16.7679
	0.50	4.35069	3.98804	4.42950	6.08505	16.0109

η = 4.0	σ \ γ	0.0	0.3	0.5	0.7	0.9
	0.00	6.24653	7.11213	7.74251	8.87144	23.0956
	0.05	6.3019	7.06839	7.67394	9.59567	22.5544
	0.10	6.35742	7.01281	7.59933	9.44676	21.9993
	0.15	6.43950	6.94232	7.51700	9.29251	21.4290
	0.20	6.52155	6.85563	7.42567	9.13213	20.8423
	0.25	6.58043	6.75461	7.31803	8.96453	20.2375
	0.30	6.63916	6.60751	7.19987	8.78828	19.6129
	0.35	6.50069	6.45588	7.06394	8.60155	18.9661
	0.40	6.29945	6.28154	6.90827	8.40203	18.29434
	0.45	6.06721	6.08479	6.73034	8.18681	17.5945
	0.50	5.81205	5.86525	6.52751	7.95224	16.8623

η = 8.0	σ \ γ	0.0	0.3	0.5	0.7	0.9
	0.00	8.53627	9.30827	12.70643	14.6080	25.5330
	0.05	8.53745	9.28370	12.5735	14.5033	25.0435
	0.10	8.52651	9.24106	12.3811	14.3751	24.5414
	0.15	8.49831	9.17484	12.1086	14.2186	24.0255
	0.20	8.44758	9.08002	11.8072	14.0302	23.4940
	0.25	8.36876	8.95281	11.4848	14.0466	22.9451
	0.30	8.25722	8.79104	11.1440	13.9581	22.3728
	0.35	8.10959	8.59404	10.7824	13.2342	21.7847
	0.40	7.92400	8.36213	10.4014	12.8864	21.1664
	0.45	7.69947	8.08585	9.99839	12.4945	20.5165
	0.50	7.43643	7.79550	9.57097	12.0569	19.8288

K_{31}

$\eta = 2.0$	σ \ γ	0.0	0.3	0.5	0.7	0.9
	0.00	3.85329	4.18500	5.10135	7.71389	22.2960
	0.05	3.78463	4.16526	4.99645	7.52400	21.7325
	0.10	3.71582	4.16018	4.88803	7.32852	21.1537
	0.15	3.66051	4.16382	4.77548	7.12701	20.5586
	0.20	3.52526	4.15638	4.65810	6.91897	19.9456
	0.25	3.42684	4.11233	4.53508	6.70381	19.3130
	0.30	3.32822	4.02800	4.40553	6.48085	18.6588
	0.35	3.25526	3.91573	4.26856	6.24927	17.9807
	0.40	3.18214	3.78514	4.12322	6.00811	17.2759
	0.45	3.01423	3.64068	3.96857	5.75618	16.5409
	0.50	2.84628	3.48412	3.80354	5.49204	15.7717

$\eta = 4.0$	σ \ γ	0.0	0.3	0.5	0.7	0.9
	0.00	4.76163	5.17401	6.35578	7.71389	22.2961
	0.05	4.64738	5.07764	6.27974	7.52427	21.7325
	0.10	4.53011	4.97504	6.14227	7.32971	21.1538
	0.15	4.40968	4.86575	5.99054	7.13001	20.5587
	0.20	4.28595	4.74928	5.83075	6.92506	19.9458
	0.25	4.15872	4.62514	5.66386	6.71506	19.3133
	0.30	4.02775	4.49283	5.48957	6.50062	18.6592
	0.35	3.89269	4.35185	5.30794	6.28496	17.9812
	0.40	3.75306	4.20158	5.11756	6.07251	17.2765
	0.45	3.60812	4.04133	4.91758	5.86756	16.5417
	0.50	3.45670	3.87018	4.70667	5.66288	15.7726

$\eta = 8.0$	σ \ γ	0.0	0.3	0.5	0.7	0.9
	0.00	4.76163	5.17401	6.53205	10.5689	22.2960
	0.05	4.64749	5.07955	6.49635	10.5323	21.7325
	0.10	4.53064	4.98331	6.45677	10.4413	21.1538
	0.15	4.41121	4.88587	6.41129	10.2968	20.5588
	0.20	4.28952	4.78789	6.35739	10.1066	19.9458
	0.25	4.16625	4.68997	6.29219	9.87896	19.3134
	0.30	4.04293	4.59241	6.21238	9.62064	18.6593
	0.35	3.92269	4.49471	6.11440	9.33509	17.9814
	0.40	3.81128	4.39517	5.99463	9.02620	17.2768
	0.45	3.71561	4.29063	5.85483	8.69267	16.5420
	0.50	3.63599	4.17662	5.69528	8.33438	15.7729

K_{42}

$\eta = 2.0$	σ \ γ	0.0	0.3	0.5	0.7	0.9
	0.00	4.85065	4.40231	5.69159	8.08961	22.3999
	0.05	4.77203	4.43130	5.64881	7.90432	21.8365
	0.10	4.69335	4.48974	5.57992	7.70939	21.2572
	0.15	4.51441	4.57182	5.47143	7.50498	20.6609
	0.20	4.3355	4.65891	5.34198	7.29138	20.0462
	0.25	4.22284	4.71023	5.19564	7.06863	19.4115
	0.30	4.11021	4.68166	5.04025	6.83971	18.7613
	0.35	3.90905	4.56429	4.87456	6.59453	18.2444
	0.40	3.70780	4.40501	4.69843	6.34187	17.5538
	0.45	3.56994	4.22893	4.51140	6.07745	16.8344
	0.50	3.43209	4.03996	4.31270	5.79984	16.0821

$\eta = 4.0$	σ \ γ	0.0	0.3	0.5	0.7	0.9
	0.00	5.84356	5.88907	6.59924	8.08961	22.3999
	0.05	5.71372	5.76284	6.43392	7.90657	21.8367
	0.10	5.58387	5.63152	6.27386	7.71833	21.2581
	0.15	5.31763	5.49442	6.10779	7.52464	20.6627
	0.20	5.05139	5.35083	5.93558	7.32524	20.0492
	0.25	4.93198	5.20002	5.75687	7.11978	19.4157
	0.30	4.81257	5.04131	5.57100	6.90781	18.7604
	0.35	4.77085	4.87402	5.37739	6.68864	18.0808
	0.40	4.72913	4.69740	5.17517	6.46116	17.3741
	0.45	4.56158	4.51058	4.96334	6.22372	16.6369
	0.50	4.39402	4.31251	4.74062	5.97397	15.8650

$\eta = 8.0$	σ \ γ	0.0	0.3	0.5	0.7	0.9
	0.00	5.86959	5.88908	6.59945	10.51124	22.3999
	0.05	5.75665	5.76412	6.49751	10.4642	21.8367
	0.10	5.64139	5.63756	6.39804	10.3690	21.2582
	0.15	5.51402	5.51039	6.30155	10.22475	20.6630
	0.20	5.38699	5.38404	6.20736	10.03655	20.0496
	0.25	5.27494	5.26044	6.11307	9.81125	19.4164
	0.30	5.17006	5.14175	6.01467	9.55470	18.7613
	0.35	5.07130	5.02945	5.90710	9.27083	18.0821
	0.40	4.97574	4.92262	5.78505	8.96179	17.3757
	0.45	4.87698	4.81661	5.64346	8.62827	16.6389
	0.50	4.76765	4.70354	5.47786	8.27735	15.8674

APPENDIX A.5

Mode \ γ	Dimensionless Eigenvalues				
	0.0	0.3	0.5	0.7	0.9
K_{10}^{LI}	2.26703	2.78506	3.78311	6.22506	18.59366
K_{1R}^{I}	2.35156	1.74485	1.41230	1.19290	1.05265
K_{20}^{LI}	4.15312	5.38803	7.46911	12.40608	37.17569
K_{2R}^{I}	5.99198	5.39050	7.11992	11.65862	34.78854
K_{3R}^{I}	9.50405	10.12981	13.98832	23.21453	69.57125
K_{12}^{I}	1.38716	0.92194	0.56885	0.32063	0.08583
K_{11}^{LI}	1.08704	0.93802	0.80171	0.69951	0.62174
K_{22}^{LI}	1.80645	1.75699	1.59841	1.39710	1.24419
K_{21}^{I}	1.66007	1.73403	1.73410	1.62484	1.48865
K_{32}^{I}	2.59454	2.46947	2.56431	2.52842	2.35375
K_{31}^{LI}	3.17302	3.04033	3.88408	6.26551	18.60433
K_{42}^{LI}	3.96699	3.71160	4.19722	6.38866	18.63560
K_{41}^{I}	3.79673	4.08514	4.41915	6.49033	18.66062
K_{52}^{I}	4.65828	4.62981	5.31924	6.90625	18.76864
K_{51}^{I}	5.89198	4.88734	6.83295	11.49253	34.73523
K_{62}^{I}	5.59369	5.51969	6.57203	11.21673	34.59274
K_{61}^{LI}	5.04904	5.50662	7.51632	12.42607	37.18106
K_{72}^{LI}	5.89803	5.86714	7.66061	12.48662	37.19671

Table A.5 Table of K values for Infinite hollow cylinder, $\sigma = 0.30$.

APPENDIX A.6.1

LUMPED IMPEDANCE MODEL OF TUNING FORK RESONATOR

A resonator can often be regarded as a lumped stiffness and a lumped mass. The mass vibrating on a spring is a classical case. Acoustically, the lumped system such as the Helmholtz resonator can be analysed as two reactances, one positive (inertial) and the other negative (stiffness). The condition for resonance is that the sum of the reactances is zero. This zero reactance condition is applicable to distributed resonances. The phenomena are, therefore, being the cases of added stiffness and added mass. There are various ways of calculating the same.

Impedance of a lumped mass

Consider the mass-spring system shown in Fig.6.2. If an alternating force is applied to the mass m, the ratio of force amplitude to velocity amplitude gives the impedance. This will be a pure reactance if they are in quadrature. Thus, if the force F is expressed as

$$F = m \ddot{x} = F_0 \ e^{j\omega t} \qquad (A.6.1)$$

where F_0 is the peak amplitude and x is the displacement, then the impedance is given by

$$Z_m = F/\dot{x} = j \omega m \ , \qquad (A.6.2)$$

which is a pure reactance.

Impedance of a long thin rod in tension

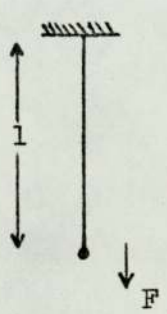

The tuning fork can be considered as a lumped mass-spring system and its impedance can be calculated by regarding the resonator as a long thin rod under tension. The force acting on the resonator under tension[71] is given by

$$F = S x = F_0 \ e^{j\omega t} \qquad (A.6.3)$$

where S is the stiffness constant given by

$$S = EA/l \qquad (A.6.4)$$

where E, A and l are the Young's modulus, area of cross-section and the length of the rod, respectively. Thus, the impedance is given by

$$Z_s = \frac{F}{\dot{x}} = -\frac{jEA}{\omega l} = \frac{\rho AC^2}{j\omega l} \qquad (A.6.5)$$

where C is the velocity of sound in the rod material.

A long thin rod can also be regarded as an acoustic transmission line. Then, the impedance of the line[5] is given by

$$Z_s = -j\,\rho\,C\,A\cot\theta \qquad (A.6.6)$$

where $\theta = 2\pi l/\lambda = \omega l/C$. When θ is small, $\cot\theta = 1/\theta$ and hence, eqn.(A.6.6) reduces to

$$Z_s = \frac{\rho C^2 A}{j\omega l} \qquad (A.6.7)$$

If a mass m (resonator) is placed at the end of the line, the resonant frequency can be obtained from the condition,

$$Z_m + Z_s = 0 \qquad (A.6.8)$$

Thus, substituting eqns.(A.6.2) and (A.6.7) in the above equation and simplifying, yields the resonant frequency as

$$\omega_0^2 = \frac{\rho C^2 A}{lm} \qquad (A.6.9)$$

Air gap as stiffness

This requires the assumption that there is no lateral motion of the gas. It is therefore compressed and rarefied, thus increasing the restoring force on the masses and increasing the frequency. If the centre is a node (equivalent to an infinitely stiff termination), the impedance at the face of each mass will be

$$Z_a = -\frac{j\,\rho C^2 A}{\omega\, t_s}\ , \qquad (A.6.10)$$

where $t_s = l$, is the half width of the air gap slot width of the tuning

fork. The stiffness can be derived from eqn.(A.6.4), as

$$S = \frac{\rho C^2 A}{t_s} \qquad (A.6.11)$$

In the actual design, the tuning fork was based on an aluminium block 1" x 1" x 1½", as shown in Fig.6.1. The resonant frequency was about 8 kHz. If it is rather arbitrarily assumed that the mass of the resonator resides in two (tines) blocks of aluminium 1" x 1" x ½" and the stiffness of the flexural spring is calculated to give an 8 kHz resonant frequency, then $Z_{spring} = 2\omega m$ Kg/sec., since $Z_m = Z_s$.

For the tuning fork shown in Fig.6.1,

$\rho_{Al} = 2.7 \times 10^3$ Kg/m^3, $\rho_{air} = 1.3$ Kg/m^3, $C_{air} = 340$ m/sec.,

$t_s = 0.51 \times 10^{-3}$ m , $A = 3.23 \times 10^{-4}$ m^2,

$v = 8.194 \times 10^{-6}$ m^3, $f = 8$ kHz.

Therefore,

Tine mass = $\rho v = 22.123 \times 10^{-3}$ Kg.;

Reactance of the mass = $2 \omega m = 2224.04$ Kg/sec.;

The stiffness arising from air in the gap between the tines (masses) is

$$S = \frac{\rho_{air} C_{air}^2 A}{t_s} = 95.18 \times 10^3 \text{ Kg/sec}^2.$$

APPENDIX A.6.2

ELECTRONIC CIRCUITS FOR TUNING FORK RESONATOR

A.6.2.1 Power Amplifier

The driving pulses of the transmitter are amplified sufficiently by using the power amplifier whose circuit diagram is shown in Fig.A.6.1. This circuit consists of two transistors T_1 and T_2 for power amplification and the transistor T_3 generates sufficient current in the coil, which, acting as an electromagnet, produces a varying magnetic field from the transmitter output. The magnetostrictive transducer (line) converts the changing magnetic field into ultrasonic energy, which drives the resonator.

A.6.2.2 Receiver

The echo signal received from the resonator, on being driven by the transmitted burst of energy, is processed in a receiver. The complete circuit diagram of the receiver is shown in Fig.A.6.2. The transmitted burst and the transients in the signal received from the resonator are suppressed and the decrement signal converted into square pulses in the comparator, after sufficient amplification. The resonant frequency of tuning fork is determined by generating a gate of ten decrement pulses using the circuits shown in the figure and then by measuring the duration of this gate using the digital counter, also shown in the figure.

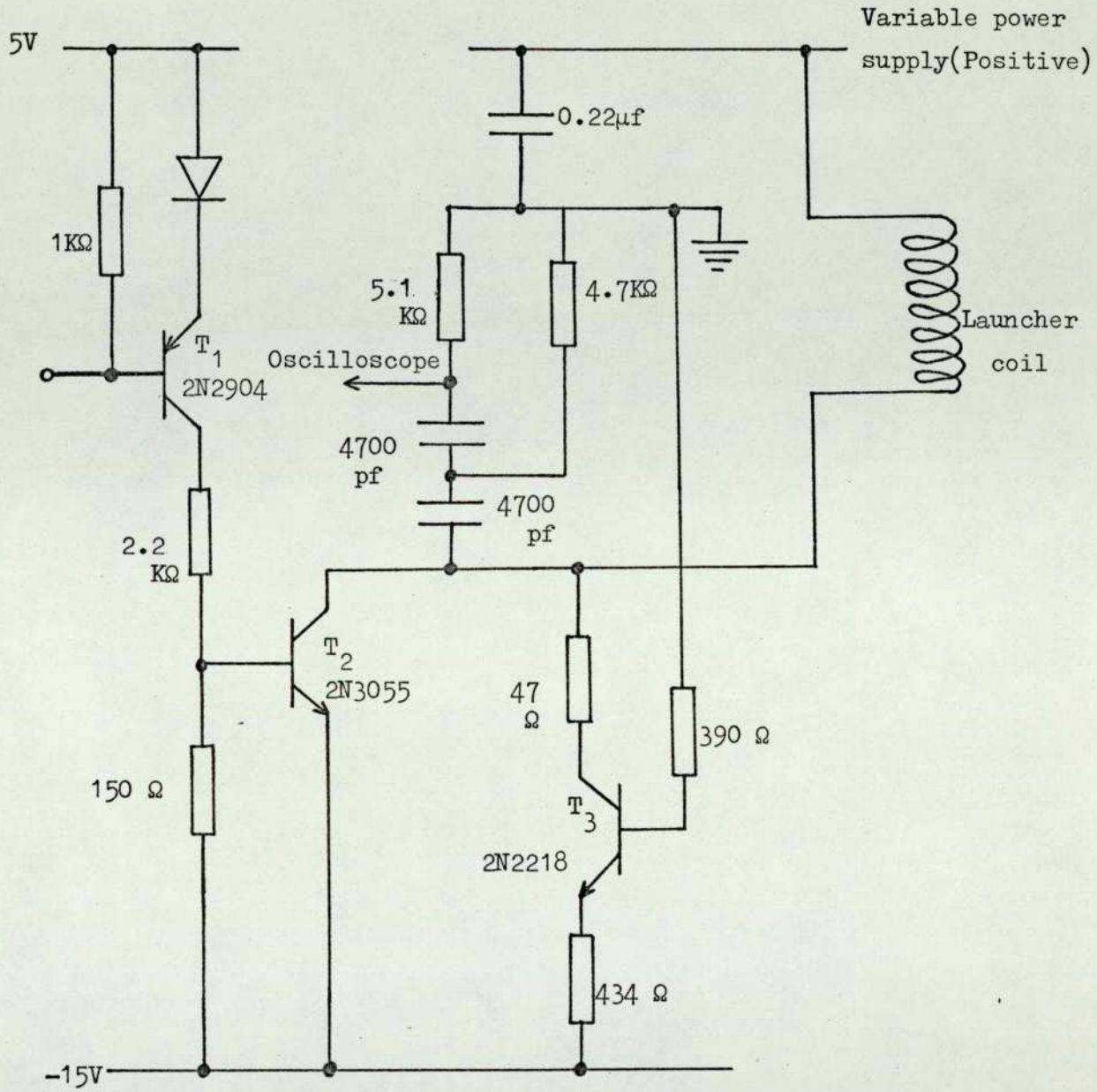

Fig.A.6.1 Circuit Diagram of the Power Amplifier.

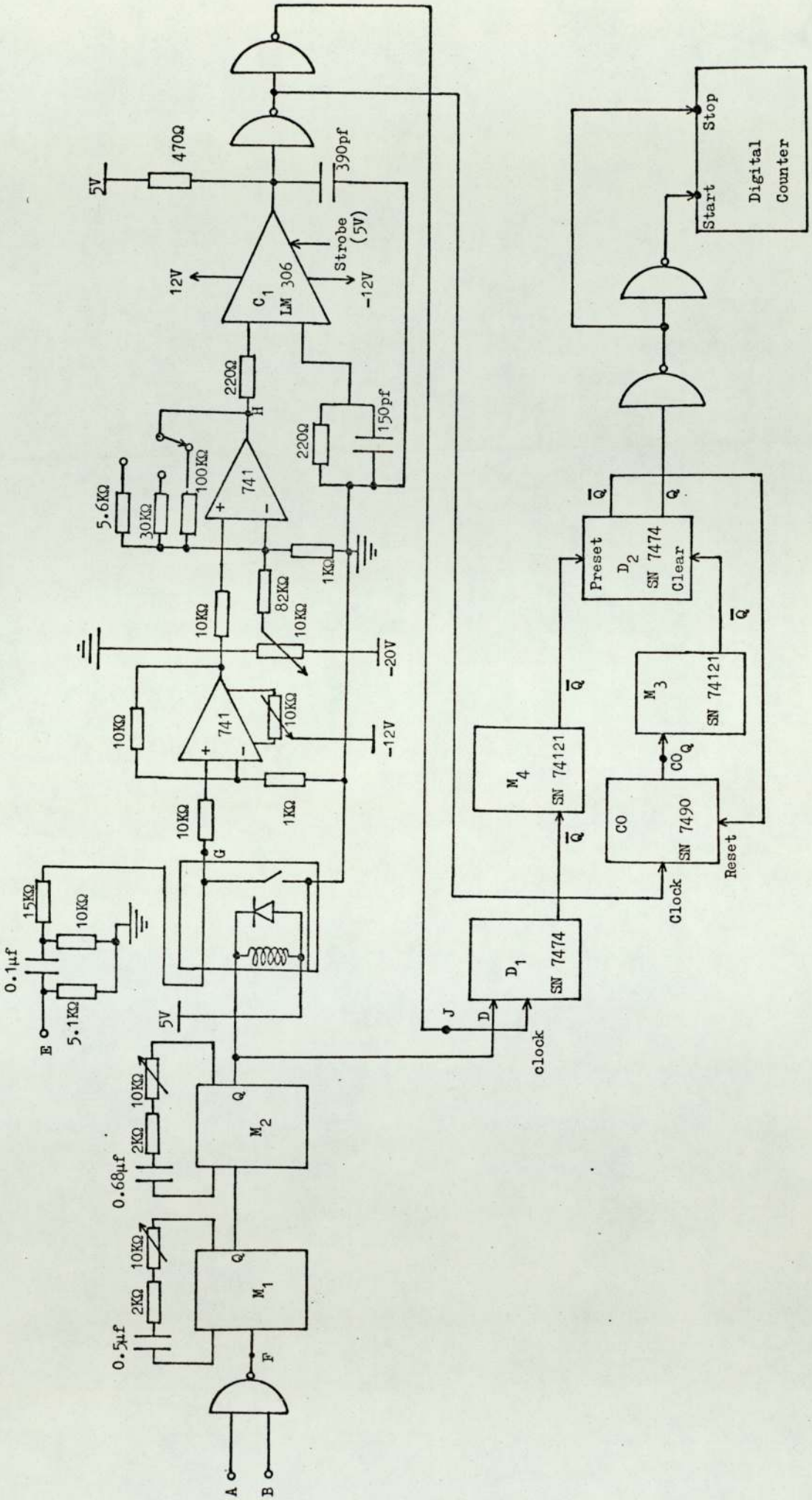

Fig.A.6.2 Circuit Diagram of the Receiver.